ALKYNYL ETHERS OF DEXTRANS AS INTERMEDIATES FOR NEW FUNCTIONAL BIOPOLYMERS

Von der Fakultät für Lebenswissenschaften

der Technischen Universität Carolo-Wilhelmina

zu Braunschweig

zur Erlangung des Grades eines

Doktors der Naturwissenschaften

(Dr. rer. nat.)

genehmighte

D i s s e r t a t i o n

von Muhammad Nazir Tahir
aus Vehari / Pakistan

1. Referentin: Professorin Dr. Petra Mischnick
2. Referent: apl. Professor Dr. Hans-Joachim Jördening
Eingereicht am: 17.10.2011
mündliche Prüfung (Disputation) am: 23.12.2011

Druckjahr 2012

VORVERÖFFENTLICHUNGEN DER DISSERTATION

Teilergebnisse aus dieser Arbeit wurden mit Genehmigung der Fakultät für Lebenswissenschaften, vertreten durch die Mentorin der Arbeit, in folgenden Beiträgen vorab veröffentlicht:

Publikationen

MN Tahir,A Adnan,P Mischnick. Lipase immobilization on *O*-propargyl and *O*-pentynyl dextrans and its application for the synthesis of click beetle pheromones. *Process Biochem*. 44: 1276-1283 (2009).

MN Tahir, C Bork,A Risberg. JC Horst, C Komoß, A Vollmer, PMischnick. Alkynyl Ethers of Glucans: Substituent distribution in peopargyl-, pentynyl- and hexynyldextrans and –amyloses and support for silver nanoparticle formation. *Macromol. Chem. Phys*. 211: 1648-1662 (2010).

Tagungsbeiträge

P Mischnick, MN Tahir, AVollmer. Unsaturated ethers of dextrans as intermediates for further functionalization. Japanese-European workshop on cellulose and functional polysaccharides, von-Thünen-Institute, Hamburg, Germany (2009).

P Mischnick, AVollmer, MNTahir. Unsaturated dextran ethers as intermediates for new functional biopolymers. Forth international symposium on the separation and characterization of natural and synthetic macromolecules (SCM-4), Amsterdam, The Netherlands (2009).

MN Tahir, P Mischnick. Propargyl ethers of dextran (PgD): Synthesis, analysis and changes during storage. Forth international symposium on the separation and characterization of natural and synthetic macromolecules (SCM-4), Amsterdam, The Netherlands (2009).

MN Tahir, P Mischnick. Synthesisof *O*-pentynyl dextran and further functionalization. 15th european carbohydrate symposium (Eurocarb-15), Vienna, Austria (2009).

ACKNOWLEDGEMENT

The work presented in the thesis was carried out in the period from July 2007 to February 2011 in Institute of Food Chemistry, Technische Universität Braunschweig, Germany, under the supervision of Prof. Dr. Petra Mischnick. During this period, I met many people, which contributed directly or indirectly to the realization of this PhD thesis. I wish to thank them in these following lines.

Petra, working with you was a pleasure; your door was always open for advice and discussions despite a busy schedule. Your motivational nature, enthusiasm and ability to see and make good use of the good sides of students while always taking care of stressful details probably has a lot to do with the relaxed atmosphere in the group. I appreciate the trust and support that I felt in these three and half years. I am also grateful for learning a lot about the other part of a scientist's job, which is not only about working in the lab or writing articles.

Dr. Magadaly Boehme, Dr. Andreas Bösch and Dr. Antje Vollmer, I am very thankful to you helping me a lot in early days of my PhD work, to conduct experiments and very useful suggestions and discussions.

Kristin Voiges, Christian Bork, Inga Unterieser, Kathrin Fiege, Marko Rother, Silke Lehmann, Dr. Anne Adden, Julia Cuers, Hauke Zinow and Rommy Müller, I am very thankful to you for a nice atmosphere, very constructive conversations in the group and for contribution, some of you have added in translation of English summary into Deutsch (Zusammenfassung).

I am very thankful to Frau Susanne Tille-Lauckner for helping in official problems, Frau Marita Baum for helping in many technical problems and in some instrumental measurements and Dr. Gerold Jerz for helping in ESI-MS measurements.

I offer my sincere thanks to the members of Institute of Food Chemistry; Karin Kadim for IR spectra, A. Risberg, KTH Stockholm, Fibre and Polymer Technology, Stockholm, Sweden for SEM images; J. C. Horst and C. Komoß, Institut für Pharmazeutische Technologie, TU Braunschweig for TEM images; Nico Lämmerhardt, Institut für Halbleitertechnik TU Braunschweig for performing spin-coating experiments and helping me to record fluorescence microscopic images; Dr. Silke Hillebrand, for her help in antioxidant experiments; C. Schmidt, Institut für Ökologische Chemie und Abfallanalytik, TU Braunschweig for ICP-OES measurements; and Elemental Analysis laboratory (Institut für Pharmazeutische

Technologie), NMR and GC-MS laboratories (Institut für Organische Chemie) for their help to carryout this research work.

I am very thankful to Deutsche Forschungsgemeinschaft (DFG Mi 398/9-1) for financial support for first one and half year. I am also very thankful to Deutscher Akademischer Austausch dienst (DAAD), Internatinal Office TU Braunschweig, and Institute of Food Chemistry, TU Braunschweig, for their financial support for next two years.

I sincerely thank Prof. Dr. H.-J. Jördening, Institut für Technische Chemie, TU Braunschweig, for agreeing to be the co-referee of my thesis.

I must mention that staying in Germany hashelped a lot in my mental and social bringing up. After all, life is much more than doingresearch and writing the thesis and research articles. Although, I have not tried much to improve my German language (Deutsch) but the opportunity to observe the German society and organized system in German institutes wasextremely vital. I am proud to say that "*Ich war in Deutschland und dort habe ichpromoviert."*

Finally, I want to dedicate this thesis to my parents, sister, brothers and my wife. I know theyhave missed me a lot when I was away and always have wished for my success and progress. And I know how much proud and happy they are on this achievement. I love you guys.

LIST OF ABBREVIATIONS

AcD	acetyl dextran
AcD-Fe	acetyl dextran complexed with iron
ATR-IR	attenuated total reflectance infrared
BSA	N,*O*-Bis-(trimethylsilyl)-acetamide
BSTFA	N,*O*-Bis-(trimethylsilyl)-trifluoroacetamide
CID	collision induced dissociation
CMC	carboxymethyl cellulose
CuAAC	copper catalyzed azide-alkyne cyclo addition
D	daltons
DCM	dichloromethane
DMAc	dimethyl acetamide
DMF	dimethyl formamide
DMSO	dimethyl sulfoxide
DNA	deoxyribonucleic acid
DP	degree of polymerization
DS	degree of substitution
DS_{EA}	degree of substitution calculated from elemental analysis
DS_{GC}	degree of substitution calculated from monomer analysis by gas chromatography
DS_{py}	degree of substitution of pentynyl
EA	elemental analysis
ECR	effective carbon response
EDC	1-ethyl-3(3-dimethylaminopropyl)carbodiimide
ESI-MS	electrospray ionization mass spectrometry
Et	ethyl
Fig.	figure
GC-MS	gas chromatography mass spectrometry
GLC	gas liquid chromatography
HMDS	hexamethyldisilazane
HPLC	high pressure liquid chromatography
ICP-OES	inductively coupled plasma optical emission spectroscopy
m/z	mass-to-charge ratio
Me	methyl
M_w	average molecular weight
MWCO	molecular weight cut-off
NMR	nuclear magnetic resonance
PEG	polyethylene glycol
PEO	polyethylene oxide
Pg	propargyl
PgD	propargyl dextran
Py	pentynyl
PyAcD	peracetylated pentynyl dextran
PyAcD-Fe	peracetylated pentynyl dextran complexed with iron
PyD	pentynyl dextran
PyD-Ag	peracetylated pentynyl dextran complexed with silver
PyD-Amb	lipase (*Rhizopus* arrhizus) immobilized on Amberlite XAD 761

PyD-Duo	lipase (*Rhizopus* arrhizus) immobilized on Duolite A568
PyD-Lew	lipase (*Rhizopus* arrhizus) immobilized on Lewatit VP OC 1600
PyD-Lip	lipase (*Rhizopus* arrhizus) immobilized on pentynyl dextran
RNA	ribonucleic acid
SEC	size exclusion chromatography
SEM	scanning electron microscopy
TBAB	tetra-n-butyl ammonium bromide
TEA	tetraethyl ammonium
TEM	transmission electron microscopy
TFA	trifluoroacetic acid
THF	tetrahydrofuran
TLC	thin layer chromatography
TMCS	trimethylchlorosilane
TMS	trimethylsilyl
UV	ultra violet

TABLE OF CONTENT

1 INTRODUCTION

1.1 Polysaccharides

Carbohydrates represent the most abundant organic compounds in the biosphere in different substances, forms and materials. The basic carbohydrates as cellulose, starch and sucrose were known and used by human being from very ancient times for different purposes. Egypt used cellulose already about 4000 B.C. to prepare a material for writing and there are indications of sugar processing to get sucrose in New Guinea as early as 10000 B.C and about 6000 B.C. in India [1].

Carbohydrates exist as monosaccharides, di-, oligosaccharides and polysaccharides [1, 2]. Biopolymers are produced by living organisms. Cellulose and starch, proteins and peptides, and DNA and RNA are all examples of biopolymers, in which the monomeric units are sugars, amino acids and nucleotides respectively. Biopolymers generally consists of C, H, N and O but proteins, DNA, RNA and a few other biopolymers contain in addition other elements like sulfur and phosphorus also in basic polymer chain [3].

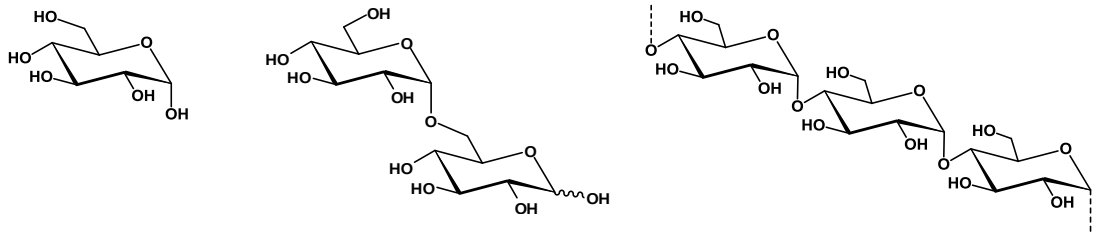

Monosaccharide (glucose) Disaccharide (isomaltose) Polysaccharide (amylose from starch)

Fig. 1.1: Examples of mono-, di-, and polysaccharides

In the nineteenth century [1], it was found that carbohydrates have the general formula $C_n(H_2O)_n$. So they are considered hydrates of carbon and hence called carbohydrates [4]. Later it was found that carbohydrates in fact contain hydroxyl groups and are polyhydroxy aldehydes or ketones. Thus now carbohydrates can be defined as polyhydroxy aldehydes or ketones or compounds that can be derived from them by any of the several means e.g. oxidation, reduction or substitution of one or more of the hydroxyl groups. In disaccharides (and polysacharides), oxygen links two rings together. The atom above it (see in di-, or polysaccharide in Fig. 1.1) is

connected to two oxygens, both of which are in ether type situation. The carbon and these oxygens form acetal linkage to connect monosaccharides to di- and polysacchardies.

Biopolymers are generally divided into polynucleotides, proteins, polysaccharides, terpenes, polyhydroxyalkanoates and lignin [3]. They are the functional basis for all living organisms on earth and constitute the largest fraction of the cell. Their three-dimensional structures provide the robustness that is required to form templates for (parts that perform) biochemical function [5, 6].

A variety of carbohydrates is produced naturally by plants, animals and microorganisms. A brief overview of selected polysaccharide is given in Table 1.1. The structure of polysaccharides can be linear e.g. cellulose, branched e.g. dextran, xanthan or heavily branched e.g. amylopectin, gum acacia etc.

Plants are the main natural producer of carbohydrates by photosynthesis in which energy from the sun is converted into chemical energy using carbon dioxide and water following a complex mechanism [1, 2].

$$6\,CO_2 + 6\,H_2O \xrightarrow[photosynthesis]{h\nu} C_6H_{12}O_6 + 6\,O_2$$

Therefore, carbohydrates played an important role in scheme of universe and in the establishment and evolution of life on earth. It is estimated that about 3.4×10^{11} tons of carbohydrates are biosynthesized each year on the earth by plants and bacteria [1].

In addition to the traditional scientific areas connected with the study of biological macromolecules, there are a number of young, yet actively expanding fields, involving biopolymers, nanoscience, biotechnology and molecular medicine. In nanoscience and molecular biotechnology, biopolymers and related compounds may be used as templates or scaffolds for various miniaturized technologies [6]. Carbohydrates, being one of the subclass of biomolecules, are intimately linked to lipids and proteins, usually as glycoconjugates e.g. glycolipids in membranes or as glycoproteins [7].

Table 1.1: Structure of polysaccharides of different origin

Polysaccharide	Source	Bond linkage	structure
Cellulose	Plants	β-(1→4)-D-glucose	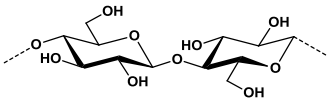
Curdlan	Bacteria	β-(1→3)-D-glucose	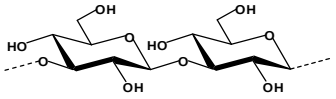
Dextran	Bacteria	α-(1→6)-D-glucose main chain	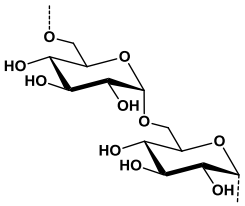
Pullulan	Fungi	α-(1→6) linked maltotriosyl units	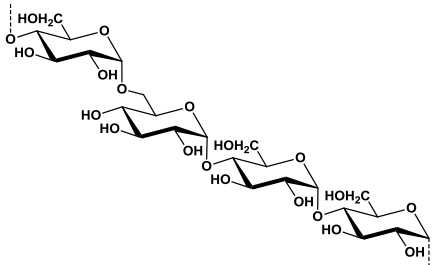
Amylose (Starch)	Plants	α-(1→4)-D-glucose	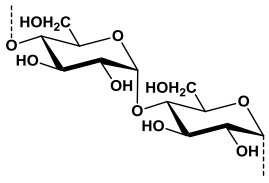
Amylopectin (Starch)	Plants	α-(1→4) and (1→6)-D-glucose	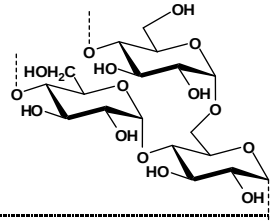
Chitin	Fungi	β-(1→4)-D-(*N*-acetyl) glucosamine	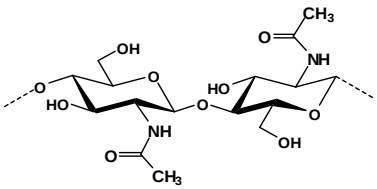
Alginate	Algae	β-(1→4)-D-mannuronic acid α-(1→4)-L-guluronic acid	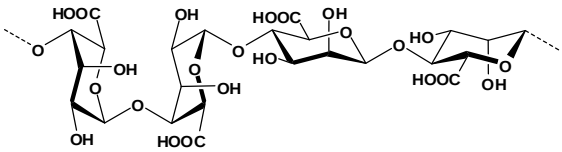 G G M M

1.1.1 Chemical Modification of Polysaccharides

Unique structure of polysaccharides combined with many promising properties like hydrophilicity, biocompatibility, non-toxicity, biodegradability (at least in the original state), stereoregularity, multi-chirality, and polyfunctionality, i.e. reactive functional groups (mainly OH, NH, and COOH) that can be modified by various chemical reactions provide an additional and important argument for their study as a valuable and renewable resource for the future. Chemical modification of polysaccharides is one of the most important paths to develop new products and materials. Along with many advantages of modified polysaccharides due to their wide applications, the change of structure made them less degradable which is a disadvantage with respect to recycling, but also a required property for some applications [8].

1.1.2 Applications of Polysaccharides in Scientific and Industrial Fields

The large amount of produced polysaccharide derivatives with their structural diversity makes them perfect materials for defined applications [9]. Most common methods for modification are based on esterification and etherification of OH. Nucleophilic substitution reactions are also used to a lower extent. Chemical modification broadens the field of applications due to control over properties of modified polysaccharides e.g. solubility, hydrophobic and hydrophilic balance, and polarity etc.

Polysaccharides and their derivatives are widely applied in building materials, paper manufacturing, pharmaceuticals, food, mucilages, textiles, fuel, cosmetics and toiletry formulations. In cosmetics, they include skin, hair and dental products. These products are used as viscosity enhancers, emulsifiers, sweeteners, stabilizers and moisturizers. In food industry, they are used for the preservation of confections, for the flavor protection and delivery, as softener in baked goods, as thickener in sauces and dressings, to improve texture and shelf-life of baked products and to improve freeze-thaw stability.

In pharmaceuticals, polysaccharide derivatives are used in tablets, liquids, coatings of chewing gums, as crystallization inhibitors, stabilization for drugs, and vitamins etc. In textiles, carbohydrates are used as humectants, antistatic agents, softeners, textile detergent and as thickener in textile sizing. They appear in the products such as

cements, paints, adhesives, lotions, creams, toothpastes, mouthwashes, skin moisturizers, hair conditioners and shampoos. An overview of applications of some selected polysaccharides is given in Table 1.2.

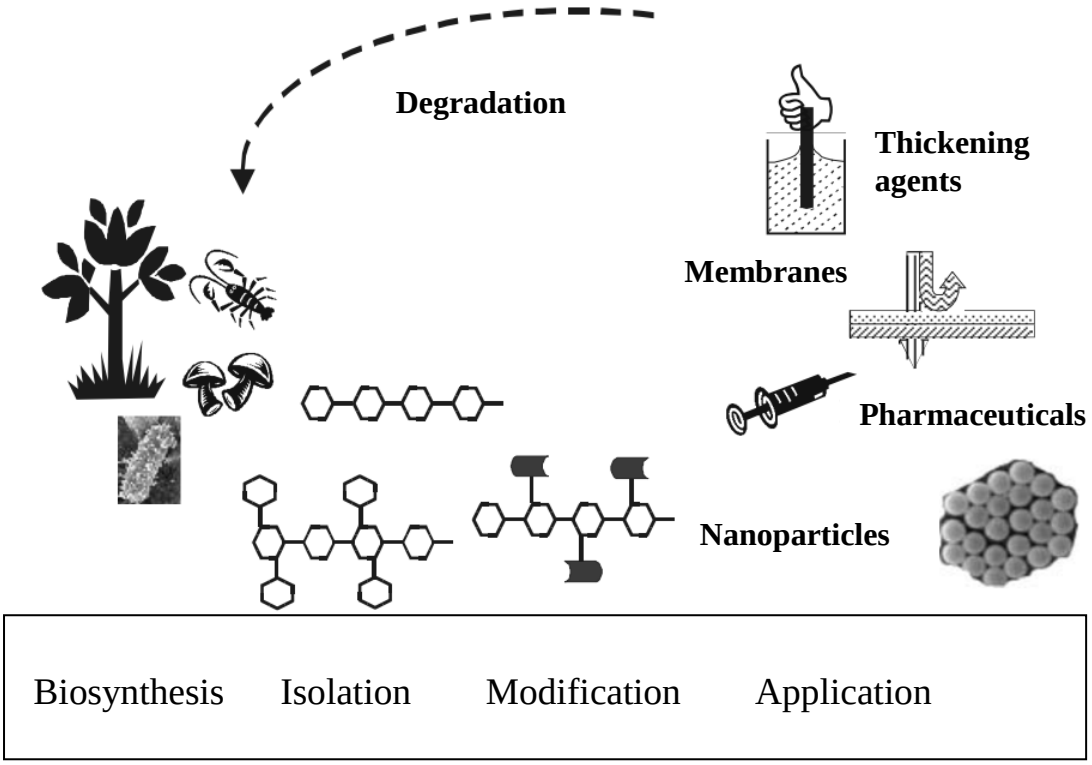

Fig. 1.2: A general scheme for production, isolation, modification and applications of polysaccharides (Adopted from [10])

Biopolymers have many applications in medical fields and can roughly be divided into three main categories: drug delivery system, wound closure and healing products, and surgical implant devices. Due to many free OH groups in polysaccharide chains, they tend to form cooperative intra- and inter chain hydrogen bonds affecting superamolecular structure in solution. It is also the reason for good film forming property in some polysaccharides [11]. Some biopolymers are applied (or employed as) for food containers, soil retention sheeting, agriculture film, waste bags and as packing materials in general. When used as non-woven, these biopolymers can be used in agriculture, filtration, hygiene and protective clothing [12]. An important feature for a potential polymer system to be used for polymer flooding in enhanced oil recovery applications is that the aqueous polymer solution has a relatively high viscosity at low polymer concentrations [13] which is for example fulfilled by carboxymethyl cellulose (CMC).

Table 1.2: Typical applications of polysaccharides and their derivatives [2, 14-17]

Polysaccharide	Function	Application
Dextran	Volume expander, lubricant, supporting material	Blood expander, eye drops, separation chromatography, immobilization of biosensors
Cellulose	Industrial raw material	Paper board, paper, paste boards, textiles
Guar	Stabilizer, water retention	Dairy ice cream, desserts, bakery products, meat products
Alginates	Stabilizer, gelation	Beverages, ice creams, puddings, pharmaceuticals
Xanthan gum	Stabilizer, thickener	Dressings, beverages, dairy products, bakery products
Gum acacia	Stabilizer, thickener, emulsifier, encapsulating agent	Confectionary, bakery, beverages, sauces
Dextran sulfate	Anticoagulant material	Substituent for heparin in anticoagulant therapy
Cellulose acetate	Synthetic fiber Film material	Artificial silk, photographic film base, cigarette filters, playing cards etc.
Methyl cellulose	Gelation, stabilizer, water retention	Fat reducer, bakery, adhesive in mortar, wall paper paste, cosmetics
Carboxymethyl cellulose	Stabilizer, thickener, water retention	Ice creams, syrups, cake mixes, meats, toothpaste, jelly, textile sizing, detergents, eye drops, paper products
Hydroxypropyl starch	Thickener, stabilizer	Bakery, soups, confectionaries

It is widely recognized that many biological compounds e.g. drugs, food additives, agrochemicals and fragrances are chiral and their physiochemical properties depend on their stereochemistry. Purity of such enantiomers is very important because mostly only one enantiomer of many drugs exhibit desired therapeutic activity while others show an antagonistic function, side effect or even toxic effect [18]. Cellulose, cyclodextrin and amylose and other polysaccharide derivatives are used as chiral packing materials or as chiral stationary phases in various chromatographic methods for enantioseparation of such biological compounds [19-25].

1.2 Analysis of Polysaccharides

The structural analysis of polysaccharides and knowledge about substituent distribution in their derivatives may offer the most fundamental understanding about the functions and properties of polysaccharides. Substitution distribution analysis is mainly focused on starch and cellulose derivatives due to their industrial importance and bulk production [26]. Diversity and irregularity of polysaccharide chains make the structural analysis a complex task. In the last two decades, many efforts have been made to improve our knowledge about substitution pattern in polysaccharide derivatives and how this modification is influenced by the method applied. The understanding of structure- properties relationship. e.g. solubility, viscosity, thermoreversible gelation, film forming, flocculation, biodegradability etc. will help to improve these properties in a more functional way by the conditions of preparation. Polysaccharide analysis requires specialized techniques, which differ from those methods used for the characterization of small molecules.

Structure analysis of polysaccharide derivatives usually starts with the determination of degree of substitution (DS): by elemental analysis, by titration method, by determination of amount of substituents after cleavage (Zeisel method for alkyl and hydroxyalkyl ethers, seponification of ester derivatives), by NMR spectroscopy, or by GLC after depolymerization and preparation of volatile derivatives [27].

Among these methods, NMR spectroscopy can give a first sight into structural analysis of polysaccharides[28] but is limited due to solubility, viscosity and polymeric nature of modified polysaccharides [27]. Average DS of cellulose acetates can be calculated by ^{1}H- and ^{13}C-NMR spectroscopy, while positions of esterification can be better resolved after perpropyonylation [10]. In contrast, chemical methods of analysis, including depolymerization and separation of monomer derivatives, although more laborious, appear to provide a reliable means to determine both the DS and the distribution of the substituents in modified polysaccharides [29].

1.2.1 Monomer Analysis of Polysaccharides

Knowing the monomer composition of polysaccharides is very important for further investigation of substituent distribution, e.g. in the polysaccharide chain or with respect to the superamolecular structure of starch granule or of cellulose fiber[30].

After modification, homoglycans can be considered as co-polymer of up to eight (one type of substituents) or more than eight (different type of substituents) constituents[28, 31]. Depolymerization is the first step in monomer analysis of polysaccharide derivatives. Cleavage of glycosidic linkage of polysaccharides can be carried our by different methods e.g. hydrolysis or methanolysis or – in case all OH are protected – by reductive cleavage using a Lewis acid and triethylsilane [32].

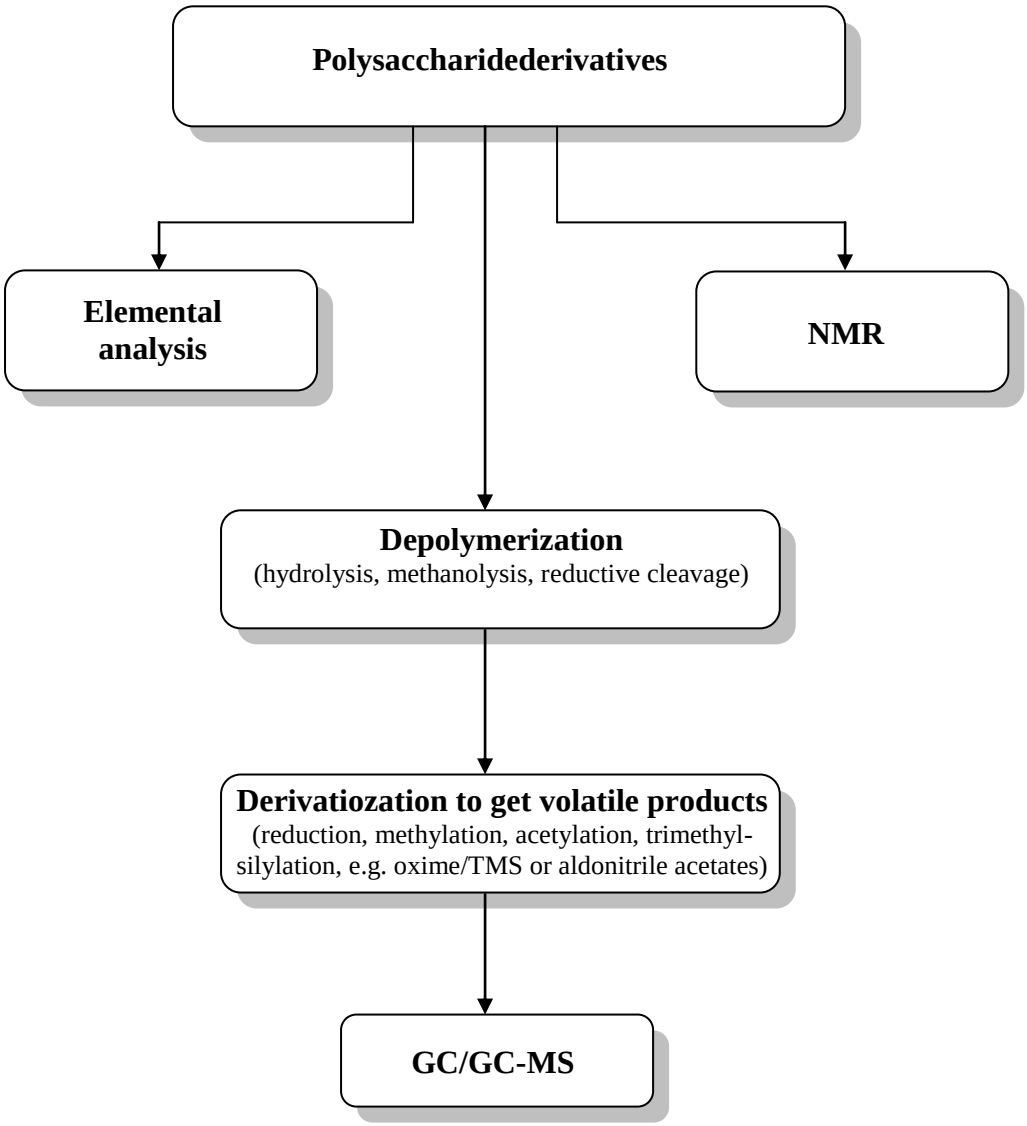

Fig. 1.3: A general scheme for analysis of polysaccharide derivatives

Hydrolysis – "cleavage by the addition of a water molecule across a bond – is the most common method to cleave glycosidic linkages in polysaccharides" [32]. It is carried out in aqueous media with an acid catalyst. Common acid catalysts are trifluoroacetic acid, sulfuric acid and hydrochloric acid [32].

If methanol is applied as a nucleophile instead of water, methyl glycosides are formed. Methanolysis is generally carried out in the presence of dry hydrogen chloride as a catalyst at elevated temperature. Water is rigorously excluded during methanolysis since presence of water will set up an equilibrium between methyl glucosides and free forms of sugars in aqueous solutions, leading to complex mixtures [32]. After completion of methanolysis, HCl can be neutralized with amberlite IRA-400 (HCO_3^-) resin [33] or simply by evaporating with co-solvent [34].

To make polysaccharides more volatile, free hydroxyl groups of polysaccharides are commonly acetylated, trifluoroacetylated, ethylated, methylated, or silylated. Among these methods, silyation and acetylation are relatively common methods to form respective ethers at free hydroxyl groups. A general scheme for analysis of polysaccharide derivatives is given in Fig. 1.3.

Sweeley *et al*. [35] introduced silylation for the analysis of carbohydrates by GLC, using trimethylchlorosilane (TMCS) and hexamethyldisilazane (HMDS) in the presence of pyridine. The drawback of this procedure is that a solid mass of the formed siloxane will deposit on the flame ionization detector resulting in decrease of detector sensitivity. Many developments have been made to improve this classic method, to avoid siloxane formation and to increase the stability of derivatized products. In modified methods, *N,O*-bis-(trimethylsilyl)-acetamide (BSA) or *N,O*-bis-(trimethylsilyl)-trifluoroacetamide (BSTFA) are used instead of TMCS and HDMS [36-39].

To prepare acetyl derivatives, a carboxylic acid itself does not react spontaneously with hydroxyls which are the major reason for poor volatility of carbohydrates. A reactive acid derivative in a proper solvent is required to achieve a fast and quantitative esterification under mild conditions to avoid any side reaction. The acetyl or trifluoroacetyl derivatives are prepared with either acetic anhydride or trifuoroacetic anhydride and pyridine or sodium acetate as base catalyst at elevated temperature [32].

Usually anomeric carbon of resulting aldoses is reduced to avoid multiple peaks for each carbohydrate. Reduction with $NaBD_4$, to produce corresponding alditol is done under alkaline conditions [40, 41]. To avoid loss of information on ring size reductive cleavage may can be used after permethylation instead of hydrolysis and reduction.

ECR Concept

Partially derivatized alditols are normally used for quantitative determination of the glycosidic linkage-isomers present in unknown polysaccharide after integration of peak areas of GLC peaks. In former times, molar response factor of the compounds under investigation was used for this purpose. It was assumed that a given weight of any organic compound will give the same peak area as the same weight of a similar organic compound [42]. The alternative to this approach is to isolate and purify each derivative and calculate each response factor, which is a very long and laborious work. Another method to calculate relative response without actually measuring each derivative is the Effective Carbon Response (ECR) concept. The ECR concept is based on empirical rules reported by Addison and Ackman[43]. It is assumed that each type of carbon atom e.g. hydrocarbon, carbonyl, ether, ester etc. contribute to the response in the flame ionization detector to the same extent in all compounds, regardless of the structure of the basic compound. The total response factor was then calculated by summing all the contributions of the different types of the carbon atoms present in the molecule. This approach is especially useful for homologous series or structurally related compounds [43]. Sweet *et al*. [42] compared ECR theory with equal molar response and equal weight response and confirmed the validity and superiority of ECR theory by applying it for quantitative analysis of partially methylated and partially ethylated alditol acetates. In this method, each carbon has 100 basic points and then total ECR value was calculated by making corrections according to the functional group in which carbon resides (Table 1.3). Thus:

$$ECR = \Sigma C \times 100 - \Sigma(\textit{correction value for each functional group})$$

Correction values for different functional groups are calculated according to Table 1.3.

Table 1.3: Calculation of correction value for different functional groups and increment value for ECR

Functional group	Formula	Correction value	Increment in ECR
Ether	C-O-C	-100	100
Prim. alcohol	CH_2OH	-45	55
Sec. alcohol	CHOH	-55	45
Ester of prim. alcohol	CH_2-OC(O)-C	-145	155
Ester of sec. alcohol	CH-OC(O)-C	-155	145
Double bond	C=C	-10	190
O-TMS	CH-O-Si$(CH_3)_3$	-25	375

1.2.2 Substitution Pattern in Polysaccharide Derivatives

The physical and biological functions of polysaccharide derivatives, e.g. methyl, hydroxyethyl or sulfate derivatives, of glucans are greatly affected by the distribution of their substituents. Position of substituent in the glucose unit is very important especially for properties where molecular recognition is involved e.g. for cellulose sulfate as heparinoidic materials. The distribution of substituent along the chain strongly influence the physiochemical properties e.g. solubility, gelation and retrogredation [30, 44]. For example, substituents preventing crystallization, or ionic substituents inducing water solubility would probably be most effective if evenly distributed while the formation of junction zones in gelation processes requires the cooperation of closely related hydrophobic or polar groups since single hydrogen bonds, electrostatic or hydrophobic interactions are too weak for stable network formation. A well known example is alginate, consisting of β-D-mannuronic acid and α-L-guluronic acids, where sequences of the latter are responsible for calcium-induced network formation. Distribution of substituents in the polysaccharide chain can be analyzed by different methods after partial degradation e.g. selective partial degradation using enzymes [45, 46], or after random chemical degradation [44, 47]. A random distribution of substituents in the monomer unit can be described by Spurlin model.

Spurlin model

Polysaccharide derivatives are prepared by polymer analogous reactions from preformed polymer chains. For statistical evaluation about distribution of substituents, Spurlin [48] made some useful calculations. Spurlin considered the glucose unit as individual constituent of cellulose and made calculations on the basis of the following assumptions.

- Cellulose chain is long enough to neglect end groups.
- Ratio of reactivities of the three types of hydroxyl groups (k_2, k_3, k_6 for the 1→4 linked cellulose) is independent of the average DS or of the state of substitution of neighbor hydroxyl groups i.e. $k_2:k_3:k_6$ remains constant during the course of the reaction.

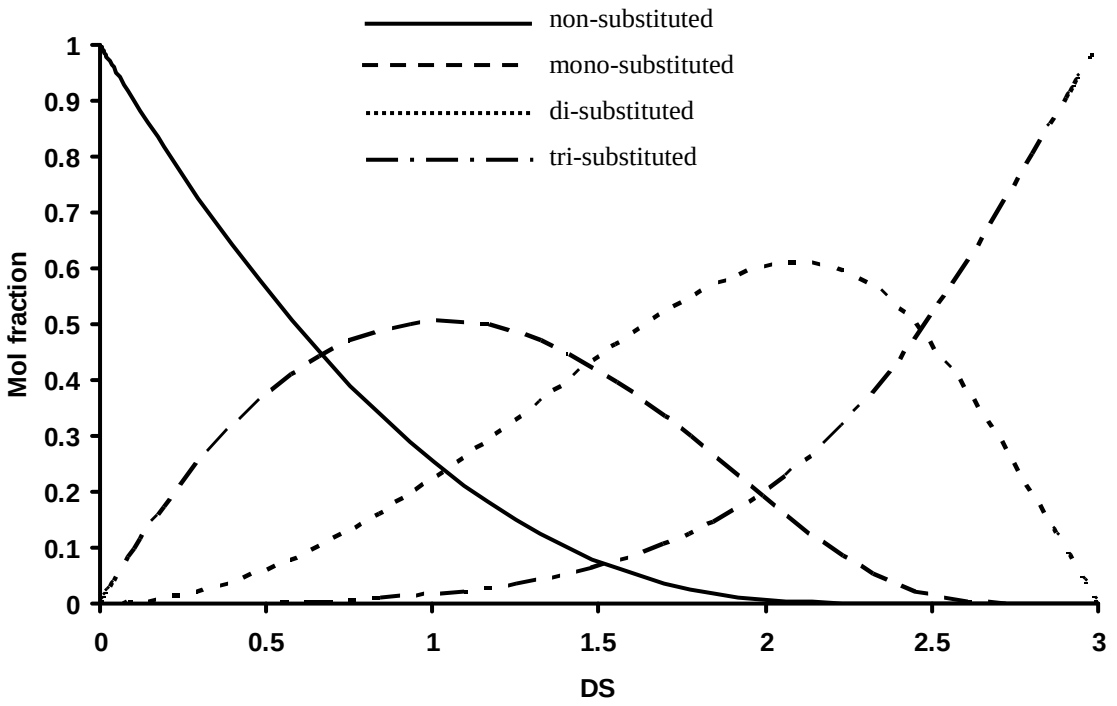

Fig. 1.4: Spurlin model diagram for statistical distribution of substituents (glucose in cellulose) at rate constants k_2: 1, k_3: 0.5, k_6: 0.67 (adopted from [49])

Reuben and Casti [50, 51] refined the Spurlin model and included the interaction of two secondary OH-2 and OH-3 hydroxyls due to their vicinity as a conditional probability. The ratio of rate constants for OH-3 k_3 (free *O*-2) and k_3' (substituted *O*-2) indicates the enhancement or decrease of *O*-3 reactivity by *O*-2 substitution.

2 DEXTRAN

2.1 Introduction

A large number of different polysaccharides from plant or bacterial sources exist. Cellulose and starch are the main polysaccharides in plants. They have been used as raw materials for chemical modification reactions since mid of the 19th century. Other glucans are produced by different fungi and bacteria e.g. curdlan, scleroglucan, schizophyllan and pullulan [52]. However, the most important polysaccharide for medical and industrial applications produced by various bacterial strains is dextran [53]. Currently, more than 1000 publications about dextran are appearing annually [17].

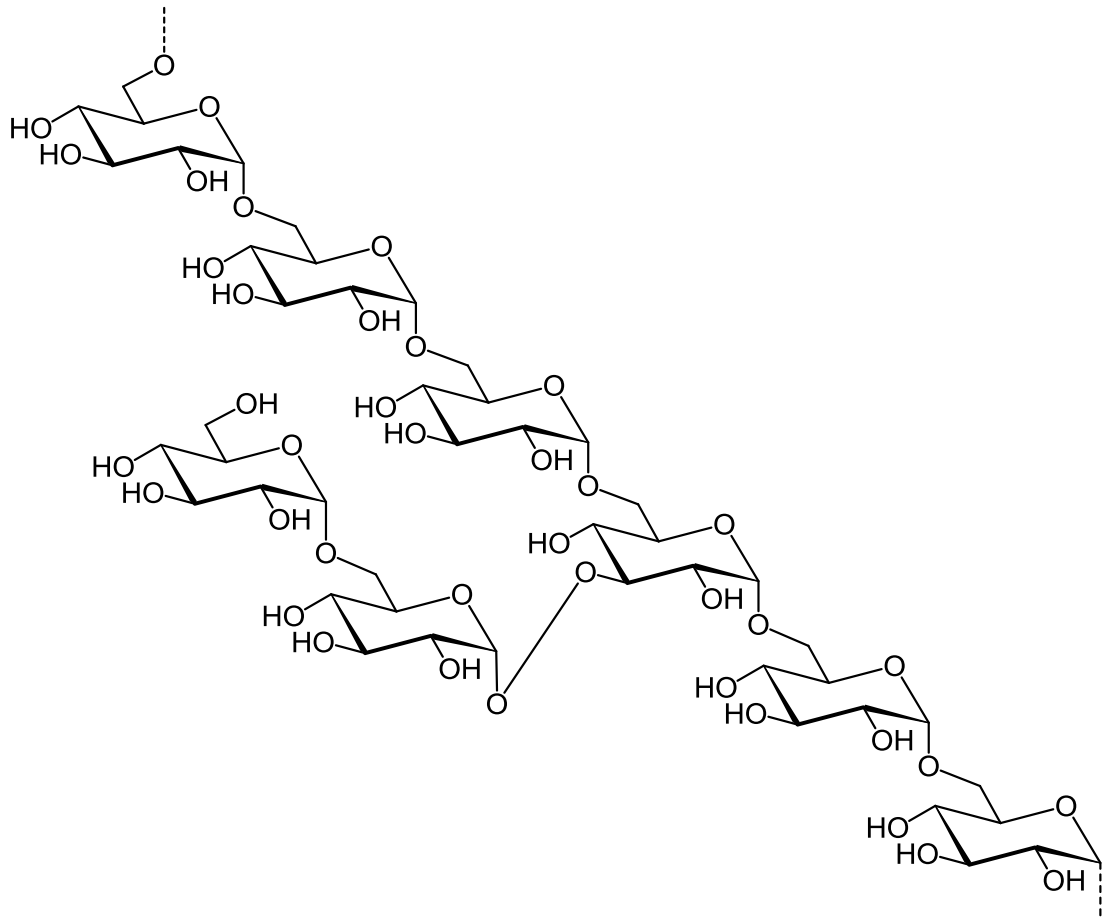

Fig. 2.1: $\alpha-(1\rightarrow 6)$ main chain of dextran with branching at $\alpha-(1\rightarrow 3)$

Dextran is a collective name of a large class of neutral polysaccharides composed exclusively of D-glucose units with varying proportions of linkages and branches [52, 54]. Up to 97% of polymer chains have α-(1→6) linkages. These α-D-glucans also posses α-(1→2), α-(1→3), and α-(1→4)-linkages usually linked as branches. The degree of branching is often about 5% and depends upon the temperature at which dextran was synthesized and on its molecular weight [55]. The distinct structure of each type of dextran depends on its specific microbial strain of origin [15, 53]. *Leuconcostoc mesenteroides* NRRL B-512 (F), and *Leuconostoc dextranicum* which are members of *Lactobacillaceae* family are used commercially. *Lactobacillus confusus* (BP 2865) is also rarely used for dextran production [56, 57].

About more than 500 metric tons of clinical dextran is produced annually [17]. Major dextran producers employ a batchwise process of *Leuconostoc* in the presence of sucrose. The dextran is then precipitated with ethanol or methanol from the visous culture broth. Fractionation of native dextran after hydrolysis in dilute acid gives dextran of desired molecular weight [17].

2.2 History

In 1861, Pasteur found lime-producing bacteria, which in 1878 were named *Leuconostoc mesenteroides* by van Tieghem [58, 59]. The segregated carbohydrate was named "dextran" by Scheibler.

Slime forming properties of filtered extracts of *Bacillus mesentericus* were first observed in 1910 by Beijerinck [60]. Subsequent investigations have shown that dextran can be formed by several gram-positive bacterial strains, facultatively anaerobic e.g. *Leuconostoc* and *Streptococcus* strains [55] but more solid prove of the dextran synthesizing activity of the *Leuconostoc* extracts were provided by Hehre *et al*. in 1939 and 1941 [61, 62]. Meanwhile, Allene Jeanes was conducting studies on dextran at Northern Regional Research Laboratory (NRRL) Peoria USA. During these studies, Benedict observed that a strain of *Leuconostoc mesenteroides* isolated from an infected root beer bottle was a vigorous dextran producer and its dextran was only slightly branched. This strain of bacteria was designated as NRRL-512. In 1948, Haynes isolated substrain NRRL-512(B) from original B-512 by selecting colonies with vigorous growth characteristics [17].

2.3 Branching

The dextran produced by *Leuconostoc mesenteroides* NRRL B-512 consists of an α-(1→6)-linked glucan with side chains attached to the 3-positions of the backbone glucosyl units. Still there is a lack of knowledge about branching activities of dextran sucrase due to incomplete knowledge of branching in native dextran [17]. Wales *et al*. [63] proposed a comb type structure for B-512 dextran. However, this model was criticized and discarded by Senti *et al*. [64]. Ebert and his colleagues [65] proposed a hypothesis for branching in which a free dextran molecule acts as an acceptor to release dextran from dextran-dextransucrase complex to form a branch linkage. They tested their hypothesis by adding a labeled low molecular weight dextran to an actively synthesizing system containing sucrose and found that labeled low molecular weight dextran incorporated into a higher molecular weight dextran. Their experiments, however, did not lead to conclusive evidence that the branching reaction occurs by an acceptor reaction with acceptor dextran because their experiments were conducted in the presence of sucrose and an actively biosynthesizing system. The incorporation of low molecular weight dextran could thus have occurred if the labeled acceptor dextran was acting as a primer to which glucose units from sucrose were added at the non-reducing ends to give a labeled product of higher molecular weight. Furthermore, they did not show that the acceptor dextran carried a newly formed branch linkage.

Robyt and Taniguchi [66] investigated the branching mechanism by treating acceptor dextran with labeled dextran sucrase in the absence of sucrose, and results show that acceptor dextran releases ^{14}C-labeled dextran from a labeled system. Results from acetolysis, reduction and acid hydrolysis confirmed that the produced dextran has a newly synthesized α-(1→3) branch linkage that was formed from the interaction of the acceptor dextran with the enzyme-dextranosyl complex. Based on these studies, their proposed mechanism is shown in Fig. 2.2.

Degree of branching is estimated as about 5% from periodate oxidation [67, 68] and methylation studies [69, 70]. It is found that degree of branching decreases on partial acid hydrolysis, although effect is not so dramatic [70]. The reason for this decrease is greater lability of α-(1→3) linkages towards acids as compared to α-(1→6) linkages [71], but after using less sensitive techniques, Bremner [72] did not find any difference in branching between native dextran and $\overline{M}_w$ 3000. Other researchers find

it from 4.8 to 5.5% by using NMR spectroscopy depending upon the integrating techniques used [17]. Larm *et al*. [73] have investigated the length of side chain by sequential degradation, in which non-reducing end groups were quantitatively eliminated and concluded that 40% of the side chains are one unit long, 45% consists of two units and remaining 15% are longer than two units. By using *endo*-dextranase, Covacevich and Richards analyzed the distribution of oligosaccharides from the hydrolysate and concluded that branches in the dextran were distributed (relatively) in a random manner and were not clustered. Kuge *et al*. [74] also investigated branching using dextrans of different molecular weight. He concluded that dextrans with $\overline{M}_w$ $<10^5$ have very low content of long branches and can be considered as linear polymer, but in general, some 5% of the residues in the dextran are branched, and the overall degree of branching does not depend upon molecular weight, however, long chain content changes with molecular weight. According to Senti *et al*. [64] long chain branches in dextran could be further branched indistinguishable from the main chain and considered dextran as a randomly branched polymer. Due to long-chain branching, dextran has a higher density and of hyper branched character.

Until now, all attempts to separate the enzyme responsible for branching have failed. Strong binding of dextran on the enzyme complicates the purification process.

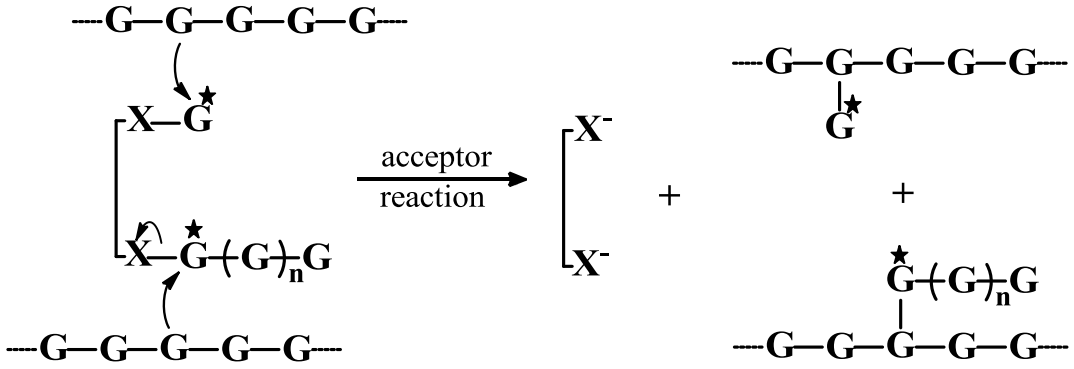

Fig. 2.2: Mechanism for the formation of branches in dextran B-512 (F). The sequence --G-G--- represents part of a dextran chain, -X-G-G--- is newly growing chain, ★ is ^{14}C label, -X- is dextran producing enzyme (adopted from Robyt *et al*. [75])

2.4 Physical Properties

Dextran NRRL B-512(F) is readily soluble in water, dimethyl sulfoxide, methyl sulfoxide, formamide, ethylene glycol, glycerol, *N*-methylmorpholine-*N*-oxide, and

hexamethylphosphoramide. Some dextran fractions may require some heating to bring them into solution due to formation of certain degree of crystallinity [17].

^{1}H-NMR of dextran in DMSO-d_6 is shown in Fig. 2.3. In addition to the ring protons, the protons of the hydroxyl groups are also visible at 4.48 ppm (OH-2), 4.84 ppm (OH-3) and 4.92 ppm (OH-4) [52, 76]. Some little peaks at 5.17 ppm are due to resonance from the reducing end anomeric protons [77]. It was not possible to assign peaks for H-2 to H-6(a/b) due to peak broadening and overlapping.

Table 2.1: ^{13}C and ^{1}H chemical shifts measured for dextran (M_w 500 000) in DMSO-d_6 (see Fig. 2.3)

	^{13}C [ppm]	^{1}H [ppm]
H-1	98.25	4.69
H-2	71.89	3.11-3.80
H-3	73.38	
H-4	70.16	
H-5	70.41	
H-6$_{(a/b)}$	66.12	
H_2O		3.40 (in DMSO-d_6 otherwise at 4.8 ppm [78])
DMSO		2.52

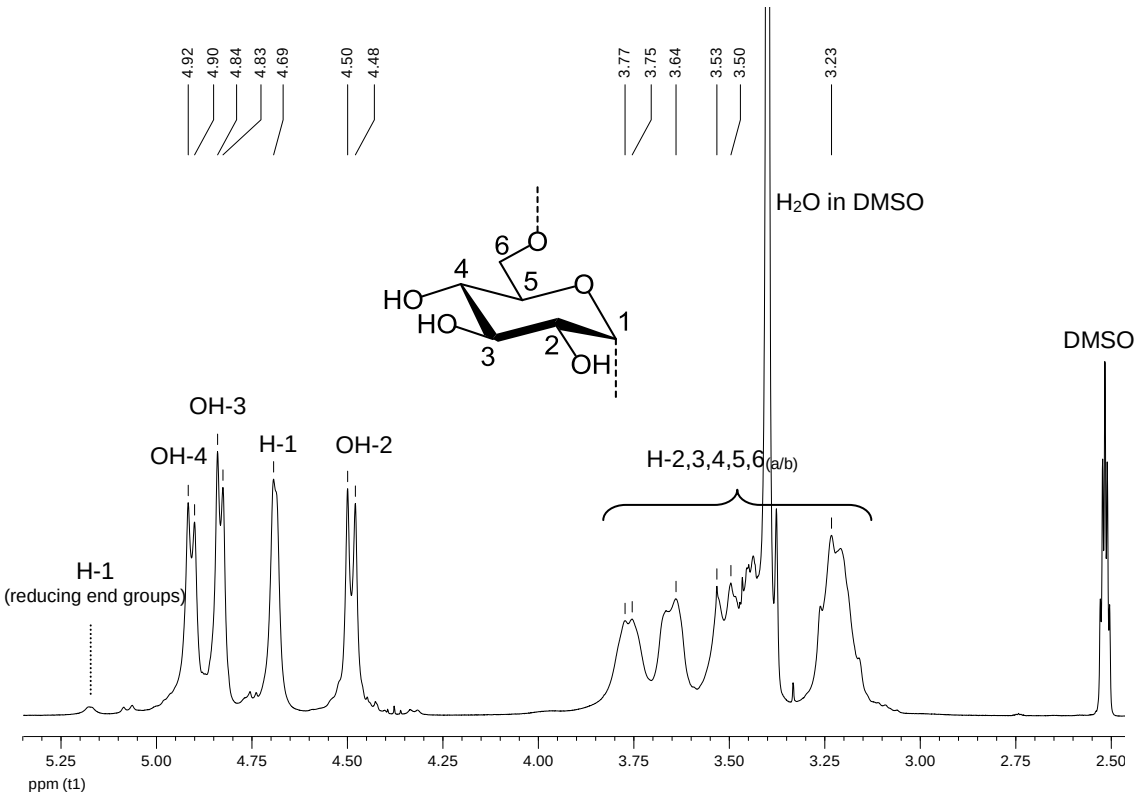

Fig. 2.3: ^{1}H-NMR (400 MHz, DMSO-d_6) spectrum of dextran from *Leuconostoc sp.* ($\overline{M}_W$ 500 000)

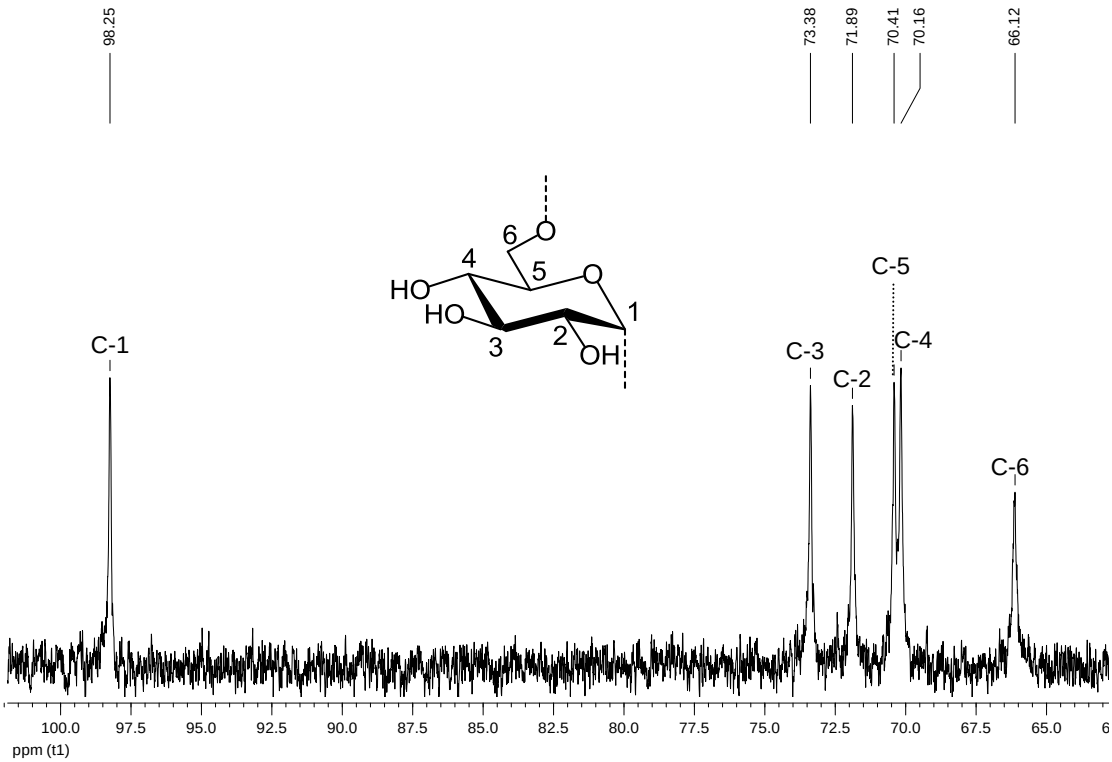

Fig. 2.4: ^{13}C-NMR (400 MHz, DMSO-d_6) spectrum of dextran from *Leuconostoc sp.*($\overline{M}_w$ 500 000)

The molecular-weight dependence of the diffusion coefficient and relation between radii of gyration and the hydrodynamic radii prove that dextran molecules behaves as random coil in aqueous solution. Comparison of the results from different sources show that dextran molecules are more compact than ideal random coils due to polymer branching in dextran molecules [79]. Roland-Sabate *et al*. have investigated structural properties of dextran and concluded that dextrans are mostly linear polymers with short and long chain branches and act like a linear coil [80].In the oligosaccharide range ($M_w < 2000$), the solution properties are best explained by a transition from a coil to a rod like conformation. The behavior of dextran coils also depends upon solvent i.e. dextran coils are more compact in poor solvents e.g. ethylene glycol and expand considerably in good solvents e.g. dimethyl sulfoxide. On the other hands it also depends upon molecular weight, i.e. radius of gyration increases as molecular weight increases. The solution properties indicate that dextran molecules with $M_w > 10^5$ behave as if they were highly branched [17].

2.5 Reactivity

The reactivity of the dextran depends upon the relative reactivities of equatorially oriented secondary hydroxyl groups, HO-2, HO-3 and HO-4. As with other glucans, the reactivity at HO-2 towards alkylating agent is higher than HO-3 and HO-4 due to higher acidity because of its proximity to the anomeric center. Spurlin [48] has shown how the relative rate constants for etherification in homogeneous reaction can be calculated from the partial DS values x_i.

In dextran, along with three adjacent hydroxyl groups in each glucose unit, the branching, which means that instead of equal numbers of 2-, 3- and 4-OH, there are about 5% less 3- and instead about 5% 6-OH. This also means that end-groups cannot be neglected anymore and should be considered for statistical comparison. Due to these factors, calculations for dextran are more complex than for cellulose. Substitution at OH-3 may not only change the reactivity at OH-2 but also at OH-4; conversely, substitution at OH-4 and OH-2 individually and combined may effect the reactivity at OH-3. Thus five additional rate constants should be considered besides those prevailing at OH-2, OH-3 and OH-4 in unsubstituted dextran [81] (Fig. 2.5).

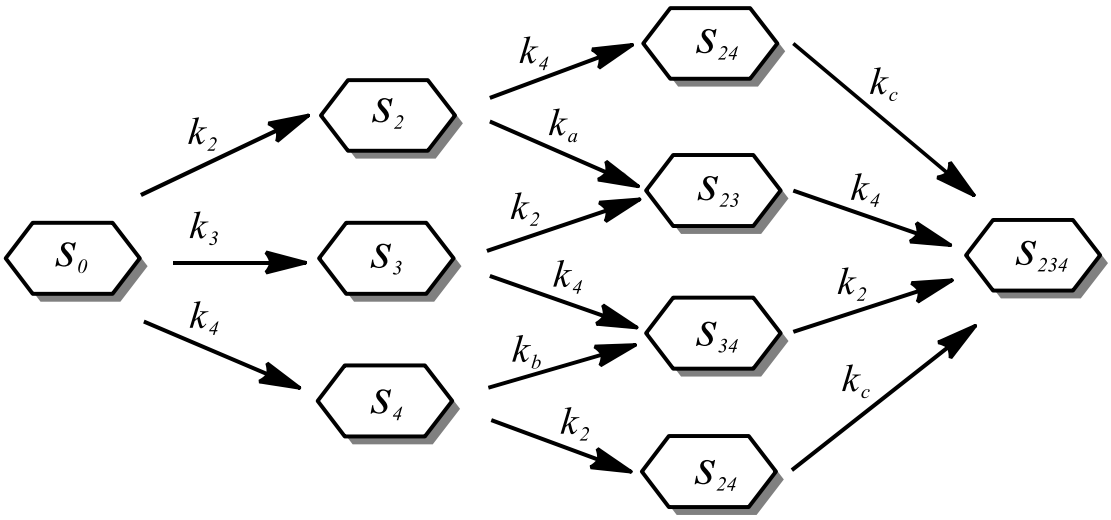

k_a= The rate constant at position 3 when position 2 is methylated
k_b= The rate constant at position 3 when position 4 is methylated
k_c= The rate constant at position 3 when position 2 and 4 are methylated

Fig. 2.5: Relative reactivities of hydroxyl groups of dextran (adopted from [81])

To make the calculations simple, Norrman [81] have assumed substitution at OH-3 not affecting the reactivity at OH-2, significantly. This assumption was based upon

the investigations of Caroon [82] and other researchers [83, 84]. Results for partially methylated dextran synthesized in methyl sulphate solution containing 19% NaOH show relative reactivities as $k_2:k_3:k_4$ = 8:1:3.5**.** Good agreement between calculated and experimental data was found when calculations were made for enhanced reactivity at HO-3 as a result of substitution at HO-2 and HO-4 [81].

2.6 Dextran Derivatives

A variety of dextran esters have been synthesized in last few decades e.g. with different chain length of carboxylic acid. Beside DS, the latter influences solubility. It was found that dextran esters of butanoic acid and hexanoic acid are water soluble with maximum DS values of 0.50 and 0.26 respectively [85]. Full protection of dextran derivatives e.g peracetylation or perpropionylation is an effective method for revealing structural features on the molecular level by NMR. The introduction of longer aliphatic acids was also achieved by acylation with the so-called impeller method. Dextran stearates and dextran myristates with DS 2.9 were prepared by treating dextran with corresponding acid in the presence of chloroacetic anhydride and $Mg(ClO_4)_2$ as catalyst [52].

Hydrogels prepared via homogeneous esterification of dextran with unsaturated carboxylic acids are advanced polysaccharide-based products useful for drug delivery systems and protective encapsulants, e.g. of viruses used in gene therapy [52]. Very promising in this regard is the dextran maleic acid mono ester [86], which can be obtained by conversion of dextran in DMF/LiCl with the maleic anhydride in the presence of tetraethylamonium (TEA) as a catalyst. DS of the products can be easily controlled by the amount of anhydride applied but is also influenced by temperature, amount of catalyst and reaction time. The dextran maleates are easily soluble in various common organic solvents such as DMSO, DMF, *N*-methyl-2-pyrrolidone (NMP) and DMA. The Hydrogels are manufactured by irradiation of dextran maleate with long-wave UV light (365 nm). The minimum DS required for proper UV cross-linking of the derivatives is 0.60. The hydrogels show a high swelling capacity (swelling ratio up to 15 fold at pH 7) depending on DS and the pH of the medium [86].

Dextran ethers are not so common as esters. Modification of dextran backbone by introduction of ether type moieties leads to comparatively stable dextran derivatives

with altered physiochemical properties. The solubility, hydrolytic-lipophilic balance, ionic strength and resistance against hydrolytic or enzymatic degradation have been tailored by etherification. Amphiphilic ethers have emulsifying properties and can form micelles in water usable as surfactants or for the encapsulation of hydrophobic materials e.g. drugs [52]. This approach has been used to synthesize biodegradable hydrogels. An appropriate chain length and chemical structure can control the drug release. An overview of common dextran ethers is given in Table 2.2.

Table 2.2: Examples of dextran ethers represented in the literature

Types of dextran ether	Functional group (R)	Reference
Methyl	$-CH_3$	[73, 81, 87, 88]
Ethyl	$-C_2H_5$	[73]
Benzyl	$-CH_2C_6H_5$	[89]
Trityl	$-C(C_6H_5)_3$	[73, 90, 91]
Trimethylsilyl	$-Si(CH_3)_3$	[92, 93]
Carboxymethyl	$-CH_2COOH$	[94, 95]
2-Mercaptoethyl	$-C_2H_4SH$	[96]
2-Cyanoethyl	$-C_2H_4CN$	[97]
2-Hydroxyethyl	$-C_2H_4OH$	[98]
2-Hydroxypropyl	$-CH_2CHOHCH_3$	[99]
2-Hydroxyalkyl	$-CH_2CHOH(CH_2)_nCH_3$	[100, 101]
(2-Hydroxy-3-phenoxy)propyl	$-CH_2CHOHCH_2OC_6H_5$	[102, 103]
(3-Chloro-2-hydroxy)propyl	$-CH_2CHOHCH_2Cl$	[104, 105]
2-Diethylaminoethyl	$-C_2H_4N(C_2H_5)_2$	[106, 107]
(3-Amino-2-hydroxy)propyl	$-CH_2CHOHCH_2NH_2$	[108]
(3-Dimethylalkylammonium-2-hydroxy)propyl	$-CH_2CHOHCH_2N^+(CH_3)_2R$	[109-112]
Polyethyleneglycol cetyl	$-(CH_2CH_2O)_{10}C_{16}H_{33}$	[113]
Polyethyleneglycol stearyl	$-(CH_2CH_2O)_{10}C_{18}H_{37}$	[113]

2.7 Important Applications of Dextrans

Many applications of dextrans in foods were patented in 1950's and 60's in USA but no application was pursued for mandatory toxicological studies. Therefore, in 1977 food and drug administration (FDA) USA deleted its GRAS (generally recognized as

safe) status. In Europe or UK, dextrans are not permitted as foodstuff additives but however, are considered as safe as components of food packaging materials [17]. One of the main reasons for less applications of dextran is its relatively high price as compared to most of the starch and cellulose based products. Dextrans most likely find applications in pharmaceuticals and in high quality and high technology products in other fields.

Clinical grade dextran with $\overline{M}_w$ of 40 000, 60 000, 70 000 $gmol^{-1}$ (designated as dextran 40, 60 and 70, respectively) in 6 or 10% aqueous solutions are used for replacing moderate blood losses [17] by substituting blood proteins, e.g. albumins, manufactured under various commercial names in different countries e.g. Polyglucin®, Dextran, Macrodex, Expandax, Intradex and Dextraven etc. [114]. Dextran 40 especially improves the blood flow by reducing the blood viscosity and by inhibiting erythrocyte aggregation.

Amino dextrans and carboxymethyl dextrans are used for the surface functionalization of biosensors. In the same way, dextran ethers are commonly used in drug delivery systems [115, 116]. Hydrogels synthesized by esterification of dextran with unsaturated carboxylic acids or by reaction of biopolymers with bifunctional reagents e.g. diisocyanates and phosphorus oxychloride or by acylation with methacrylate groups and subsequent UV irradiation [117-119] are used as drug carrier in site specific drug delivery systems or in control release of drugs.

Dextran is used as cryoprotective agent for human, animal and plant cells [120, 121]. A mixture of 5% methyl sulphoxide and 9% dextran 70 was found to afford optimal cryoprotection of human bone marrow committed stem cells [17]. Dextrans can be used as adjuvant for prolonging local anesthesia, and prolongation of anesthetic effect up to more than three fold is observed depending upon the M_w of dextran, the type of dextran derivative and compound used for anesthesia but results are somehow a matter of debate.

Dextran sulfates have shown anticoagulant activity, cationic spermine-dextran conjugates have been tested as vectors for gene transfection [122]. Mann *et al*. prepared termini-labeled aminopropyl dextrans for target drug release [123]. Amphiphilic dextrans [102, 124] have also been applied for nanoparticle coating and as drug carrier system in emulsion polymerization [125] and for direct nanoparticle formation [126]. Heinze *et al*. have modified dextrans into a wide range of ester

derivatives which form nanoparticles by dialysis from DMAc solution against water [127-129].

2-Phase polymers systems, especially dextran-PEG systems are used for the partition of sub-cellular particles and macromolecules e.g. separation of enzymes for example pullulanase from *Klebsiella pneumoniae cells*. Fractions of dextran with narrow molecular weight distribution are used as size exclusion chromatography (SEC) standards [52]. Cross-linking can be achieved by physical interactions and chemical reactions. Concentrated solutions of dextran with low M_w (6 000 $gmol^{-1}$) form hydrogels by crystallization [130].

Sephadex® is formed by cross-linking of dextran with epichlorohydrin [52]. A variety of Sephadex® products have been prepared in last decades for use in different separation techniques. The most porous gel, Sephadex® G-25 can fractionate proteins in the molecular weight range 4000-800000. Sephadex® gels are frequently used for fractionation and purification of biopolymers. Sephadex® G-25 is used for desalting or buffer exchange in large scale operations. Insulin producers use Sephadex® G-50 to remove proinsulin and protease impurities in the final stage of purification of porcine or bovine insulins. These gels are commercially used for fractionation of plasma proteins, specially in human serum albumin, blood clotting factors etc. [17]. Another matrix for separation of macromolecules is Sephacryl® formed by cross-linking of allyl dextran by *N*,*N´*-methylene bisacrylamide [131].

Purified dextran fractions with high clarity and low chloride level are used in the photographic industry. Additions of low concentrations of dextran to the silver emulsion are found to enhance the quality of the images significantly [17].

3 ALKYLATION OF CARBOHYDRATES

Among alkylation reactions, methylation is of special importance for structural analysis of carbohydrates [132]. Over 100 years have passed since the first *O*-methylated sugar was prepared [133]. Methyl ethers of sugars have proved being valuable derivatives in the elucidation of carbohydrate structures because of their stability towards acids and alkali [134]. In the early fifties, Hodge *et al*. [135] applied methylation and ethylation reactions with sodium and methyl iodide in liquid ammonia for structure analysis of polysaccharides. The alkylation of polysaccharides e.g. dextran can be applied to investigate the interglycosidic linkages e.g. the branching pattern, i.e. the number and length of side chains in polysaccharides [52].

The most common method for methylation of polysaccharides has involved the use of methylsulfinyl carbanion in DMSO, introduced by Hakomori [136] as alkoxide-forming reagent and is used almost universally [137]. This reagent is freshly prepared by treatment of dry DMSO with sodium or potassium hydride [138]. However, this method has some disadvantages [139], e.g. the preparation of sodium methylsulfinyl methanide in methyl sulfoxide is troublesome and the reagent is not stable. Moreover, polysaccharides often resist complete alkylation in one step; repetition of methylation can cause severe depolymerization.

A direct method for alkoxide formation in sugars using solid base e.g. NaOH, KOH in DMSO is reported by Ciucanu *et al*. [140]. The other bases used for this purpose are metal hydrides e.g. KH, NaH, Potassium tert-butoxide [139], metal oxides e.g. Ag_2O and deprotonated DMSO e.g. Na-dimsyl, which will be discussed in Chapter 3.3.

An overview of different systems for alkylation is given in the following.

3.1 Solid Alkali Hydroxide as Basic Reagent in Aprotic Solvents

NaOH was the first solid base used for *O*-methylation of carbohydrates with dimethyl sulfate in 1956 [141]. THF was used as solvent in this experiment. THF is aprotic but no solvent for carbohydrates. So in this completely heterogeneous experiment, carbohydrates were only partially methylated. The polar aprotic solvents such as DMF, DMAc, and DMSO are good solvents for carbohydrates and also for their methylated derivatives. Later on in 1958, $Ba(OH)_2$ in DMF was used for *O*-methylation of carbohydrates with methyl iodide which in one step gave good yield

of per-*O*-methylated product [140]. This method was modified by using DMSO instead of DMF as solvent while methyl iodide was replaced by dimethyl sulfate. Some other researchers have used NaOH or KOH with DMSO and dimethyl sulfate. The method uses a fine powdered NaOH or KOH in DMSO, DMF or DMAc [142, 143]. The active base in deprotonation of carbohydrate hydroxyl group is OH^- ion. The solid NaOH is sparingly soluble in DMSO, but it is very hygroscopic and can absorb water produced in the deprotonation equilibrium reaction. This is one of the important properties of solid NaOH.

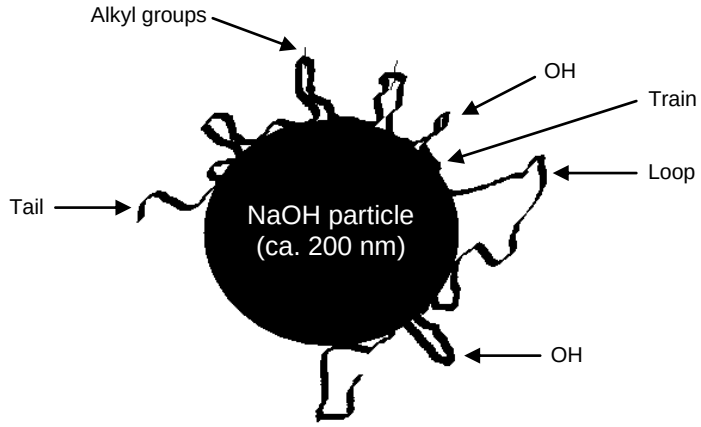

Fig. 3.1: Alkoxide formation of polysaccharides with solid NaOH in aprotic solvent [44]

Using optimal proportions of methyl iodide and powdered NaOH, the method gives high yields in one step within minutes at room temperature for small carbohydrates and without formation of side product [140]. Moreover, the method works without special care and no need to avoid exposure to air and moisture, but rate of reaction also depends upon the size of NaOH particles, i.e. particles with larger size will have less surface area and vice versa. Polymer chain will cover the NaOH particle on the surface forming trains, loops and free tails (Fig. 3.1). In such situation, it is not possible for all OH groups to have contact with NaOH particle, resultantly all OH would not have equal chances for alcoholate ion formation. In such situation, it will effect not only final DS but heterogeneity of the product will also be increased. Moreover, in case of alkali sensitive reagents permanent presence of base can enhance side product formation. But all these drawbacks can be minimized by using very fine particles of NaOH. The speed and simplicity of this technique prompted its application in the methylation of simple carbohydrates, oligosaccharides, polyalcohols, and hydroxy fatty acids etc.

3.2 Alkali Hydride as Basic Agent in Aprotic Solvents

In 1962, the per-*O*-methylation of two sugars with NaH in THF was reported [144]. Later on THF was replaced by DMF, DMAc, and DMSO [145-147] and *O*-methylation was completed in one step.

NaH is a very strong base and can even be used for *O*-methylation of sterically hindered hydroxyl groups. Using NaH as a base, the basic agent is the H^- ion. However, due to the contact with moisture during handling, small portions will be transformed into NaOH. So OH^- ion may also be present. NaH will alsoconvertDMSO into $CH_3SOCH_2^-Na^+$.

3.3 Dimsyl Anion as Basic Agent

In 1964, Hakomori [136] used sodium dimsyl as basic agent for the methylation of glycolipds. The method has been applied extensively for carbohydrates analysis but final methylation products contain small amount of side products, which was difficult to separate and identify by gas chromatography. Analysis of these products by GC-MS indicates the presence of a small amount of methylated derivatives of DMSO. Dimsyl anion can also be prepared by other methods e.g. using KH instead of NaH. KH reacts with DMSO at room temperature in minutes and yields a pale yellow-green solution of potassium dimsyl. Dimsyl anion generated from KH has been reported to offer better methylation results than NaH [140].

Since 1985, the lithium salt of methylsulfinyl carbanion obtained by reaction of butyl lithium or methyl lithium with DMSO have shown superior performance compared with sodium or potassium salts [148, 149].

3.4 General Mechanism of Alkylation of Carbohydrates

O-Alkylation of carbohydrates is based on the substitution of the proton from carbohydrate hydroxyl with an alkyl group. The direct reaction of the carbohydrates with common alkylating agents e.g. alkyl halides or dimethyl sulfate is not possible, because OH is a weak nucleophile and no alkylated product was obtained by mixing these reagents [140]. The *O*-alkylation mechanism for carbohydrates relies upon a two-step reaction (Fig. 3.2). The first step is base-promoted deprotonation of the

alcoholic OH to alcoholate (step 1). In the second step, the nucleophilic anion attacks an alkylating reagent (RX) (step 2). The second step usually is irreversible and this Williamson etherification is kinetically controlled. Order of reactivity is glycosidic (hemiacetal) > primary > secondary OH. By the electron withdrawing effect of the anomeric center, the acidity of the neighboring 2-OH is usually enhanced, thus being more reactive than the primary OH at low base concentration.

Step 1 is an equilibrium process, which depends upon the strength and concentration of the base, the reactivity of the carbohydrate hydroxyl groups, the reaction medium (solvent), and temperature.

The polar aprotic solvents are very good solvents for polarizable, neutral and ionic species. By increasing the polarity of the solvent, the rate of the reaction also increases. The polarity of these solvents follows the following order DMSO > DMAc ≈ DMF having dielectric constants 46.68, 37.78 and 37.00 respectively. The general mechanism of the reaction is:

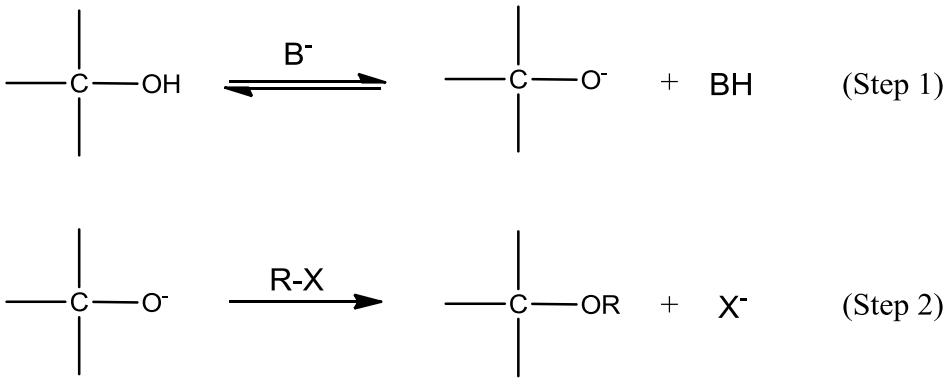

Overall reaction

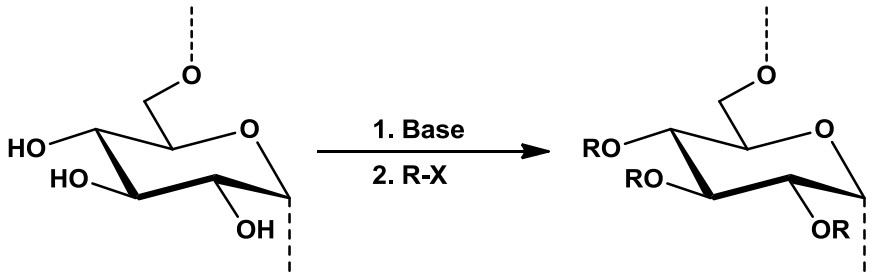

Fig. 3.2: General mechanism of alkylation of carbohydrates

4 ALKYNYL CHEMISTRY

Alkynyl ethers of polysaccharides are interesting products themselves, and also as intermediates to introduce a number of further functionalities. Tankam *et al*. [150] stated that the geometry of the acetylenic function corresponds to a rigid carbon rod with acidic hydrogen at the tip. Such alkynyl groups show many special properties, e.g. solvent-dependent self-association and a wide range of reactivities. Self-association depends on the ability of acetylenic groups to act as both, a hydrogen bond acceptor as well as donor. When linked to a polymeric backbone, supramolecular structures associated with cooperative effects and not only hydrophilic-hydrophobic balance can be expected.Combination of acetylenic and carbohydrate chemistry links a carbon rich, rod like hydrophobic reactive group with an oxygen rich, strictly stereoregular, hydrophilic polymer. By the reaction of alkynyl ethers of polysaccharides with base and electrophiles, a variety of derivatives having different functional groups e.g. alcohol, carboxylic acid, aldehyde etc. can be synthesized (Fig. 4.1).

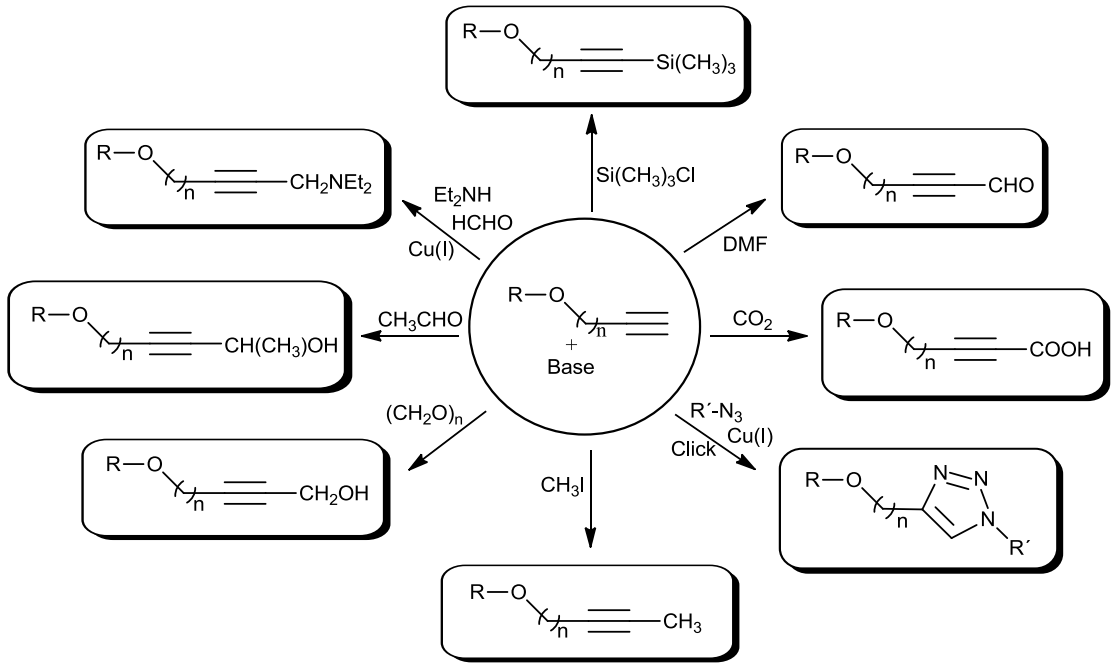

Fig. 4.1: Functionalyzation of alkynyl ethers of polysaccharides (adapted from Tankam *et al*. [150, 151])

Carbohydrates with acetylenic groups have been used and described by several authors, e.g. Belghiti *et al*. [152] Aversa *et al*. [153], or Bernet and Vasella [154]. *O*-Glycosyl compounds and *O*-alkynyl glycosides have since 1995 been the subject of a series of systematic studies of oligosaccharide analogues of polysaccharides by Vasella and co-workers [155-157]. Different researchers have synthesized propargyl ethers of cellulose in various ways [158-162]. Tankam *et al*. have demonstrated the concept of unsaturated polysaccharide ethers as reactive intermediates [150] with propargyl starches and methyl 2,3-di-*O*-propargyl glucosides as model compounds [151].

4.1 Click Chemistry

The Cu(I) catalysis of the well-known 1,3-dipolar cycloaddition reaction between azide and alkyne was discovered independently by the groups of Meldal [163, 164] and Sharpless [165] in 2002. In this cycloaddition reaction (Fig. 4.2), an organic azide reacts with an alkyne to form a triazole ring, similar to classical Huisgen cycloaddition reaction [166]. However, in the presence of Cu(I) the reaction proceeds faster even under ambient reaction conditions and only 1,4-disubstituted ring is formed in contrast to the classical Huisgen cycloaddition reaction in which 1,4- and 1,5-disubstituted triazole regioisomers are formed [167]. In order to get 1,5-disubstituted 1,2,3-triazoles from organic azide and alkyne, ruthenium(II) catalyst can be used as reported by Fokin and Jia [168]. The introduction of this concept has not only gradually but conceptually changed the way in which material design problems are approached [169]. In broad sense, "click chemistry" may be taken to denote a reaction that has the following attributes [170]:

- Quantitative
- Rapid
- Free of side reactions
- Regioselective
- Functional group tolerant
- Mild reaction conditions
- Broadly applicable

The idea of *facilitation* is the essence of the "click chemistry" [171] while simplicity lies at the core of the click concept. Likely the advantages of enhanced efficiency and specificity have allowed click methods to flourish so vibrantly. By means of the "click reaction" concept, large (bio)macromolecules can be synthesized by coupling small building blocks via heteroatom-containing linkages. Such a coupling reaction should meet several criteria: It should be modular, high-yielding and generate only harmless side products and it should be carried out under mild reaction conditions, preferentially in the presence of other functional groups using readily available starting materials and reagents [172].

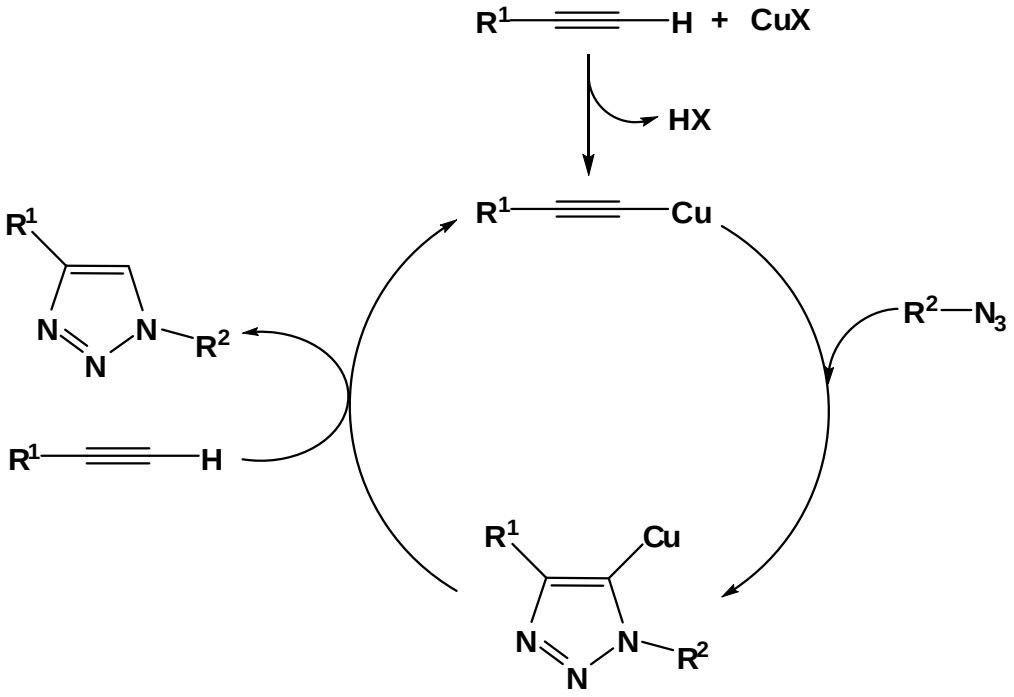

Fig. 4.2: Proposed mechanism for the formation of 1,2,3-triazoles [173]

Pahimanolis *et al*. [174] have prepared dextran-g-poly(ethylene glycol) by copper catalyzed azide-alkyne cycloaddition (CuAAC) reaction in aqueous media and at ambient temperature. In this reaction, epichlorohydrin was reacted with NaN_3 to synthesize 1-azido-2,3-epoxypropane which was etherified on to the backbone of dextran using base catalysts. In the second step, azide was clicked with alkyne-end-functionalyzed poly(ethylene glycol) monomethyl ether. Yeoh *et al*. [175] have reported the synthesis of 5-azidouridine which was clicked with a series of

α-propargyl glycosides in aqueous media to provide a series of natural uridine di-phosphate (UDP)-sugar analogues as potential glycosyl transferase inhibitor. Carbohydrates are involved in a number of biological processes such as cell-cell recognition and cell-protein interactions. Srinivasachari *et al*[176, 177] have clicked acetylated di-azido trehalose and dialkyne oligoethylamine to synthsise non-viral biopolymer based delivery vehicles for cellular delivery of plasmide DNA (pDNA).

Click reaction sometimes provide solutions to the problems which otherwise are very difficult to overcome in a traditional way. e.g., there is a great interest in using peptides as building blocks for the synthesis of peptide-based polymers for pharmaceutical applications. However, the synthesis of peptide-based polymers imposes several major synthetic challenges. CuAAC is a very suitable method because the formed 1,2,3-triazole moiety is a mimic of a native peptide bond [178, 179]. Due to disparate reactivity, some monomer combinations can not be employed to synthesize block copolymers e.g. styrene and vinyl acetate or ethylene. To overcome such a principal problem, it is conceivable that an efficient reaction links two separately prepared polymer chains [169]. Using this technique, Hest *et al*. [180] in 2005 prepared diblock copolymers of polystyrene, polymethylmethacrylate and polyethyleneglycol using Cu(I) catalyzed 1,3-dipolar cycloaddition between azides and acetylene units.

Multivalent ligands often bind much more strongly to the interacting proteins than their monovalent counterparts. Pieters *et al.*[181] developed a versatile microwave assisted CuAAC method to develop conjugation of azido carbohydrates with different kinds of alkyne-bearing dendrimers. These glycodendrimers can be used to increase affinities in different applications e.g. binding with bacteria, bacterial toxins and lectins. Nanoparticles have great potential in the biomedical and pharmaceutical fields as vehicles for drugs [182]. Caruso *et al*. [183, 184] developed a general approach for the synthesis of ultrathin polymer films on planar substrates for the preparation of pH-responsive nanocapsules from polyacrylicacid with either alkyne or azide functionalities. Tankam *et al*. [150, 151] have shown in model studies of methyl-4,6-*O*-propargyl-α-D-glucoside and starch that Mannich type amination and 1,3-dipolar cycloaddition of azides ("click reaction") are most appropriate for carbohydrates containing free –OH beside alkynyl residues (Fig. 4.3).

Advantegous is the tolerance of click reaction against many common functional groups. Hofren *et al*. [9] have modified cellulose in its native solid state (filter paper)

to a highly fluorescent material by click reaction without using any solvent or toxic catalysts.

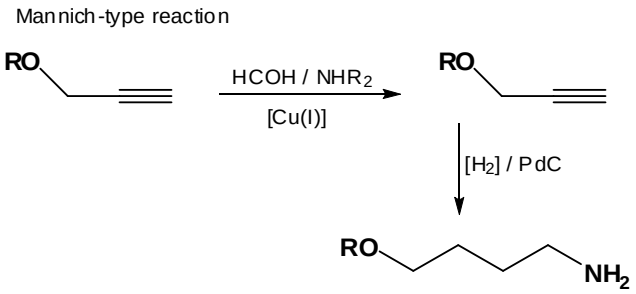

Fig. 4.3: Mannich-type ammination reaction (according to [150, 151])

5 SCOPE OF THE THESIS

Polysaccharide derivatives are of great interest due to their wide range of properties and applicability. Due to their biocompatibility, dextrans are widely used in bioanalysis and medical applications.Many publications can be found on the physiological activity of dextran and its derivatives or about their applications, but comparably few on detailed structure analysis of chemically modified dextrans. Therefore, in this research project dextran was selected for chemical modification.

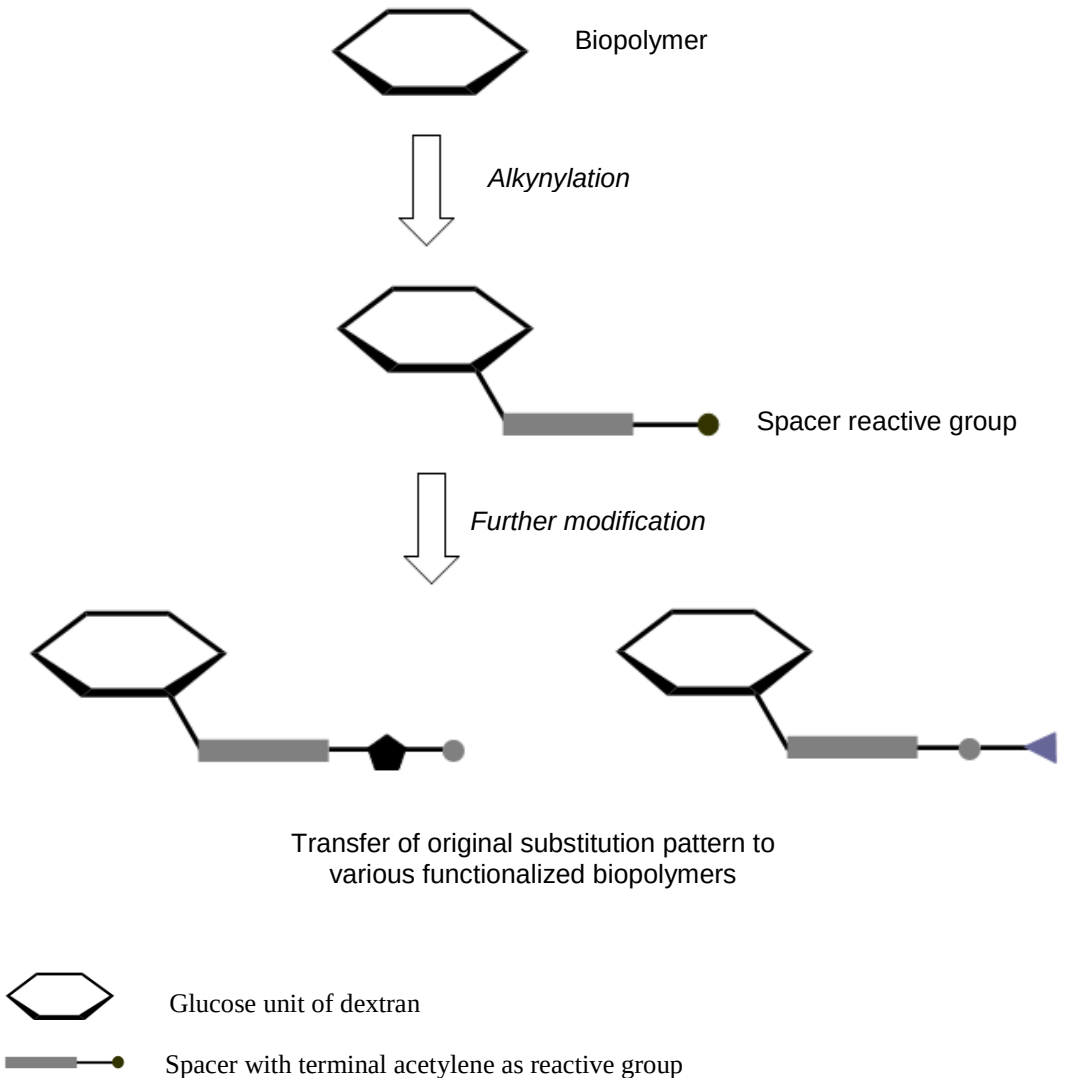

Scheme 5.1: Representation of the scope of the thesis

Alkynyl groups have been selected as primary substituent due to their special properties: the ability to act as hydrogen bonding donor as well as acceptor,

CH-acidity and partner for 1,3-diplar cycloaddition to azides, which allows the introduction of a wide range of functionalities or signal molecules in a second reaction step. Based on functional studies on propargyl starches, alkynyl ethers of dextran should be prepared.. The concept is summarized in Scheme 5.1.
Since properties of polysaccharide derivatives beside the chemistry of the substituents and the degree of substitution (DS) strongly depend upon the distribution of functional groups, analysis of the substitution pattern is also part of the project.

To summarize, the scope of the thesis comprises:

- Combination of two well developed fields of research i.e. modification of polysaccharides and acetylenic chemistry
- Synthesis of *O*-alkynyl dextrans under various conditions and with variation of alkynyl chain length
- Characterization of the products with respect to DS and substituent distribution
- Studying the properties of *O*-alkynyl dextrans
- Further modification of terminal alkynes by click reactions to introduce different functional groups and bioactive molecules
- Application tests of the follow-up products of *O*-alkynyl dextrans

6 ALKYNYL ETHERS OF DEXTRAN: SYNTHESIS AND ANALYSIS

Propargyl ethers of dextran were synthesized. Reaction conditions i.e. solvent, type and amount of base eq./OH of dextran were optimized. Products were characterized using different analytical techniques.

6.1 Propargyl Dextrans

6.1.1 Synthesis of Propargyl Dextrans

In the master thesis [185], preceding this work, propargyl ethers of dextran had been prepared. In these studies, dextran was dissolved in DMSO and reacted with various bases and propargyl bromide (PgBr, or PgCl). Products are designated as PgD and are listed in Table 6.1.

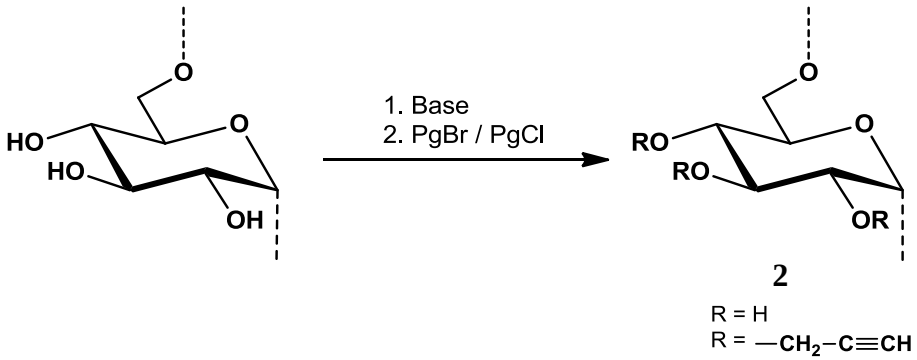

Scheme 6.1: Synthesis of propargyl dextran (PgD)

In most cases, it was observed that during dialysis against water a part of the product was precipitated while leaving rest in the form of fine suspension in water. To look whether these two portions differ from each other, they were separated in case of PgD-15 (Table 6.1) and analyzed separately [185].

6.1.2 Characterization of Propargyl Dextrans

Characterization of PgDs was carried out by ATR-IR spectroscopy, elemental analysis (EA), and monomer analysis by GLC after hydrolysis and acetylation. Details and results are given in [185]. It was observed that while the amount of base

was increased linearly for all three series of PgDs, in contrast to the usually observed decreasing reaction efficiency with increasing amount of reagents, here it first increased, but strongly decreased again, when excess of base was applied(Table 6.1). This behavior indicates that there might be some side reaction running which is consuming extra propargyl halide and favored by an excess of base. Tankam *et al*. [151] have observed the same phenomenon with relatively higher DS for *O*-propargyl starches.

Table 6.1: Synthesis of PgD using various bases and PgBr

Sample	Base	Base eq./OH	DS_{GC}	PgBr eq./OH
PgD-1	Li-dimsyl	0.50	0.76	2.0
PgD-2		0.75	1.47	2.0
PgD-3		1.00	1.66	2.0
PgD-4		1.25	1.67	2.0
PgD-5		1.50	1.66	2.0
PgD-6	NaOH	0.50	0.14	2.0
PgD-7		0.75	0.26	2.0
PgD-8		1.00	0.61	2.0
PgD-9		1.25	0.62	2.0
PgD-10		1.50	0.64	2.0
PgD-11	NaH	0.50	0.47	2.0
PgD-12		0.75	0.77	2.0
PgD-13		1.00	0.57	2.0
PgD-14		1.25	0.69	2.0
PgD-15a		1.50	0.78	2.0
PgD-15b			0.99	

Dextran (M_w: 500 000) in DMSO was used in all reactions
PgD 15-a: Part of PgD not precipitated during dialysis against water
PgD 15-b: Part of PgD precipitated during dialysis against water

Elemental analysis of some selected PgDs (Table 6.2) show a reasonable amount of S, which increases with the amount of base applied, indicates that DMSO is involved in the side reaction. At the same time, the amount of C also increases, giving apparently to high DS values from EA.

Table 6.2: Elemental analysis of some selected PgD samples

Sample	C [%]	H [%]	S [%]	C/H	C/S	Base eq./OH	DS_{GC}	DS_{EA}
PgD-14	51.37	5.64	1.53	9.11	33.57	1.25	0.69	0.65
PgD-10	52.27	5.62	1.59	9.30	32.87	1.50	0.64	0.76
PgD-15b	59.93	5.46	2.88	10.97	20.81	1.50	0.99	(1.84)*

* cannot be evaluated due to side product impurity

6.1.2.1 Side Product formed in Propargyl Dextrans

In control reactions (Scheme 6.2), PgCl and Li-dimsyl were reacted in DMSO, and also without DMSO (Scheme 6.2, SP-3), without addition of sugar under identical conditions used for *O*-propargyl dextran synthesis including dialysis against water and freeze-drying.

Elemental analysis shows 10.86% sulfur content along with C, H and O in both cases where reaction was conducted in DMSO (Table 6.3, SP-1, SP-2). The formation of brown-black color in control reaction without DMSO (SP-3) shows that a side product is also formed from hydroxide and PgCl only, but in case of Li-dimsyl, this base is finally assembled in the side product. Tankam *et al*. [151] carried out a control reaction with NaOH and PgBr in DMSO. Brown flakes formed instantaneously, containing 5% sulfur, and after dialysis and freeze-drying showed *C≡C-H, C-H,* and *C=O* vibrations in the ATR-IR spectrum.

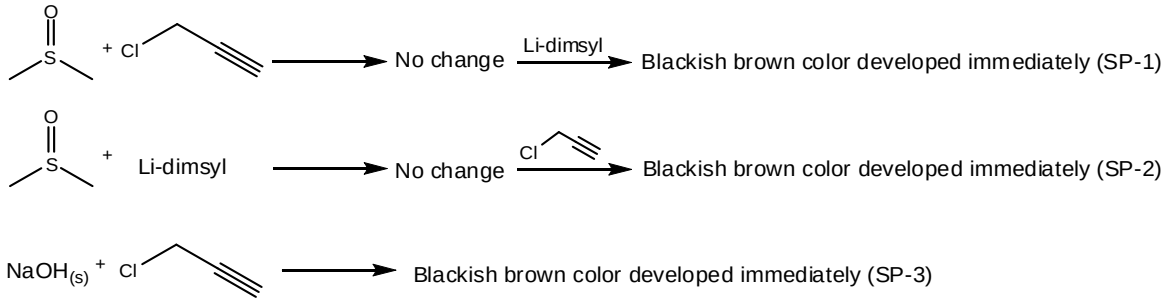

Scheme 6.2: Formation of side product in control reactions

Table 6.3: Elemental analysis of side products formed in control reactions

Sample	C [%]	H [%]	S [%]	C/H	C/S
SP-1	66.49	5.32	10.86	12.50	6.12
SP-2	66.69	5.13	10.86	13.00	6.14
SP-3	51.12	4.98		10.26	

From these experiments, it is obvious that side reaction occurs between base (dimsyl or hydroxide ion) and the alkynyl halide. Elemental analysis of SP-1 and SP-2 (Table 6.3) showed that formation and nature of side product did not depend upon order of addition of reagents. Product formed in control reactions (SP-1, SP-2, SP-3) were not soluble in any solvent.ATR-IR spectra of SP-2 and SP-3 (Fig. 6.2) show terminal alkyne and probably C=C absorption bands, while ether and carbonyl groups are only present if OH^- is used as base.

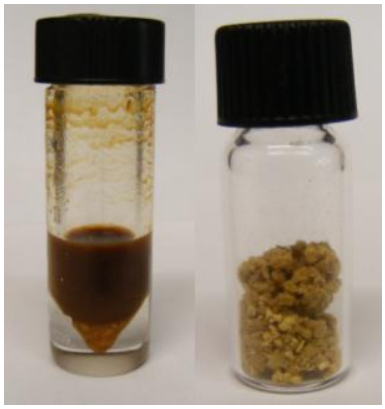

Fig. 6.1: Side product (SP-3) formed from propargyl chloride and NaOH (left), dialyzed against water (MWCO 14000) and freeze-dried (right).

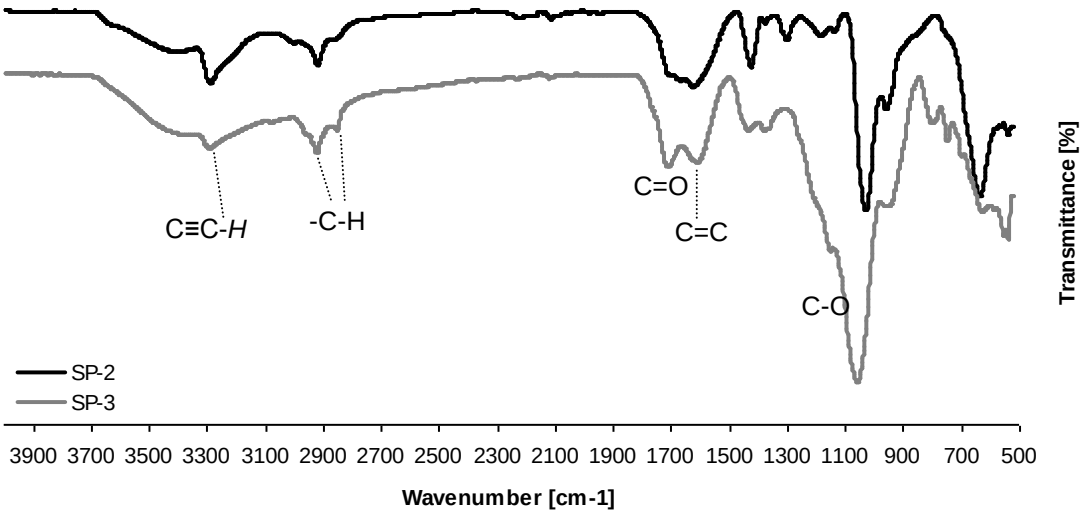

Fig. 6.2: ATR-IR spectra of products formed from PgCl and Li-dimsyl in DMSO (SP-2) and from PgCl and NaOH without DMSO (SP-3). Absorption bands were assigned according to [186].

Polymerization of propargylic compounds has been the subject of many researchers as propargyl chloride or bromide are reactive compounds and polymerize efficiently [187]. Klusener *et al.*[188] have reported conversion of pent-3-en-1-yne into dimers and trimers by treatment with butyl-lithium in THF. Tankam *et al*. [151] have reacted propargyl bromide and NaOH in DMSO, and ATR-IR spectrum of the product has indicated the presence of C≡C-H, saturated C-H, C=O,enol ethers (1700-1710, 1665, 1610 cm^{-1}), C-O or S=O(1025 cm^{-1}) and a pronounced absorption at 630 cm^{-1} for δ(C≡C-H)which shows that terminal alkynes groups are at least partially retained during polymerization of propargyl bromide. Kunzler *et al*. have documented the polymerization of propargyl halides (PgX) to polyconjugated products with CH_2X

side chains using $MoCl_3$ and WCl_6 based initiators. Cross-linking occurs by addition of CH_2X groups to other double bonds and subsequent HX elimination resulting into dark brownish or black colored polymer which does not dissolve in common organic solvents [189]. Kabanov *et al.*[190] have reported conjugated systems formed by reacting propargyl chloride with poly(4-vinylpyridine) in methanol. It was found that pyridine reacts with propargyl chloride to form propargylpyridinium chloride which polymerizes spontaneously at the triple bond of preorganized propargyl chloride (Scheme 6.3). Gal *et al*. [191] have polymerized propargyl bromide by reacting with 2-ethynylpyridine under reflux in methanol. It was supposed that mechanism of polymerization was the same as reported by Kabanaov *et al*. [190]. Balcar *et al*. [192] have prepared nitrophenyl propargyl ethers which were polymerized in benzene using molybdenium based metathesis catalyst system.

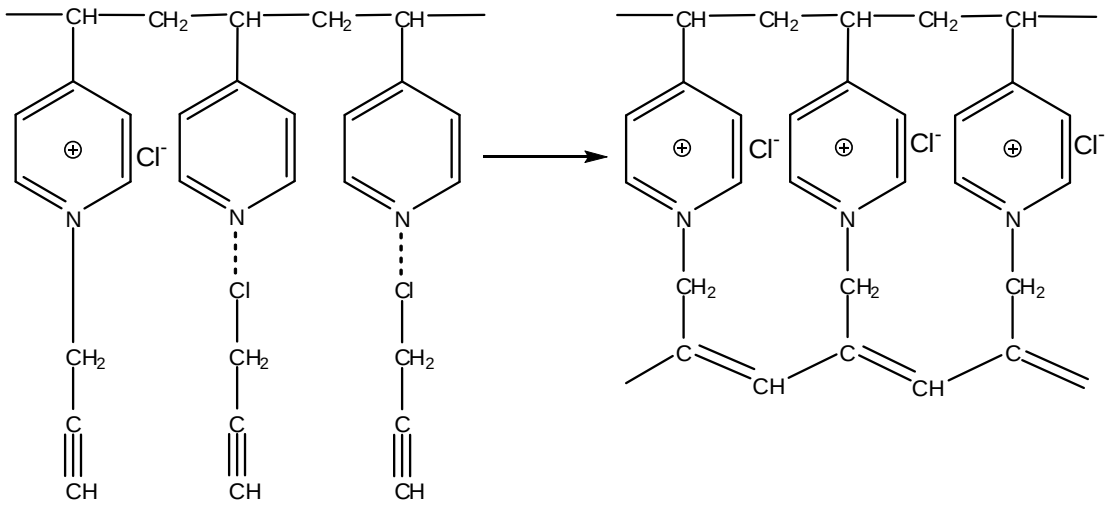

Scheme 6.3: Proposed mechanism for the polymerization of propargyl chloride in the presence of poly-4-vinylpyridine according to [190]

In our PgD samples, an absorption at about 1630 cm^{-1}, which is considered characteristic for conjugated dienes [186], was observed in all samples and its intensity increases with increasing amount of base. Such absorption was also observed by the mentioned researchers [190-192]. ATR-IR spectra of SP-2 and SP-3 (Fig. 6.2) also show intensive absorption in the same area, indicating that polymer containing conjugated ene-structures formed during these control reactions. In all examples from the cited literature [189-191], products were reddish brown, dark brown or blackish brown and were not or not completely soluble in common organic solvents which is in

agreement with our observations for PgD samples and product from control reactions (SP-1, SP-2 and SP-3).

Along with conjugated diene systems, another reason for dark color and poor solubility of PgD samples is the possibility of deprotonation of terminal CH of PgCl/PgBr and reaction with another molecule to form $\left[\text{-CH}_2\text{-C}\equiv\text{C-}\right]_n$ with skipped acetylenic bonds, which should further isomerize under basic conditions. Furthermore, the methylene group is activated and deprotonation and subsequent "self-alkylation" can occur at this position. The thermodynamically less acidic methylene group of alkyne has a higher kinetic acidity and, therefore might be substituted with further $\text{-CH}_2\text{-C}\equiv\text{C-H}$ resulting into highly branched network, which will reduce the solubility of the final product.

Elemental analysis of SP-1 and SP-2 (Table 6.3) show that empirical formula of the product should be $C_{16.14}H_{15.4}S_{0.98}O_{0.98}Cl_{0.98}$ or simply $C_{16}H_{15}SOCl$. While calculating this formula, content of C, H and S was taken according to their EA (Table 6.3) and it was supposed that oxygen will be only with S (S=O) and rest was considered for Cl. On the basis of these calculations, an additional structural feature could look like shown in Fig. 6.3, which partially could be further cross-linked forming the observed ene-structures.

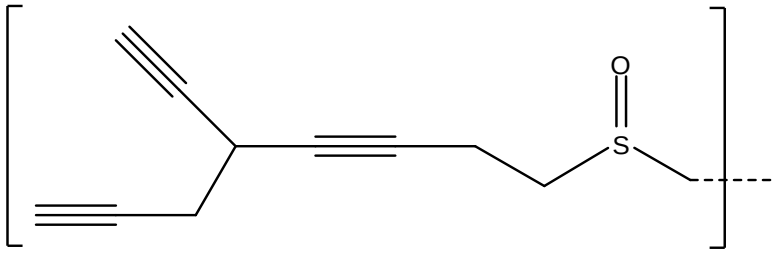

Fig 6.3: Possible structural element of the polymeric side productformed in SP-1, SP-2

It looks that in contrast to methylation reaction of dextran, alkynylation is more sensitive against the alkaline reaction conditions. Propargyl halides form an insoluble dark polymer which contains sulfur, oxygen, conjugated dienes, and terminal alkynyl functions. It is probably formed by reactions of the dimsyl anion with PgCl or PgBr, by nucleophlic attack of α-deprotonated PgX, and by C-C-crosslinking of the alkynyl-rich intermediates.

6.1.2.2 Distribution of Substituents in Propargyl Dextrans

DS and distribution of substituents in PgDs was determined by GLC after hydrolysis and acetylation while positions of substituents were deduced from shifted fragments by GLC/MS [193]. With Li-dimsyl, PgDs with relatively higher DS (0.76 - 1.67) and with relatively less side product were formed. With NaH, PgDs of generally deeper color and relatively lower DS (0.47 - 0.99) than with Li-dimsyl were obtained. While with NaOH, PgDs of lowest DS (0.14 – 0.64) and deepest color in this serieswere obtained [185]. Substitution pattern of these PgDs strongly deviate from the random distribution (Table 6.5-6.7), which was calculated weighting the partial DS values (x_i) at *O*-2, *O*-3 and *O*-4 according to Spurlin model for cellulose derivatives[48]. Branched glucosyl units and 6-*O*-substitution from terminal residues was neglected. Although PgD 3-5 have almost the same DS, comparison with the random model shows increasing deviation and thus increasing heterogeneity (Table 6.5). The also observed decrease in regioselectivity with increasing amount of base applied is not unexpected for kinetically controlled reactions, since the difference in acidity of OH is leveled of in the presence of excess base.

6.1.2.3 Solvent Effect on Propargylation of Dextran

From elemental analysis of PgD samples it was clear that side product involve S which was possible only from solvent (DMSO). All attempts to replace DMSO failed. Different solvents with different bases (Table 6.4) were used but in most cases DS was very low or even zero. In case of PgD-17, where NaH was used in THF, although DS was not so low (0.67) but yellow color was developed on addition of PgCl, indicating the formation of side product.

Table 6.4: Different solvents or mixture of solvents used to replace DMSO

Sample	Base	Base eq/OH	Solvent	DS_{GC}
PgD-16	NaOH	1.25	THF	0.14
PgD-17	NaH	5.00	THF	0.67
PgD-18	NaH	1.50	Formamide	0
PgD-19	NaOH	1.50	Formamide	0
PgD-20	Li-dimsyl	1.00	Formamide	0
PgD-21	Li-dimsyl	5.00	Formamide	0

Alkylating agent was PgCl (2.0 eq./OH) in all reactions

Table 6.5: Monomer composition (Mol %) of PgD 1-5, prepared with Li-dimsyl (0.5, 0.75, 1.0, 1.25, 1.5 eq./OH) and Propargyl bromide (2.0 eq./OH) in DMSO, as obtained after acid hydrolysis and acetylation. s_i: glc substituted at O-*i*, x_i: partial DS in position *i*, c_i: Mol fraction in % of i-fold substituted glc.

Sample / **Position**	**PgD-1**		**PgD-2**		**PgD-3**		**PgD-4**		**PgD-5**	
	Exp	**Random**	**Exp**	**Random**	**Exp**	**Random**	**Exp**	**Random**	**Exp**	**Random**
s_0	49.60	37.80	12.12	5.97	8.53	3.24	14.77	5.33	20.43	6.44
s_2	23.24	35.67	40.02	43.30	31.55	34.73	27.20	27.44	22.70	25.08
s_3	0.00	2.00	0.00	1.74	0.00	1.22	0.00	2.46	0.00	3.58
s_4	1.85	11.06	0.00	3.41	0.00	2.96	1.50	5.80	0.00	6.69
s_{23}	4.53	1.89	11.50	12.63	12.19	13.09	5.92	12.66	5.90	13.94
s_{24}	20.29	10.44	25.28	24.74	32.55	31.17	24.95	29.85	21.15	26.07
s_{34}	0.00	0.59	0.00	1.00	0.00	1.11	0.00	2.68	0.00	3.72
s_{234}	0.50	0.55	11.08	7.21	15.18	11.95	25.66	13.78	29.82	14.49
DS	0.76	0.76	1.47	1.47	1.67	1.67	1.67	1.67	1.66	1.66
c_0	49.60	37.80	12.12	5.97	8.53	3.24	14.77	5.33	20.43	6.44
c_1	25.09	48.73	40.02	48.45	31.55	38.90	28.70	35.70	22.70	35.35
c_2	24.82	12.91	36.78	38.36	44.74	45.91	30.87	45.19	27.05	43.73
c_3	0.50	0.55	11.08	7.21	15.18	11.95	25.66	13.78	29.82	14.49
x_2	0.49	63.7 %	0.88	59.8 %	0.92	54.7 %	0.84	50.0 %	0.79	47.9 %
x_3	0.05	6.6 %	0.23	15.4 %	0.27	16.4 %	0.32	18.9 %	0.35	21.4 %
x_4	0.23	29.7 %	0.36	24.7 %	0.48	28.6 %	0.52	31.2 %	0.51	30.7 %
H₁	22.1		9.0		7.8		18.2		24.4	

H1: Heterogeneity parameter = $(\Sigma \Delta Si^2)^{1/2}$, where ΔS_i is the difference between experimental and calculated S_i values[27]

Table 6.6: Monomer composition (Mol %) of PgD 6-10, prepared with NaOH (0.5, 0.75, 1.0, 1.25, 1.5 eq./OH) and Propargyl bromide (2.0 eq./OH) in DMSO, as obtained after acid hydrolysis and acetylation. s_i: glc substituted at O-*i*, x_i: partial DS in position *i*, c_i: Mol fraction in % of i-fold substituted glc.

Sample / Position	PgD-6		PgD-7		PgD-8		PgD-9		PgD-10	
	Exp	Random	Exp	Random	Exp	Random	Exp	Random	Exp	Random
S_0	91.54	86.30	79.99	74.99	56.10	47.47	83.64	79.56	55.06	45.97
S_2	3.97	7.97	14.07	18.31	25.65	32.17	10.45	13.59	27.43	34.05
S_3	0.00	3.51	0.00	1.91	0.00	3.45	0.00	1.65	0.00	3.64
S_4	0.00	1.67	0.38	3.39	3.50	8.10	1.78	4.12	2.38	7.26
S_{23}	2.59	0.32	1.62	0.47	3.68	2.34	0.98	0.28	3.87	2.70
S_{24}	0.58	0.15	3.06	0.83	7.97	5.49	2.10	0.70	7.78	5.38
S_{34}	0.00	0.07	0.00	0.09	0.00	0.59	0.00	0.09	0.00	0.58
S_{234}	1.32	0.01	0.87	0.02	3.09	0.40	1.05	0.01	3.47	0.43
DS	0.14	0.14	0.26	0.26	0.61	0.61	0.62	0.62	0.64	0.64
C_0	91.54	86.30	79.99	74.99	56.10	47.47	83.64	79.56	55.06	45.97
C_1	3.97	13.15	14.45	23.61	29.15	43.71	12.23	19.36	29.81	44.95
C_2	3.16	0.55	4.68	1.38	11.65	8.41	3.09	1.07	11.65	8.65
C_3	1.32	0.01	0.87	0.02	3.09	0.40	1.05	0.01	3.47	0.43
X_2	0.08	59.3 %	0.20	74.2 %	0.40	65.4 %	0.15	67.7 %	0.43	66.9 %
X_3	0.04	27.4 %	0.02	9.4 %	0.07	10.9 %	0.02	9.4 %	0.07	11.5 %
X_4	0.02	13.3 %	0.04	16.3 %	0.15	23.6 %	0.05	22.8 %	0.14	21.4 %
H1	8.1		7.9		12.9		6.2		13.4	

H1: Heterogeneity parameter = $(\Sigma \Delta Si^2)^{1/2}$, where $\Delta S_i$is the difference between experimental and calculated $S_i$values [27]

Table 6.7: Monomer composition (Mol %) of PgD 11-15, prepared with NaH (0.5, 0.75, 1.0, 1.25, 1.5 eq./OH) and Propargyl bromide (2.0 eq./OH) in DMSO, as obtained after acid hydrolysis and acetylation. s_i: glc substituted at O-*i*, x_i: partial DS in position *i*, c_i: Mol fraction in % of i-fold substituted glc.

Sample / Position	PgD-11		PgD-12		PgD-13		PgD-14		PgD-15a		PgD-15b	
	Exp	Random	Exp	Random	Exp	Random	Exp	Random	Exp	Random	Exp	Random
S_0	61.87	57.41	47.15	36.95	58.76	50.45	53.35	41.96	35.89	25.83	47.54	36.59
S_2	26.26	30.42	31.61	37.99	25.76	31.9	29.58	36.69	32.85	37.37	30.97	38.24
S_3	0	1.76	0	4.26	0	3.37	0	4.42	0	4.43	0	4.1
S_4	3.49	6.01	2.15	7.26	2.5	6.97	0	6.3	4.98	9.06	1.36	7.38
S_{23}	2.39	0.93	4.82	4.38	3.34	2.13	4.01	3.87	5.3	6.41	4.7	4.28
S_{24}	5.41	3.19	8.76	7.47	6.71	4.41	7.54	5.51	11.64	13.11	10.06	7.71
S_{34}	0	0.18	0	0.84	0	0.47	0	0.66	0	1.55	0	0.83
S_{234}	0.58	0.1	5.51	0.86	2.93	0.29	5.52	0.58	9.34	2.25	5.37	0.86
DS	0.47	0.47	0.77	0.77	0.57	0.57	0.69	0.69	1	1	0.78	0.78
C_0	61.87	57.41	47.15	36.95	58.76	50.45	53.35	41.96	35.89	25.83	47.54	36.59
C_1	29.75	38.19	33.76	49.51	28.26	42.25	29.58	47.42	37.83	50.86	32.33	49.72
C_2	7.8	4.3	13.57	12.68	10.04	7.01	11.55	10.04	16.94	21.07	14.76	12.82
C_3	0.58	0.1	5.51	0.86	2.93	0.29	5.52	0.58	9.34	2.25	5.37	0.86
X_2	0.35	73.6%	0.51	65.4%	0.39	67.8%	0.47	67.3%	0.59	59.3%	0.51	65.5%
X_3	0.03	6.3%	0.1	13.3%	0.06	10.9%	0.1	13.7%	0.15	14.7%	0.1	12.9%
X_4	0.09	20.1%	0.16	21.2%	0.12	21.2%	0.13	18.8%	0.26	26.0%	0.17	21.5%
H_1	7.4		14.6		12.3		16.4		14.6		15.9	

PgD 15-a: Soluble part of PgD 15 (which was not precipitated during dialysis),
PgD 15-b: Insoluble part of PgD 15 (which was precipitated during dialysis)

H1: Heterogeneity parameter = $(\Sigma \Delta Si^2)^{1/2}$, where $\Delta S_i$is the difference between experimental and calculated $S_i$values [27]

6.1.2.4 Loss of Propargyl Groups in PgDs

Repeated monomer analysis of PgD samples, recorded after a few month storage at room temperature showed that PgDs were not stable. All samples show continuous loss of propargyl residue at all positions (Fig. 6.4-6.5). Tankam *et al*. [151] have also observed such loss of propargyl residues for propargyl starches and have proposed a mechanism suggesting an intramolecular reaction between the C≡C triple bond and a neighboured OH group of the sugar, thus forming a six-membered ring including an enol ether linkage. This is easily hydrolyzed and after tautomerisation to an enolether cleaved by hydrolysis (Scheme 6.4). This interpretation was supported by corresponding changes in ATR-IR spectra.

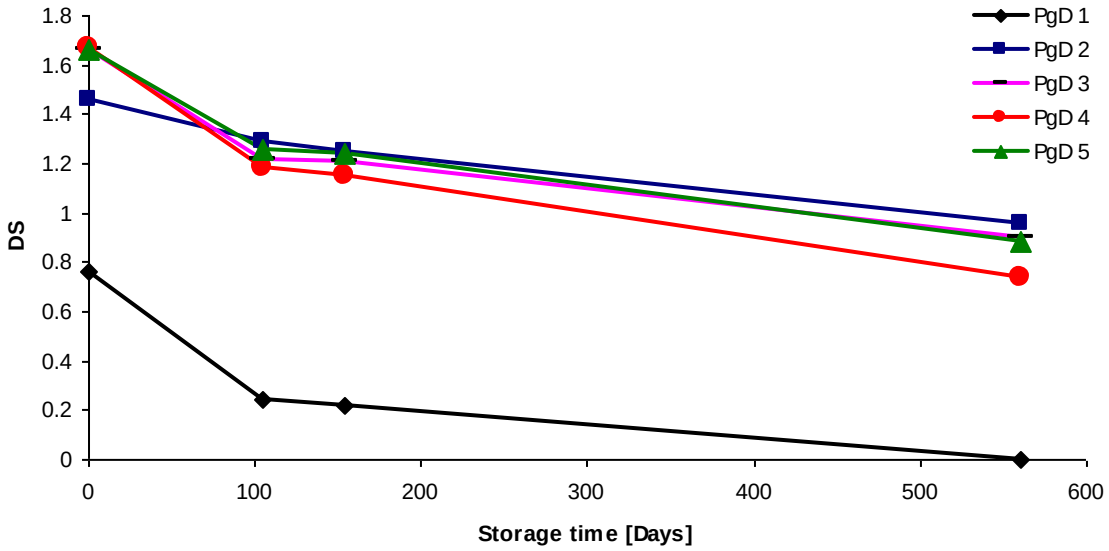

Fig. 6.4: PgD 1-5 (Li-dimsyl 0.5-1.5 eq./OH , PgBr 2.0 eq./OH), loss of DS during storage.

However, the IR spectra also showed a relative increase for the terminal alkyne C-H absorption for PgD 4 and 5 compared to PgD 3, indicating another DS trend than calculated for the depolymerized samples as discussed above.

Figure 6.6 shows the ATR-IR spectra (transmittance) of the series of PgD prepared with Li-dimsyl. While the intensity of OH-vibration decreases from PgD 1–5, its maximum is shifted to higher wave numbers (from 3335 cm^{-1} for dextran to 3501 cm^{-1} for PgD 5) indicating an average decrease in hydrogen bond strength. Absorption for terminal

C≡C-H occurs constantly at 3282 cm^{-1} with increase in intensity, while C≡C vibration at 2 118 cm^{-1} is weak, but also increasing. In the area of C-O absorption at 914, 1002–1008 and around 1150 cm^{-1}, a new vibration occurred between 1060 and 1078 cm^{-1} also showing a shift to higher wave number with DS. For semiquantitative evaluation, transmittance data were converted to absorption data and the areas of terminal alkyne peak, normalized by internal reference to C-O vibration mode at 1006 cm^{-1}, was taken as a measure for DS. Careful elucidation of the wave number of the OH-stretching mode showed a polynomial correlation ($R^2 = 0.989$) with this relative DS scale.

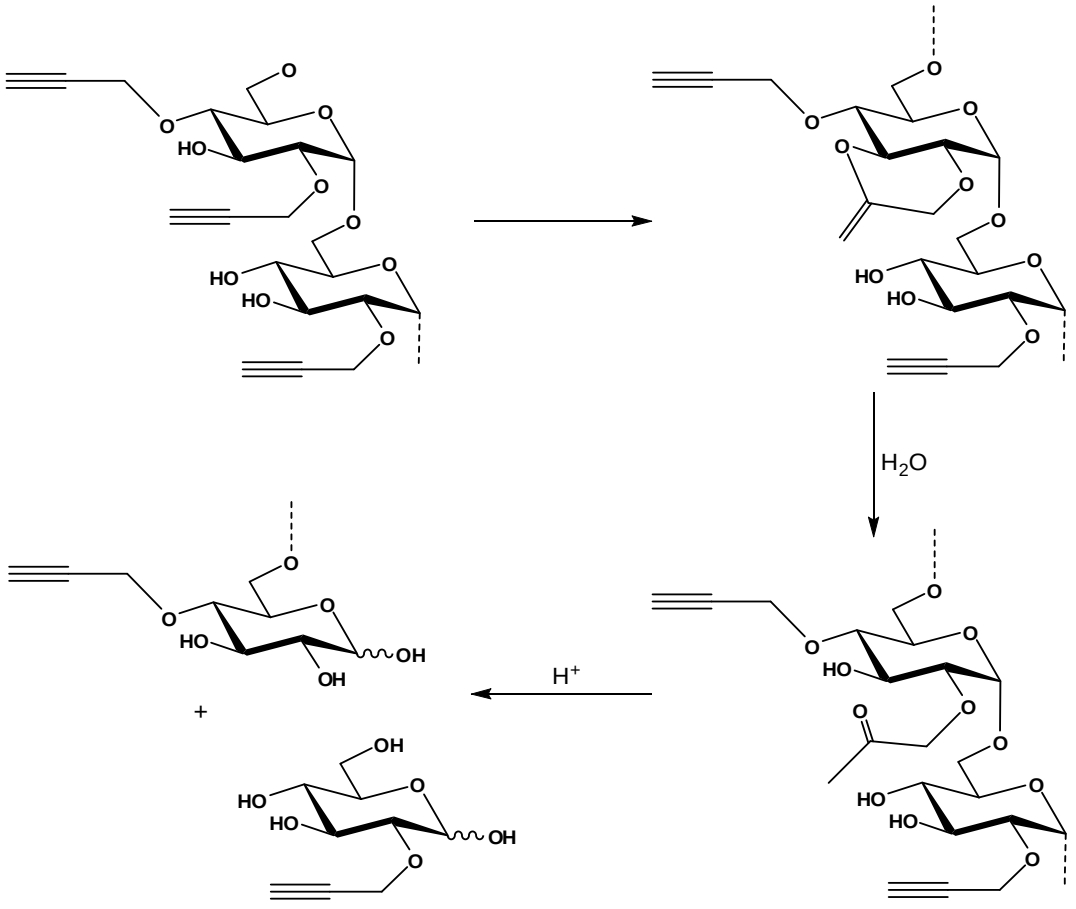

Scheme 6.4: Proposed mechanism for propargyl loss in propargyl dextran by cycloisomerization and hydrolysis as described for propargyl starches in [151]

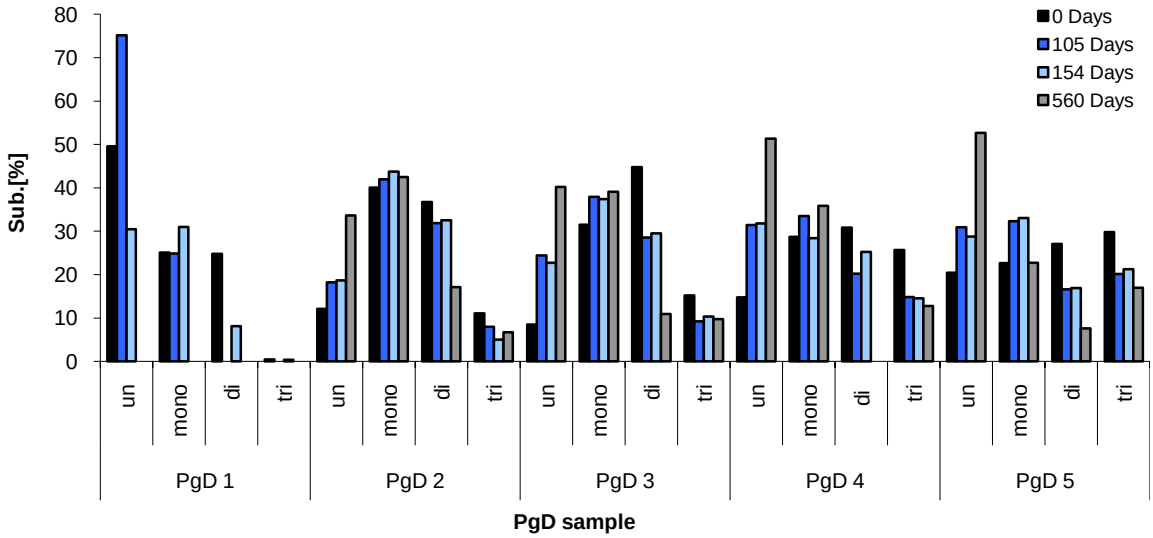

Fig. 6.5: Loss of propargyl residues (in Mol % of the originally present groups) from PgDs after various storage times

To estimate absolute DS values from this correlation, the range was fixed between dextran at 3335 cm^{-1} and DS 0, and a theoretical value for unbound secondary OH at 3630 cm^{-1} and DS 3. This is in agreement with effects on dilution of alcohols on the OH stretching modes in IR spectroscopy [194, 195].

By weakening the hydrogen bonds, the average strength of O-H increases and thus the maximum of the broad absorption is shifted to higher wave numbers. Due to the cooperativity of hydrogen bonds, changes and thus relative shifts with DS are larger in the beginning and level out when less and less OH are left. From this correlation DS calculated from ATR-IR spectra (DS_{IR}) values of 1.84, 2.08 and 2.27 are obtained for PgD 3–5. Although, these are only rough estimations and not yet absolute values, loss of substituents during acid hydrolysis and thus a lower DS_{Hy} compared to DS_{IR} is very probable.

At the same time, signals at 1725, 1680 and 1627 cm^{-1} which are referred to intramolecular side reactions (see above) increase in the PgD series. It is concluded that substituents are lost during hydrolysis, preferably from enol ethers and oxopropyl residues formed by internal side reactions as mentioned above [150].

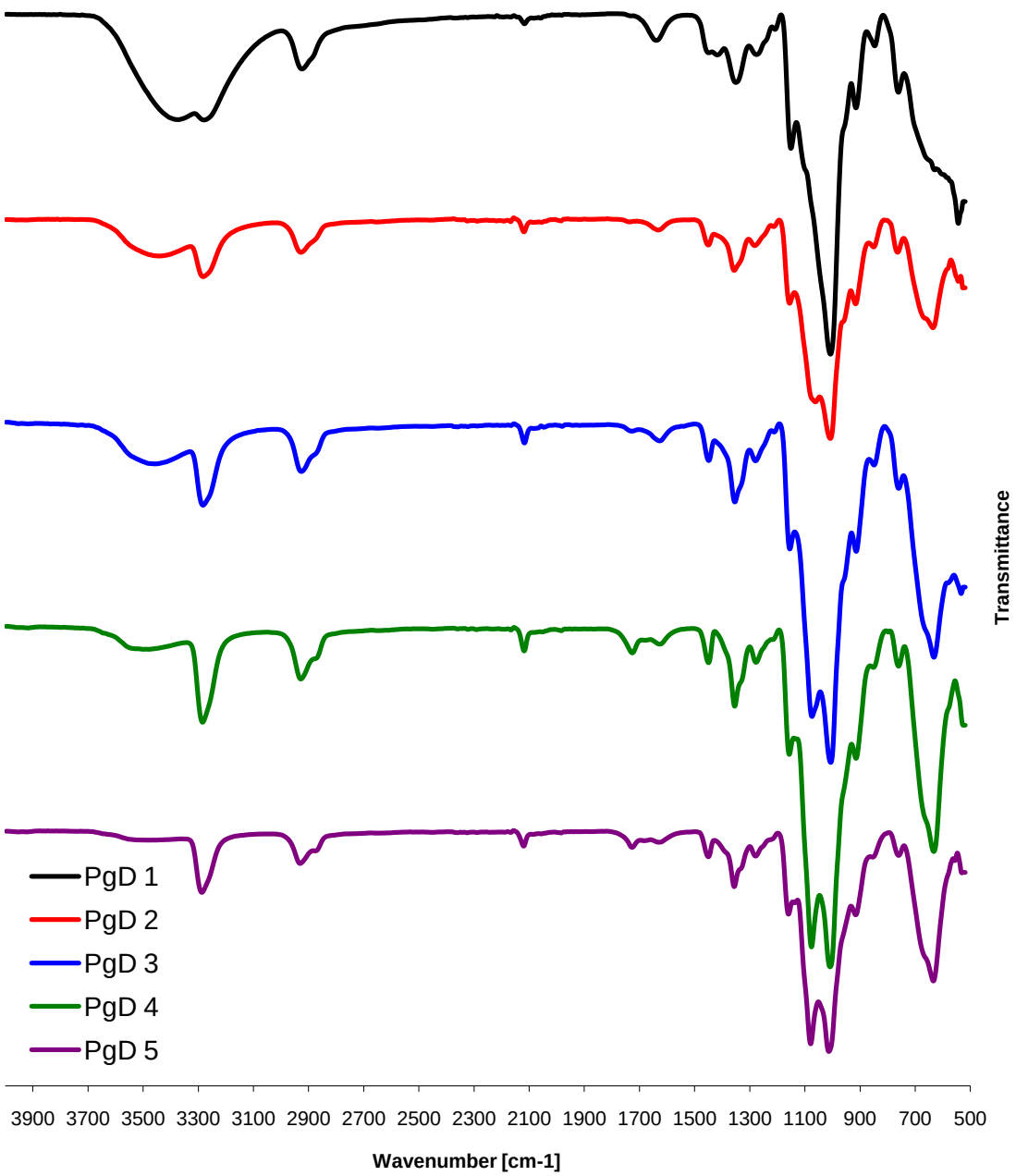

Fig. 6.6. ATR-IR spectra of PgD 1–5 prepared with 0.5–1.5 equiv./OH Li-dimsyl and 2 equiv./OH PgBr in DMSO from dextran (M_w 500 000); 1: 0.5, 2: 0.75, 3: 1.0, 4: 1.25, 5: 1.5 equiv. Li dimsyl/OH.

However, not only the total, but also the DS_{IR} for propargyl is obviously higher than DS_{Hy}. Therefore, it is assumed that acid catalyzed internal addition might also be favored by formation of a six-membered ring. Furthermore, in contrast to basic conditions applied at room temperature, acid hydrolysis is performed at 120 °C. Internal attack of the carboxonium ion formed during hydrolysis as is well known for hydroxyalkyl and allyl

ethers, is excluded due to steric reasons and lack of subsequent products. Significant rearrangement to allenyl residues or internal alkynyl ethers, which would also be sensitive to acid hydrolysis, could not be confirmed by IR spectroscopy. Only for PgD 4 and 5, very tiny allene signals could be detected at 1963 and 1967 cm^{-1}, respectively (Fig. 6.6).

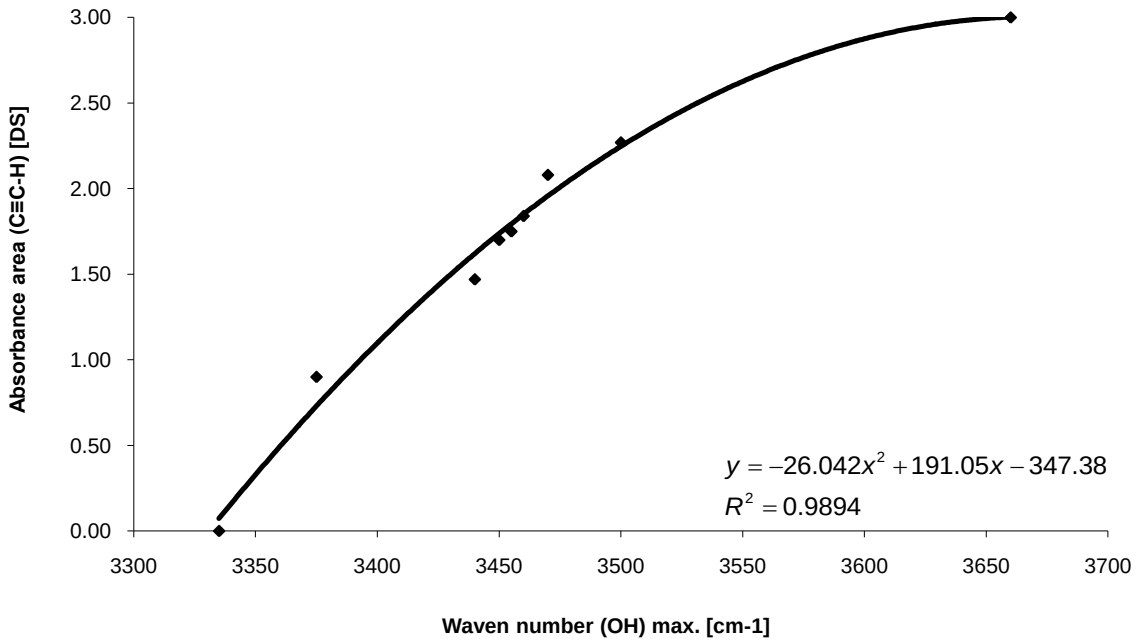

Fig. 6.7: Correlation of the absorption maximum of OH stretching mode in PgD with DS. Normalized peak area of C≡C-H absorption (IR) was taken as measure for DS

After 4 months of storage of solid PgD at room temperature, more pronounced changes in the IR spectra had occurred. Absorption typical for terminal alkynes at 3282, 2218 and 632 cm^{-1} now had decreased and already mentioned vibrations at ca. 1627, 1680 and 1725 cm^{-1} had appeared or further increased with a intensity shift from the absorption ascribed to C-O in enol ethers to that referred to C=O in the oxopropylether residue. Thus the DS obtained after acid hydrolysis by monomer analysis further decreased. A control experiment with *O*-(3-trimethylsilyl propargyl) dextran confirmed that the terminal hydrogen is not involved in the side reaction, since loss of propargyl groups was also observed for this compound after storage. Substitution patterns and DS were followed over a long period of storage (Figure 6.4, 6.5). PgD 3–5 showed losses of 2,4- and

2,3-di-*O*-Pg-glc at a decreasing rate, while the relative portion of 2-*O*-Pg-glc remained on a high level and even increased in the early stage, indicating that Pg was mainly lost from position 3 and 4. No mono-substituted 3- and nearly no 4-*O*-Pg-glc was observed. That neither 3-, nor the 3,4-di-*O*-Pg-glc have been present in any of these samples is also indicative for the higher instability of Pg in these positions.

In the series of PgD 3–5 prepared with increasing equivalent of Li-dimsyl, but all showing the same DS, change is most pronounced for PgD 3 with H_1 increasing from 8 to 14, while for PgD 4 it increases from 18 to 21, and remained unchanged for PgD 5 at 24. This increase in heterogeneity, i.e., the average deviation from the random pattern, confirms that loss of propargyl residues is not an unspecific random process, but is faster for di- and mono- than for trisubstituted residues. But, since the portion of trisubstituted residues is also decreased, even though at a lower rate, the mechanism proposed cannot be the only responsible one, or must include intermolecular reactions or participation of water as well. Otherwise, fully substituted residues should be stable.

Since methanolysis is known to prevent some side reactions observed during aqueous acid hydrolysis of polysaccacharide ethers, e.g., the intramolecular additions of 2-*O*-(2-hydoxyalkyl)- and 2-*O*-allyl ethers to the carboxonium ion intermediate, a new PgD was prepared and submitted to hydrolysis/acetylation and methanolysis/trimethyl-silylation. Pinitol was added as an internal standard to calculate glucose recovery. From IR spectra, DS_{IR} = 1.75 was calculated for this PgD. After hydrolysis, a DS_{Hy} of 1.12 was determined, while from the trimethylsilylated methyl glucosides a DS of 1.62 was obtained reproducibly. Exact monomer pattern could not be determined, since mono- and disubstituted anomers were coeluting, allowing only rough estimation. However, the average DS was not significantly affected by this incomplete separation. Recovery of glucose units was always higher for methanolysis, but was only 45%. One reason is the presence of polymeric by-product from the synthesis, but this only counts for a much smaller portion. As has been thoroughly studied by Horner and Saake on hydrolysis of carboxymethyl celluloses, recovery of sugar units is sometimes very low without affecting relative ratios of substituted units and thus DS [196]. Compared to methanolysis, 19% less substitution was found for *O*-2 after hydrolysis, 48% less at *O*-3 and 43% less at *O*-4.Heterogeneity slightly increased from 11.5 to 13.2. Differences of

DS_{Hy} and DS_{IR} were between 10 and 20% for most of the PgD samples, but cover the range from 0 to 36% in this extreme case (DS_{IR} =1.75).

From the present data, it can be concluded that propargyl ethers in partially substituted polysaccharides are not completely stable under acidic and basic conditions. During storage in solid form, changes occur that enhance losses of substituents during hydrolysis, preferentially from positions 3 and 4 and from mono- and disubstituted glucosyl units. Participation of vicinal free OH is supported by experimental data, but mechanisms are not fully understood presently and will be object of further studies. Pg ethers seem to be less sensitive against methanolysis conditions compared to those applied in aqueous hydrolysis. Heterogeneity is not only the result of selective Pg losses during hydrolysis, but is also observed after methanolysis and also for methyldextrans prepared under similar conditions [26]. As PgDs were not stable under normal storage conditions and show a continues loss of propargyl residues, chain length of alkyl group was extended from 3 to 5 carbon atoms in next series of experiments.

6.2 Pentynyl Dextran

6.2.1 Synthesis of Pentynyl Dextran

Dextran ($\overline{M}_w$ 500 000) was reacted with 5-chloro-1-pentyne (2 eq./OH) and Li-dimsyl (1.5 eq./OH) in DMSO (scheme 6.5). To find out, whether dialysis against water or precipitation in ethanol as applied for large scale preparations is suitable for purification of PyD, the product was divided into two parts after stirring for 72 hours at r.t. First part was dialyzed against deionized water and freeze dried (PyD-1a) while second part was precipitated in ethanol, washed with ethanol and dried at r.t. and then under vacuum (PyD-1b). Both parts were characterized to compare their DS and distribution of substituents.

The color of dialyzed portion was whitish while, that of precipitated was light brown. According to our experience with PgDs, intensity of brownish color is proportional to amount of side product, so light brownish color in precipitatated part indicated that some side product was formed along with desired product and that was not washed out with

ethanol. In case of PgD side product was also not separated by dialysis but in case of PyD synthesis the color of the dialyzed product indicated better purification result.

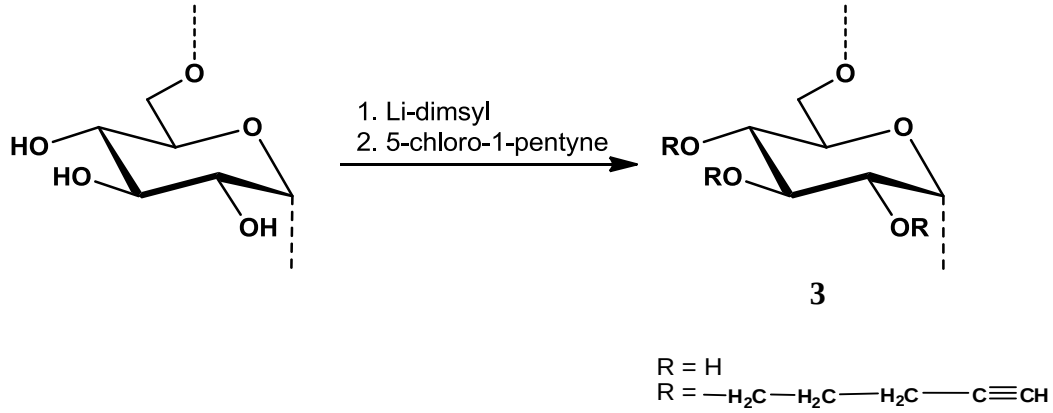

Scheme 6.5: Synthesis of pentynyl dextran (PyD)

6.2.2 Comparison of Purification Methods for Pentynyl Dextran

Both fractions of PyD-1, i.e. dialyzed against water (PyD-1a) and precipitated in ethanol (PyD-1b), were characterized by ATR-IR spectroscopy, EA and monomer analysis. The latter comprises methanolysis of glucosidic bonds, *O*-trimethylsilylation of the resulting methyl glucosides and gas chromatographic analysis of the volatile products. The IR-spectra are shown in Fig. 6.8. As for side product containg PgDs a strong absorption at about 1417 cm^{-1} appeared for the precipitatated part PyD-1a. Moreover, color and 4.47% S (Table 6.8) also indicate that the precipitated fraction contains a reasonable portion of side product.

In contrast, dialysis against water looks much better method as the product contains only a little amount of S (0.24%), indicating that relatively pure product was obtained by this method. Obviously, in contrast, the side product from pentynyl chloride is not of polymeric, but low molecular weight character and thus removable by repeated dialysis over longer period, although probably non-water soluble. In contrast, non-solubility in ethanol and/or co-precipitation with the polymer is indicated by the higher content in the precipitated fraction.

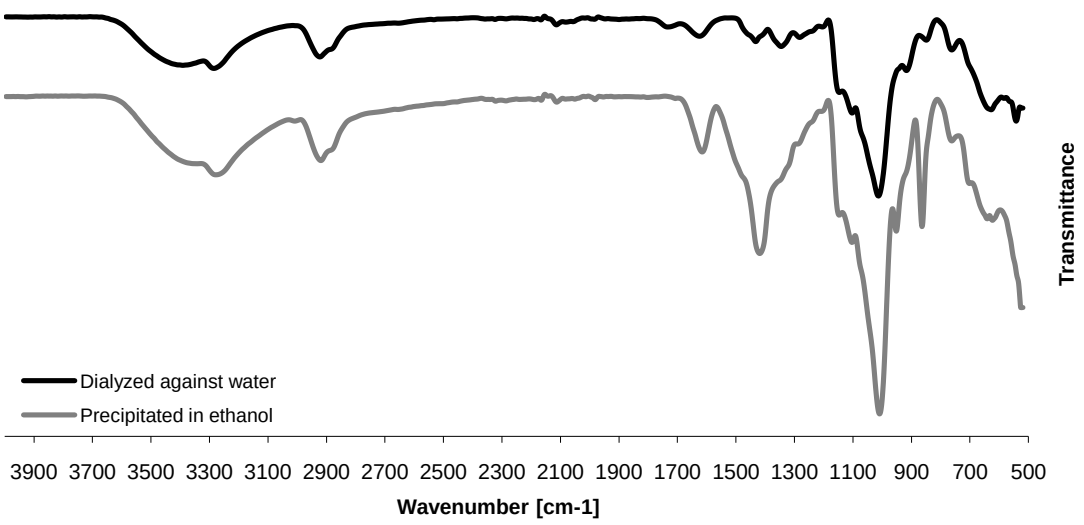

Fig. 6.8: Comparison of ATR-IR spectra of PyD-1 portions, dialyzed or precipitated in ethanol after synthesis

Table 6.8: Elemental analysis of dialyzed and precipitated portion of PyD-1

	C [%]	**H [%]**	**S [%]**	**C/H**	**DS_{EA}**
Dextran	44.43	6.22	-	7.14	-
PyD-1a (dialyzed against water)	50.84	6.84	0.24	7.43	0.40
PyD-1b (precipitatated in EtOH)	42.78	5.83	4.47	7.34	0.12

C and H content in precipitated part is even lower than in dextran (Table 6.8) which indicated further contamination with inorganic or low-carbon compounds and therefore the C/H ratio and S content are more informative than C and H content. In contrast, dialyzed part show reasonable increase in C and H content and corresponds to DS very close to DS determined from monomer analysis. Table 6.9 and Fig. 6.9 show molar proportions of glucose units substituted in position *i* (s_i);c_i summarizes the *i*-fold substituted residues and x_i gives the partial DS values at O-*i*. Considering only the substituted part, there is not much difference in both fractions. Probably, part of the material was nearly unsubstituted, as we have found in other cases and this material was preferably precipitated.

Due to these results, dialysis against water was used for purification of the product in all PyD synthesis reactions.

Table 6.9: Monomer composition of PyD-1a (dialyzed against water) and PyD-1b (precipitated in ethanol); comparison with random distribution, calculated for the experimentally found partial DS values

Sample / Position	PyD-1a (dialyzed)*		PyD-1b (precipitated)*	
	Experimental	**Random**	**Experimental**	**Random**
S_0	69.49	59.93	73.53	64.08
S_2	12.80	16.56	11.50	15.52
S_3	1.56	7.33	1.39	6.68
S_4	5.86	9.88	4.76	8.82
S_{23}	3.16	2.03	2.71	1.62
S_{24}	2.11	2.73	2.00	2.14
S_{34}	2.61	1.21	2.05	0.92
S_{234}	3.57	0.33	3.29	0.22
DS	**0.47**	**0.47**	**0.41**	**0.41**
C_0	69.49	59.93	73.53	64.08
C_1	20.22	33.77	17.65	31.02
C_2	7.88	5.96	6.76	4.68
C_3	3.57	0.33	3.29	0.22
X_2	0.22	46.4%	0.20	47.5%
X_3	0.11	23.3%	0.09	23.0%
X_4	0.14	30.3%	0.12	29.5%
H_1	**13.0**		**12.7**	

*1198 mg dextran was used. 312.5 mg (24 %) from dialyzed part and 1008.0 mg (76 %) was obtained from precipitated part.

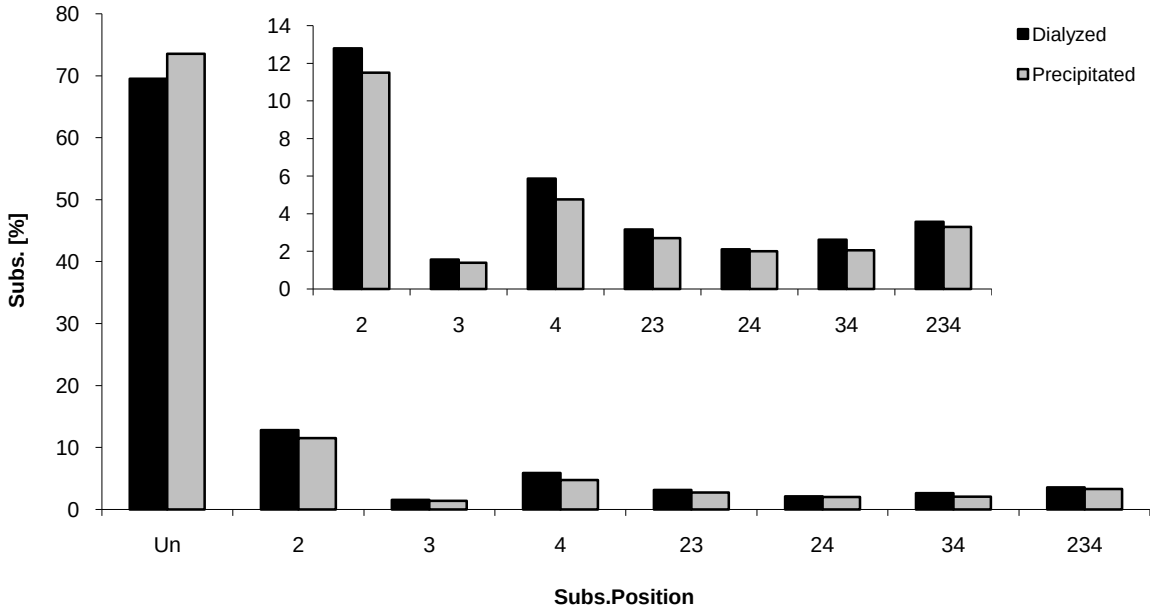

Fig. 6.9: Monomer composition of PyD-1 (black: dialyzed against water, gray: precipitated in ethanol). Inset: excluding un-substituted units.

6.2.3 Side Product Formed From Pentynyl Chloride

Side product formation during PyD synthesis was less pronounced than during propargylation, and of lower molecular weight and higher solubility, allowing separation by dialysis against water or by Soxhlet extraction in CH_2Cl_2. During PyD studies, a model reaction was conducted, in which pentynylation of methyl α-D-glucopyranoside was carried out using Li-dimsyl in DMSO. Analysis of the isolated lipophilic product showed that pentynylation of methyl α-D-glucopyranoside was not successful, but only side product had been isolated (SP-4).

Table 6.10: EA of side product isolated from Li-dimsyl and pentynyl chloride reaction in DMSO

Sample	C [%]	H [%]	S [%]	C/H
SP-4 ("PyG")	70.89	7.81	0.72	9.08

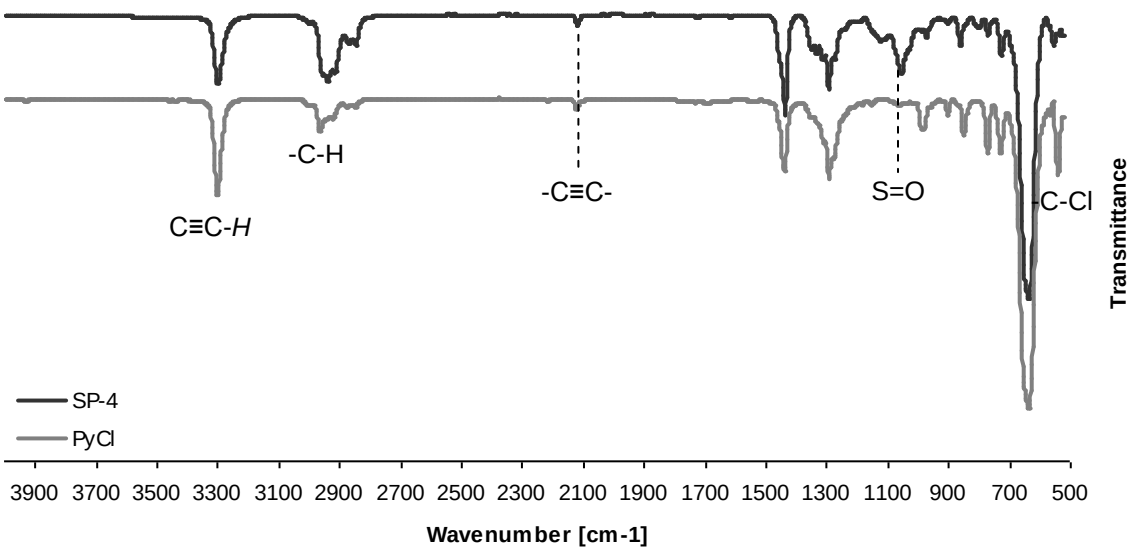

Fig. 6.10: ATR-IR spectra of side product (SP-4) isolated from pentynylation of methyl α-D-glucopyranoside and pentynyl chloride (PyCl)

Elemental analysis of SP-4 (Table 6.10) showed 0.72% S, indicating that nature of side product formed was different from that of SP-1 and SP-2 formed from PgCl and Li-dimsyl in DMSO and without sugar (Scheme 6.2). ATR-IR spectra (Fig. 6.10) show strong absorption at 3302 cm^{-1} and a weak absorption at 2120 cm^{-1} corresponding to C≡C-*H* and -C≡C- respectively, very similar to that of PyCl with some residual C-Cl

stretching at 538 cm^{-1} and S=O absorption at 1047 cm^{-1} which was not present in PyCl.However,absence of typical absorption of carbohydrate confirmed that only residual reagent and side product had been isolated.

^{1}H-NMR spectroscopy of SP-4 in $CDCl_3$ also shows high similarity with PyCl (Fig. 6.11). Many additional signals are caused by reaction of PyCl with Li-dimsyl. ^{1}H-NMR spectrum of SP-4 shows two sets of triplet signals between 3.6 and 3.7 ppm, one of which corresponding to PyCl protons H-1 (Cl-*CH_2*-), while the second slightly high field-shifted belongs to a substitution product.

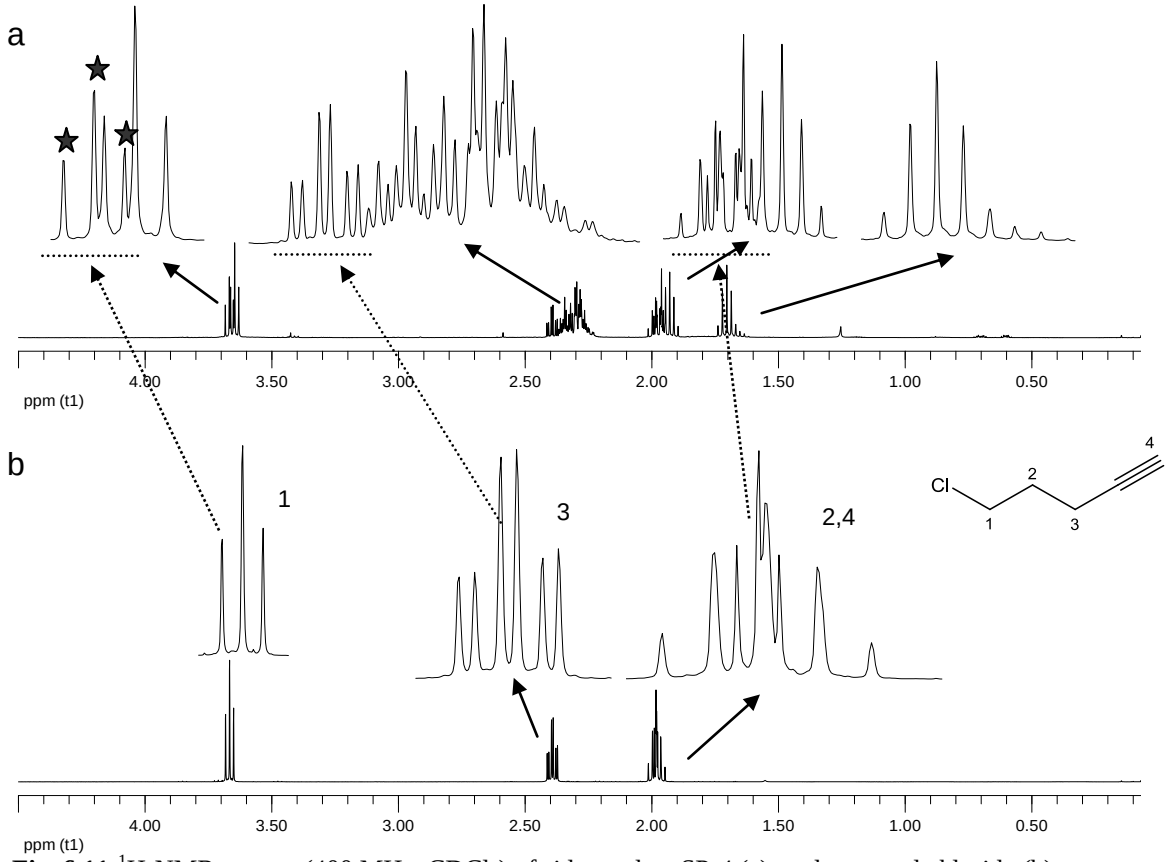

Fig. 6.11: ^{1}H-NMR spectra (400 MHz, $CDCl_3$) of side product SP-4 (a), and pentynyl chloride (b)

Beside double triplett of H-3 (-*CH_2*-C≡C) from residual PyCl, about 4 high-field shifted signal sets are visible (Fig. 6.11). Some new signal sets also appeared in the area corresponding to H-2 (Cl-CH_2-*CH_2*-) and the terminal H-4 (-CH_2-C≡*CH*). In ^{13}C-NMR of the same side product and PyCl (Fig. 6.12) also up to 4 signals appeared in each area of the PyCl-C atoms. Surprisingly ESI-MS (Fig. 6.13 shows *m/z* values which by chance are

in agreement with Na adducts of mono-, di-, and trisubstituted methyl glucosides. Some signals e.g. *m/z* 589.6, 633.5 and 677.6 with Δ = +44 refer to contamination with polyethylene oxide (PEO).

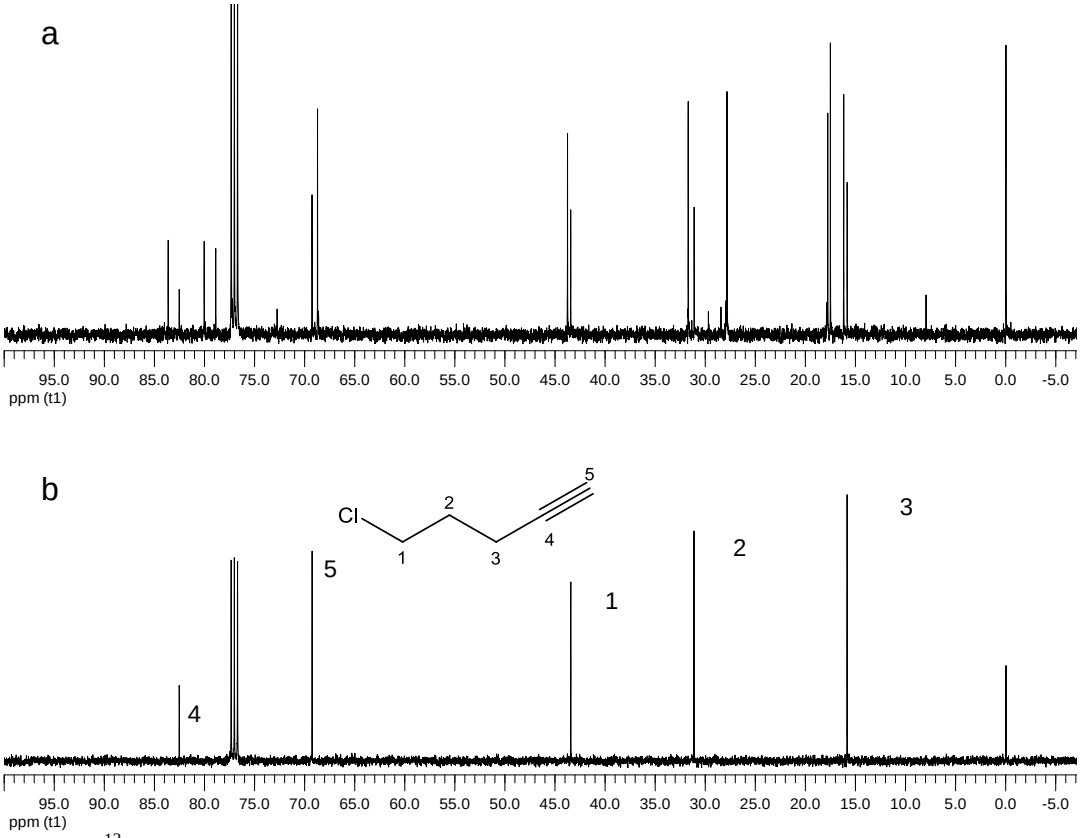

Fig. 6.12: ^{13}C-NMR spectra (400 MHz, $CDCl_3$) of side product SP-4) (a), and pentynyl chloride (b)

As ESI-MS (Fig. 6.13) showed a series ofcompounds, the mixture was submitted to column chromatography. Single spot in TLC (Fig. 6.14) was an indication that main fraction was collected. Color of the side-product before purification was yellow while after purification was a colorless liquid. EA (Table 6.11), TLC (Fig. 6.14) and ATR-IR spectrum (Fig. 6.15) confirmed that main fraction was isolated. A little amount having yellow color was sticked with silica gel (silica gel 60) used in column and was not eluted.

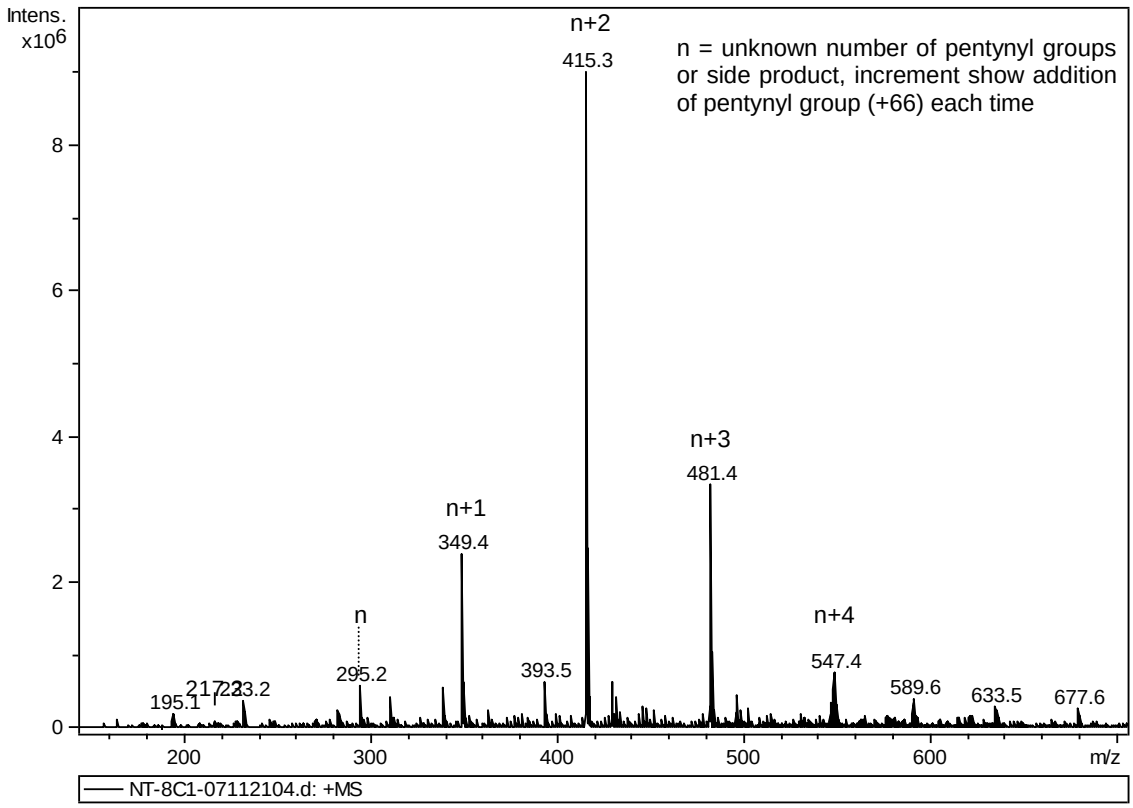

Fig. 6.13:ESI-MS of side product SP-4 form PyCl and Li-dimsyl

Fig. 6.14: TLC of SP-4 before (A) and after purification by column chromatography (B) [n-hexane/EtOAc (10:1)]

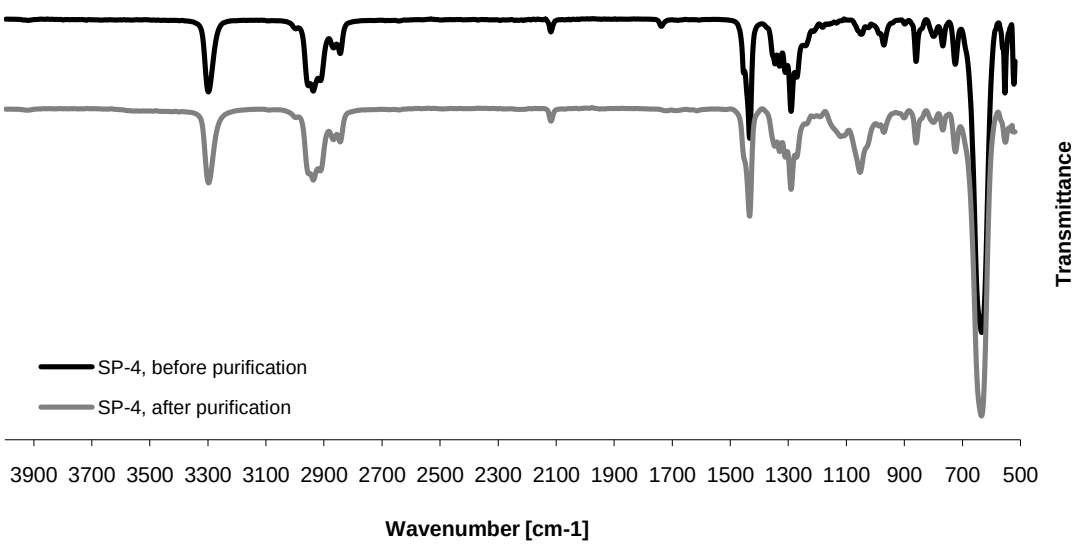

Fig. 6.15: ATR-IR of side product (SP-4) before (upper) and after purification (lower)

There is not much difference in EA of SP-4 before and after purification (Table 6.11). Before,0.72% S were found, but sulfur was absent after purification, indicating that a little yellow colored product that was not eluted from column was S containing fraction. 17.66% chloride in the separated fraction confirms that about 50% is residual pentynyl chloride. Oxygen seems to be absent since the sum of CHS and Cl is 98%.

For control, reaction of PyCl and Li-dimsyl was conducted without sugar (SP-5) and thus side reaction was forced (Scheme 6.6). The product was isolated with CH_2Cl_2, washed with water and dried over $CaCl_2$.

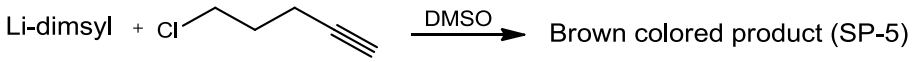

Scheme 6.6: Product formed in control reaction from Li-dimsyl and 5-chloro-1-pentyne in DMSO

On TLC of SP-5 (Fig. 6.16), some weak spots below the main spot were observed, same as in case of SP-4. During purification by column chromatography, again a little amount of yellow product was not eluted from the column.

SP-5 (raw, 273.08 mg) contained 3.19% S, while the product contained no S after purification (SP-5a, 212.42 mg) but 13.34% Cl which had not been determined from raw product (Table 6.11). NMR and ATR-IR spectra (Fig. 6.18, 6.20) also showed that same

type of side product which probably contains a mixture of various compounds was formed in both cases (SP-4, SP-5).

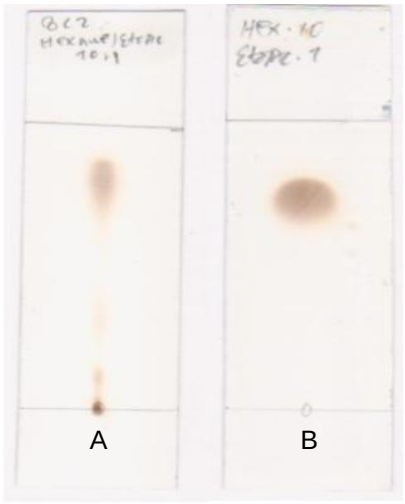

Fig. 6.16: TLC of side product (SP-5) formed from pentynyl chloride and Li-dimsyl in DMSO in control reaction before (A) and after purification (B) [n-hexane/EtOAc (10:1)]. PyCl could not be detected on TLC under the applied conditions.

Thus, the low molecular weight colourlesse main fraction is due to residual pentynyl chloride and its oligomeric products (Fig. 6.17), formed by nucleophilic attack of the acetylide or the 3-deprotonated pentynyl halide, thus giving branched oligomers. The average DP correlates with the number of Cl. For 17.66% Cl (SP4-a, Tab. 6.11), an average DP of 3 is obtained, while 13.34% Cl correspond to an average DP of 4. In contrast, the S-containing yellowish, non migrating side product is probably formed by multiple alkynylation of the dimsyl anion. This portion was much higher in the control experiment with 3.19% sulfur in the raw product.

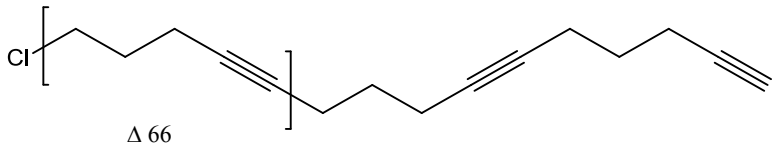

Fig. 6.17: Possible structure of the sulfur-free sideproducts from PyCl in SP-4 and SP-5

Table 6.11: EA of SP-4 and SP-5 before and after purification by column chromatography

Sample	C [%]	H [%]	S [%]	Cl [%]	C/H
SP-4 (raw product)	70.89	7.81	0.72	Not measured	9.08
SP-4a (after purification)	72.34	7.92	0.00	17.66	9.13
SP-5 (raw product,)	57.27	8.23	3.19	Not measured	6.96
SP-5a (after purification,)	77.76	7.77	0.00	13.34	10.00

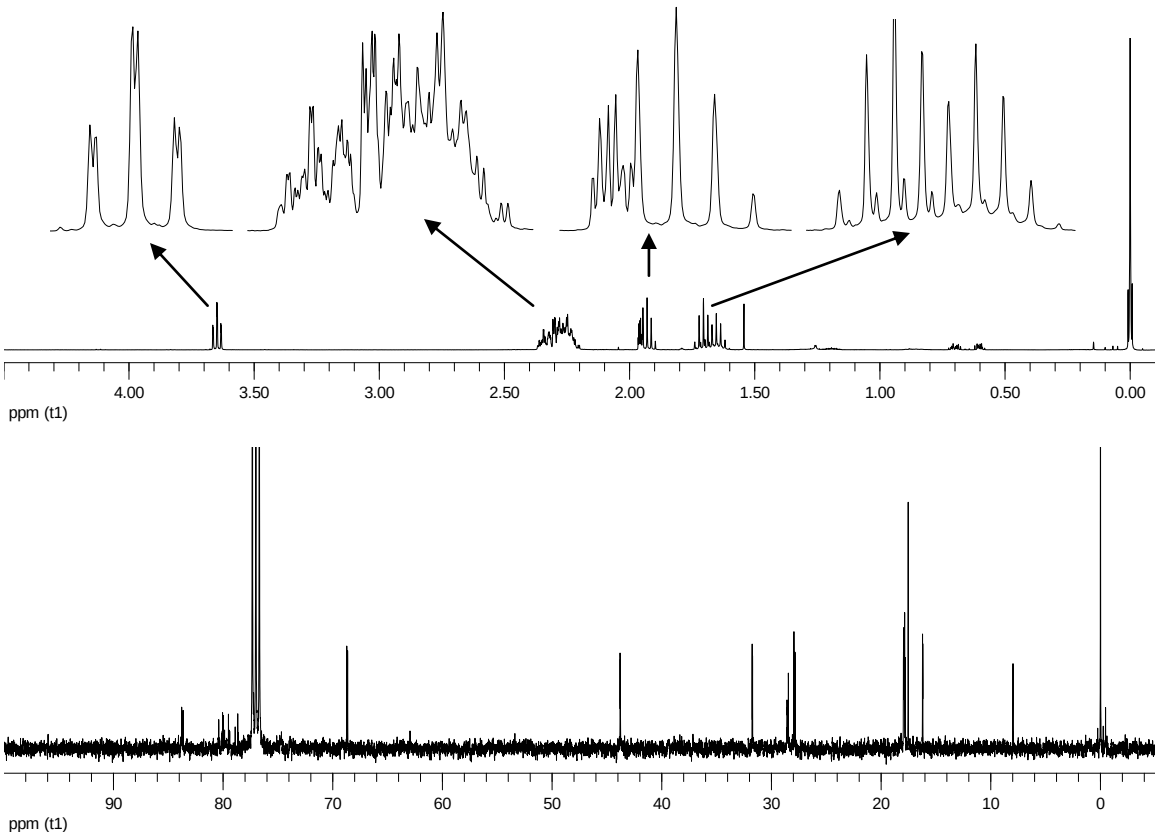

Fig. 6.18: ^{1}H and ^{13}C-NMR (400 MHz, $CDCl_3$) spectra of control reaction productformed from pentynyl chloride and Li-dimsyl in DMSO after purification (SP-5a)

ESI-MS of SP-5 (Fig. 6.19) shows two series of signals. One is the same as have been observed in mass spectrum of SP-4 (Fig. 6.14) having *m/z* 217.2, 283.2, 349.4, 415.3 and 481.4 while second series also has signals at *m/z* with Δ = +66 i.e. 233.1, 299.2, 365.3, 431.4, 497.4 and 563.5, thus shifted by +16 compared to the first series. This apparently corresponds to the series of lithiated and sodiated adducts. Li is present from the Li-dimsyl and dominated the ESI-MS of SP-4, while sodium is ubiquitous. This interpretation corresponds to M = 78 + (n x 66) and thus to DMSO + n Py. The maximum

in MS is found at n = 3 and 4, but up to n = 7 (*m/z* 563) could be observed for SP-5. No chloride-containing products were visible. However, this can be due to much lower ion yield compared to the sulfoxide.

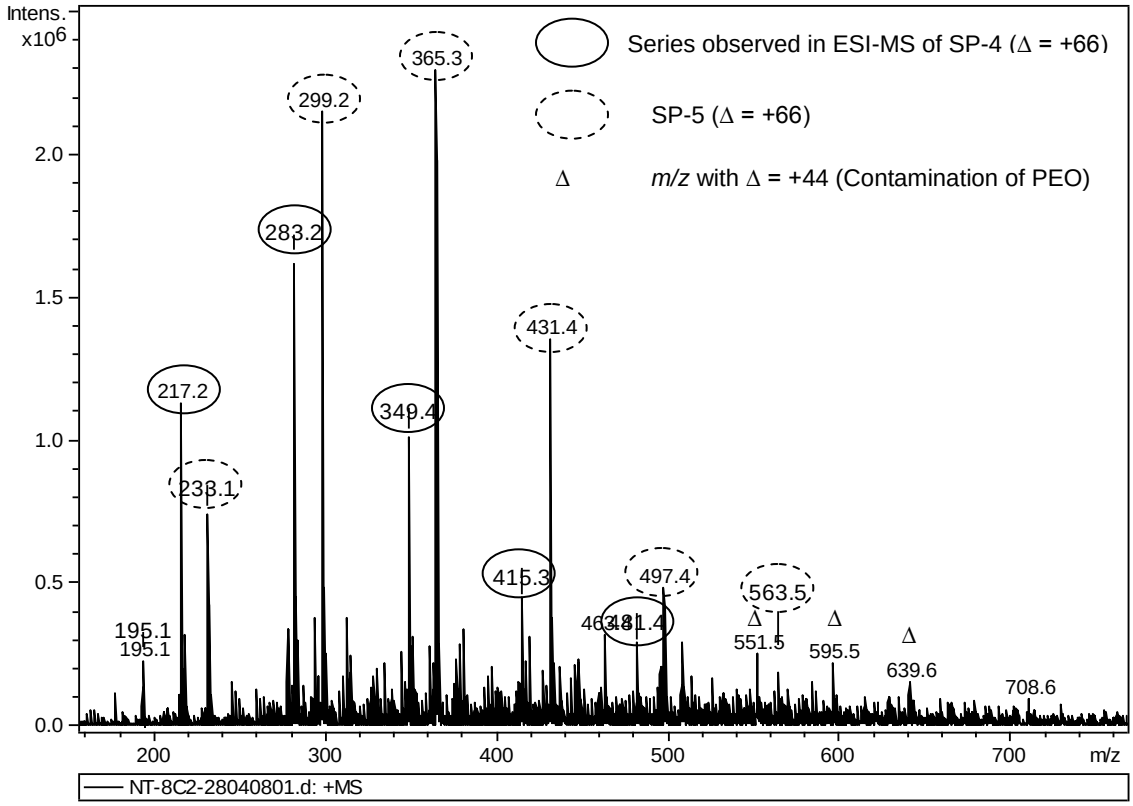

Fig. 6.19: ESI-MS of control reaction product SP-5 formed from pentynyl chloride and Li-dimsyl in DMSO; according to the structure interpretation, [M+Li] were formed in the SP-4 series (Li^+ from Li-dimsyl, see Fig. 6.13), while [M+Na] adducts dominated SP-5

To confirm that same type of side product (as observed in SP-4, SP-5) was formed during PyD synthesis, a new PyD sample (PyD-2) was synthesized under identical conditions used for PyD-1. After 48 hours, side product formed was isolated with CH_2Cl_2, washed several times with water to remove DMSO, dried over $CaCl_2$ and analyzed. ATR-IR spectrum of organic phase of PyD-2 (Fig. 6.21) is comparable to that of SP-4 and SP-5.

Thus side product was also formed during synthesis of PyD but most of its part was removed during dialysis against water. Obviously, pentynyl halides are much less pruned to side reactions than the corresponding propargyl derivatives. In case of PyCl,

oligomerisation of the reagent up to an average DP of 3-4 seems to occur and on the other hand multiple pentynylation of DMSO.

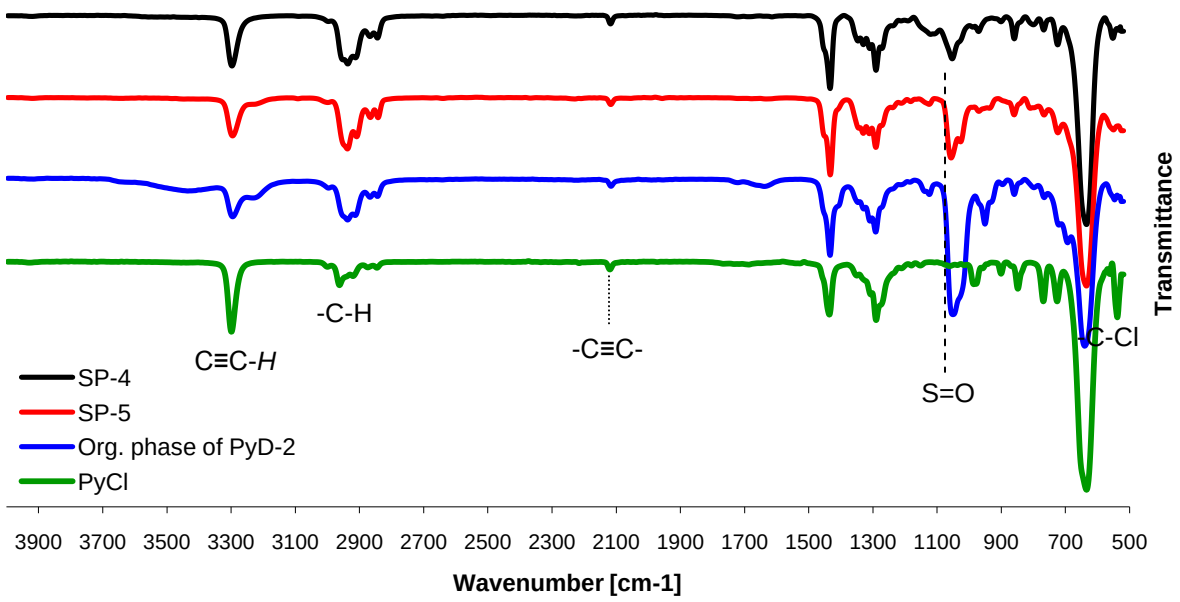

Fig. 6.20: ATR-IR spectra of side product (SP-4) isolated from pentynylation of methyl α-D-glucopyranoside, side product formed in control reaction of PyCl and Li-dimsyl in DMSO (SP-5),organic phase (isolated with CH_2Cl_2 from reaction mixture) of PyD-2 and PyCl

6.2.4 Optimization of Reaction Conditions for Synthesis of Pentynyl Dextran

To optimize other reaction parameters for PyD synthesis, a series of reactions was performed. As known from our experience with PgD synthesis, in spite of side-product formation, DMSO was proved to be a more appropriate solvent than THF, formamide or a mixture of DMSO and THF with respect to reaction efficiency. Thus, DMSO was used in nearly all PyD syntheses. Since Li-dimsyl is largely consumed prior to alkynyl halide addition and thus best allows avoiding alkali-promoted side reactions, it was employed in all reactions except one where NaOH in water was used. Most of the reactions were performed at room temperature, while only some were conducted at 70 °C. 5-Chloro-1-pentyne was kept constant at 2.0 eq./OH in all reactions. Tetra-*n*-butyl ammonium bromide (TBAB) was applied as phase transfer catalyst in some reactions but did not

show any significant effect on DS. An overview of PyD syntheses and reaction conditions is given in Table 6.12.

Part of the modified dextran precipitated during dialysis against water while the residual part remained in a dispersed state. In case of PyD-5, -7 and -16 (Table 6.12), these two parts were collected and freeze-dried separately.

From the series PyD-9 – PyD-16 it is obvious that DS did only slightly increase after 48 hrs and did not change significantly after 12 days. Deepening of yellow color indicates that formation of side product increases at prolonged reaction time. Therefore, 48 hrs was considered as suitable reaction time for PyD synthesis. Using NaOH in water also failed as it did not show any substitution. Mixtures of DMSO and THF as solvent showed relatively low DS as compared to DMSO alone.

Table 6.12: Conditions of PyD syntheses. 5-Chloro-1-pentyne was 2.0 eq./OH in all entries. Base was 1.5 eq. Li-dimsyl/OH in all reactions (except PyD-8, where NaOH was used instead)

Sample	Dextran (mg)	Solvent	Reactiontime (h)	Product(mg)	DS_{GC}
PyD-3	200.81	DMSO	24	201.55	0.15
PyD-4*	210.73	DMSO	24	210.12	0.08
PyD-5[a]	199.63	DMSO	24	30.37	0.19[b]
				197.76	0.32[c]
PyD-6*	188.32	DMSO+THF (1:1)	24	183.14	0.02
PyD-7*,[a]	205.66	DMSO+THF (3:1)	24	37.51	0.23[b]
				182.97	0.27[c]
PyD-8*	199.45	H_2O	48	195.68	0.00
PyD-9**	644.44	DMSO	48	120.12	0.45
PyD 10**			120	123.47	0.29
PyD-11**			145	112.64	0.29
PyD-12**			288	95.84	0.35
PyD-13**			388	98.33	0.35
PyD-14**			557	118.31	0.48
PyD-15**			755	110.22	0.34
PyD-16	200.70	DMSO	48	34.54	0.37[b]
				206.93	0.51[c]

a: Reaction conducted at 70 °C
b: Portion of sample which did notprecipitate in water during dialysis
c: Portion of sample which precipitated in water during dialysis
*: Tetra-*n*-butyl ammonium bromide (TBAB) was used as phase transfer catalyst (2.0 eq./OH)
** Samples withdrawn from the same reaction mixture after specific interval

Keeping in mind the reaction conditions described in Table 6.12, PyD-17 was prepared on gram scale (conditions like for PyD-1) for detailed analysis of distribution of substituents, for further functionalization and applications.

6.2.5 Characterization of Pentynyl Dextran

Since up-scaled PyD-17 was the compound employed in all further studies, its structural characterization shall be described in more detail. From all techniques applied, i.e. ATR-IR spectroscopy, NMR spectroscopy, ESI-MS, and GLC, presence of a small amount of side product was indicated. From color of the product and elemental analysis, it was expected that proportion of side product in PyD should be much lower than in PgDs. To remove the side product, Soxhlet extraction with dichloromethane (DCM) was carried out. Out of 3.098 g of PyD-17, only 37.4 mg (1.2%) could be extracted with DCM during 24 hrs. The color of the DCM-extract (PyD-17a) was yellowish brown while that of the purified PyD-17 (PyD-17b) was more whitish than starting material. Both fractions, PyD-17a and PyD-17b were further analyzed (see below).
Beside the techniques already mentioned, scanning electron microscopy (SEM) was used to characterize the product's morphology.

6.2.5.1 Infrared Spectroscopy of Pentynyl Dextran

In IR spectroscopy of dextran (Fig. 6.21), a broad absorption band at 3000-3600 cm^{-1} gives the maximum absorption corresponding to the stretching of the hydrogen-bonded OH groups and at about 2900 cm^{-1} for –CH stretching vibration of dextran while C≡C–*H* vibration from PyD appears at 3280 cm^{-1}.
ATR-IR comparison of purified PyD-17 (PyD-17b) DCM-and the extract (PyD-17a) (Fig.6.21) showed the latter also having a strong vibration at about 3280 cm^{-1}, but at the same time an absorption at ≈ 1700 cm^{-1} appears which was not present in PyD-17 before Soxhlet extraction and is not present in PyD-17b.From the results of ATR-IR analysis of PyD-17a and PyD-17b (Fig. 6.21), it is concluded that side product along with some

highly substituted product (PyD) was dissolved in CH_2Cl_2, which was further confirmed from elemental analysis (Table 6.13).

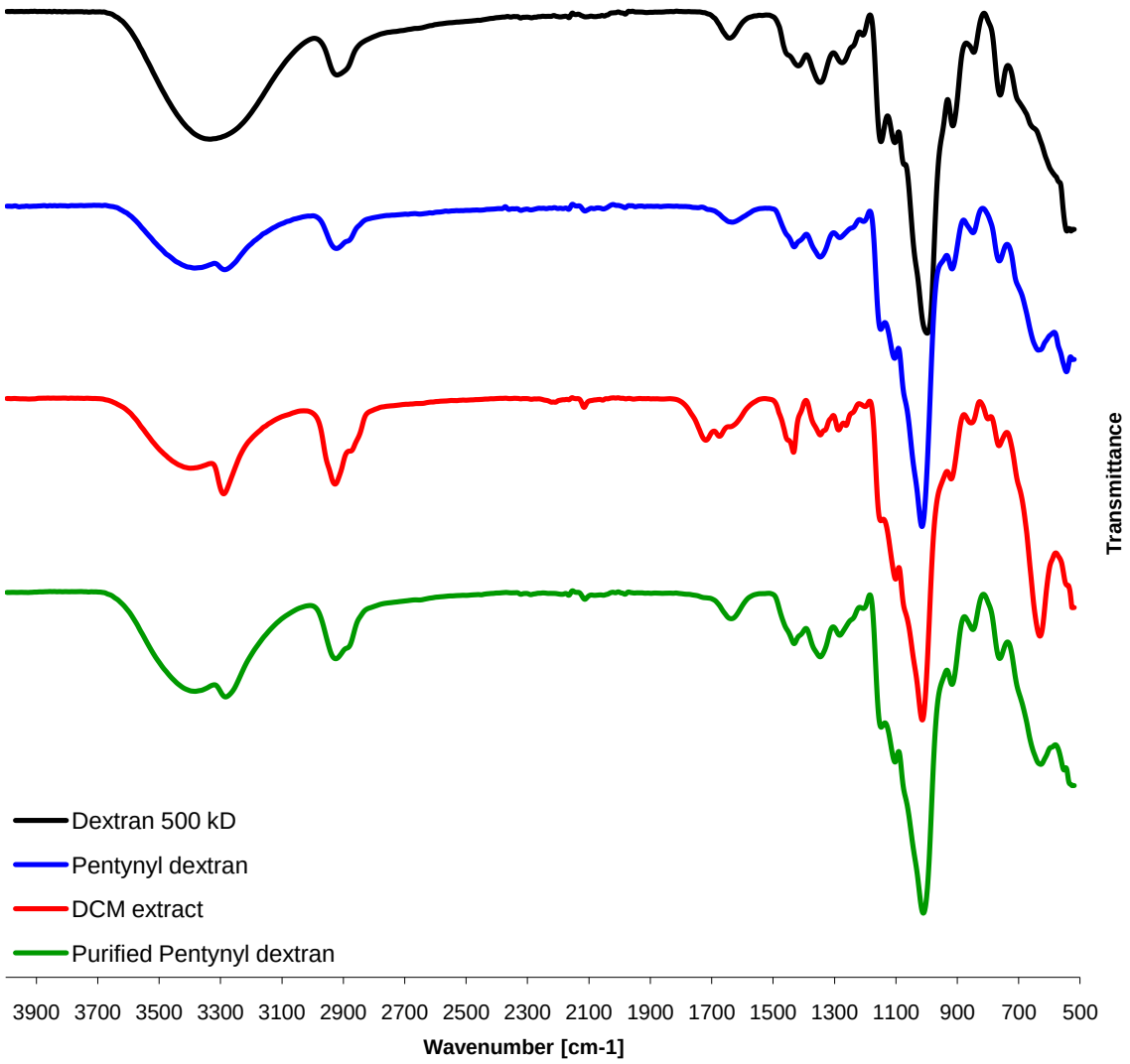

Fig. 6.21: ATR-IR spectra of dextran, raw PyD-17, DCM-extract (PyD-17-a), and purified PyD-17-b

6.2.5.2 Elemental Analysis of Pentynyl Dextran

EA (Table 6.13) of dextran (starting material), and its pentynyl derivative (PyD-17), raw product and Soxhlet-extracted batch, was used to calculate DS and to see the effect of side product. In the portion of PyD-1 dialyzed against water, 0.24% S had been detected

(Table 6.8) but, after decreasing reaction time from 72 to 48 hours, no sulfur was detected in elemental analysis of PyD-17 (Table 6.13).

Before Soxhlet extraction, the S content in PyD-17 was so low that that it was not detectable by elemental analysis but in the side-product rich fraction, S content was detectable in EA (Table 6.13). Moreover, comparison of color of DCM-extract and purified PyD-17 fractions of PyD also support this assumption.

Table 6.13: EA of dextran, PyD-17 (raw product) and after Soxhlet extraction with CH_2Cl_2

	C [%]	H [%]	C/H	S [%]	DS_{EA}
Dextran	44.43	6.22			
PyD-17 (raw product, 3.09 g)	51.82	7.06	7.34	0.00	0.48
PyD-17a (CH_2Cl_2 extract, 37.4 mg)	60.61	6.98	8.68	0.64	(1.29)*
PyD-17b (purified, 3.05 g)	51.40	6.64	7.74	0.00	0.43

* apparent DS

DS_{EA} of purified PyD-17b is 0.43, which is a realistic decrease of the DS of the raw PyD-17 (EA: 0.48, GLC: 0.43).

It is interesting to note that DS of PyD-17 calculated from monomer analysis (before Soxhlet extraction) and that of PyD-17b calculated from EA is exactly the same (0.43), while that calculated from NMR (0.62, Fig. 6.22) and EA before Soxhlet extraction (0.48) is higher. It is quite logical because elemental analysis measures only elemental content and does not care about its source, whether, it is from product or from the side product. It is almost the same with NMR spectroscopy, it measures proportion of a certain functional group and from NMR spectra of a polysaccharide, it is very difficult to distinguish whether a proton from terminal alkyne belongs to product or to side product (see 6.2.5.3) but it is not the case with GLC. In GLC, side product also shows peaks (Fig. 6.28) but it does not mix up with the peaks representing substituted sugar and does not increase DS artificially.

6.2.5.3 NMR Spectroscopy of Pentynyl Dextran

Nuclear magnetic resonance (NMR) spectroscopy, ^{1}H-NMR, of PyD-17 was recorded in DMSO-d_6, since PyD-17 was not soluble in other solvents commonly used for NMR spectroscopy. Peaks were assigned according to couplings observed in 2D-NMR

experiments. $^{1}H^{13}C$-HSQC (Heteronuclear Single Quantum Coherence) spectra show that H at 4.69 ppm (Fig. 6.22) strongly couples with C-1 of dextran, indicating that it should be H-1 (H at C-1 of glucosyl unit of dextran). Shoulders appearing downfield following the main peak of H-1 and that of OH groups probably represent the corresponding protons of 2-*O*-substituted glucosyl units. The terminal acetylenic proton of the substituent (H-11) appeared at 2.71 ppm and two of the three methylene groups were also detected separately from the sugar ring-protons at 1.69 and 2.24 ppm and thus allowed calculation of the DS.

The DS was calculated from relative intensities of H-11 and that of H-1 according to the formula:

$$DS_{Py} = \frac{\int \text{H-11}}{\int \text{H-1}}$$

DS_{Py} =0.62

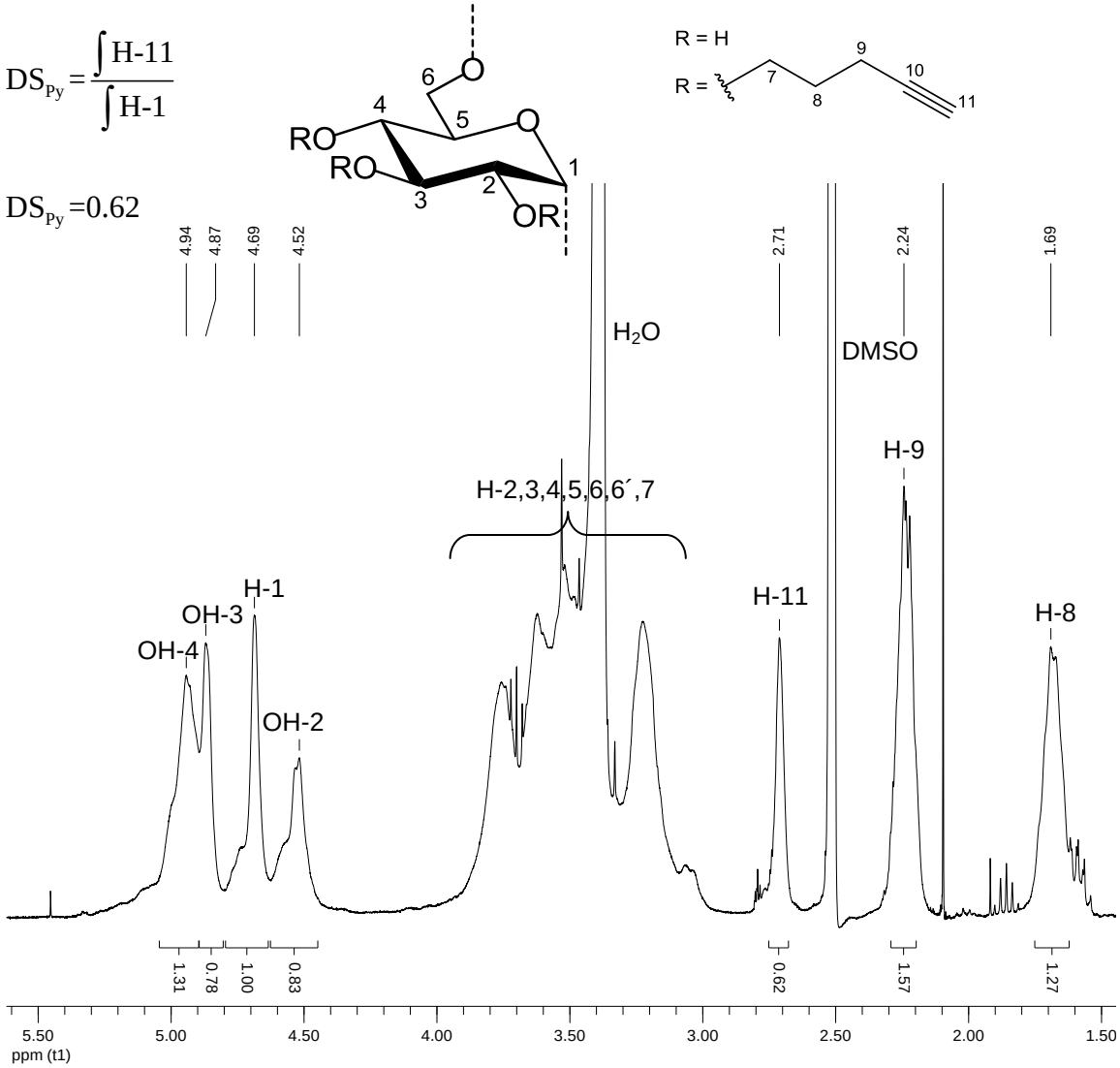

Fig. 6.22: ^{1}H-NMR spectrum of PyD-17-b (400 MHz, DMSO-d_6)

Intensity of H-11 and consequently DS was higher than expected but most probably this is due to side product present in the sample which contains terminal alkynyl residues.

When ^{1}H-NMR spectrum of the same sample was recorded in pyridine (Fig. 6.23), all peaks were shifted a little bit downfield, and a very broad peak appeared at 6.08 ppm corresponding to OH-2, OH-3 and OH-4. Such peak broadening is typical in NMR proton spectra for O-H or N-H resonances (here only O-H is concerned).

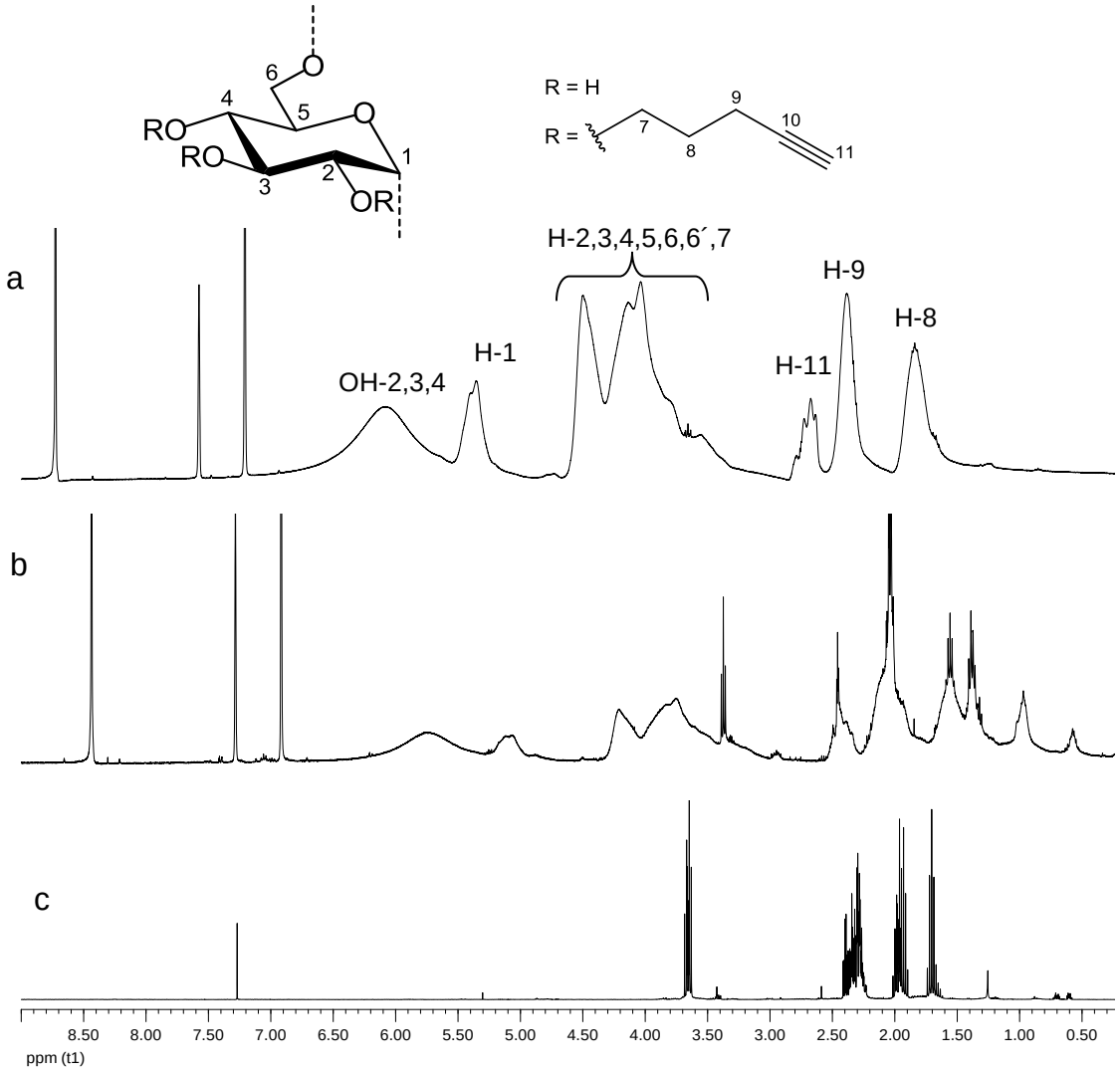

Fig. 6.23: ^{1}H-NMR spectra of PyD-17, raw product (a), DCM-extract (PyD-17a), obtained by Soxhlet extraction of PyD-17 (b) (300 MHz, pyridine-d_5) that of control reaction (c) (400 MHz, $CDCl_3$)

Comparison of NMR of raw PyD-17 and PyD-17a shows three additional peaks between 0 and 3 ppm for the latter (Fig. 6.23). In addition, shape and relative intensities of former

visible three pentynyl representing signals in this area have changed. Probably the more narrow signals "on top" of the broad ones are related to the lower molecular mass side product, indicating that its chemical structure is similar to pentynyl derivatives.
Comparison of ^{1}H-NMR spectra of the product of control reaction (see 6.2.3) and that of PyD-17a (Fig. 6.23) shows that DCM-extract (PyD-17a) contains a reasonable amount of side product along with PyD.

6.2.5.4 ESI-MS of Pentynyl Dextran

In electrospray ionization, a liquid solution of analyte is passing through a nozzle. The solution leaving the capillary is sprayed into the plume of charged micro droplets because of the difference in applied voltage between the tip of the sprayer and inlet of a small internal-diameter capillary transfer tube located a few millimeter away [197]. The solution fed to the needle is normally drawn into a liquid cone (so-called Taylor cone) by the applied potential (Fig. 6.24).

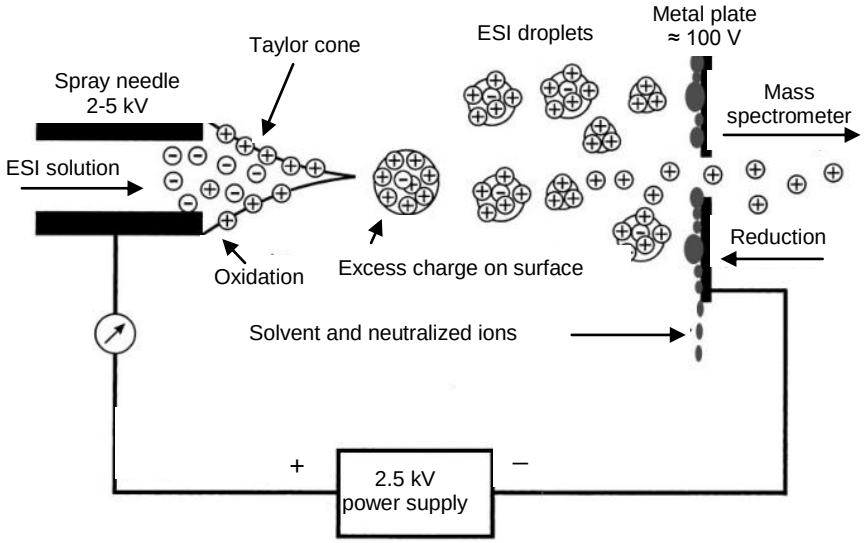

Fig. 6.24: Schematic representation of electrospray ionization (adopted from [198])

For ESI-MS, PyD-17 was submitted to methanolysis and the residue obtained after evaporation of MeOH/HCl was dissolved in MeOH. Mass spectrum (Fig. 6.25) shows *m/z* values for sodiated un-, mono-, di- and tri-substituted methyl glucosides (DP1) and

disaccharides (DP2) from pentynyl-dextran. Along with expected masses, some unexpected masses e.g. masses for tetra- (*m/z* 481.3) and penta-PyD (*m/z* 547.4) etc. were also observed. Tetra-*O*-pentynyl glucoside is at least theoretically possible due to terminal groups while, a pentasubstituted glucoside would only be possible by tandem-reaction of the terminal alkynyl residues. However, there are no indications for such a nucleophilic reaction from GC analysis. However, it was found that the side product gives a series of products with Δ 66 and *m/z* values, that by accident coincide with those of methyl glucosides (see 6.2.3, Fig. 6.13 and 6.19).

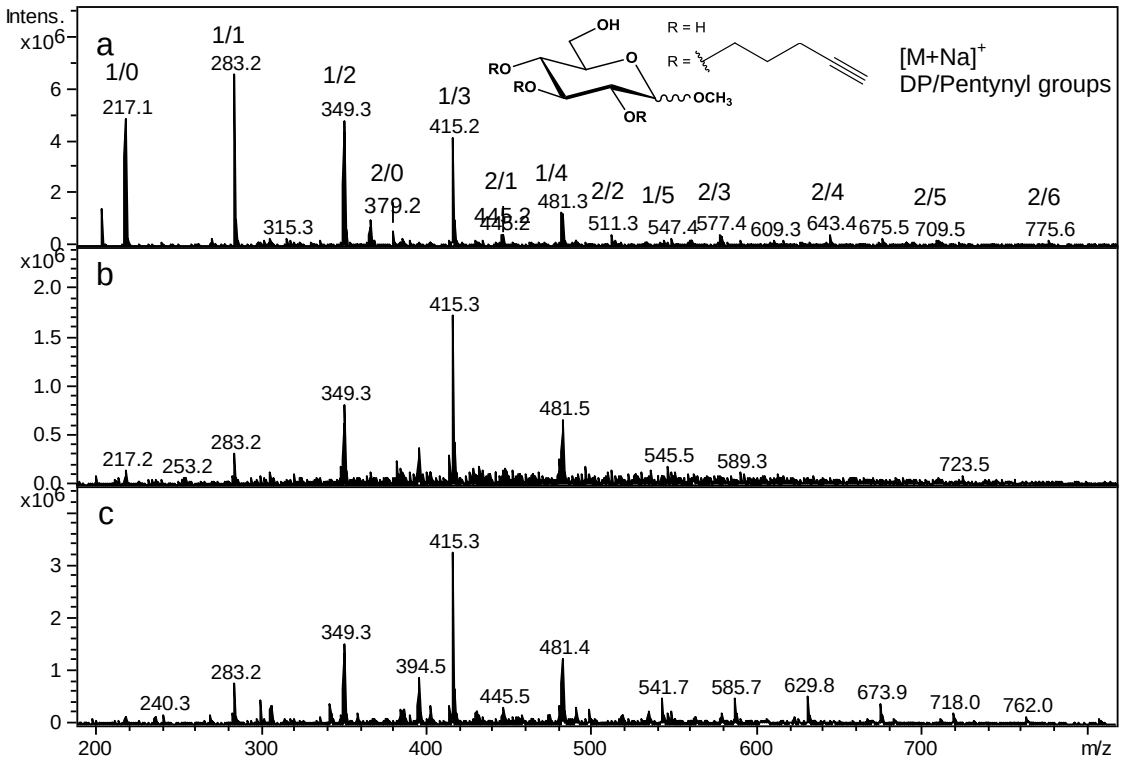

Fig. 6.25: ESI-MS of PyD-17 (raw product) (a), CH_2Cl_2 extract (b) and purified PyD-17b (c) after methanolysis under the same conditions for all samples. Signals area assigned according to DP and n times Δ66 (Py)

ESI-MS spectra of raw (PyD-17), purified (PyD-17b) and its DCM-extract (PyD-17a) from Soxhlet extraction (Fig. 6.28), all show signals at *m/z* 217, 283, 349, 415, 481, and 547 which are in accordance with sodium adducts of mono-, di-, tri-,tetra-, and penta-*O*-pentynyl methyl. Signals at *m/z* 511, 577, 643, 709 and 775 respectively corresponding to disaccharides with 2- 6 pentynyl groups in raw sample show that methanolysis was

incomplete. Signals at *m/z* e.g. 541, 585, 629, 673, 718, 762, 806 etc. with Δ (*m/z*) = 44 are caused by a contamination with polyethylene oxide $–(CH_2\text{-}CH_2\text{-}O)_n\text{-}$.

ESI-MS spectra of PyD-17a and PyD-17b look very similar. Obviously, the products from high pentynylated dextran extracted (corresponding to less than 1% of total PyD) dominate the mass spectrum. In addition, it was found that the fresh side product by chance gave the same *m/z* values with a Δ+66 pattern, corresponding to various numbers of pentynyl groups incorporated. NMR (see 6.2.3., Fig. 6.13, 6.19) and EA of the extract (Table 6.13) also strongly indicate that major portion of DCM-extract consists of side product. Most probably, molecular weight of side product was very high and it was not possible to detect it by ESI-MS but it contributes in EA and NMR spectrum.

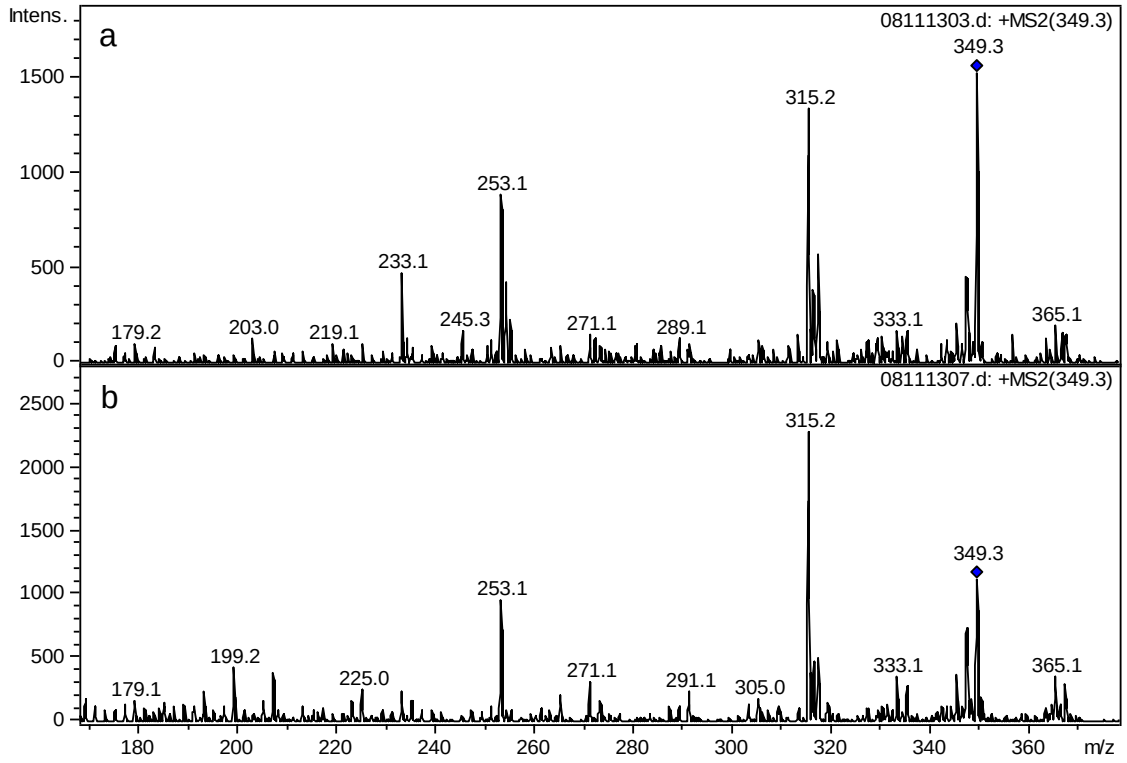

Fig. 6.26: Fragmentation of *m/z*349 (corresponding to DP1/Py_2) from Fig. 6.25) in the methanolysate of the DCM-extract (a) and purified (b) PyD-17-b

Fragmentation of *m/z* 349 and 415 (Fig. 6.26, 6.27) from both, the methanolysate of the DCM-extract and of the purified PyD-17-b, by collision induced dissociation (CID) gave very similar mass spectra. However, it is known that sodium adducts of monosaccharides [199] give very poor fragmentation, since dissociation under loss of the counter ion

occurs at the high energy required. Therefore, Li-adducts are usually preferred. The CID spectra in Figs. 6.29 and 6.30 show very uncommon fragmentations (M-2, -34, -96) which are not in agreement with sugar fragmentation [200]. Surprisingly, fragmentation of *m/z* 349 produces *m/z* 365, which is only possible, if the mother ion was double-charged (which is not the case) or in this case might be explained by comprising Na- and Li-adducts of various compounds, which can exchange the counter ion during fragmentation. This could explain the partial "disproportionation" to *m/z* 333 and 365. Apparent M-2 could than be interpreted as M-18 of *m/z* 365. Corresponding M+16 is not visible in MS^2 of the homolog *m/z* 415 (Me-glc-Py_3), but apparent M-2.

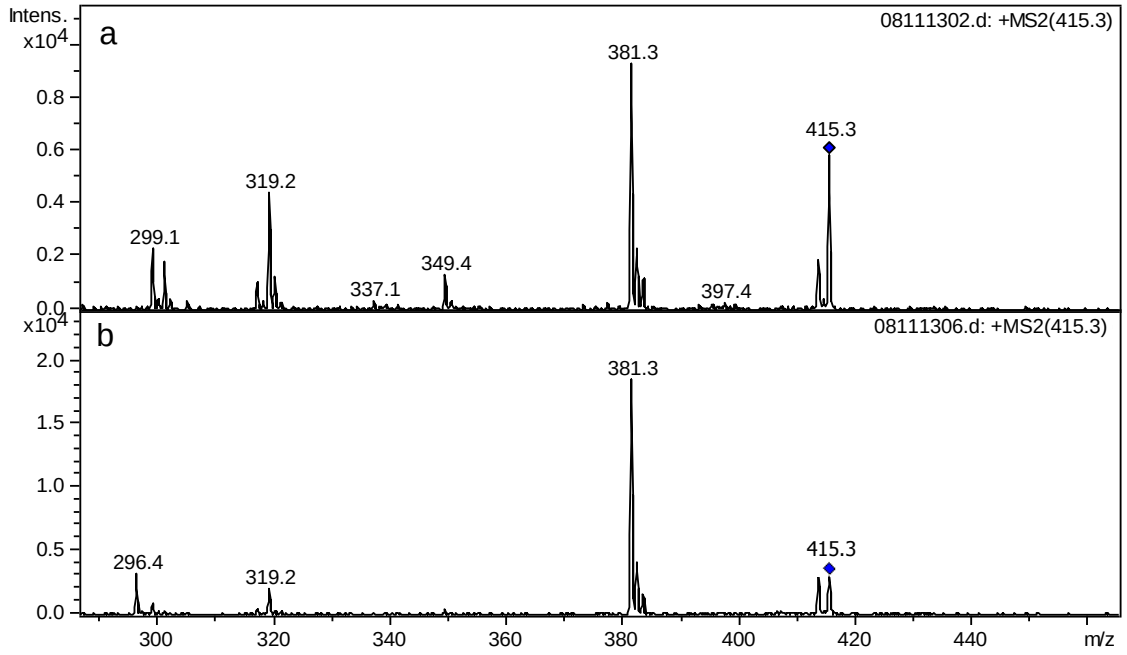

Fig. 6.27: Fragmentation of *m/z* 415 (corresponding to DP1/Py_3) (from Fig. 6.25) in the methanolysate of DCM-extract (a) and purified (b) part of PyD-17.

6.2.5.5 Monomer Analysis of Pentynyl Dextran

Monomer analysis of PyD was carried out using gas liquid chromatography (GLC) after methanolysis and trimethylsilylation. Peaks were assigned using GC-MS.

It is common in polysaccharide analysis to reduce monosaccharide obtained by hydrolysis with $NaBH_4$ to avoid multiple peaks due to α- and β-glycosides for each substitution pattern. However, in case of PyD, this was not possible because, triple bond

in pentynyl does not remain unaffected during reduction. Therefore, formation of two peaks i.e. one for α and one for β glucoside, were accepted. Fortunately, glucose does not tend to form furanosides too, but since substitution also influences equilibria of α,β-pyranosides and furanosides, formation of minor amounts of the latter cannot be excluded. The gas chromatogram with peak assignments according to the pentynyl positions is shown in Fig. 6.28.

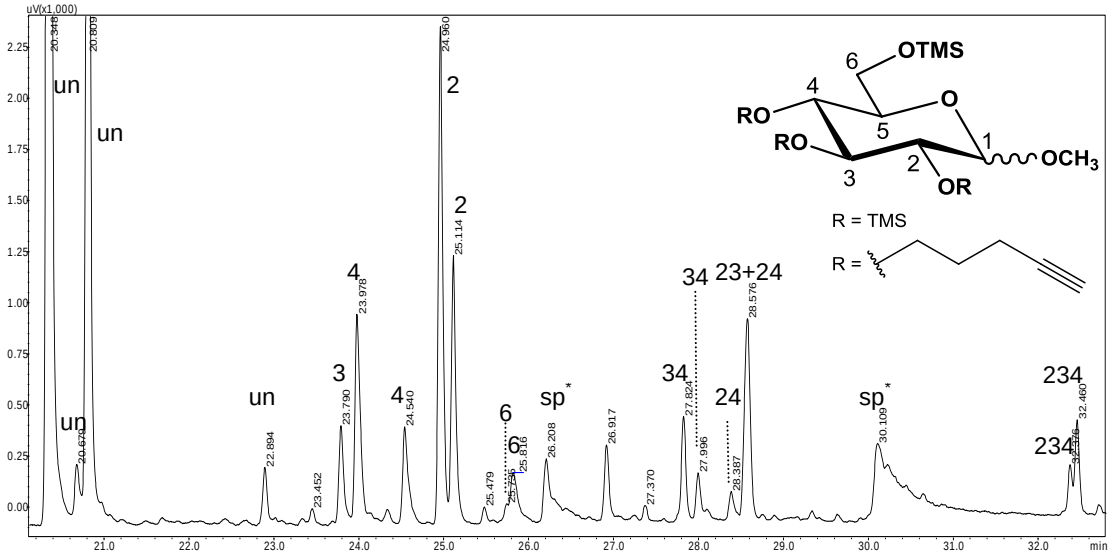

Fig. 6.28: Gas chromatogram of raw PyD-17 (DS_{GC}: 0.43) after methanolysis and trimethylsilylation, column: zebron ZB 5 (5% phenylmethyl polysiloxan), carrier gas: He, temperature program: 60 °C (1 min) - 20 °C/min 130 °C - 4 °C/min 290 °C (10 min) - 20 °C/min 310 °C (10 min).
* from side product

The number and location of substituents in the methyl *O*-trimethylsilyl-*O*-pentynyl-D-glucosides were deduced from the EI-mass spectra (GC/MS). Fragmentation of methyl glucosides is well known [201]. Therefore, position of alkynyl groups can be deduced from characteristic fragment shifts, as has been described by Tankam *et al*. for propargylated glucosides [150].

Along with expected peaks for un-substituted glucosides and pentynyl derivatives, some additonal peaks were observed in the gas chromatogram. Peaks at 25.47 and 26.91 minutes (Fig. 6.28) appeared due to 1-*O*-TMS derivative of glucopyranosides (caused by humidity in MeOH/HCl). Two little peaks at 25.73 and 25.81 min. are due to mono-substitution at *O*-6 at terminal glucosyl residues in dextran. (In some samples of PyD, di-

substituted glucosides involving 2,6-di-*O*-pentynyl were also observed just after 28 minutes but in most cases, its intensity was too low to detect it.)

In the gas chromatogram of PyD-17 (Fig. 6.28), there is only one peak for 3-*O*-Py-glc (23.79 min), while its second peak coincides with 4-*O*-Py-glc (23.97 min). Second peak of 2,4-*O*-Py-glc and both peaks of 2,3-*O*-Py-glc were also not separated (28.57 min). Area for second peak of 2,4-*O*-Py-glc was subtracted from the peak at 28.57 min, after estimating its amount according to the α,β-ratio of 3,4-*O*-Py-glc. The remaining peak area was divided in two peaks of 2,3-*O*-Py-glc in the same way.

Table 6.14: Retention times of monomer derivatives obtained from PyD-17 by methanolysis and trimethylsilylation (GC conditions: seeFig. 6.28 and Experimental)

Ret. Time (min)	**Pentynyl in passion**
20.348	un (α / β)
20.809	un (α / β)
23.790	3 (α / β)
23.978	4 (α / β)
24.540	4 (α / β)
24.960	2 (α / β)
25.114	2 (α / β)
25.735	6 (α / β)
25.816	6 (α / β)
27.824	34 (α / β)
27.996	34 (α / β)
28.387	24 (α / β)
28.576	23 + 24 (α / β)
32.376	234 (α / β)
32.460	234 (α / β)

Peaks at 26.20 and 30.10 min. refer to side product, as is obvious from the reduction of these peaks after purification of PyD (Fig. 6.29). Comparison of gas chromatograms of PyD-17a and PyD-17b (Fig. 6.29) confirms that most of the side product was dissolved in CH_2Cl_2 during Soxhlet extraction. Intensity of peaks at 26.92 and 30.11 min., which were much prominent in raw PyD-17, is very low intensity in PyD-17b while its intensity have multiplied in PyD-17a (Fig. 6.29).

Comparison of the results of monomer analysis of PyD-17a and PyD-17b (Table 6.15) does not show much difference between two fractions. Total DS, partial DS at different

substitution positions and heterogeneity is comparable except relatively higher proportion of tri-substituted PyD in PyD-17a but they differ from monomer analysis of raw PyD-17.

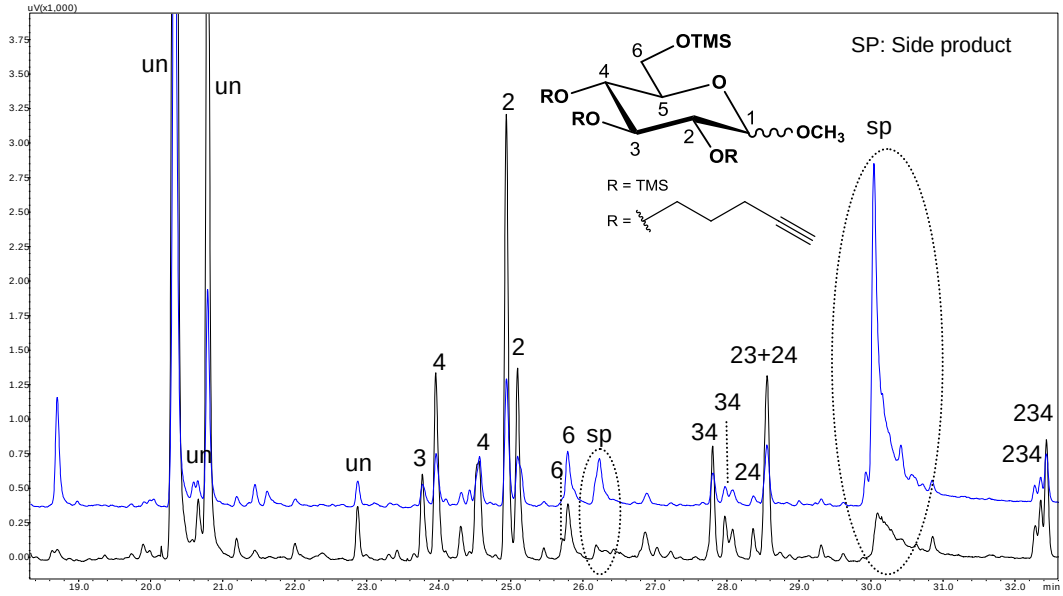

Fig. 6.29: Gas chromatograms of methyl-*O*-pentynyl-*O*-TMS-glucosides obtained from DCM-extract (blue, upper, DS: 0.44) and purified PyD-17 (black, lower, DS: 0.43) fractions of PyD-17. For GC temp. program, see Fig. 6.28 and Experimental

Table 6.15: Monomer composition (Mol%) of raw PyD-17, its DCM-extract (PyD-17a) and purified PyD-17 (PyD-17b).

Sample / Position	Raw PyD-17		DCM-extract (PyD-17a)		Purified (PyD-17b)	
	Experimental	**Random**	**Experimental**	**Random**	**Experimental**	**Random**
s_0	70.06	62.50	70.37	62.09	71.28	63.71
s_2	11.54	14.74	11.65	14.97	11.53	15.03
s_3	1.64	6.34	1.36	6.60	1.75	6.18
s_4	6.73	10.97	6.51	10.74	5.48	10.04
s_{23}	1.83	1.49	1.87	1.59	1.83	1.46
s_{24}	2.46	2.59	1.87	2.59	2.86	2.37
s_{34}	2.48	1.11	2.33	1.14	2.40	0.97
s_{234}	3.25	0.26	4.04	0.28	2.87	0.23
DS	**0.43**	**0.43**	**0.44**	**0.44**	**0.43**	**0.43**
c_0	70.06	62.50	70.37	62.09	71.28	63.71
c_1	19.92	32.04	19.52	32.31	18.76	31.26
c_2	6.77	5.19	6.09	5.32	7.09	4.80
c_3	3.25	0.26	4.04	0.28	2.87	0.23
x_2	0.19	44.2%	0.19	44.4%	0.19	45.9%
x_3	0.09	21.3%	0.10	21.9%	0.09	21.3%
x_4	0.15	34.5%	0.15	33.7%	0.14	32.8%
***H*$_1$**	**10.87**		**11.9**		**10.9**	

Comparison of DS of PyD before and after Soxhlet-extraction, calculated from monomer analysis and from EA (Table 6.16) shows, that actual DS of the sample is 0.43 and that almost all side product present in PyD was collected in DCM-extract (PyD-17a). Apparently higher DS of PyD-17a (1.29) calculated from EA is just due to relatively higher C content in the side product formed.

Table 6.16: comparison of DS calculated from EA and GC of PyD-17 before and after Soxhlet extraction

	DS_{EA}	DS_{GC}
PyD-17 (Raw product)	0.48	0.43
PyD-17a (DCM-extract)	(1.29)	0.44
PyD-17b (Pure)	0.43	0.43

All these results have confirmed that side product was formed during synthesis of *O*-pentynyl dextran but most of its part was removed during dialysis. Soxhlet extraction with DCM is successful method to purify the product. Gas chromatogram (Fig. 6.29) indicates that side product is still present in the *O*-pentynyl dextran, but its content is strongly reduced.

Purified *O*-pentynyl dextran was used for complexation of metals ions (chapter 7), further functionalization e.g. in click-reactions (chapter 8), and in direct applications e.g. for immobilization of enzymes (chapter 9).

6.2.6 Fractionation of Pentynyl Dextran

Monomer analysis of PyD had shown an unexpected strong deviation from the random pattern, calculated from the partial DS-values. This high heterogeneity most probably is caused by a DS gradient in the material. For better understanding of distribution of substituents in *O*-pentynyl dextran in the unit, within the polymer chain or among the polymer chains, it is necessary to fractionate the material e.g. according to polarity or on the basis of other factors e.g. length of polymer chains. The Soxhlet extraction had been applied successfully for purification of the *O*-pentynyl dextran, so same technique was applied for its fractionation.

6.2.6.1 Fractionation of Pentynyl Dextran by THF

It was tried to fractionate PyD-17 on the basis of its solubility in THF. Soxhlet extraction with THF was carried out for 24 hours. Unexpectedly, the entire material was finally dissolved in THF. Therefore, this method was not appropriate for fractionation of PyD.
It was tried to reduce solubility by treating PyD-17 in THF at room temperature. After stirring for 3 days, 24 mg (14%) out of 169 mg of raw material had been dissolved. THF-soluble and -insoluble fractions were separated by filtration. Soluble portion was a sticky yellow-colored solid while the insoluble fraction was a white solid. Color, physical appearance and monomer analysis of both fractions of PyD-17 (Fig. 6.30, Table 6.17) show that a little fraction of side product that was not removed by Soxhlet extraction with CH_2Cl_2 was dissolved in THF along with some higher substituted *O*-pentynyl dextran.

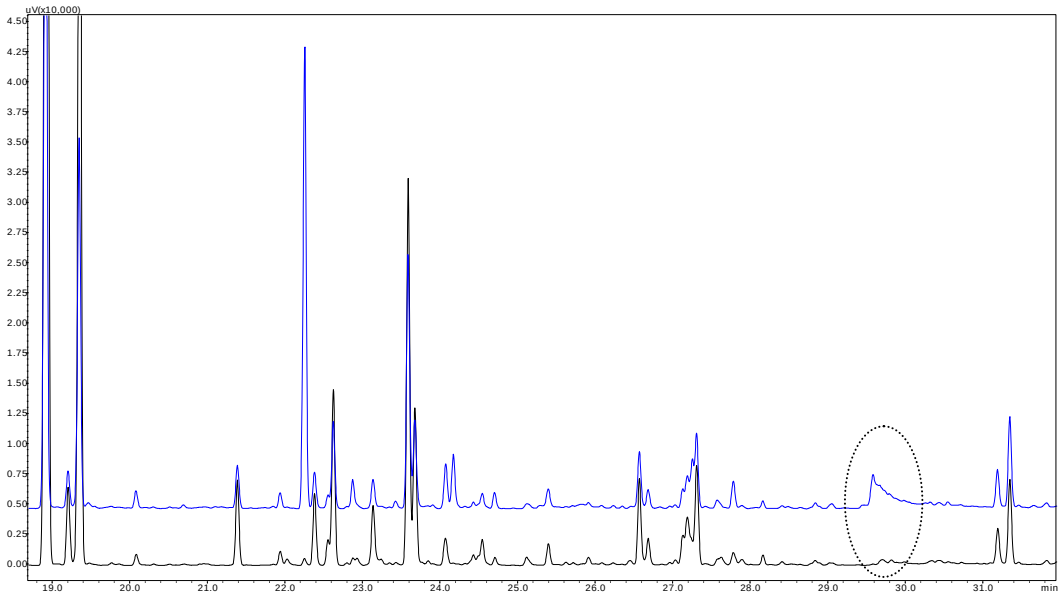

Fig. 6.33: Monomer analysis of cold-THF-soluble (blue, upper, 14%) and -insoluble (black, lower, 86%) fractions of PyD-17 after methanolysis and trimethylsilylation. For GC temp. program, see Fig. 6.28 and Experimental

Monomer analysis of THF soluble and insoluble fractions (Table 6.17) gave DS of 0.59 and 0.35, and heterogeneities H_1 of 14.8 and 9.8, respectively. Gas chromatogram (Fig. 6.31) of both fractions show that the soluble portion contains the characteristic peaks caused by side product (compare Fig. 6.28, 6.29). Proportion of tri-substituted

O-pentynyl glucoside units is much higher in the THF-soluble fraction than in the insoluble fraction but relative portions of *O*-2, *O*-3 and *O*-4-substitution (x_i in %) are comparable in both fractions.

Calculating the average DS from both weighted fractions gives 0.39 which is close to the original DS of 0.43.

Table 6.17: Monomer composition of cold-THF-soluble and -insoluble fractions of PyD-17

Sample / Position	THF Soluble		THF Insoluble	
	Experimental	**Random**	**Experimental**	**Random**
S_0	61.57	51.53	75.61	69.14
S_2	15.45	19.42	10.10	13.23
S_3	2.30	9.92	1.79	7.08
S_4	5.37	9.38	4.49	7.01
S_{23}	5.29	3.74	3.31	1.35
S_{24}	1.47	3.53	0.52	1.34
S_{34}	3.39	1.80	2.05	0.72
S_{234}	5.16	0.68	2.14	0.14
DS	**0.59**	**0.59**	**0.35**	**0.35**
C_0	61.57	51.53	75.61	69.14
C_1	23.13	38.71	16.37	27.31
C_2	10.15	9.07	5.87	3.41
C_3	5.16	0.68	2.14	0.14
X_2	0.27	46.5%	0.16	46.5%
X_3	0.16	27.4%	0.09	26.9%
X_4	0.15	26.1%	0.09	26.6%
H_1	**14.8**		**9.8**	

7 COMPLEXATION OF PENTYNYL DEXTRAN WITH METALS

7.1 Complexation of Pentynyl Dextran with Silver

It is well known that terminal alkynes can complex various metal ions. Avny *et al*. [160]tested propargylated cellulose membranes for the binding of various metal salts. Mercury, aluminium, and silver were bound efficiently as estimated from weight gain which for silver corresponded to a molar ratio of 0.8 :1 (Ag to C≡CH) . Therefore, PyD-17 (DS 0.43) was dialyzed against $AgNO_3$ solution under exclusion of light and washed several times to remove unbound salt, and subsequently freeze-dried. Slightly pink product was formed which was analyzed by elemental analysis, inductively coupled plasma optical emission spectroscopy (ICP-OES), ATR-IR spectroscopy and transmission electron microscopy (TEM).

Table 7.1: Silver complexation with PyD-17. –Elemental composition (w/w %)

	C [%]	H [%]	C/H	Ag [%][1]	Ag [%][2]
PyD-17 (DS 0.43)	51.40	6.64	7.74		
PyD-17-Ag	38.72	5.18	7.47	23.3	24.5

1 Determined by ICP-OES
2 Calculated from EA (C/H) difference to 100%

Elemental analysis of freeze-dried material corresponds with a PyD content of 75.5% in the product which corresponds well with an Ag content of 23.3 g per 100 g of the product, determined by ICP-OES after hydrolysis with nitric acid (Table 7.1).

Molar ratio of Ag/C≡CH is 1.3:1 which might indicate not only roughly stoichiometric 1:1 Ag/C≡C complexation but a more complex structure. Chen *et al*. [202] have prepared ribbon like structure of cationic complex $[Ag_3(C{\equiv}CBu^t)_2]^+$ from [BuC≡CAg] and $AgBF_4$, while Abu-salah *et al*. [203] have reported $[Ag_{14}(C{\equiv}CBu^t)_{12}]^{2+}$using a different ratio of [BuC≡CAg] and $AgBF_4$.

Exposure of a small amount of the material to light produced a red-brownish material. Since it is known that silver nanoparticles absorb light in the range of 380-450 nm due to surface plasmon excitation [204], the slightly reddish color probably indicates the formation of silver particles.

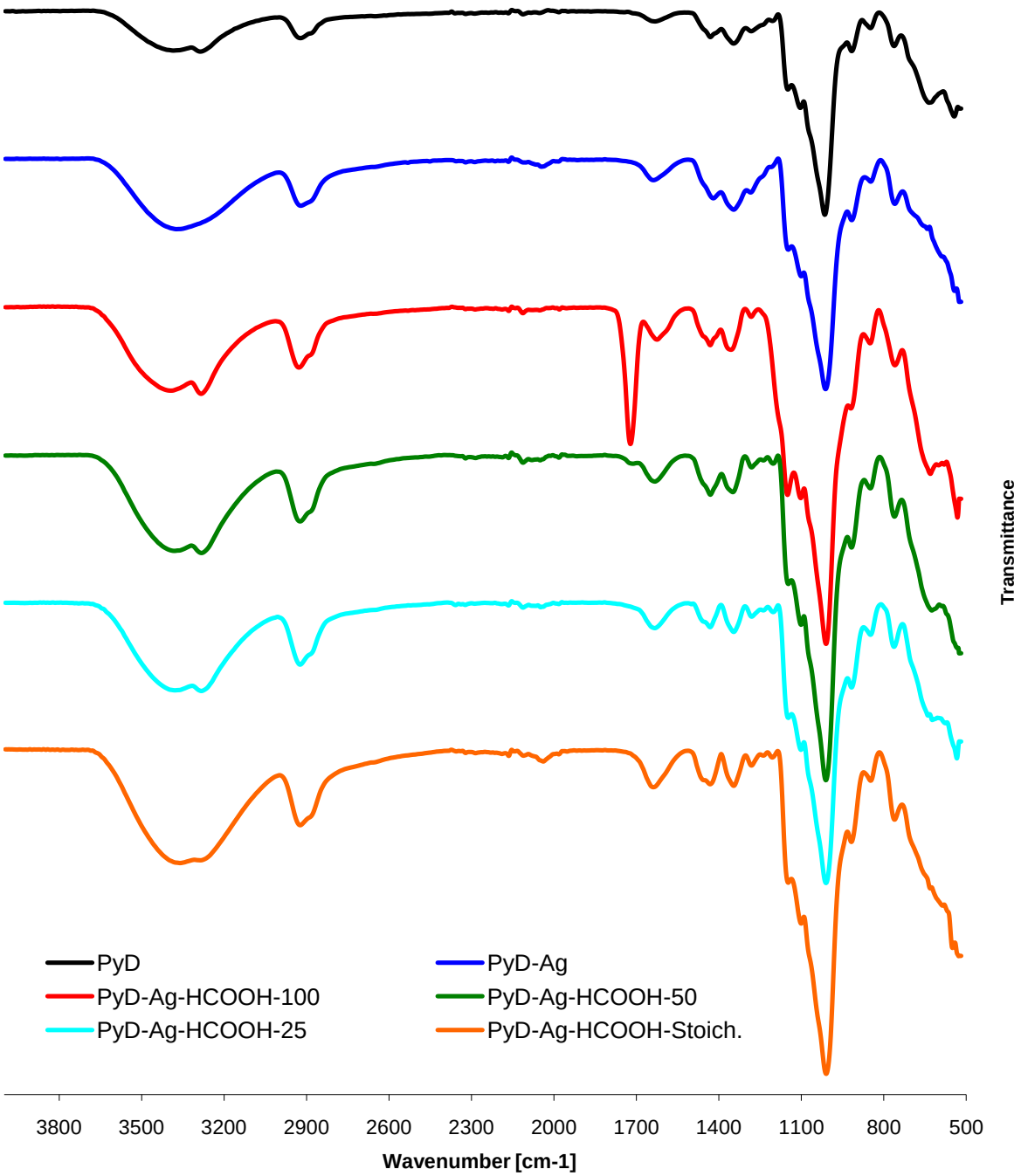

Fig. 7.1: Comparison of ATR-IR spectra of PyD-17, PyD-17-Ag before and after treatment with 100%, 50%, 25% and stoichiometric amount of formic acid

In the ATR-IR spectrum of PyD-17-Ag, the C≡C–*H* vibration had disappeared, indicating the formation of alkynyl silver salt. Treatment with concentrated formic acid for reduction of Ag^+ gave a slightly colored clear solution. Beside the regenerated terminal

alkyne vibration at 3280 cm^{-1}, ATR-IR spectrum of the dialyzed and freeze-dried product showed *O*-formylation of dextran (*C=O* at 1716 cm^{-1} in Fig. 7.1).

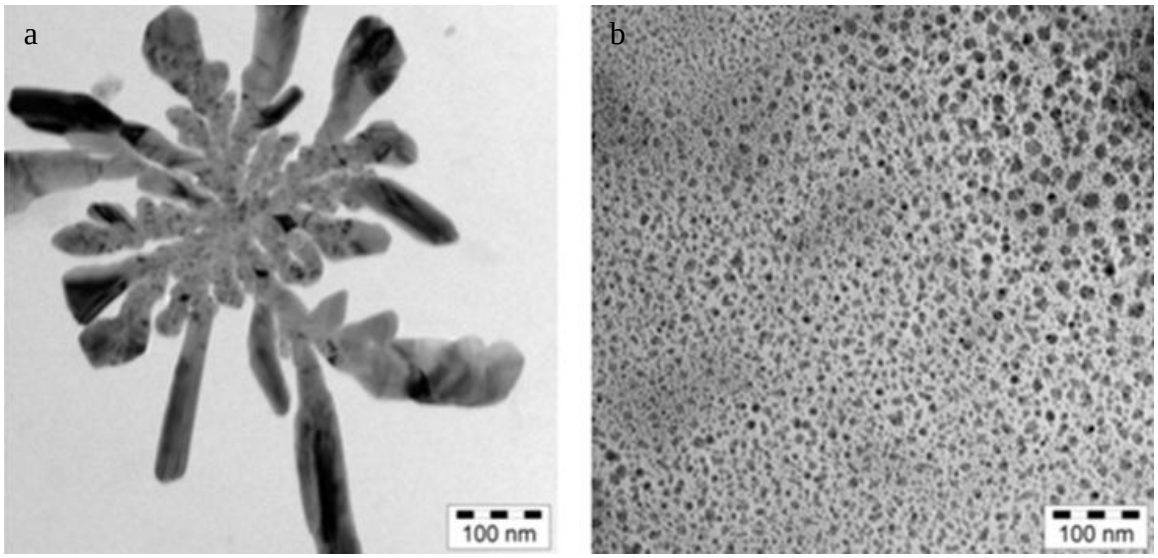

Fig. 7.2: TEM images of PyD-17-Ag prepared from suspension in water (a) and after reduction with formic acid (b)

TEM of PyD-17-Ag displayed star-shaped dendritic structures with black domains (Fig. 7.2). Since the freeze-dried sample was suspended in water to deposit it on the carbon grid, artifact formation during drying can not be excluded. However, silver acetylide is not water soluble and all water soluble low molecular weight material was removed during dialysis against demineralized water. SEM micrographs (Fig. 7.3) show spherical shape of particles for PyD-17-Ag. Therefore, the origin of the star-shaped Ag-rich particles with an extension of a few hundred nm, can not be elucidated unambiguously at present. In contrast, the TEM image of the formic acid-reduced sample showed a uniform distribution of small Ag nanoparticles, about 4-10 nm in diameter (Fig. 7.2). These probably result from the disintegration of the compact dextran structure due to formylation of OH groups, which is also evident from ATR-IR spectrum (Fig. 7.1).

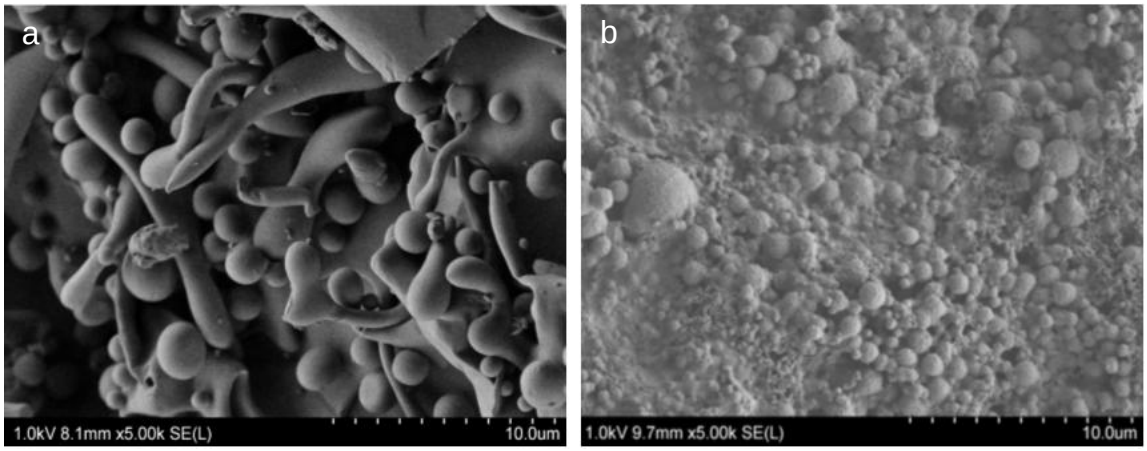

Fig. 7.3: SEM images of PyD-17 (DS 0.43) (a), and PyD-17-Ag (b) obtained by dialysis from DMSO solution of PyD-17 against $AgNO_3$ in water

7.2 Complexation of Pentynyl Dextran with Iron

After successful complexation of silver ion with PyD, dialysis experiment was performed against iron salt solutions (Fe^{2+}, Fe^{3+}). Unmodified dextran ($\overline{M}_w$ 500 000) and its pentynyl derivative (PyD-17) was dissolved in DMAc and dialyzed against $FeCl_3$ solution in water. Before freeze-drying, the samples were exhaustively dialyzed against demineralized water to remove unbound iron. Elemental analysis did not show any iron complexation for unmodified dextran or its pentynyl derivative (Table 7.2). Thus, in contrast to silver, iron did not show any complexation with PyD.

For further studies, PyD-17 was peracetylated with acetic anhydride and pyridine in formamide ($HCONH_2$). Dialysis of peracetylated pentynyl dextran (PyAcD) against of $FeCl_3$ solution in water produced an ochrous-brownish product while water outside the dialysis remained colorless. Iron content of the freeze-dried product was 9.44 g per 100 g of material (Table 7.2). This corresponds to about 13.5% Fe_2O_3. The molar ratio of Fe/AGU was 0.5–0.6, corresponding to 1.2–1.3 for Fe/C≡CH. For comparison and to confirm that iron oxide was not simply the product of pH-dependent dehydration and precipitation, beside unmodified dextran, dextran triacetate (AcD, DS 3.0) was prepared and also dialyzed against $FeCl_3$ in water under the same conditions. Product was colorless and elemental analysis did not show any reasonable change (Table 7.2). Thus unlike Ag complexation with PyD, both alkynyl and acetyl groups are required for efficient iron

binding and might cooperate. SEM images of PyAcD-17 without and with iron (Fig. 7.4) no longer show spherical structures like for PyD (Fig. 7.3).

Table 7.2: EA of dextran and its derivatives before and after dialysis against $FeCl_3$ solution in water

	C [%]	**H [%]**	**Fe [%]**[1]	**Fe [%]**[2]
Dextran	44.43	6.22		
Dextran-Fe	41.77	6.63		
PyD-17	51.40	6.64		
PyD-17-Fe	50.90	7.01		
AcD	49.23	5.53		
AcD-Fe	49.52	5.55		
PyAcD-17	55.23	5.90		
PyAcD-17-Fe	46.78	5.24	9.44	7.6
PyAcD-17-Fe[3]	46.91	5.33		7.3

1 Determined by ICP-OES
2 Calculated from EA (C/H)
3 Repeated experiment

A similar experiment with $FeCl_2/FeCl_3$ in a 1:1.5 molar ratio to give Fe_3O_4 ($FeO \cdot Fe_2O_3$) performed under nitrogen gave a relatively darker product. The product showed superparamagnetic properties during and after dialysis against water. Paramagnetic properties however, were lost after freeze-drying. The iron content determined by ICP-OES was 13.0 g per 100 g of the material corresponding to 18.0 g per 100 g when calculated as Fe_3O_4 (Table 7.3).

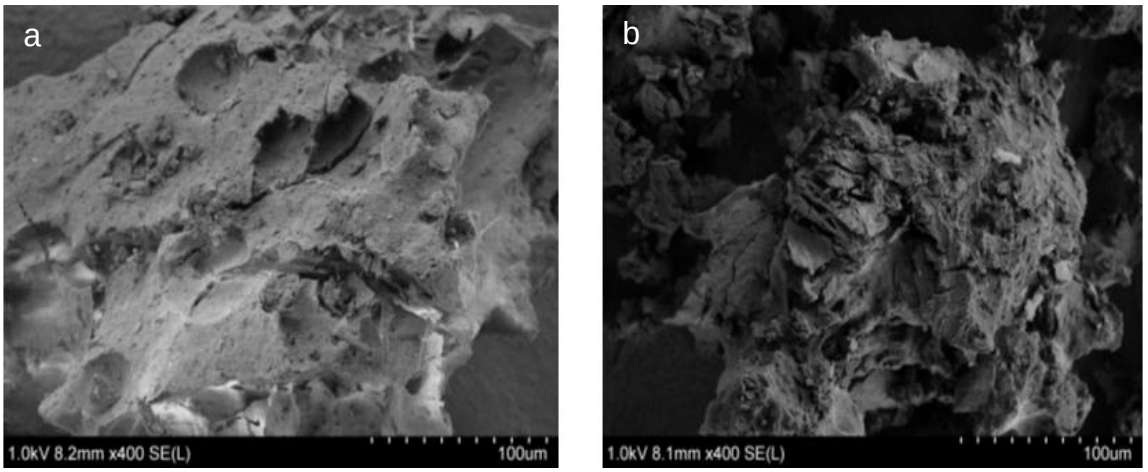

Fig. 7.5: SEM image of PyAcD (DS_{py} = 0.43, DS_{Ac} = 2.57) dialyzed from pyridine solution against water (a) and PyAcD-Fe (b) dialyzed from DMAc solution against aqueous $FeCl_3$ and freeze-dried

Table 7.3: Elemental analysis of PyAcD-Fe (Fe^{2+}/Fe^{3+})

	C [%]	H [%]	Fe [%][1]	Fe [%][2]
PyAcD	55.23	5.90		
PyAcD-Fe (Fe^{2+}/Fe^{3+})	41.28	4.78	13.0	13.5

1 Determined by ICP-OES
2 Calculated from EA (from assumed PyAcD content based on C/H)

It was observed that during dialysis against demineralized water, a part of material always precipitated while another stayed in solution (Fig. 7.5). Color of dissolved part was always darker than precipitated part. In another experiment of Fe^{2+}/Fe^{3+}-complexation with PyAcD-17, both portions were separately freeze-dried. Weight of dissolved portion was only 3.75% of the total weight.

Table 7.4: Elemental analysis of precipitated and dissolved portions of PyAcD-17-Fe (Fe^{2+}/Fe^{3+})-complexation experiments

	C [%]	H [%]	C/H	PyAcD [%]*	$Fe [\%]_{EA}$
PyAcD	55.23	5.90	9.36	101	
PyAcD-Fe (Fe^{2+}/Fe^{3+}) (Soluble)	17.14	2.62	6.54	60	39.8
PyAcD-Fe (Fe^{2+}/Fe^{3+}) (Insoluble)	47.36	6.42	7.37	94	5.8

* Apparent PyAcD recovery calculated from EA

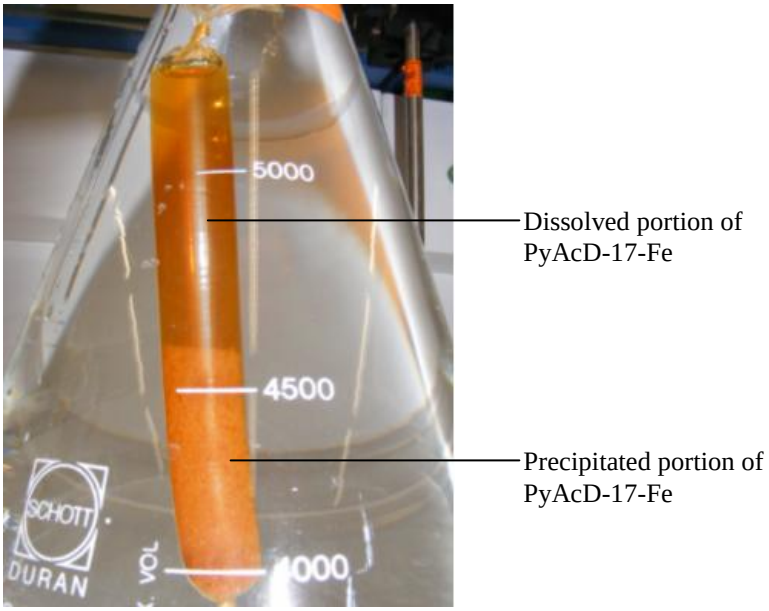

Fig. 7.5: Precipitated and dissolved portions in Fe^{2+}/Fe^{3+}-Complexation experiment with PyAcD-17

There was an interesting observation during metal complexation with PyD-17 or PyAcD-17. By Ag complexation of PyD, weight increased , while in case of Fe complexation experiments weight was always lower after complexation (Table 7.5). Moreover, ATR-IR spectra showed a slight loss of acetyl residues after all iron complexation experiments (Fig. 7.7), in agreement with the loss of weight.

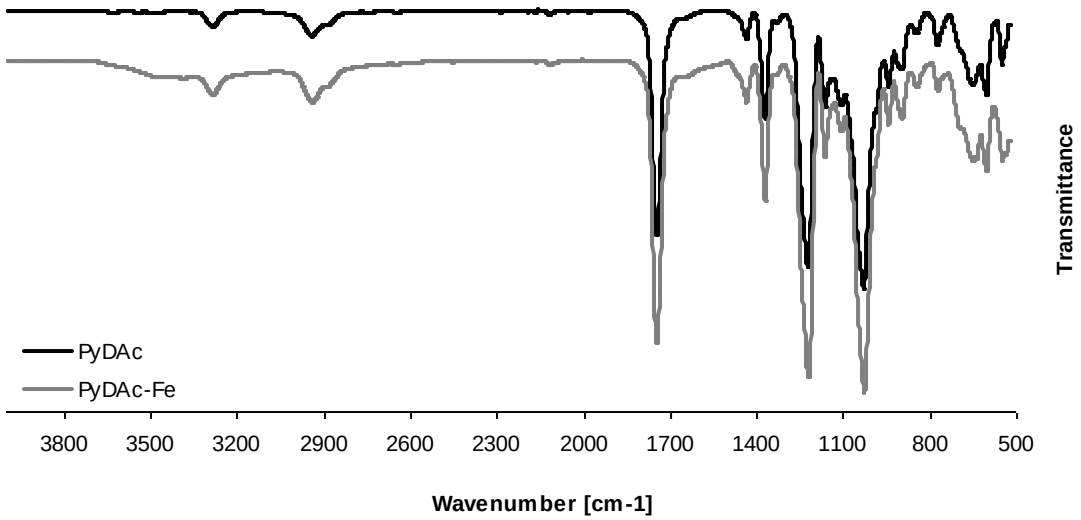

Fig. 7.6: ATR-IR spectra of PyAcD-17 and (PyAcD-17-Fe)

Table 7.5: Weight loss or increase after metal complexation of PyD and PyAcD

Sample	Starting material (mg)	Final product (mg)	Δ
PyAcD-Fe^{3+} (a)	98.40	81.13	-17.6 %
PyAcD-Fe^{3+} (b)	60.21	40.89	-32.1 %
PyAcD-Fe^{3+} (c)	76.60	68.00	-11.2 %
PyAcD-$Fe^{2+/3+}$	102.60	87.58	-14.6 %
PyD-Ag	248.96	290.56	+16.7 %

8 FUNCTIONALIZATION OF PENTYNYL DEXTRAN

Alkynyl dextrans can be considered as reactive intermediates for new products based on polysaccharides. Beside nucleophilic substitutions employing the acetylide anion, click chemistry offers a straight forward and efficient way to elegantly tailor the properties of natural-based polymers without involving multiple reactions and purification steps [174]. Moreover, basic features of click chemistry e.g. ambient reaction temperature and high tolerance towards oxygen and water, conveniently match with the chemical needs for the modification of biopolymer based materials.

8.1 Azides Synthesis and their Click Reactions with PyD

Residues bearing various functional groups, -NH_2, free and Boc protected, -OH, -COOH, -SH, or the vitamins biotin and α-tocopherol, were grafted on the backbone of dextran by forming 1,2,3-triazoles between terminal alkynes of PyD and azides of the respective compound. For this purpose, 2-bromoethylamine hydrobromide, 3-chloro-1-propanol, 4-chlorobutyric acid, 3-chloro-1-propanethiol, and biotin were converted into their respective azides **4 -7, 9**.

Above mentioned azides were prepared according to Scheme 8.1. The carboxy group of the biotin side chain was activated with *N*-hydroxy-succinimide (NHS) and subsequently the amide of **4** form under promotion of EDS, giving the biotin-azide (**9)**. 6-azido-*N*-Boc-hexyl-1-amine (**10**) was commercially available while *O*-Acetyl-α-tocopherol acetate azide (**11**) was a gift from Prof. Thomas Rosenau, University of Natural Resources and Applied Life Sciences, Department of Chemistry, Vienna, Austria.

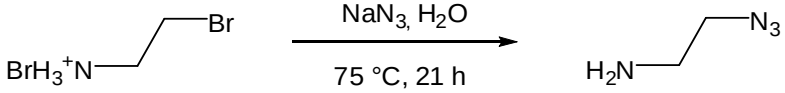

4 86%

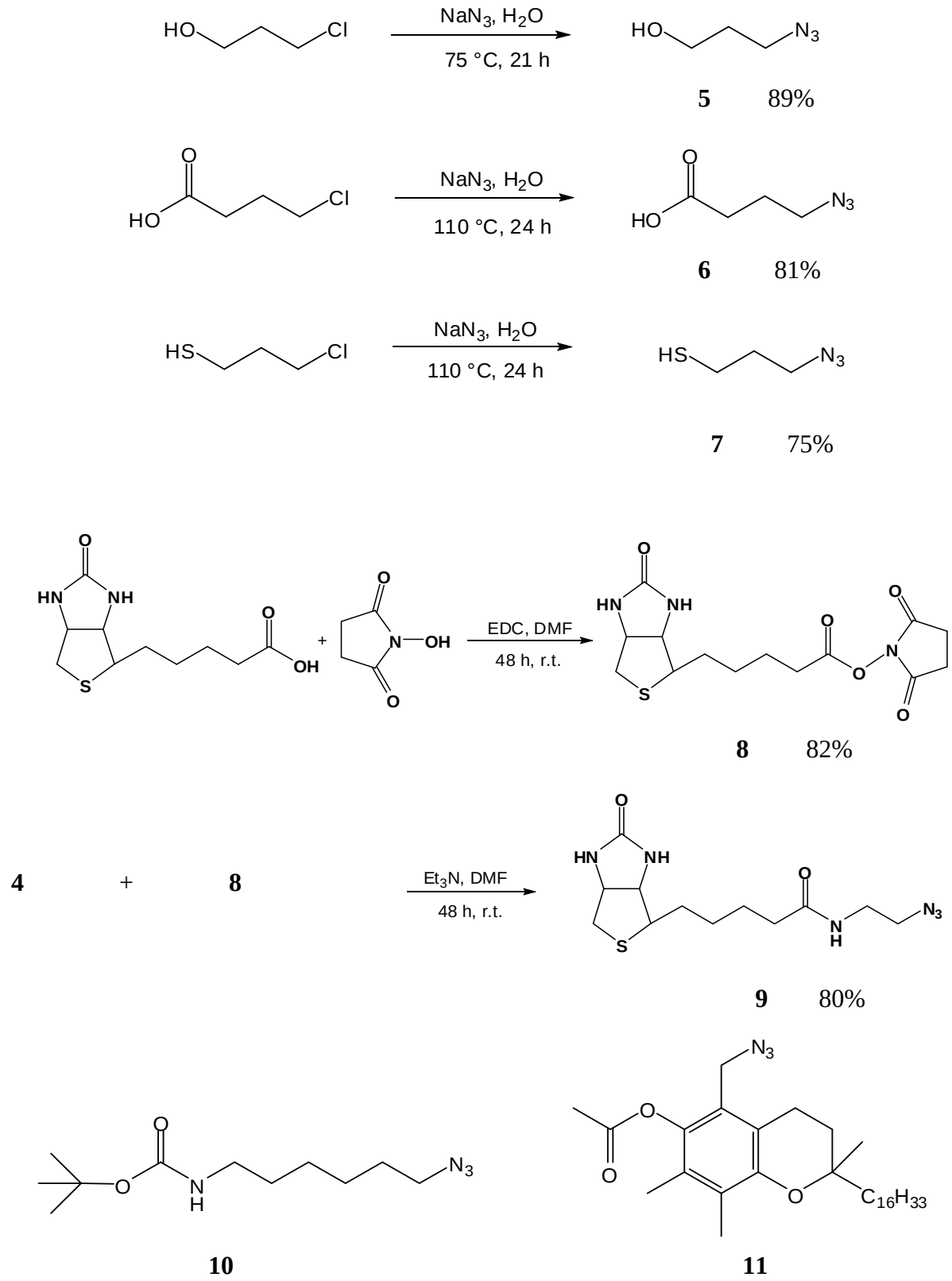

Scheme 8.1: Synthesis of azides for click reactions on pentynyl dextran

PyD-17 was used in all click reactions (Scheme 8.2). Conditions were nearly the same for all reactions. All reactions were carried out in a mixture of DMSO and water (v/v, 4:1) at room temperature for 96 hours with $CuSO_4$/Na-ascorbate as the catalyst system. High conversion (60-100%) was observed for all entries.

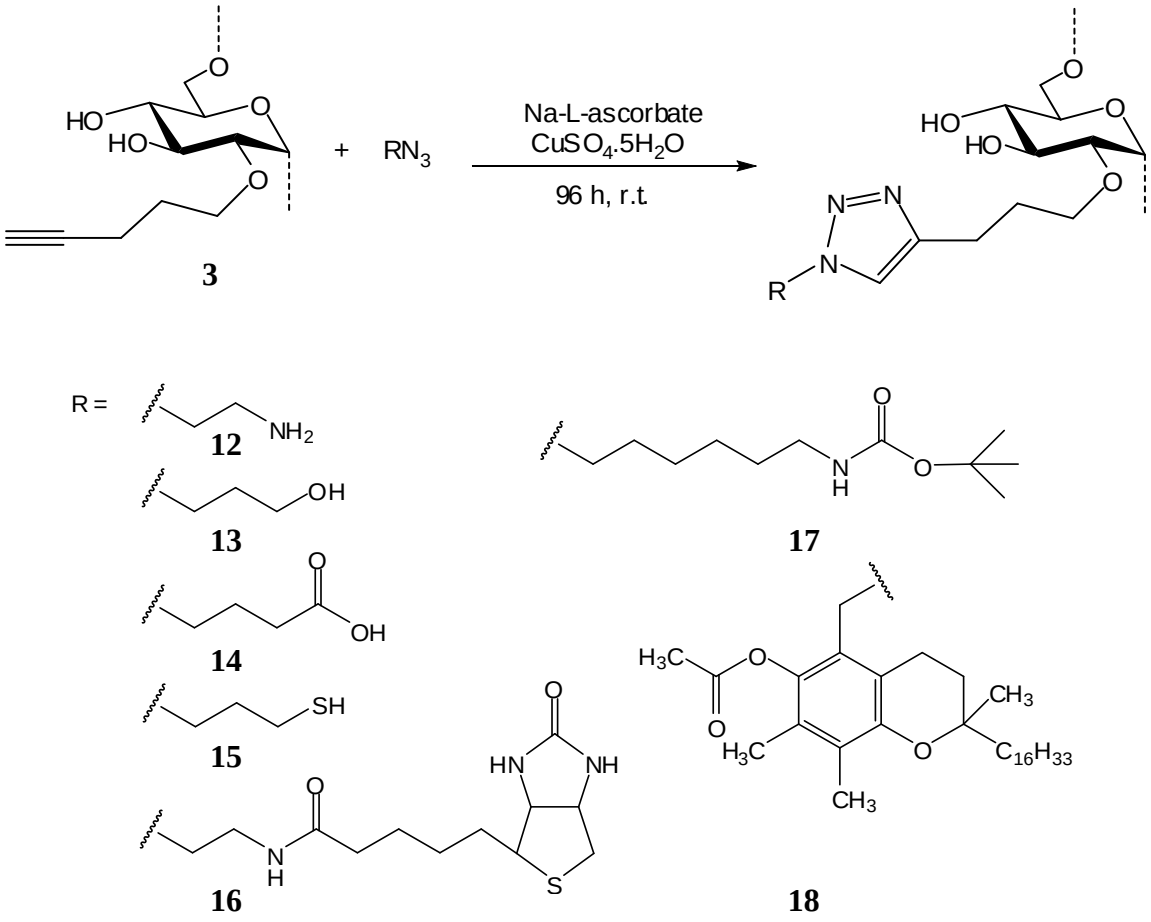

Scheme 8.2: Click reactions of azides with PyD-17

8.2 Characterization of Functionalized Pentynyl Dextran

Products were characterized by ATR-IR and NMR spectroscopy, and - after methanolysis - by means of GLC and ESI-MS. Due to insufficient solubility of some products, it was not always possible to record NMR spectra.

8.2.1 Infrared Spectroscopy and Elemental Analysis

Comparison of ATR-IR spectra of PyD before and after click reactions with different azides (Fig. 8.1) shows a significant decrease (PyD-COOH, PyD-NH-Boc, PyD-SH, PyD-biotin, PyD-Toc) or even total disappearance (PyD-NH_2, PyD-OH) of the C≡C-*H* vibration at about 3280 cm^{-1}. 1,2,3-Triazoles give absorption normally at 1600-1700 cm^{-1}[205]. Absorption at 2100 cm^{-1} in the ATR-IR spectra of PyD-SH and PyD-Toc can be due to incomplete conversion or due to unreacted azides [206]. Other analytical techniques e.g. EA, GLC and NMR confirmed that all click reactions were very efficient. Since polysaccharides and their hydrophilic derivatives easily adsorb water and might have entrapped other minor compounds, which cannot easily be removed by dialysis or extraction, data must be corrected for moisture content and impurities. In case of amino compounds salt formation and complexation of metal ions must also be considered. Therefore, elemental analysis data did not allow simply calculating the $DS_{triazole}$ from the nitrogen content, and thus not the exact rate of conversion, since the ratios of C, H and N did not fit to one distinct pair of DS values for most of the products (Table 8.1).

Conversion in click reactions was calculated from the nitrogen content of the products Since residual azide is present in PyD-NH_2, PyD-SH and PyD-toc, too high apparent conversions are obtained for these sample, but even for PyD-OH, apparent conversion exceeds by far 100% (Table 8.1). Calculations can also be made on the basis of S in some cases but due to low accuracy of S determination and moreover, it was present only in two samples, conversion was calculated only on the basis of N.

Table 8.1: Elemental analysis of PyD-17 and its click reaction products with azides **4** – **7**, **10**, and **11**

Sample	C [%]	H [%]	N [%]	S [%]	C/H	$DS_{triazole}$	Conv. [%]
PyD-17 (**3**)	51.40	6.64			7.74		
PyD-OH (**13**)	43.95	6.60	10.05		6.66	0.60	(140)*
PyD-NH_2 (**12**)	44.07	6.50	10.11		6.78	0.41	95
PyD-NH-Boc (**17**)	51.47	7.69	7.41		6.69	0.37	86
PyD-COOH (**14**)	44.76	6.08	6.32		7.36	0.36	83
PyD-SH (**15**)	42.85	6.05	8.83	9.08	7.08	0.53	(123)*
PyD-biotin (**16**)	48.78	6.62	9.32	3.03	7.36	0.33	76
PyD-toc (**18**)	61.29	8.38	4.54		7.31	0.46	(107)*

* Residual unreacted azide is present in the product

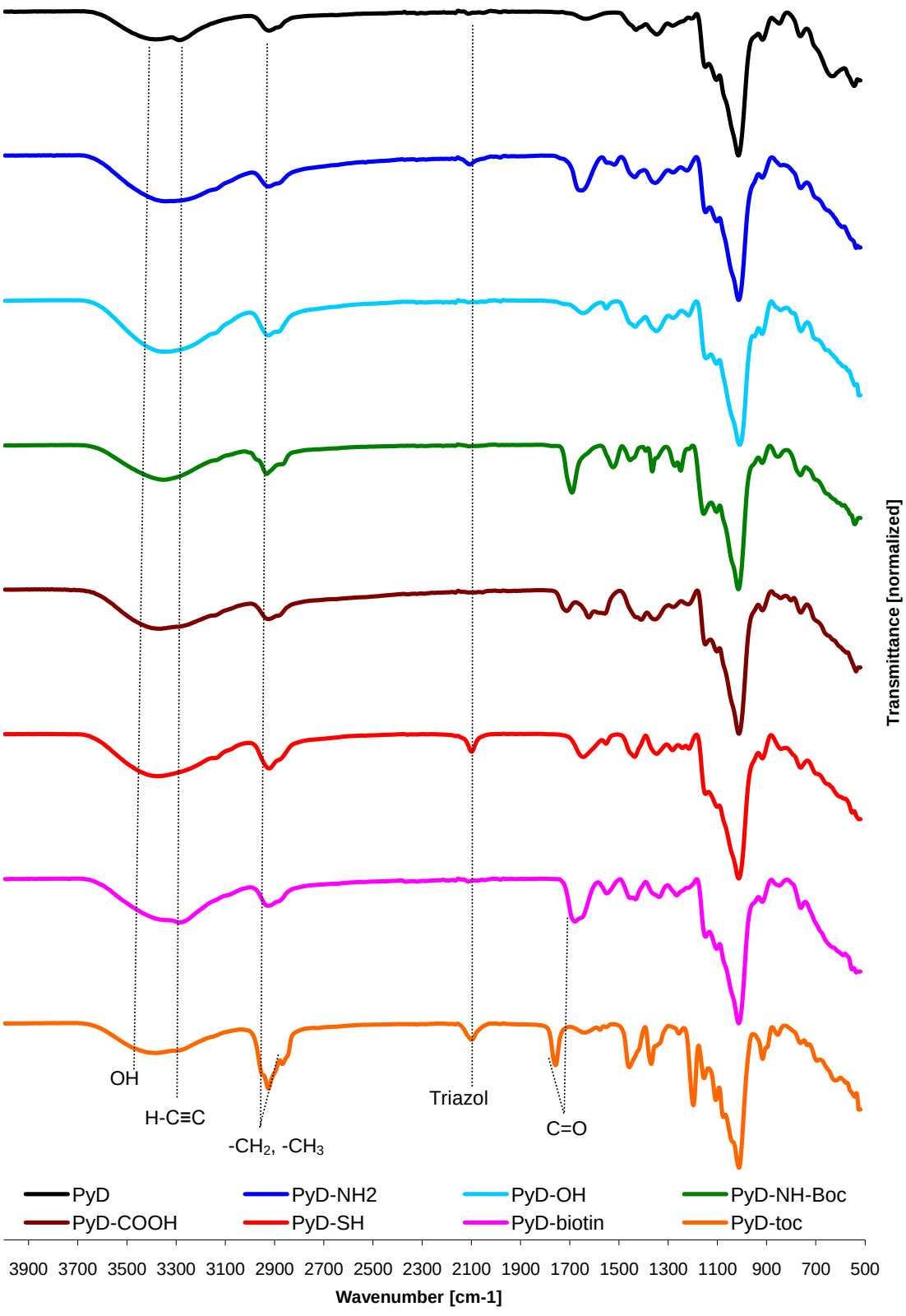

Fig. 8.1: ATR-IR spectra of PyD before and after its functionalyzation

8.2.2 Monomer Analysis

Monomer analysis of all triazole products was carried out by GLC after methanolysis and trimethylsilylation. D-Pinitol was added as internal standard after methanolysis to calculate sugar recovery from relative intensities of the peaks for D-pinitol (17.19 min) and for glucosyl units or on the basis of only unsubstituted glucosyl units (18.49, 18.89 min, Fig. 8.2).

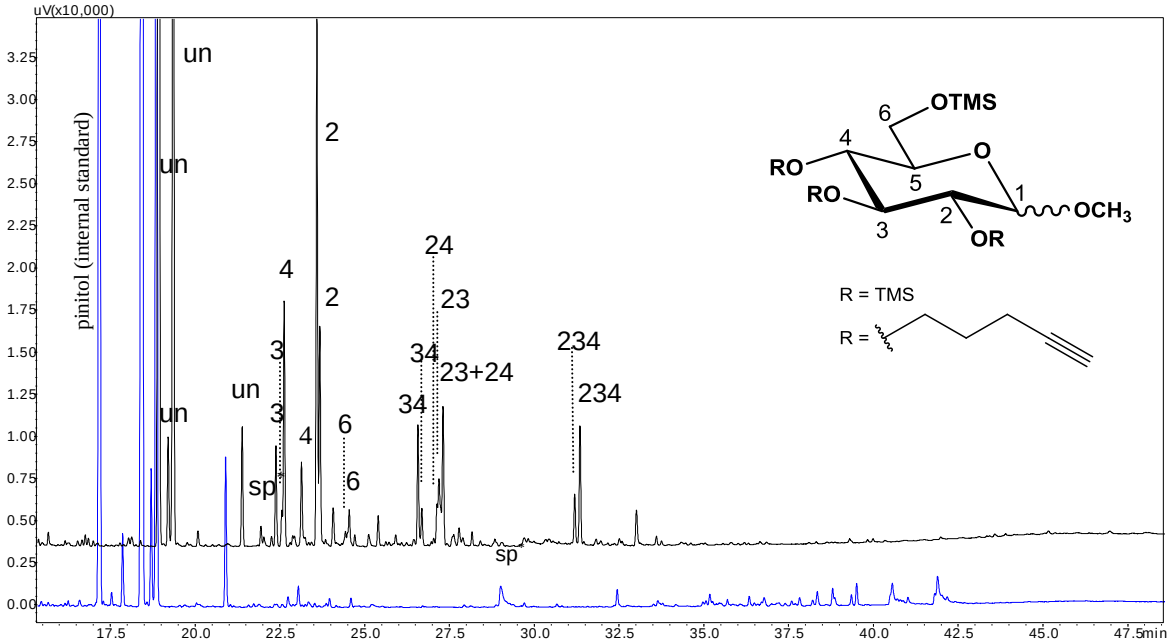

Fig. 8.2: Gas chromatogram of PyD-17 (upper-black) and PyD-NH_2 (lower-blue), column: zebron ZB 5 (5% phenylmethyl polysiloxan), carrier gas: He, temperature program: 60 °C (1 min) - 20 °C/min 130 °C - 4 °C/min 290 °C (10 min) - 20 °C/min 310 °C (10 min).
* Side product

Calculation of the conversion of pentynyl groups to respective 1,2,3-triazoles from GLC was based on the disappearance of *O*-pentynyl glucosides compared to the starting material, since the triazole derivatives could not be detected in gas chromatogram.

The gas chromatogram of PyD-NH_2 is shown in Fig. 8.2. Due to very high conversion, only the peaks representing un-substituted units appear beside a few minor peaks e.g. at 29.01 minutes due to little amount of side product present in PyD. As DS of PyD used in this experiment is 0.43, DS of unreacted pentynyl glucosides i.e. which did not form triazoles was calculated from gas chromatogram (Fig. 8.2). Conversion was estimated as:

DS for pentynyl groups before triazole formation	0.43
DS for pentynyl groups after triazole formation	0.01
$DS_{cal.}$ of 1,2,3-triazole (0.43-0.01)	0.42
Conversion of pentynyl into triazole	98%
Sugar recovery	61%

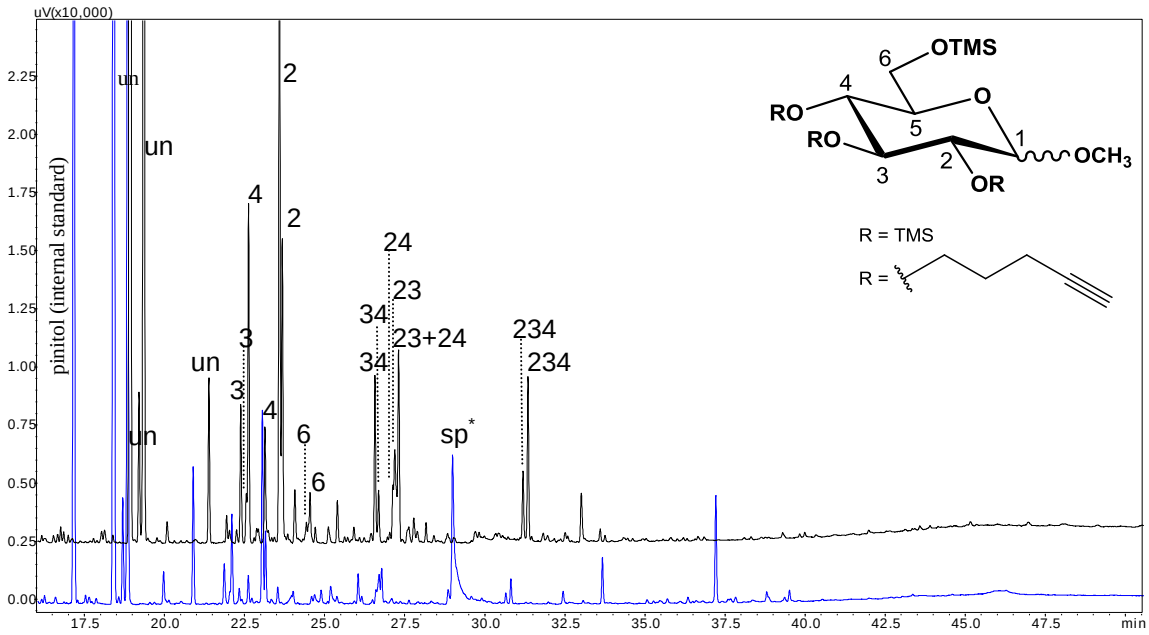

Fig. 8.3: Gas chromatogram of PyD-17 (upper-black) and PyD-biotin (lower-blue). For GC temperature program and other conditions, see Fig. 8.2 and Experimental
* Side product, since performed prior to Soxhlet purification, see section 6.2.5

It should be mentioned that due to its high heterogeneity, PyD-17 in spite of its modest DS of 0.43 contains about 6 Mol% of di- and 4 Mol% of even tri-substituted glucosyl residues (see Tab. 6.15). If only one of the pentynyl groups of a multiple substituted glucose reacts in the click reaction, the peak also disappears. This means that estimating alkyne conversion on the basis described will show an increasing overestimation with decreasing conversion.

In some cases, where conversion was not complete e.g. PyD-biotin, peaks for non-reacted *O*-pentynyl glucosides can also be observed (Fig. 8.3). An overview of conversion and sugar recovery for all click reactions is given in Table 8.2.

Table 8.2: Conversion of pentynyl glucosides to 1,2,3-triazoles by click-reaction with azides **4**-**7**, and**9**-**11**, as estimated from residual DS(Py) obtained by GLC

Sample	$DS_{py\text{-}exp}$	$DS_{triazole\text{-}calc.}$	Conv. [%]	Sugar recov. [%]
PyD (**3**)	0.43			
PyD-NH_2 (**12**)	0.01	0.42	98	61
PyD-OH (**13**)	0.01	0.42	98	53
PyD-NH-Boc (**17**)	0.10	0.33	77	58
PyD-COOH (**14**)	0.07	0.36	84	54
PyD-SH (**15**)	0.03	0.40	93	27
PyD-biotin (**16**)	0.16	0.27	63	35
PyD-toc (**18**)	0.19	0.24	56	27

8.2.3 Electrospray Ionization Mass Spectrometry (ESI-MS)

ESI-IT-MS of pentynyl triazole products was recorded after methanolysis and using methanol as solvent. Almost all samples show mono-, di-, and tri-substituted triazole products. Although relative ion abundances do not simply reflect the molar ratios of components, they were as expectedi.e. mono > di > tri.

*PyD-NH_2 (**12**)*

ESI-MS of PyD-NH_2 was recorded after methanolysis (Fig. 8.4). *M/z* 347.3 is the main signal in the mass spectrum corresponding to $[M+H]^+$ of the mono-substituted glucose (**19**). Second intensive signal at 361.4 with Δ= +14 compared to 347 is most probably due to methylation of triazole (**20**), since a product shifted by 14 u was observed for all triazole derivatives. A tiny peak at *m/z* 375 might be caused by additional *N*-methylation of the amino group as a result of the methanolysis at elevated temperature (methanolic HCl, 120 minutes at 90 °C) , although this is commonly not observed. The relative intensities do not reflect the molar proportions. The signal of the sodiated non-substituted methyl glucoside at *m/z* 217 is nearly completely suppressed, although this component presents about 70 Mol% of the sample.

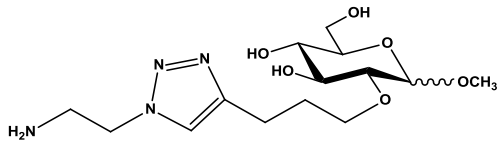

M: 346

19

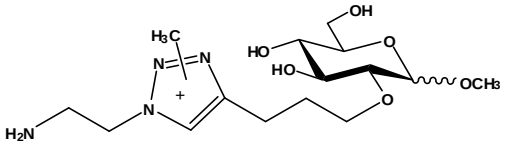

M: 361

20

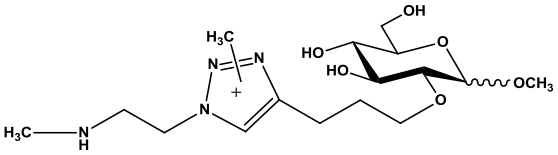

M: 375

21

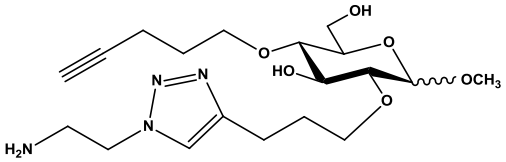

M: 412

22

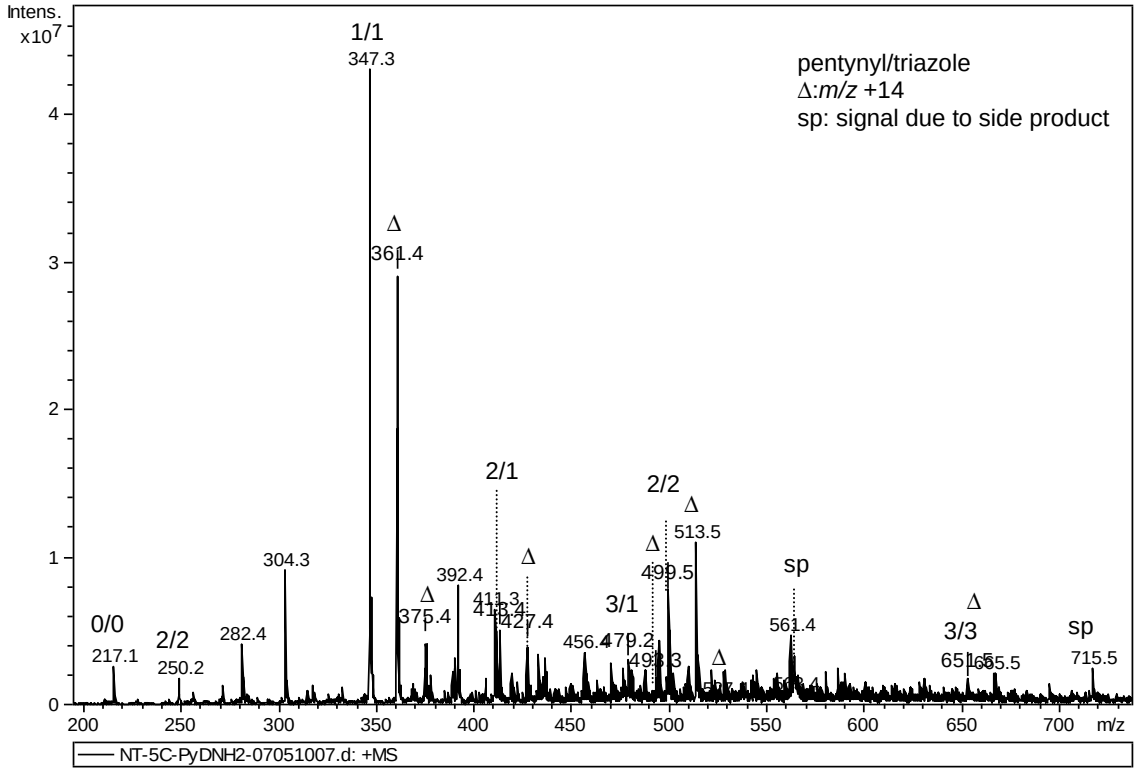

Fig. 8.4: ESI-MS of PyD-NH_2 (**12**) after methanolysis; peaks are assigned (n/m) according to the number of pentynyl groups (n) and converted groups (m)

Intensity of di-substituted triazole product (*m/z* 499.5) is much lower than that of mono-substituted one (*m/z* 347.3) but still tri-substituted product (*m/z* 651.5) can be detected. *M/z* 563.4 cannot be assigned to a glucose derivative, but occurrence of *m/z* 715.5 (563+152) indicates that it might bear various numbers of triazole groups.

Table 8.3: Assigned *m/z* values from ESI-MS of methanolysis products of PyD-NH_2 (**12**)

m/z	**Pentynyl groups**			**Remarks**
	Total	**Conv.**	**Un-conv.**	
217.1	0	0		
250.2	2	2		(498+2)/2
347.3	1	1		**19**
361.4	1	1		**20**
375.4	1	1		**21**
413.4	2	1	1	**22**
427.4	2	1	1	**22-Me**
479.2	3	1	2	**22-Py**
493.3	3	1	2	**22-Py-Me**
499.4	2	2		**22a**
513.5	2	2		**22a-Me**
527.4	2	2		**22a-Me_2**
651.5	3	3		**22b**
665.5	3	3		**22b-Me**
715.5				Side product

sp = side product

*PyD-OH (**13**)*

ESI-MS of PyD-OH (**13**) after methanolysis (Fig. 8.5) shows the main signal at *m/z* 362.3, 529.5 and 696.5 representing mono-, di-, and tri-substituted functionalized glucosides respectively. Again, signals following the main signals X at *m/z* X+14 were detected. Weak signals with Δ = +66, e.g. 362+66 = 428, 529+66 = 595 and 696+66 = 762, represent products containing one unconverted pentynyl group in mono-, di-, and tri-substituted triazole product, respectively.

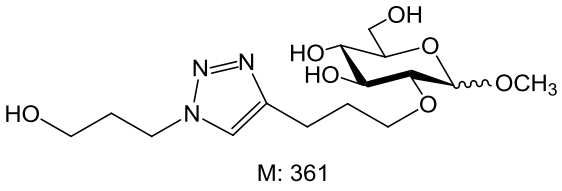

M: 361

23

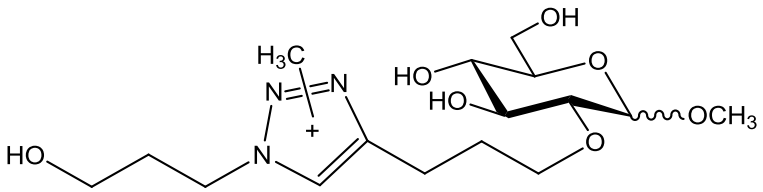

M: 376

24

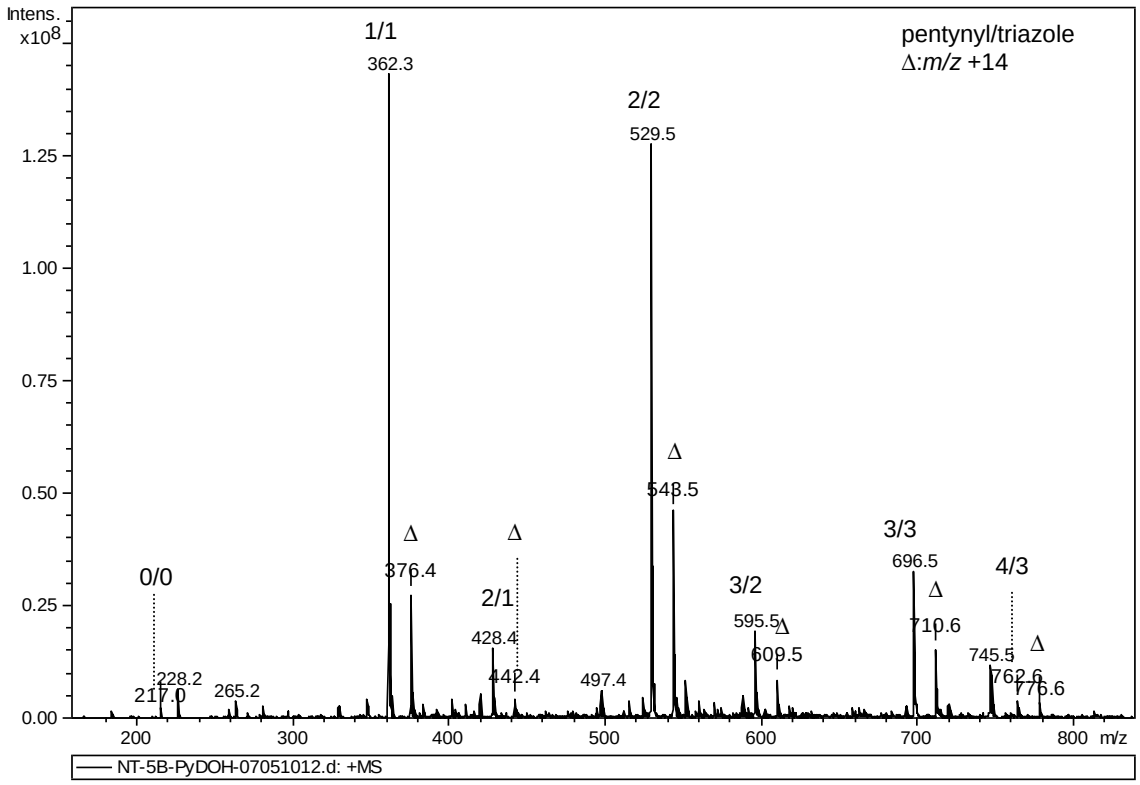

Fig. 8.5: ESI-MS of PyD-OH (**13**) after methanolysis. Signals are assigned (n/m) according to the number of pentynyl groups (n) and converted groups (m)

Table 8.4: Assigned *m/z* values from ESI-MS of PyD-OH (**13**)

m/z	**Pentynyl groups**			**Remarks**
	Total	**Conv.**	**Un-conv.**	
217.0				unsubs.
362.3	1	1		**23**
376.4	1	1		**24**
428.4	2	1	1	**23-Py**
442.4	2	1	1	**23-Py-Me**
529.5	2	2		**23a**
543.5	2	2		**23a-Me**
595.5	3	2	1	**23a-Py**
609.5	3	2	1	**23a-Py-Me**
696.5	3	3		**23b**
710.6	3	3		**23b-Me**
762.6	4	3	1	**23b-Py-Me**
776.6	4	3	1	**23b-Py-Me$_2$**

Signal Δ = +14 (376.4, 543.5, 710.6) following the main signals in mass spectrum of PyD-OH (Fig. 8.5) are referred to the already mentioned *N*-methylation at triazole.

Surprisingly, even signals corresponding to tetra-*O*-substituted glucosides are observed at *m/z* 762.6 and 776.6 in this very clear mass spectrum, and are most probably due to end groups. This might be due to an increasing surface activity and increasing probability of protonation of methylation with number of substituents, and thus a strong overestimation.

*PyD-NH-Boc (**17**)*

ESI-MS of methanolyzed PyD-NH-Boc (**17**) (Fig. 8.6) shows mainly mono-substituted product but di-, and tri-substituted monomers are also present. Boc group has been lost during sample preparation for ESI-MS. Table 8.5 lists the *m/z* values observed and their interpretation. Doubly charged (*m/z* 306) signals with Δ = +14 are again due to triazole-methylation ($M+CH_3^+$ instead of $M+H^+$). Some other masses e.g. *m/z* 469.4, 535.5, 677.6 with Δ = +66 following the mono- and di-substituted products shows unconverted pentynyl glucosides.

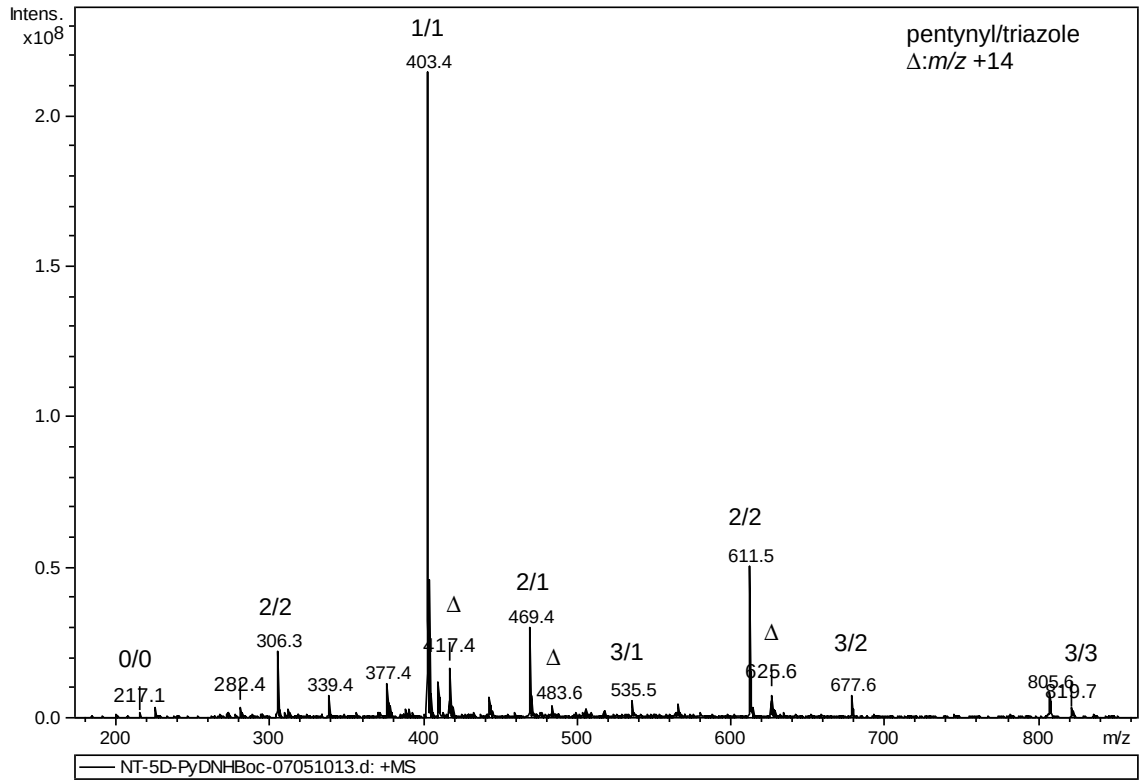

Fig. 8.6: ESI-MS of PyD-NH-Boc (**17**) after methanolysis, peaks are assigned (n/m) according to the number of pentynyl groups (n) and converted groups (m)

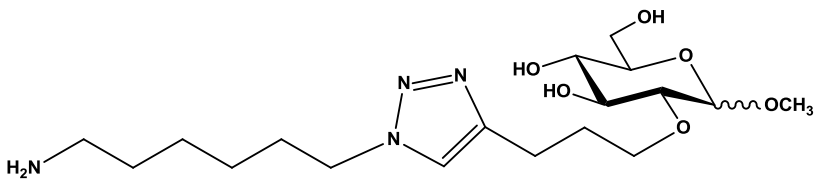

M: 402

25

Table 8.5: Assigned *m/z* values from ESI-MS of PyD-NH-Boc (**17**)

m/z	**Pentynyl groups**			**Remarks**
	Total	**Conv.**	**Un-conv.**	
217.1				unsubs.
306.3	2	2		(610+2)/2
403.4	1	1		**25**
417.4	1	1		**25-Me**
469.4	2	1	1	**25-Py-Me**
483.6	2	1	1	**25-Py-Me$_2$**
535.5	3	1	2	**25-Py$_2$-Me**
611.5	2	2		**25a**
625.6	2	2		**25a-Me**
677.6	3	2	1	**25a-Py**
819.7	3	3		**25b**

*PyD-COOH (**14**)*

ESI-MS of methanolyzed PyD-COOH (**14**) (Fig. 8.7) shows signals for mono-, (*m/z* 404.3) di, (*m/z* 613.5) and tri-substituted (*m/z* 822.6) triazole products (methyl esters) and the typical accompanying signals with Δ = +14 (404+14 = 418, 613+14 = 627, 822+14 = 836) due to formation of methyl triazole as has been observed in all former ESI-MS spectra.

Along with expected *m/z* signals for PyD-COOH e.g. signals with Δ = +66 (*m/z* 470.4, 536.4, 693.5) due to some residual alkynyl groups, some signals which do not correspond to any expected mass for PyD or PyD-COOH were also observed. These signals, e.g. at *m/z* 675.4, 741.4 and 884.5 (Fig. 8.7) also show a difference of Δ = 66 and 209, corresponds to the pentynyl or triazolyl substituent, respectively. *M/z* 675 was present in ESI-MS of PyD-17 (Fig. 6.25) before Soxhlet extraction with CH_2Cl_2 and was considered as side product. Therefore, possibly *m/z* 675.4, 741.4 and 884.5 belong to side product with terminal alkyne residue which was converted into triazole after click reaction with 4-azidobutyric acid, while 741.4 refers to a higher homolog.

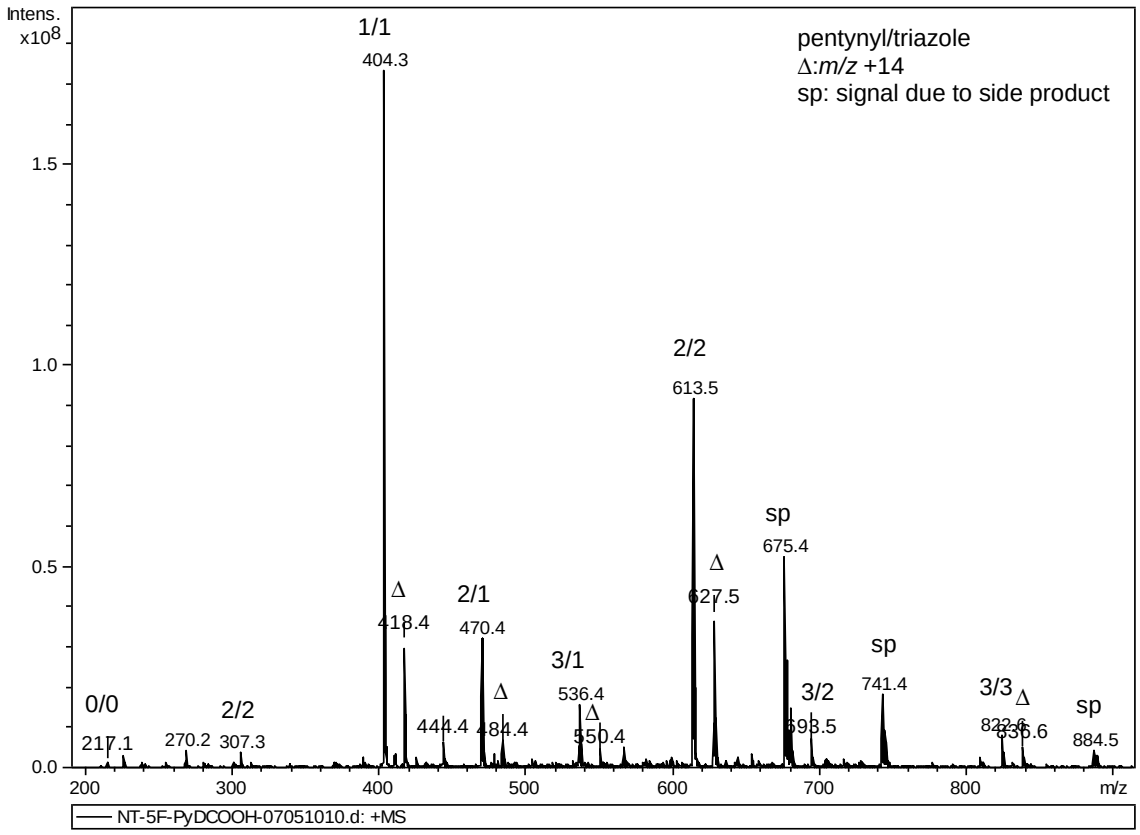

Fig. 8.7: ESI-MS of PyD-COOH (**14**) after methanolysis. Signals are assigned (n/m) according to the number of pentynyl groups (n) and converted groups (m)

Table 8.6: Assigned *m/z* values from ESI-MS of PyD-COOH (**14**)

m/z	**Pentynyl groups**			**Remarks**
	Total	**Conv.**	**Un-conv.**	
217.1				unsubs.
307.3	2	2		612+2/2
404.3	1	1		**26**
418.4	1	1		**26-Me**
470.4	2	1	1	**26-Py**
484.4	2	1	1	**26-Py-Me**
536.4	3	1	2	**26-Py$_2$**
550.4	3	1	2	**26-Py$_2$-Me**
613.5	2	2		**26a**
627.5	2	2		**26a-Me**
693.5	3	2	1	**26a-Py-Me**
822.6	3	3		**26b**
836.6	3	3		**26b-Me**
675.4				Side product
741.4				Side product
884.5				Side product

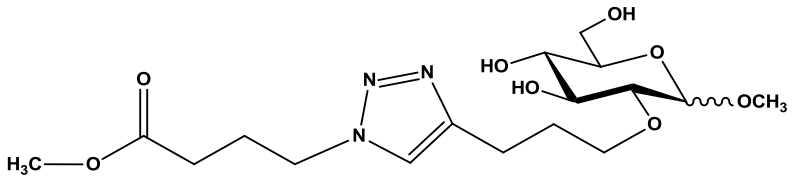

M: 403

26

*PyD-SH (**15**)*

ESI-MS of PyD-SH (**15**) after methanolysis (Fig. 8.8) shows many peaks which do not correspond to any expected product of PyD or PyD-SH.

Only a few peaks could be assigned. *m/z* 217.1 is due to un-substituted dextran, 392.3 represents mono-substituted glucoside with methylation of triazole (**27**), *m/z* 406.4 corresponds to molecular mass of **28.** *M/z* 559.4 corresponds to formation of a intramolecular S-S bridge (**29**) while 573.4 is in agreement with compound formed by S-S bridge between two different mono-substituted units (**30**).

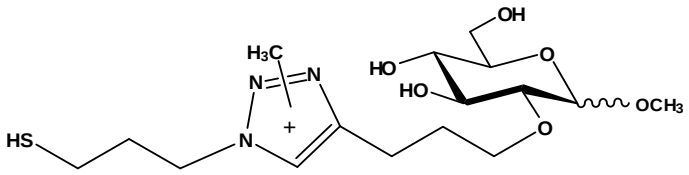

M: 392

27

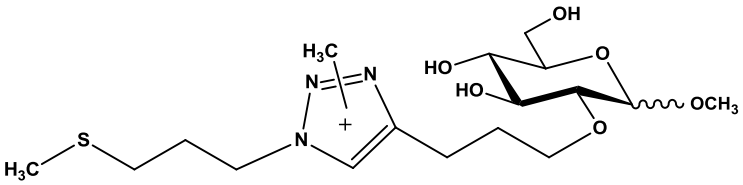

M: 406

28

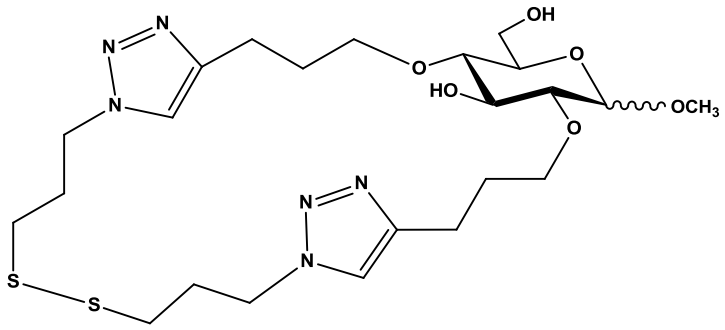

M: 558

29

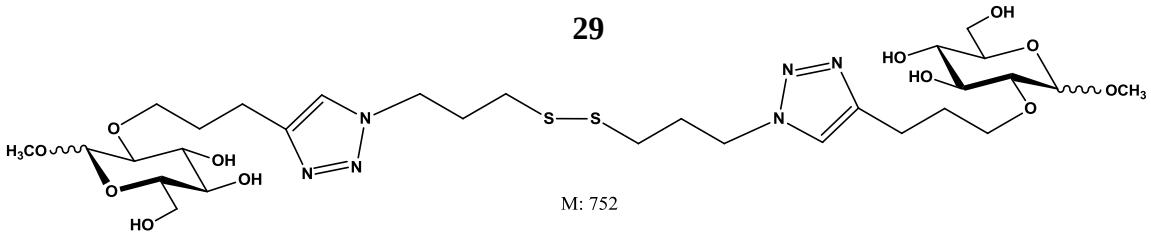

M: 752

30

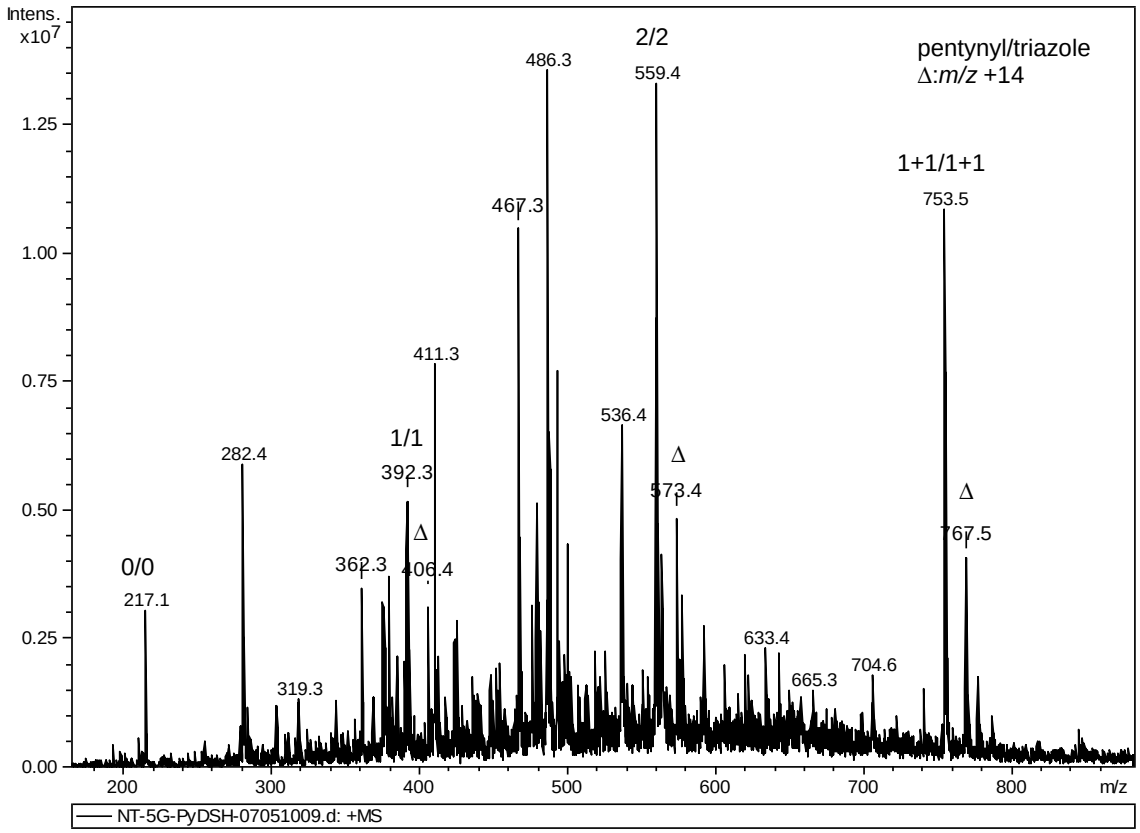

Fig. 8.8: ESI-MS of PyD-SH (**15**) after methanolysis. Signals are assigned (n/m) according to the number of pentynyl groups (n) and converted groups (m)

Table 8.7: Assigned *m/z* values from ESI-MS of PyD-SH (**15**) after methanolysis

m/z	**Pentynyl groups**			**Remarks**
	Total	**Conv.**	**Un-conv.**	
217.1				unsubs.
392.3	1	1		**27**
406.4	1	1		**28**
559.4	2	2		**29**
573.4	2	2		**29-Me**
753.5	1+1	1+1		**30**
767.5	1+1	1+1		**30-Me**

*PyD-biotin (**16**)*

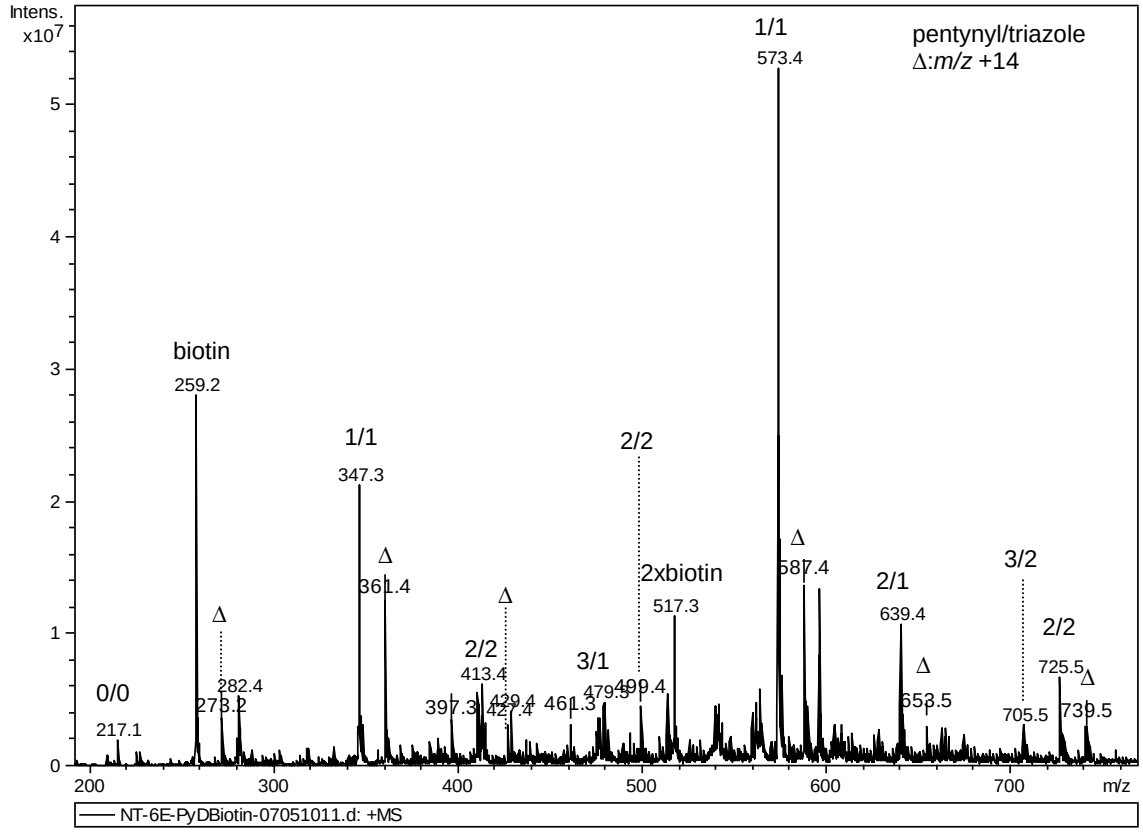

Fig. 8.9: ESI-MS of PyD-biotin (**16**) after methanolysis. Signals are assigned (n/m) according to the number of pentynyl groups (n) and converted groups (m)

ESI-MS of PyD-biotin (**16**) carried out after methanolysis is shown in Fig. 8.9. Along with masses representing $[M+H]^+$ of mono-, di-, and tri-substituted PyD-biotin products, masses with $\Delta = +14$, due to $[M+CH_3]^+$ were observed again. Some little signals with $\Delta = +66$ following main signals correspond to residual alkynyl substituents. A strong

signal at *m/z* 259.2 shows that biotin was partially release (**31**) during methanolysis as its methyl ester yielding aminoalkyl triazole (*m/z* 347.3/*m/z* 361.4). Mono-substituted methyl glucoside (*m/z* 573.4) is the strongest signal, while di-substituted product shows just a weak signal at *m/z* 725.5.

Table 8.8: Assigned *m/z* values from ESI-MS of PyD-biotin (**16**) after methanolysis

m/z	**Pentynyl groups**			**Remarks**
	Total	**Conv.**	**Un-conv.**	
217.1				unsubs.
259.2				**31**
273.2				**31-Me**
347.3	1	1		**19**
361.4	1	1		**20**
413.4	2	1	1	**19-Py**
479.3	3	1	2	**19-Py$_2$**
499.4	2	2		**19a**
517.3				Cluster of **31**
573.4	1	1		**32**
587.4	1	1		**32-Me**
639.4	2	1		**32-Py**
653.5	2	1		**32-Py-Me**
705.5	3	2	1	**32a-Py**
725.5	2	2		**33**
739.5	2	2		**33-Me**

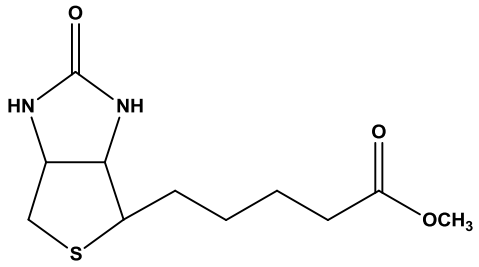

M: 258

31

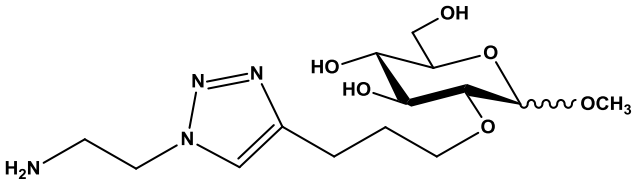

M: 346

19

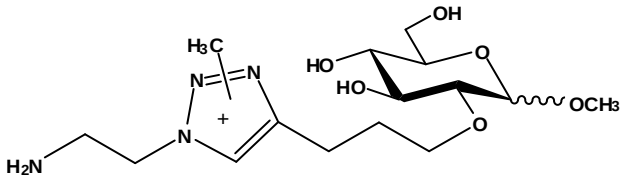

M: 361

20

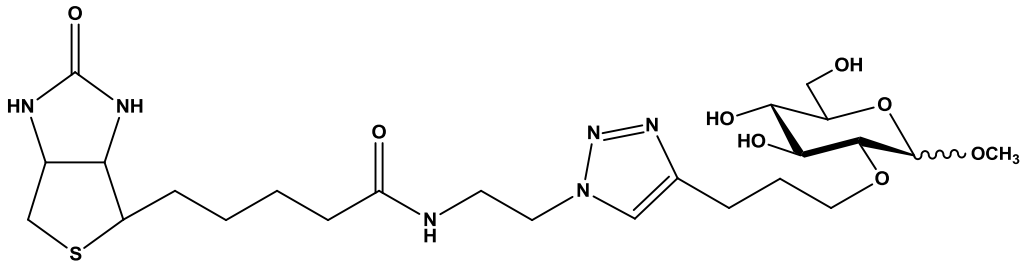

M: 572

32

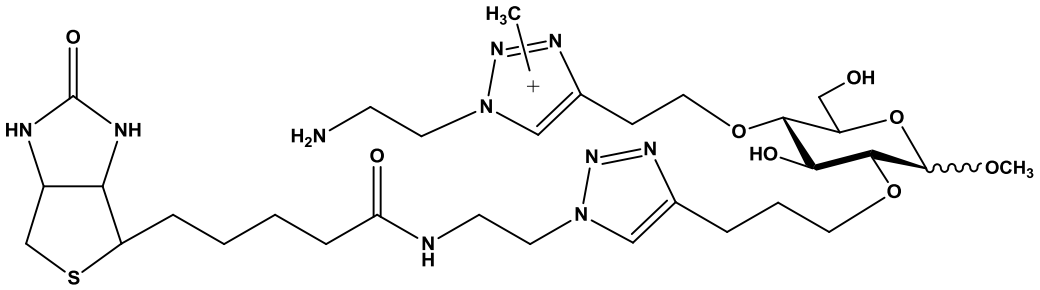

M: 725

33

*PyD-toc (**18**)*

ESI-MS of PyD-toc recorded after methanolysis (Fig. 8.10) show mono-, di-, and tri-substituted products along with some typical signal with Δ = +66 corresponding to residual alkynyl groups following the main signals. Ester hydrolysis of tocopheryl acetate occurred during methanolysis. Thus the mass increase is +471.7, but due to the formation of $[M+H]^+$, instead of [M+Na]+ for the methyl *O*-pentynyl glucoside, here the increase in

m/z is only 449.7 (*m/z* 283.2→*m/z* 732.7). Obviously sterical hindrance has not affected reactivity so much.

Degree of conversion looks even higher than determined by GC (see Table 8.2, 56%). The tocopheryl moiety seems to enhance the signal strength significantly.

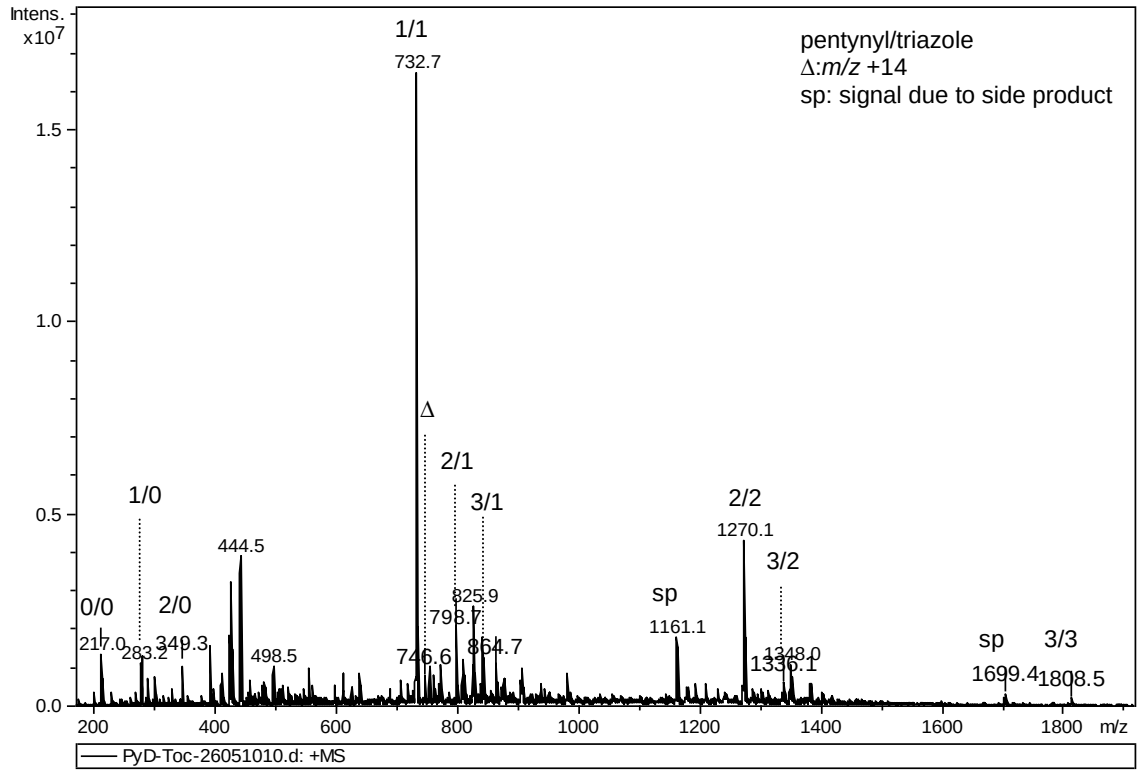

Fig. 8.10: ESI-MS of PyD-toc (**18**) after methanolysis. Signals are assigned (n/m) according to the number of pentynyl groups (n) and converted groups (m)

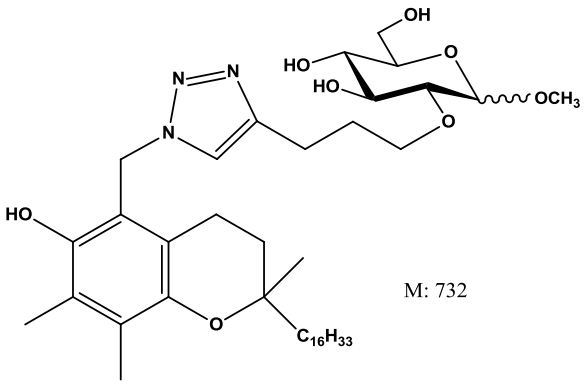

M: 732

34

Table 8.9: Assigned *m/z* values from ESI-MS of PyD-toc (**18**) after methanolysis

m/z	Pentynyl groups			Remarks
	Total	Conv.	Un-conv.	
217.0				unsubs.
283.2	1	0	1	
349.3	2	0	2	
732.7	1	1		**34**
746.6	1	1		**34-Me**
798.7	2	1	1	**34-Py**
864.7	3	1	2	**34-Py$_2$**
1270.1	2	2		**34a**
1336.1	3	2	1	**34a-Py**
1699.4				Side product
1808.5	3	3		**34b**

From ESI-MS mass spectra of all click reaction products, it also appears that the cycloadditon of PyD with more bulky azides like PyD-NH-Boc, PyD-biotin and PyD-toc is less efficient than with smaller azides like PyD-NH_2, PyD-OH, PyD-COOH and PyD-SH. DS and mol% of mono-, di-, and trisubstituted glucosyl units calculated from ESI-MS (Table 8.10) cannot agree with GLC data, since signal for non-substituted glucoside units is completely suppressed while presenting 70% of the glucose moieties as known from monomer analysis (Table 6.15). Normalization without these highly discriminated chemically different constituents shows much higher similarity (Table 8.10).

Table 8.10: Comparison of mono-, di-, and tri-substituted glucosyl units (rel. signal intensity in %) in PyD-17 and its triazole products calculated from ESI-MS

Sample	un	mono	di	tri	DS[a]
PyD[b]	71.28	18.76/65.3[c]	7.09/24.7[c]	2.87/10.0[c]	0.43/1.45[c]
PyD	23.72	32.19	23.60	20.48	1.41
PyD-NH_2	2.30	67.26	24.34	6.09	1.34/1.37
PyD-OH	0.00	38.17	43.40	18.43	1.80
PyD-NH-Boc	0.45	68.52	26.11	4.93	1.36
PyD-COOH	0	49.41	40.67	9.93	1.61
PyD-biotin	1.30	69.66	23.56	5.48	1.33[d]/1.35
PyD-toc	4.92	60.6/63.7	27.4/28.8	7.2/7.5	1.37/1.44

a Only substituted glucosyl units were considered for calculation of DS
b Calculated from GLC
c Calculated by omitting non-substituted units
d including aminoethyl triazoleformed from the loss of biotin

8.2.3.1 Synthesis of a Model Triazole Compound

In ESI-MS of methanolyzed click reaction productsions at *m/z* with Δ = +14 followedthe main signals for mono-, di-, and tri-substituted triazole glucose derivatives. Since these additional signals were observed for all compounds independent on the individual functional group, it was supposed that they appear due to methylation at triazole.

To confirm this hypothesis, a simple triazole compounds was synthesized by cycloaddition of phenylacetylene and benzylazide in a mixture of *t*-butanol and water at room temperature for 48 hours. In this model compound (**35**), there is no chance for methylation at any position except the triazole. The product (**35**) was submitted to methanolysis conditions used for PyD-sample preparation, and measured by ESI-MS (Fig. 8.11).

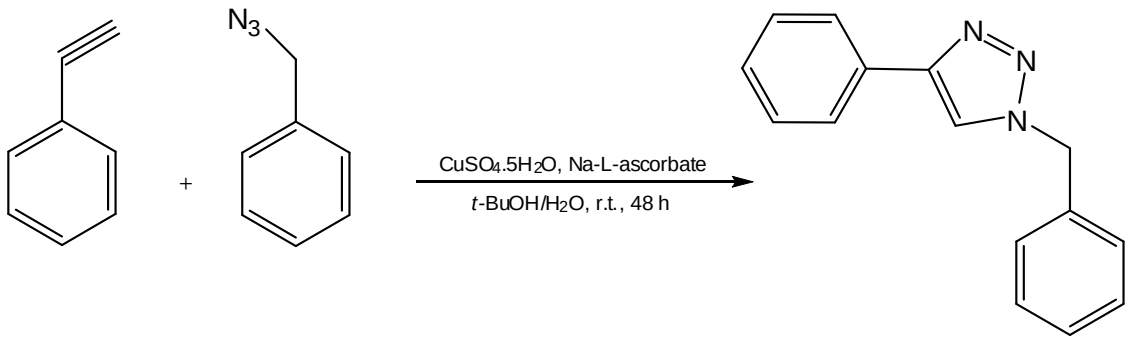

35

Scheme: 8.3: Synthesis of 1-*N*-benzyl-4-phenyl-1,2,3-triazole (**35**)

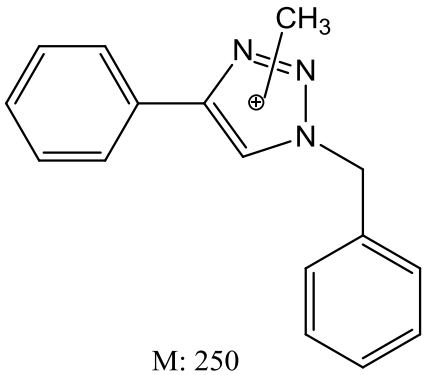

M: 250

36

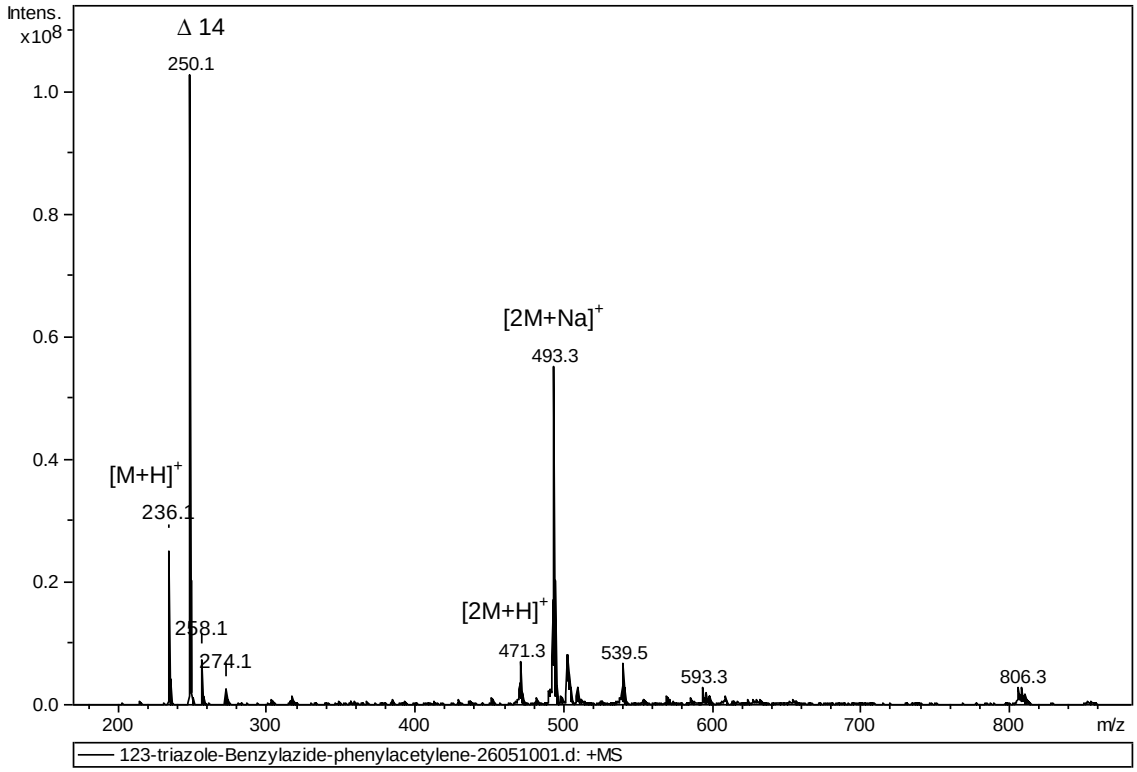

Fig. 8.11: ESI-MS of 1-*N*-benzyl-4-phenyl-1,2,3-triazole (**35**) after methanolysis

Table 8.11: Assigned *m/z* values from ESI-MS of 1-benzyl-4-phenyl-1,2,3-triazole (**35**)

m/z	**Increment**	**Remarks**
236.1	$[M+H]^+$	**35 + H^+**
250.1	$[M+CH_3]^+$	**36**
258.1	$[M+Na]^+$	
471.3	$[2M+H]^+$	
493.3	$[2M+Na]^+$	

Signal at *m/z* 236.1 and *m/z* 258 correspond to $[M+H]^+$ and $[M+Na]^+$ of the target compound (**35**) while *m/z* 250.1 is the most prominent signal in mass spectrum (Fig. 8.11) which is in agreement with methylation of triazole (**36**). Some other signals corresponding to higher masses e.g. 471.3 and 493.3, are appearing due to cluster formation of **35** ($[2M+H]^+$, $[2M+Na]^+$)**.**

The position of triazole methylation is not confirmed. In 1,2,3-triazoles, the non-binding electron pair at the sp3 nitrogen can form a double bond between N1 and N2 and as a consequence, the pi-electrons of the N2-N3 double bond will be located at N3, which will

be negatively charged in this mesomeric structure while N1 will be positively charged. But In our case with R having a +I effect, the opposite polarization is more probable and thus N3 is the most nucleophilic position to attack a protonated MeOH under the loss of water. Thusmethyl group is probably located at N3, while the positive charge is delocalized between N1 and N3.

8.2.4 NMR Spectroscopy

NMR spectra of the various triazolylpropyldextrans were recorded in DMSO-d_6 or in pyridine-d_5 because these samples were not soluble in other solvents commonly used for NMR spectroscopy. PyD-NH_2 (**12**) and PyD-SH (**15**) even were not soluble in DMSO or pyridine at all. Therefore, it was not possible to record ^{1}H- or ^{13}C-NMR spectra for these samples.

*PyD-OH (**13**)*

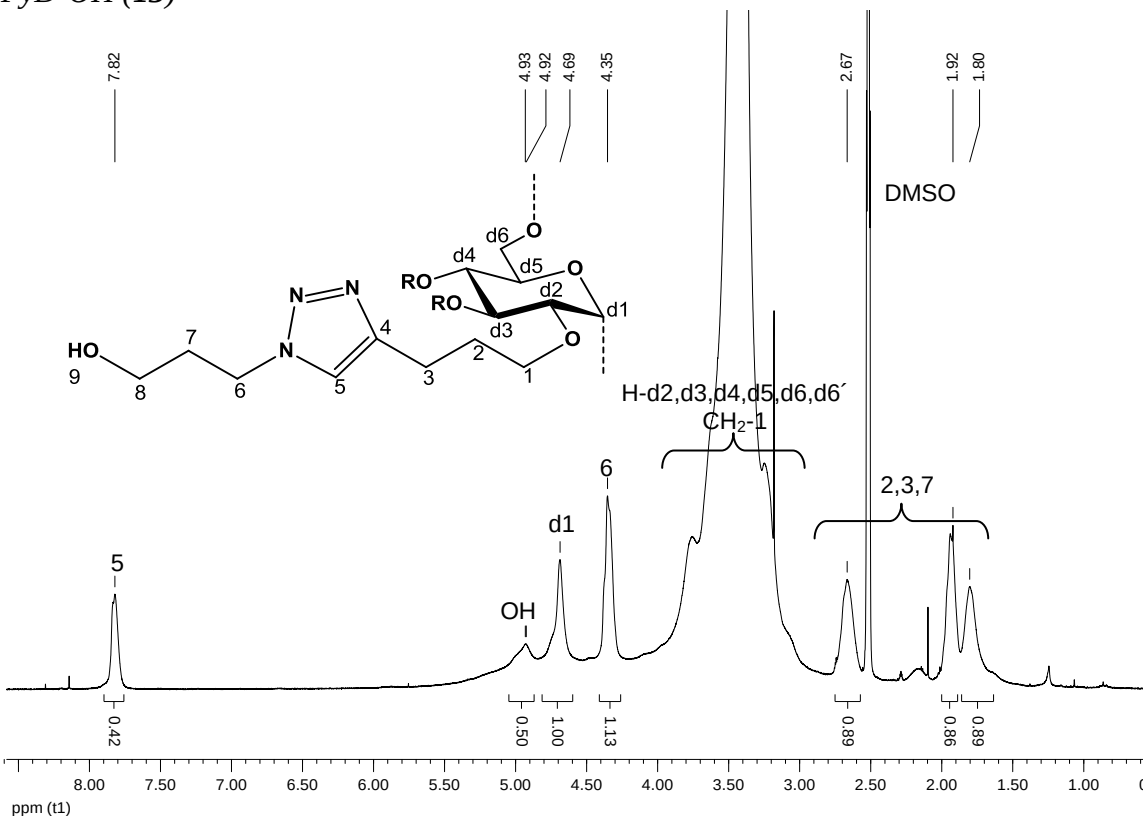

Fig. 8.12: ^{1}H-NMR spectrum of PyD-OH (**13**) (400 MHz, DMSO-d_6)

^{1}H-NMR of PyD-OH (**13**) was recorded in DMSO-d_6. Keeping in mind that DS of pentynyl in PyD-17 used in this experiment is 0.43, conversion of pentynyl groups into triazoles was calculated from the ratio of intensities of the anomeric proton (d-1) i.e. proton of C-1 in dextran (4.69 ppm. Fig. 8.12), and the proton in the triazole ring (H-5,7.82 ppm) as follows:

$$DS_{triazole} = \frac{\int CH\text{-}5}{\int d\text{-}1}$$

$$DS_{triazole} = 0.42$$

To make calculations simple, integral for d1 is set to 1.
Calculation can also be made on the basis of relative intensities of CH_2-7 (1.92 ppm), or triazole CH-5 (7.82 ppm) referred to the anomeric proton d-1 (4.69 ppm).

$$DS_{triazole} = \frac{\frac{\int CH_2\text{-}7}{2}}{\int d\text{-}1}$$

$$DS_{triazole} = 0.43$$

Conversion of pentynyl groups into respective 1,2,3-triazole is estimated to be 98% and 100%, respectively, which is in agreement with conversion calculated from GLC (98%, Table 8.2). Terminal -OH of alcohol was not visible in NMR spectrum.

*PyD-NH-Boc (**17**)*

^{1}H-NMR spectrum of PyD-NH-Boc (**17**) was recorded in DMSO-d_6. Conversion of pentynyl groups into triazoles was calculated from relative intensities of H-5 (7.82 ppm) and that of anomeric proton (d-1, 4.69 ppm).

$$DS_{triazole} = \frac{\int CH\text{-}5}{\int d\text{-}1}$$

$$DS_{triazole} = 0.47$$

Apparent conversion exceeds 100%. Other characterization methods i.e. EA (86%) and GLC (77%) show less conversion. Most probably, intensity of d-1 (4.69 ppm) was under-estimated due to many additional signals in this area.

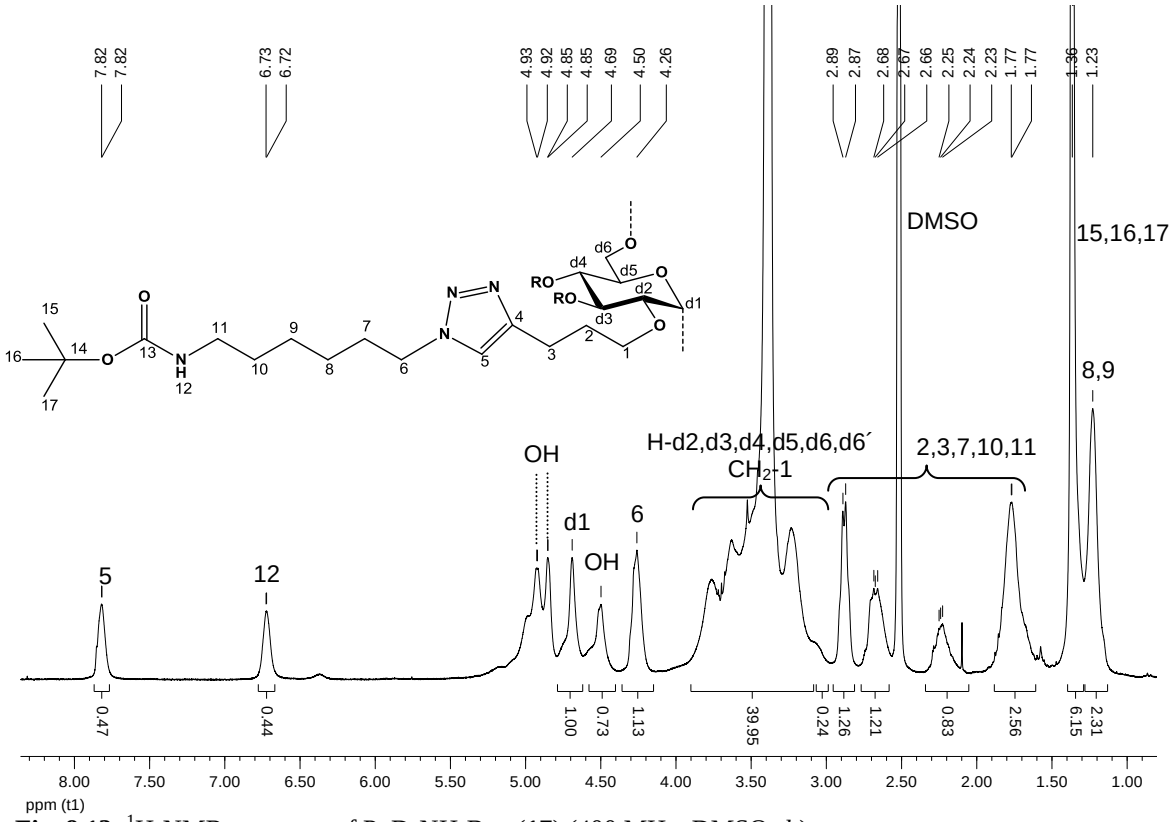

Fig. 8.13: ^{1}H-NMR spectrum of PyD-NH-Boc (**17**) (400 MHz, DMSO-d_6)

*PyD-COOH (**14**)*

^{1}H-NMR spectrum of PyD-COOH (Fig. 8.14) recorded in DMSO-d_6 shows that 77% of alkyne groups were converted into respective 1,2,3-triazoles. Calculations were made on the basis of relative intensities of H-5 (7.84 ppm) and that of d-1 (4.67 ppm).

$$DS_{triazole} = \frac{\int CH\text{-}5}{\int d\text{-}1}$$

$$DS_{triazole} = 0.33$$

Triazole DS 0.33 (77%) is comparable with conversion calculated from EA (83%) and GLC (85%).

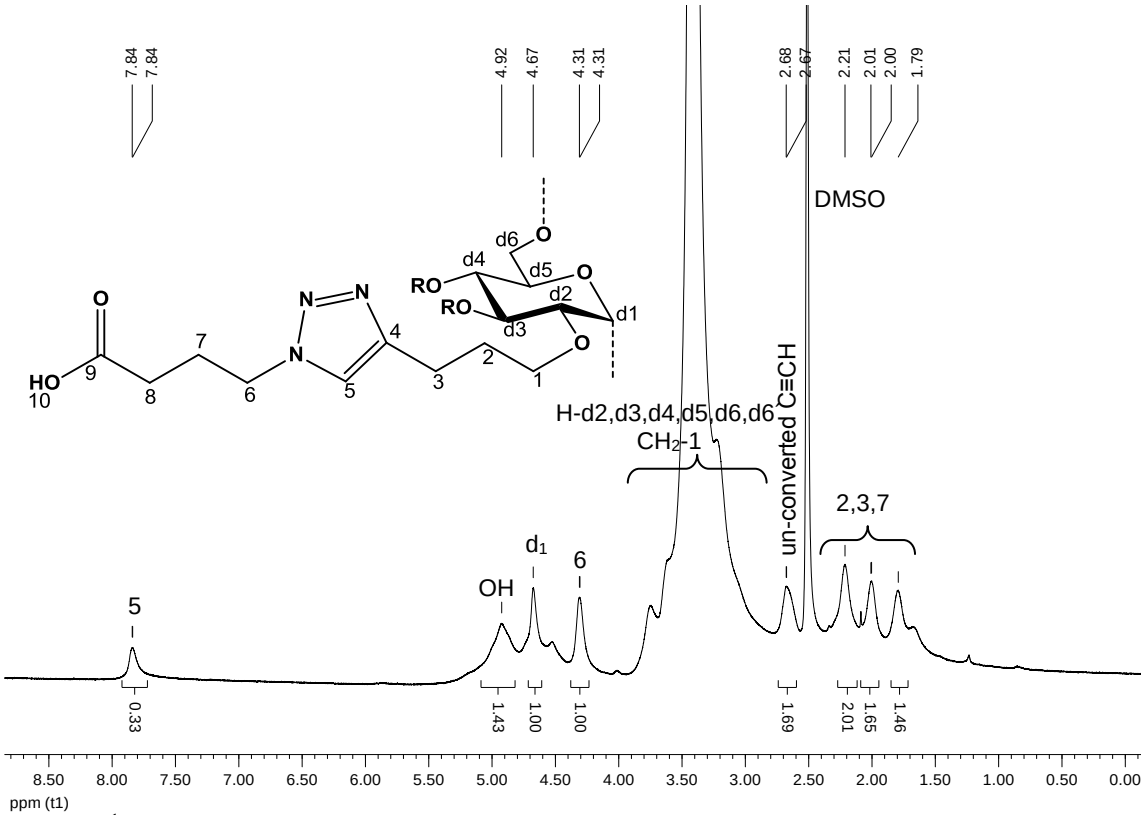

Fig. 8.14: ^{1}H-NMR spectrum of PyD-COOH (**14**) (400 MHz, DMSO-d_6)

*PyD-biotin (**16**)*

^{1}H-NMR spectrum of PyD-biotin (Fig. 8.15) recorded in DMSO-d_6 show 79% conversion which is in close agreement with EA (76%) and not much away from conversion calculated by GLC (63%). Calculation was made as:

$$DS_{triazole} = \frac{\int CH\text{-}5}{\int d\text{-}1}$$

$$DS_{triazole} = 0.34$$

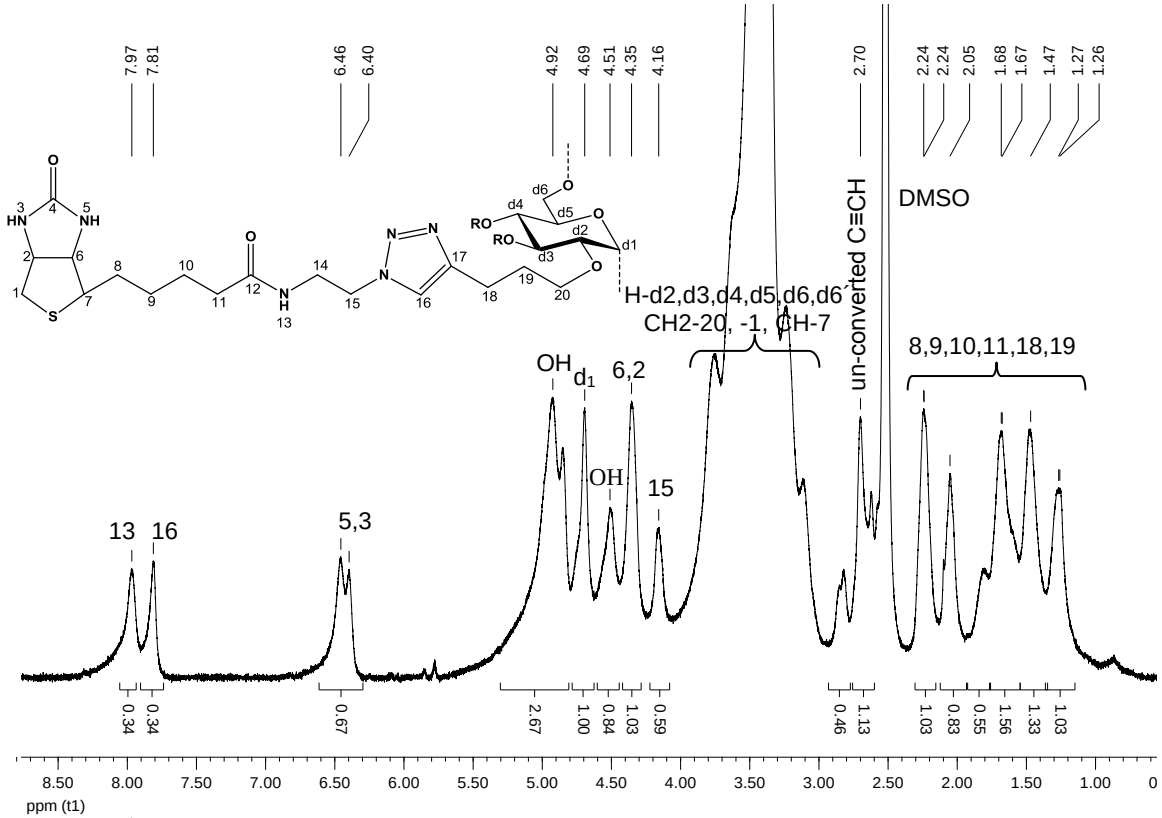

Fig. 8.15: ^{1}H-NMR spectrum of PyD-biotin (**16**) (400 MHz, DMSO-d_6)

*PyD-toc (**18**)*

^{1}H-NMR spectrum of PyD-toc (**18**) was recorded in pyridine-d_5(Fig. 8.16). Calculation of the conversion of pentynyl groups into respective 1,2,3-triazoles by comparing intensity of anomeric proton (d-1) and that of triazole proton was not possible in this case because two peaks at 4.43 ppm and 4.49 ppm were not separated in pyridine used as solvent in this case since product was not soluble in DMSO-d_6. Already from ^{1}H-NMR of PyD-17, recorded both in DMSO-d_6 and pyridine-d_5 (Fig. 6.22, 6.23), it is known that chemical shifts are less well resolved in pyridine-d_5 as compared to DMSO-d_6.

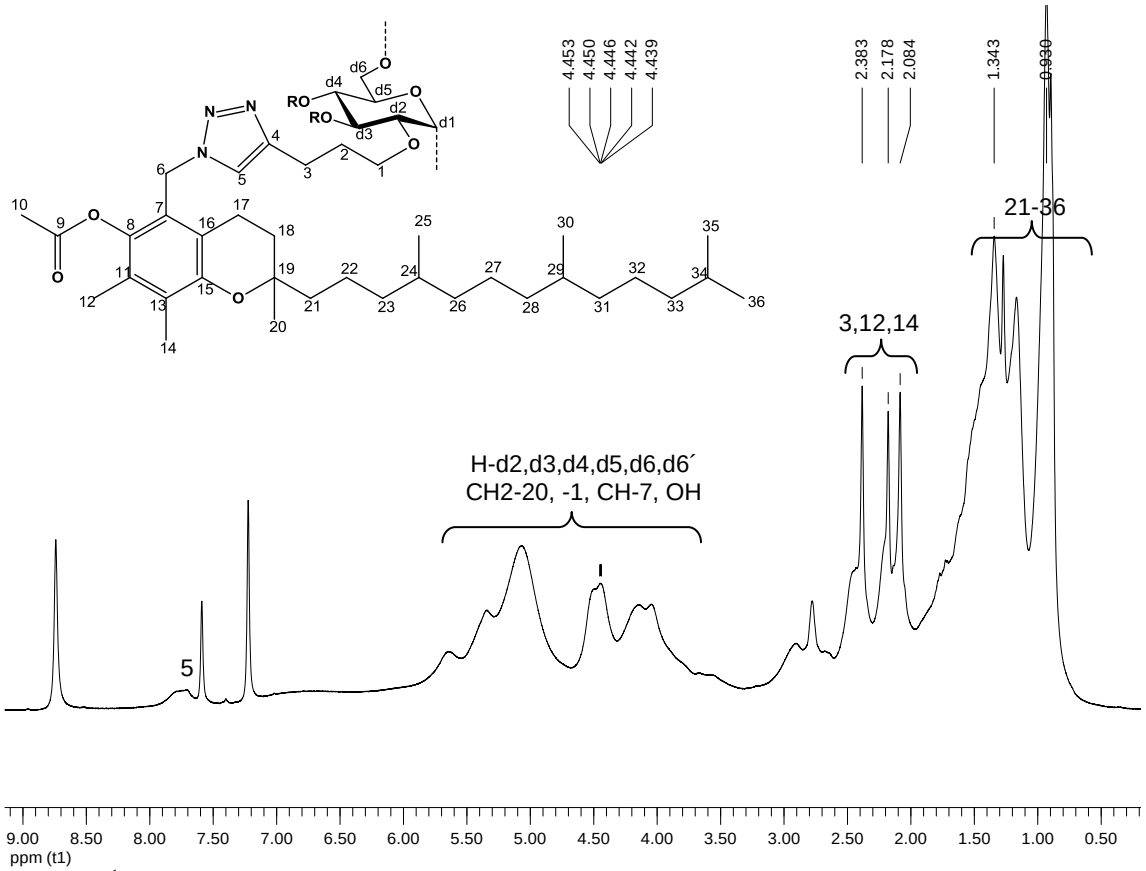

Fig. 8.16: ^{1}H-NMR spectrum of PyD-toc (**18**) (400 MHz, Pyridine-d_5)

Conversion of alkyne groups into triazoles calculated by EA, GLC and NMR is summarized for all samples and methods in Table 8.12.

Table 8.12: Comparison of pentynyl conversion into 1,2,3-triazole by EA, GLC and NMR spectroscopy

Sample	Conversion [%]		
	EA	GLC	NMR
PyD-NH_2 (**12**)	95	98	
PyD-OH (**13**)	(140)	98	98
PyD-NH-Boc (**17**)	86	77	109
PyD-COOH (**14**)	83	84	77
PyD-SH (**15**)	(123)	93	
PyD-biotin (**16**)	76	63	79
PyD-toc (**18**)	(107)	56	

Conversion exceeding 100% from EA (PyD-OH, PyD-SH, PyD-toc) is most probably due to residual azide in theproduct. GLC values are expected to be too high, and deviation should be the higher, the lower the real conversion is since incomplete

transformation of two- and threefold pentynylated glucosyl units causes overestimation. In NMR, also too high values are expected due to inaccurate integration of the broad, often not fully resolved signals. And probably incomplete integration of all signals belonging to H-1 of dextran.

8.3 Conjugation of Biotinylated PyD with Labeled Streptavidin

Streptavidin is a 52,800 Datetrameric protein purified from the bacterium*Streptomyces avidinii* [207]. It finds wide use in molecular biology through its extraordinarily strong affinity for biotin. The dissociation constant (K_d) of the biotin-streptavidin complex is on the order of ~10^{-15} mol/L [208], ranking among the strongest non-covalent interactions known in nature.

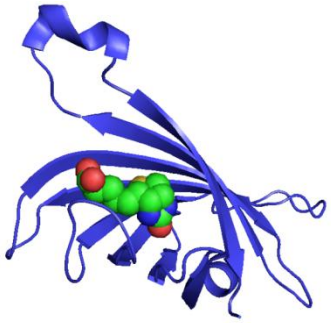

Fig. 8.17: Monomeric streptavidin (ribbons) biotin (spheres)-complex [209, 210]

The crystal structure of the streptavidin-biotin complex was determined in 1989 by Hendrickson *et al*. [211]. The structure of a streptavidin monomer is composed of eight antiparallel β-strands, which fold to give an antiparallel beta barrel tertiary structure. A biotin binding-site is located at one end of each β-barrel. Four identical streptavidin monomers (i.e. four identical β-barrels) associate to give streptavidin's tetrameric quaternary structure. Thus, streptavidin is a tetramer and each subunit binds biotin with equal affinity.

Labeled streptavidin was complexed with PyD-biotin simply by stirring aqueous solution of streptavidin with PyD-biotin. To confirm that streptavidin was attached only to biotin and not unspecifically adsorbed to PyD, a control experiment was carried out with PyD.

After incubation with streptavidin, both, PyD and PyD-biotin were washed thoroughly with water and dried. Fluorescence was recorded for both redispersed samples in DMSO (Fig. 8.18). PyD-biotin shows strong absorption at 555 nm while PyD did not show any absorption, confirming that streptavidin was specifically bound to biotin.

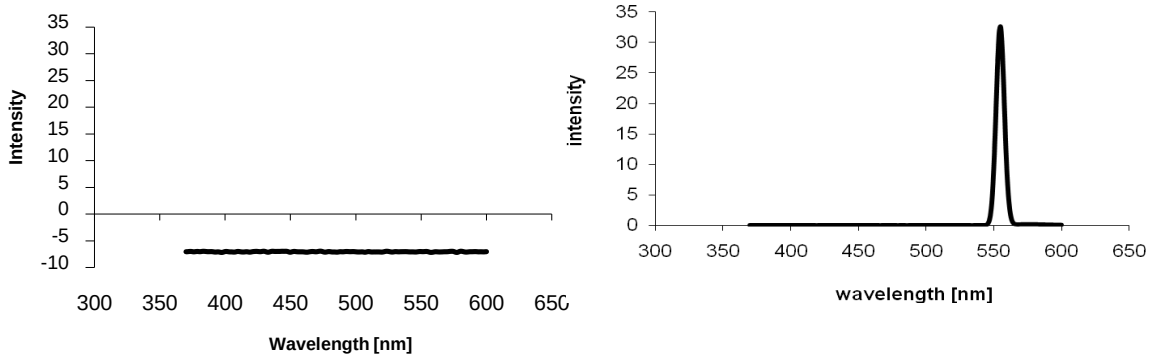

Fig. 8.18: Fluorescence of PyD (left) and PyD-biotin (right) treated with labeled streptavidin

In next step, PyD-biotin after dissolving in DMSO and pyridine (1% and 3.3%) was spin-coated on silicon wafers. These experiments were carried out by Nico Lämmerhardt at the institute of semiconductor technology. For control, PyD was also used in parallel. For some samples where solution was not clear, aliquots of the sample solutions were centrifuged and/or microfiltered.

Silicon wafers were cleaned with Piranah solution, etched with HF etching solution, and heated at 800 °C for 2 hours for thermal oxidation. The oxidation produces about12 nm of oxide layer checked by elipsometric measurements.

For removal of contamination, the silicon wafers were sonicated for 3 minutes in ethanol just before spin coating of PyD and PyD-biotin at 2000 rpm for 5 minutes. The film thickness of samples is given in Table 8.13.Comparison of centrifuged and un-centrifuged samples of the same concentration show slightly lower film thickness in case of centrifuged samples due to removal of insoluble parts resulting into lower concentration (Table 8.13), a parameter determining film thickness[212]. Comparison of PyD and PyD-biotin samples of the same concentration show that PyD-biotin samples have slightly higher film thickness due to its bigger molecules (entry 1,2,5,6, Table 8.13).

Slight difference in film thickness of sample 5,7 and 6,8 could be due to different solvents,probably solvents with low viscosity (pyridine) and higher volatility leads to lower film thickness. Filtration of samples did not show any strong effect on film thickness.Moreover, samples with 3.3% solution show a higher variation of several successive measured values on the same sample with a higher film thickness in the middle and a lower at the edges of the same substrate while 1% sample solution shows a lower variation in film thickness over the substrate, so this concentration was chosen for further binding experiments of fluorescence-marked streptavidin.

PyD and PyD-biotin samples were incubated in a 0.008% aqueous solution of Atto-550 labelled streptavidin for 10 minutes. Samples were washed thoroughly with deionized water and dried under nitrogen.

Film thickness measured after incubation with Atto-550 labeled streptavidin show almost no difference for PyD samples (no matter centrifuged or not centrifuged, Table 8.13). Even a slight decrease in film thickness, was observed. On the other hand, PyD-biotin samples (7, 8, Table 8.13) show an increase of about 15 nm in film thickness after incubation with Atto-550 labeled streptavidin.

Table 8.13: Ellipsometric data and calculated film thickness of PyD-17 and PyD-biotin (**16**) coated on silicon wafers and after incubation with Atto-550 labelled streptavidin for selected samples (data provided from Nico Lämmerhardt)

Sample No.	Sample	c/f	Thickness (nm)	Streptavidin Thickness (nm)
1	PyD[1]	c	6.0 ± 0.3	< 0
2	PyD[1]	-	7.3 ± 2.2	< 0
3	PyD[2]	c	55.3 ± 2.9	
4	PyD[2]	-	57.4 ± 14.4	
5	PyD-biotin[1]	c	7.8 ± 0.6	
6	PyD-biotin[1]	-	10.2 ± 1.7	
7	PyD-biotin[1]	c	10.0 ± 0.3	15.1 ± 1.8
8	PyD-biotin[1]	-	13.2 ± 0.8	15.8 ± 2.0
9	PyD-biotin[2]	c	39.9 ± 1.2	
10	PyD-biotin[2]	f	59.3 ± 5.8	
11	PyD-biotin[2]	c,f	27.5 ± 3.0	

All samples were dissolved in DMSO except 5 and 6 which were dissolved in pyridine

1 1% solution
2 3.3% solution
c Centrifuged
f Filtered

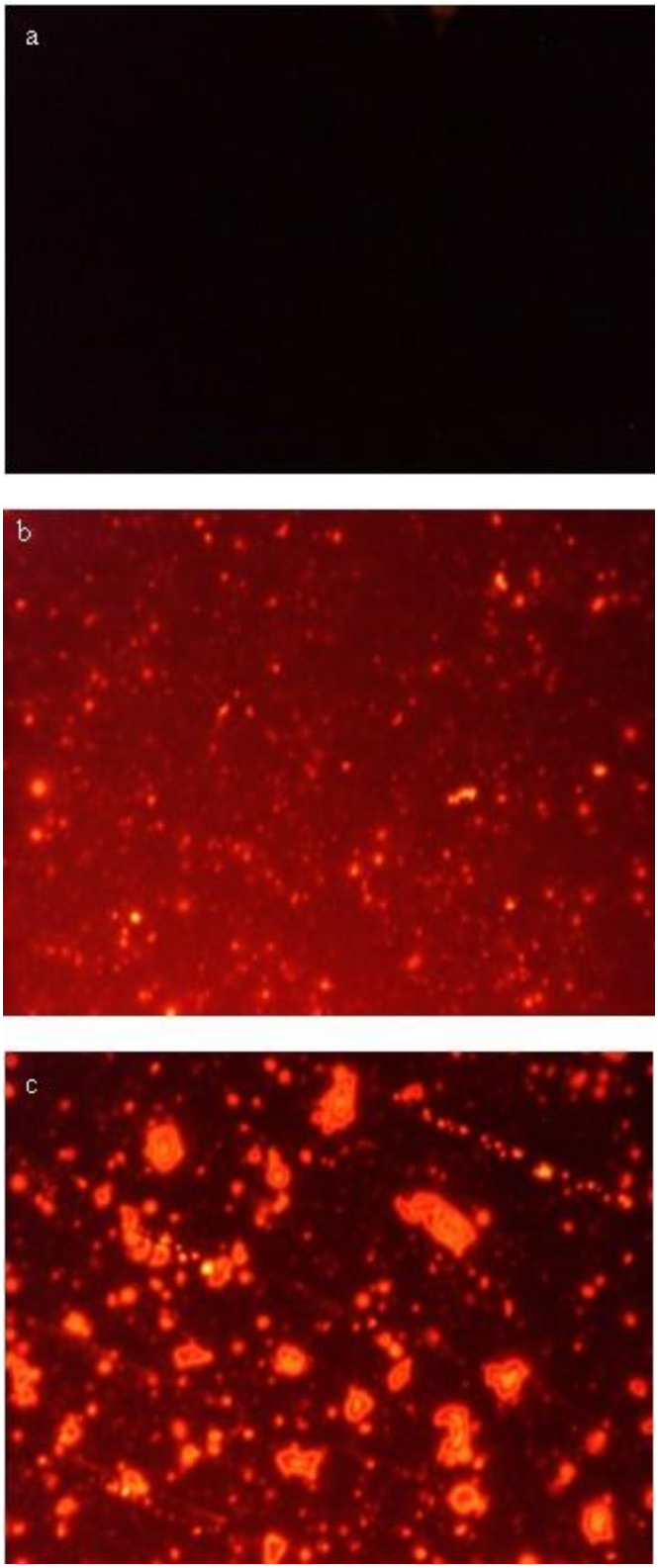

Fig. 8.19: Fluorescence microscope images (500x) of spin-coated PyD-17 and PyD-biotin after incubation in Atto-550 labeled streptavidin. PyD-17 (sample 2 in Table 8.13) in DMSO (a), centrifuged PyD-biotin (sample 7 in Table 8.13) in DMSO (b) and non-centrifuged PyD-biotin (sample 8 in Table 8.13) in DMSO (c).

The calculated thickness of the streptavidin film is about three times higher than its normal size of 4.5 x 4.5 x 5 nm^3 [213]. This seems to be too much because more than one layer of streptavidin molecules should not be bound. The main reason for this deviation is that the refractive indices used for the calculations are those of streptavidin and dextran instead of streptavidin-Atto550 and PyD-biotin. The fluorescence microscope images of streptavidin-Atto550 treated PyD and PyD-biotin samples show a great difference with almost no fluorescence for unmodified PyD control (Fig. 8.19, a) and strong fluorescence for PyD-biotin samples (Fig. 8.19, b, c). Comparison of centrifuged (Fig. 8.19, b) and non-centrifuged (Fig. 8.19, c) samples of PyD-biotin show that the latter contains larger biotinylated aggregates, while these have been removed by centrifugation..

9 LIPASE IMMOBOLIZATION ON PROPARGYL AND PENTYNYL DEXTRAN

9.1 Introduction

Lipases (triacetylglycerol ester hydrolases, E.C. 3.1.1.3) are proteins with molecular weights above 20,000 Da, and molecular size above 4 nm in diameter [214]. They are the most popular enzymes in biocatalysis, because they can be used in a variety of reactions due to their regio- and enantioselectivity, and their reusability [215-218]. During the last decade, lipases have become of high interest due to their applications in chemical and pharmaceutical industries e.g. for hydrolytic reactions, esterification, transesterification, for kinetic resolution of racemic or pro-stereogenic drugs [215], i.e. for reactions in both, aqueous and organic media [219-221]. Lipases are able to catalyze the hydrolysis of triacylglycerols in aqueous medium and ester synthesis in organic media [222]. It is not possible to employ free lipase in organic solvents, since medium and substrates can denature the enzyme by extracting the last traces of water from the protein, a minimum of which is essential for maintaining the quaternary structure of the enzyme protein and is also required for these esterification reactions [223, 224]. There are many issues related to the applications of free enzymes e.g. high cost and instability etc. To exploit their technical and economical advantages, it is recommended to immobilize the lipase to reduce costs and enhance its stability. Immobilized enzymes have many advantages over their un-immobilized counterparts due to their storage, operational, thermal and conformational stability, simple recovery of catalyst and products after reaction, reutilization, possibility of continuous reaction and easy operation and design of bioreactor [219, 225]. Moreover, quality of the products can be improved by avoiding byproducts or unwanted intermediates and easier separation [226].

Many techniques for lipase immobilization have been developed over last three decades. Generally they can be divided into four classes: adsorption on polymer-based or inorganic materials, encapsulation, covalent attachment to a carrier, and cross-linking for example using glutardialdehyde [225, 227, 228]. Among these techniques, adsorption is most popular due to simpleness and high activity yield [225]. The technique of immobilization greatly influences the properties of the biocatalyst (means: enzyme on

adsorbent) and kinetics of the organic reaction. All above mentioned techniques have their own advantages and drawbacks. Each of these techniques have been further improved by developing new materials [229, 230]. Surface area, porosity and hydrophobic-hydrophilic balance are the important parameters of the support used for immobilization of enzymes.

A variety of supports have been used for different kinds of lipases e.g. polystyrene anion exchange resins for amyloglucosidase [215], glycidyl methacrylate-divinyl benzene copolymers and macroporous cation exchange methacrylate for penicillin-G-acylase [231], amino functionalized magnetic supports for covalent immobilization of *Candida cylinderica* lipase [232], agarose and cross-linked dextran for trypsin and lipase B from *Candida antartica*[233, 234], carboxymethyl cellulose and hydrophobic supports for hydrolases [231, 232], alginate and chitosan for lipase from *Yarrowia lipolytica*[222] and lignocellulose for *Candida regusa* [226]. Among these different kinds of supports, polysaccharides, beside low cost in some cases, are non toxic, biocompatible, inert in physiological conditions and can offer appropriate micro environment to avoid severe conformational changes of the enzyme. By chemical modification, the hydrophilic/hydrophobic balance can be turned to adapt it to the enzyme structure and to provide the well-known interfacial activation of lipases upon adsorption onto this type of surfaces [235]. In the presence of hydrophobic support, the open form of the lipase become adsorbed to the hydrophobic support and thus shifting the equilibrium of "open form" and "closed form" in the favor of open form of the lipase [234, 236]. Attachment on hydrophobic support usually increases the rigidity of the immobilized enzyme, making them more resistant to small conformational changes induced by heat, organic solvents and denaturing agents [217]. Due to a wide variety of conditions applied, lipases are often easily inactivated and difficult to be separated from the reaction system for reuse which limits their industrial applications [222]. Operational cost of industrial processes can be significantly reduced by reusing the enzyme immobilized on a suitable support along with improvement in its activity and stability [234].

9.2 Comparison of Lipase Immobilization on Propargyl Dextran andOther Adsorbents

Extracellular lipase from *R. arrhizus* was immobilized on PgD, celite, alumina, wood shaving, fuller's earth, and silica gel. 1 mL of 2% aqueous solution per 100 mg of adsorbent was used. Mixtures were stirred at room temperature for 1 hour, centrifuged to remove un-adsorbed lipase and freeze-dried. Amount of lipase adsorbed on different supports (Table 9.2) was calculated from the nitrogen content in the biocatalyst according to Mariotti *et al*. [237] using the following formula:

$$\text{Protein (\%)} = \text{N (\%)} \times 6.25$$

To investigate the dependence of lipase adsorption on the DS of PgD, samples with different DS were used. PgD-14 with DS_{GC} 0.69 (see Table 6.1) corresponding to 13.7% (w/w) hydrophobic groups linked to the hydrophilic polysaccharide backbone showed maximal lipase adsorption.

Table 9.1: Dependence of lipase immobilization on DS of PgD (see Table 6.1)

Sample	DS	N [%]	Protein adsorbed [%]*
PgD-7	0.26	0.75	4.68
PgD-14	0.69	1.93	12.06
PgD-15b	0.99	0.46	2.89
PgD-4	1.68	0.32	2.00

* Protein (%) = N (%) × 6.25

Table 9.1 shows that a very low DS is not suitable for immobilization due to remaining high polarity of the only slightly modified dextran, and at higher DS, the hydrophilic/hydrophobic balance seem to run out of optimum again. The substitution pattern of PgD-14 (DS 0.69) showed remarkable deviation from a random distribution (Spurlin model) with high density of alkynyl residues and a high portion of unsubstituted domains. Thus, the very good binding properties of PgD correspond to the observations reported by Naka *et al*. that block-copolymers with hydrophilic and lipophilic sequences are very well suited for enzyme stabilization [238]. Bushan *et al*. systematically varied the composition of epoxy copolymers and found a narrow range of optimal binding and

activity at a certain hydrophilic/lipophilic balance [215]. The surface area of PgD-14 a water-insoluble powder was determined to be 10.5 ± 1.1 m^2/g. For comparison: Bushan *et al*. [215] reported surface areas in the range of 47–130 m^2/g for macroporous synthetic polymers with highest protein loading observed 3.4%. Due to high protein adsorption, PgD-14 was selected for further studies.

Hydrolytic activity of the pure and immobilized enzyme was determined titrimetrically on the basis of olive oil hydrolysis by the modified method of Samad *et al*. [239]. For this purpose, gum acacia was dissolved in aqueous solution of $CaCl_2$. Olive oil was added and homogenized. Tris maleate buffer (pH 7) was added to maintain the pH. Then, the biocatalyst was added to the mixture. A blank sample was prepared in parallel containing all reagents except biocatalyst. The enzyme substrate mixture was incubated at 30 °C in a shaking incubator for 60 minutes before adding ethanol-acetone mixture (1:1, v/v) to stop the reaction. The liberated fatty acids were titrated against ethanolic KOH. For the hydrolytic activity, a lipase unit was defined as the amount of the biocatalyst which released 1 µmol fatty acid per minute at 30 °C.

Table 9.2: Amount of immobilized lipase on different adsorbents and its hydrolytic activity

Lipase immobilized on	**Protein absorbed (%)**[a]	**Hydrolytic activity (u g^{-1})**[b]
-(free enzyme)		9600
PgD-14	12.06	1130
Celite	10.30	745
Fullers earth	9.50	400
Silica gel	7.11	214
Wood shavings	7.05	382
Alumina	6.82	70

a: Protein present in the final dried biocatalyst (adsorbent+enzyme).

b: Activity unit of lipase per gram of the biocatalyst (adsorbent + enzyme), 1u = 1 µmol fatty acids released per minute.

Hydrolytic activity for all biocatalysts was determined using the following formula (for details see Experimental):

$$\text{Hydrolytic activity} = V \times 166$$

V is the difference in volume of KOH used for biocatalyst and for blank sample.

9.2.1 Evaluation of Lipase Immobilized on Propargyl Dextran and other Adsorbents for Esterification of Geraniol and Octanoic Acid

Larvae of click beetles (family *Elateridae*) are most important soil dwelling pests. Some of their species are very harmful for a variety of crops e.g. corn and grain [240]. Females of these click beetles produce long rang sex pheromones to attract males. Toth *et al*. [241] have already determined chemical composition of these pheromones. Many researchers have tested these compounds as bait for beetle traps. The optimized bait combination for some click beetle species are as follows [242, 243]: geranyl octanoate (**37**) and geranyl butanoate (**38**) for *Agriotes lineatus*, geranyl isovalerate (**39**) for *A. litigiosus*, geranyl hexanoate (**40**) and geranyl octanoate (**37**) for *A. obscurus*, geranyl butanoate (**38**) for *A. sputator*, and (E,E)-farnesyl acetate (**41**) for *A. ustulatus*.

The biological activity of these compounds depends upon their isomeric purity e.g. geraniol and nerol are isomers but geranyl and neryl esters have entirely different fragrances. Production of isomerically pure geranyl esters by conventional chemical methods is hampered by isomerization in the presence of acid catalyst at elevated temperature. However, the lipase-catalyzed esterification is a promising technique yielding products of absolute isomeric purity.

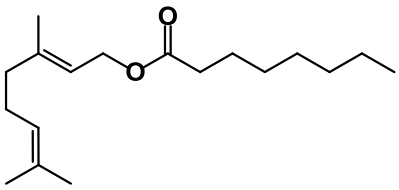

37

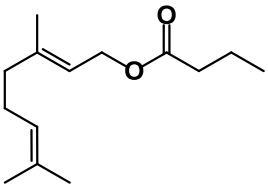

38

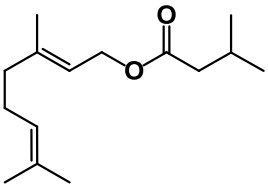

39

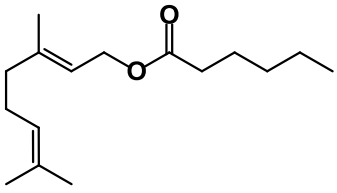

40

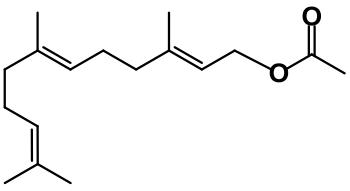

41

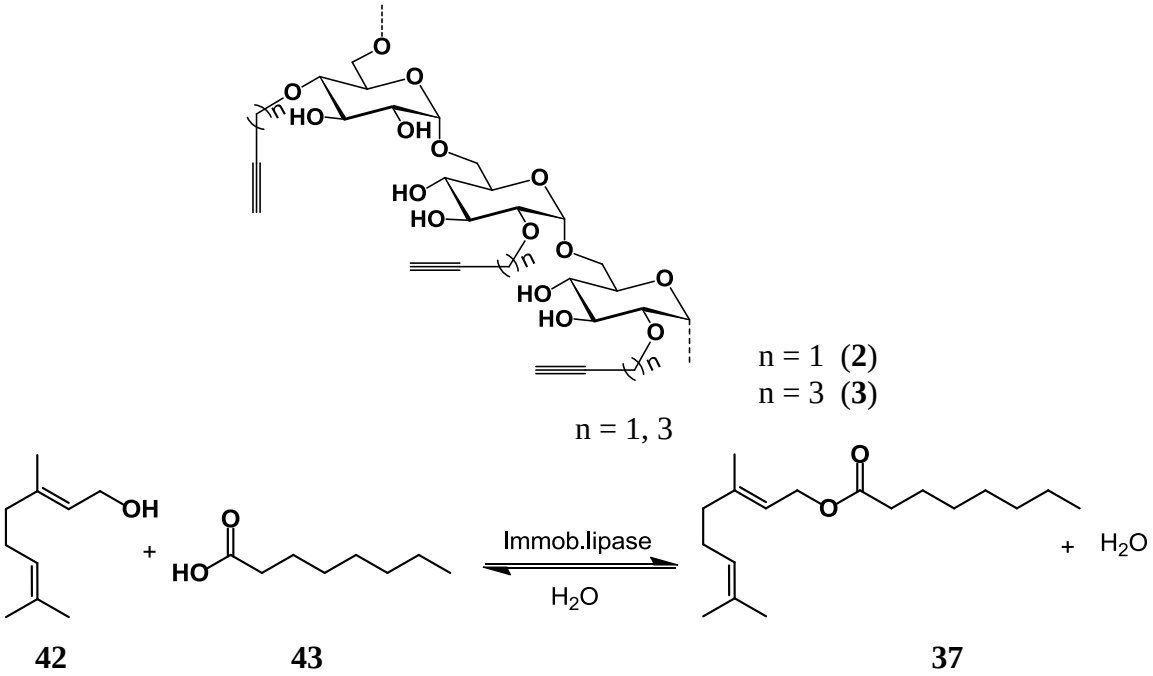

Scheme 9.1: Synthesis of geranyl octanoate (**37**).

Lipase (*R.arrhizus*) immobilized on different adsorbents was used to catalyze the esterification of geraniol (**42**) and octanoic acid (**43**). Starting conditions were chosen according to earlier findings for other supporting materials [244]. Free lipase or the lipase immobilized on wood shaving, fuller's earth, silica gel, alumina, and PgD, each corresponding to 500 units (hydrolytic activity) of lipase (calculated according to the protein content of the immobilized enzymes and hydrolytic activity of free lipase), were added to the reaction mixture containing equimolar amounts of both geraniol and octanoic acid in *n*-hexane. Samples were drawn periodically and its composition analyzed to determine esterification activity of lipase from the yield of geranyl octanoate (**37**). The data in Table 9.3 show that the free lipase did not catalyze the esterification at all. The lack of synthetic activity of soluble lipases in non-aqueous media has also been reported by other workers [245, 246].

The amount of fatty acids consumed in the esterification reaction per minute and gram of biocatalyst, i.e. $\mu mol \cdot min^{-1}g^{-1}$, is defined as esterification activity of the biocatalyst. Since the biocatalyst might need a few minutes to adapt to the conditions of the reaction system. it is a general practice to calculate average esterification activity (Table 9.3) for the first hour of the reaction. Esterification activity for all biocatalysts was determined by

titrating an aliquot of the sample withdrawn after one hour of the reaction, against KOH (alcoholic).

Comparison of lipases immobilized on different insoluble supports had shown that PgD-14 did adsorb maximum amount of lipase and showed a hydrolytic activity of 1130 units g^{-1} corresponds to 98% activity yield reported by Chang *et al*. [220], thus showing no loss of activity by immobilization. However, it was also very active in the organic reaction medium and esterified 987 µmol $min^{-1}g^{-1}$ of octanoic acid referred to immobilized enzyme (adsorbent + enzyme) in *n*-hexane (initial rate of esterification). Therefore, the Esterification activity is 87% of the hydrolytic activity, corresponding to 85% activity yield with respect to the free enzyme, to the best of our knowledge not found before.

Table 9.3: Effect of different adsorbents on lipase hydrolytic and esterification activities

Lipase immobilized on	**Hydrolytic activity (u g^{-1}) referred to biocatalyst**	**Esterification activity (µmol min^{-1} g^{-1})[a]**	**Ratio of Esterification to hydrolytic activity**
-(free enzyme)	9600	0	
PgD-14	1130	987	0.87
Celite	745	115	0.15
Fullers earth	400	51	0.13
Silica gel	214	12	0.06
Wood shavings	382	161	0.42
Alumina	70	42	0.60

a: 1 µmol of fatty acid consumed in the esterification reaction per minute per gram of biocatalyst [240]

As has been discussed by Cabrera, Mateo and Fernandez-Lafuente [234, 247, 248], binding of lipases to a hydrophobic support shifts the equilibrium between the active (‘‘open’’) and non-active (‘‘closed’’) conformation, where the active site is isolated by an oligopetide ‘‘lid’’ [249], in favor of the active form due to binding and thus fixation of this conformation by hydrophobic interaction. This is also the explanation for the hyperactivating effect of immobilization.

In contrast to the considerable hydrolytic activity of 745 ug^{-1} in aqueous system (75% activity yield), the celite-adsorbed lipase, exhibits only low esterification activity in non-aqueous solvents (115 ug^{-1}, corresponding to 15% of hydrolytic activity). In case of the lipase adsorbed on wood shavings, although the esterification activity referred to lipolytic activity was relatively high (42%), while both, hydrolytic and synthetic activities

were low. Thus lipase of *R. arrhizus* on PgD-14 was used as biocatalyst for further studies on the synthesis of geranyl octanoate.

9.3 Optimization of Reaction Conditions for Esterification of Geraniol and Octanoic Acid Catalyzed by Immobilized lipase of *R. Arrhizus*

9.3.1 Effect of Solvent on Esterification Reactivity of Lipase

It is known that the nature of the reaction medium greatly influences the activity of the biocatalysts. Different organic solvents namely *n*-hexane, *n*-octane, petroleum ether, diethyl ether, benzene, toluene, carbon tetrachloride, chloroform, acetone, THF, and *N*,*N*-dimethyl formamide were studied as non-aqueous reaction media. The PgD-14 immobilized lipase of *R. arrhizus* was used at an amount of 0.44% (w/v) for the biocatalysis of the esterification. Fig. 9.1 shows that in *n*-hexane (dielectric constant ε at 20 °C, 1.9), the enzyme exhibited maximum esterification activity. Other non-polar hydrocarbon solvents such as *n*-octane (ε = 2.0) and petroleum ether were also quite suitable for lipase-catalyzed esterification. Polar and aprotic solvents such as acetone (ε =20.7), THF (ε = 7.52) and DMF (ε = 38.3) were not found to support enzymatic ester synthesis. This might be due to extraction of residual water from the enzyme by the hydrophilic solvents which is essential for conformational integrity of the protein. A structural change in the protein results in an inactive or less active conformation. In contrast, hydrophobic solvents such as *n*-hexane do not disturb the aqueous microenvironment of the enzyme protein, while in the p-electron rich aromatic solvents benzene and toluene as well as in the halogenated chloroform and carbon tetrachloride, the esterifying activity also is very low. This behavior of the immobilized lipase of *R. arrhizus* in different solvents is similar to that of lipozyme reported by Miller *et al*. [245]. However, these results are somewhat different from those reported for immobilized lipase of *Mucor miehei* which was found to retain some activity even in solvents like THF, and DMF [250].

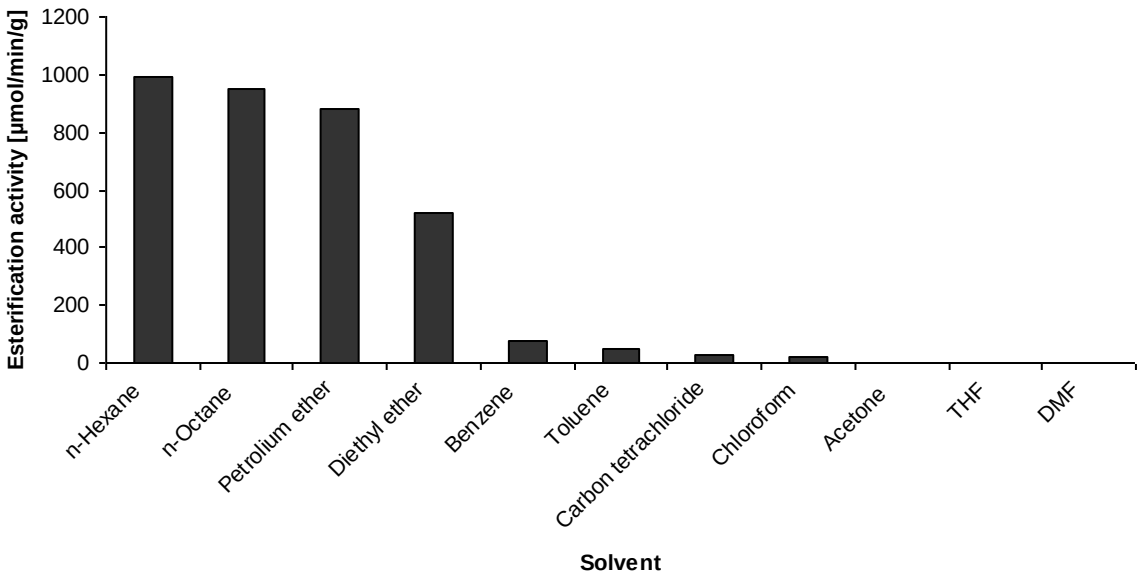

Fig. 9.1: Effect of solvent on esterification activity of the lipase (*R. arrhizus*) immobilized on PgD-14 (DS 0.69).

9.3.2 Effect of Substrate Concentration on Lipase-Catalyzed Synthesis of Geranyl Octanoate

In enzymatic esterification, the concentration of the acid and alcohol affect the activity of the enzyme, the rate of esterification and the yield of the ester. The concentration of octanoic acid was ranged from 0.1 mol L^{-1} to 1.2 mol L^{-1}, while geraniol was constant at 0.4 mol L^{-1}. The initial rate of esterification increased with increase in concentration of the acid until reaching an equimolar ratio at 0.4 mol L^{-1} (Fig. 9.2). This loss of esterification activity of the immobilized lipase beyond 0.4 mol L^{-1} of the acid may be attributed to acidification of the hydration layer of the enzyme protein [246]. Similarly the concentration of geraniol was varied between 0.1 mol L^{-1} and 1.2 mol L^{-1} with octanoic acid kept constant at 0.4 mol L^{-1} (Fig. 9.2). Again maximum of initial reaction rate was reached at equimolar 0.4 mol L^{-1}. However, in contrast to octanoic acid, the maximum activity remained constant within experimental error at higher alcohol concentrations.

Using these concentrations of the substrates and 0.44% (w/v) immobilized lipase of *R. arrhizus* (1130 lipase u/g), an esterification rate of 987 µmol $min^{-1}g^{-1}$ was achieved.

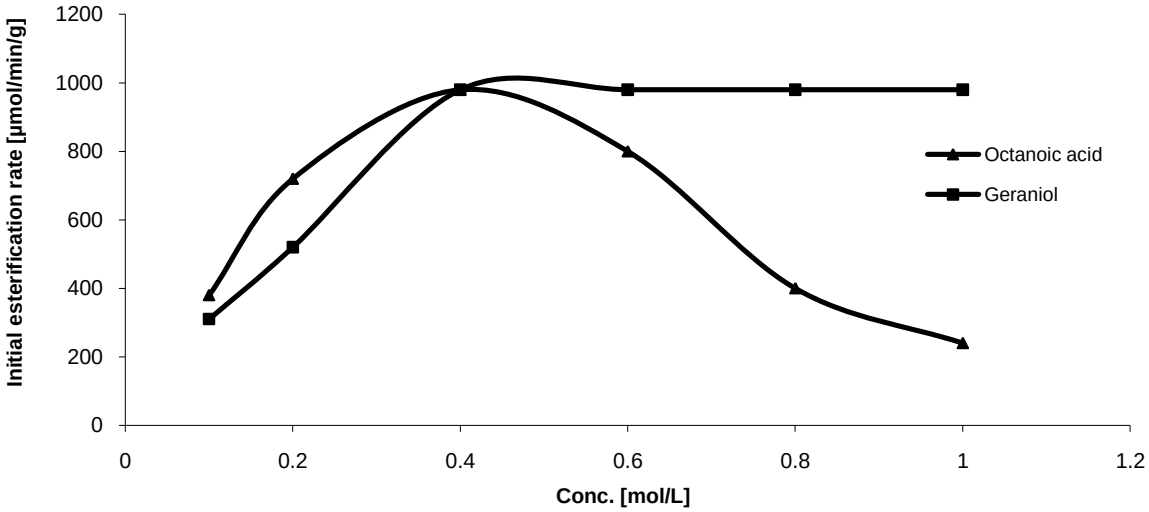

Fig. 9.2: Effect of concentration of octanoic acid at constant geraniol concentration of 0.4 mol L^{-1} and of geraniol at constant octanoic acid concentration of 0.4 mol L^{-1} on initial esterification rate.

9.3.3 Effect of Moisture on Lipase Mediated Esterification

The esterification is a reversible reaction. To avoid hydrolytic reaction and shift the equilibrium of the reaction to the ester side, removal of water from the reaction mixture is necessary. However, as mentioned above, the presence of some water is vital for all enzymatic activities. Forces such as salt bridges and hydrophobic interactions, which are responsible for active conformation of the proteins, are very much related to water. So level of water in the reaction mixture is very critical to achieve a reasonable esterification rate and the ester yield (Scheme 9.1).

The freeze-dried biocatalyst used for the catalysis was found to retain 0.51% (w/w) moisture. Different amounts of water were added to the reaction mixture containing 0.44% biocatalyst (i.e. x + 0.0022% moisture with x = moisture content of solvent and substrates = constant) to give rise to the moisture levels ranging from x + 0.0022% to x + 0.25%. Fig. 9.3 shows that the maximum yield of the ester was observed at a moisture level of x + 0.05% (w/v). Increase in moisture level beyond x + 0.05% lowered the consumption of octanoic acid by shifting the equilibrium to the hydrolysis side.

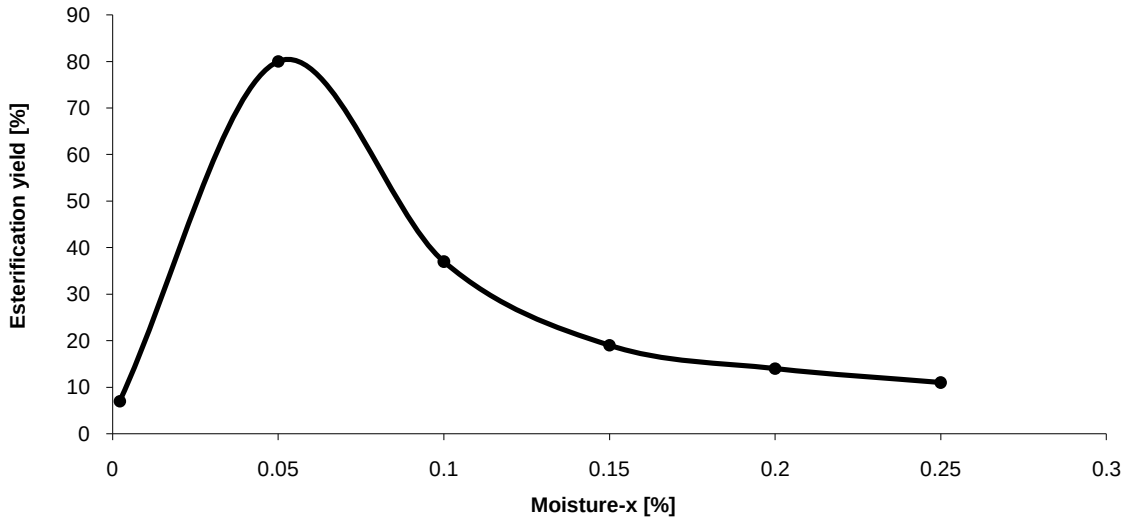

Fig. 9.3: Effect of moisture on lipase mediated esterificationm, *x* = constant moisture from solvent and substrates.

9.3.4 Effect of Temperature on Lipase Mediated Esterifcation

Effect of temperature, both, on synthetic activity and stability of the immobilized fungal lipase, was determined. The influence of temperature on enzyme activity was studied over the range of 20–60 °C by measuring the initial rates of synthesis of geranyl octanoate in *n*-hexane. Maximum initial rates were obtained at 30 °C (Fig. 9.4). At temperatures higher than 40 °C and lower than 30 °C, the reaction rates fell rapidly. There was only a slight change in the initial rates of esterification between temperatures of 40 °C and 30 °C.

When the enzyme in the reaction mixture was incubated (under shaking) at different temperatures for 48 hours, then recovered, washed, and then analyzed first for its hydrolytic activity, it was found that during 48 hours incubation at 40 °C, 45 °C, and 50 °C, the immobilized enzyme lost 27%, 54% and 82% activity, respectively, compared to no loss during 48 hours incubation at 20 °C, 25 °C and 30 °C. A temperature of 30 °C was used in all other experiments to avoid excessive evaporation of the organic solvent and to minimize enzyme denaturation.

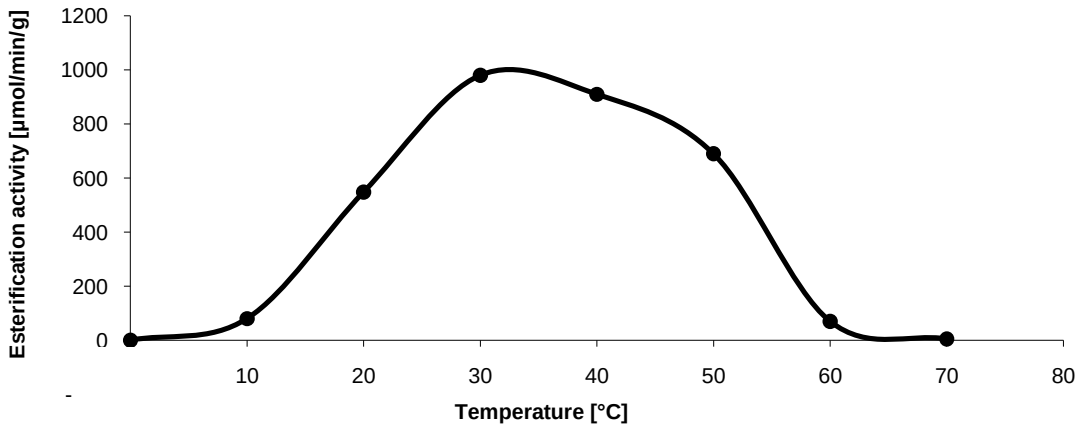

Fig. 9.4: Effect of temperature on esterification activity

9.4 Repeated Use of Lipase Immobilized on Propargyl Dextran

The potential for reusing the immobilized enzyme was considered because the economics of the process would be enhanced if the enzyme could be reused. The lipase of *R. arrhizus* immobilized on PgD-14 maintained its full activity up to three cycles for the synthesis of geranyl octanoate. During first three cycles 80% conversion of the reactants was achieved, while in the fourth cycle a loss in synthetic activity was observed, and only 70% conversion was achieved. An interesting phenomenon observed during repeated use of biocatalyst was that time required to reach equilibrium point decreases from first to the fourth cycle, i.e. in first cycle 80% conversion was achieved after 120 h, in second cycle after 54 h, in third cycle after just 8 h and in the fourth cycle 70% conversion was achieved after 4 h. This might be due to the binding capacity of the modified dextrans for water produced during esterification [224]. It can also be speculated that in a slow dynamic process a more appropriate conformation or topology of the enzyme-dextran complex is adopted.

9.5 Lipase Immobilization on Pentynyl Dextran and its Comparison with Commercial Adsorbents for the Synthesis of Geranyl Octanoate

As detailed analysis have proved that PgD, contain a reasonable amount of side product in it. Moreover, repeated monomer analysis, have shown that PgD is not a stable product. Therefore, in next step, PyD was applied for immobilization of lipase from *R. arrhizus* and was compared with some well known adsorbents used commercially for this purpose. Lewatit VP OC 1600 provided by Lanxess, Germany is a macroporous resin of poly(methyl methacrylate) with a bead size 0.32–0.45mm, surface area 130 m^2/g, pore volume, 0.5 cm^3/g, pore diameter 15 nm aprox. Amberlite XAD 761 (granular cross-linked phenol-formaldehyde polycondensate, particle size 0.560-0.760 mm, surface area 200 m^2/g, pore diameter 60 nm) and Duolite A568 (granular cross-linked phenol-formaldehyde polycondensate, main functional group tertiary amine, surface area 92.8 m^2/g, pore size 27.3 nm, pore volume 0.53 cm^3/g) were provided by Rohm and Haas, France (technical data provided by suppliers).

9.5.1 Effect of Incubation Time on Immobilization of Lipase

To study the effect of incubation time on the amount of lipase immobilization on PyD-17 (PyD-Lip, DS 0.43), Lewatit VP OC 1600 (Lew-Lip), Amberlite XAD 761 (Amb-Lip) and Duolite A568 (Duo-Lip), 2% aqueous solution of lipase was stirred with all four adsorbents at r.t. and a little amount of sample was withdrawn after every 60 minutes (up to 5 hours), centrifuged to remove non-absorbed lipase, freeze-dried and analyzed by elemental analysis (Table 9.4).

Table 9.4: Elemental analysis of different adsorbents after immobilization of lipase. N content relates to adsorption of protein (N x 6.25)

Incub.	PyD-Lip			Lew-Lip			Duo-Lip[a]			Amb-Lip		
(Hrs)	C	H	N	C	H	N	C	H	N	C	H	N
1	52.44	6.80	0.84	70.83	8.06	0.20	64.85	7.44	8.74	72.29	5.59	0.17
2	52.36	6.81	0.88	70.84	8.06	0.20	64.80	7.46	8.77	72.33	5.54	0.17
3	52.70	6.77	0.92	71.09	8.12	0.18	64.68	7.40	8.78	72.27	5.55	0.15
4	52.52	6.54	0.82	70.96	8.13	0.19	64.66	7.47	8.75	72.27	5.52	0.18
5	52.37	6.78	0.86	70.79	8.13	0.18	64.59	7.45	8.77	72.26	5.55	0.18

[a] N-content of Duo-Lip = 8.38%

Results of elemental analysis show (Table 9.4) that adsorption of enzyme does no longer significantly increase after 1 hour.

Hydrolytic activity of free and immobilized enzyme was determined titrimetrically on the basis of olive oil hydrolysis as described for PgD (section 9.2). Results are summarized in Tab. 9.5.

While protein adsorbed on PyD (5.4%) is much lower than that of PgD (12.1%), hydrolytic activity of PyD-Lip is the highest among all adsorbents compared in this study.

9.5.2 Comparison of PyD and other Adsorbents for Lipase Immobilization

Results in Table 9.5 show the protein content of the adsorbents after immobilization of enzymes as a measure for the enzyme adsorption, the hydrolytic activities and esterification activities of the free and immobilized lipases of *R. arrhizus* on different supports. PyD-Lip was about three times as active as Lew-Lip and Amb-Lip, and even four times as active as Duo-Lip. Referred to the amount of protein bound, the order is Lew-Lip > Duo-Lip > PyD-Lip > Amb-Lip (numbers in brackets). Hydrolytic activity of the biocatalysts decrease in the same order as esterification activity, while referred to the immobilized enzyme, the specific hydrolytic activity is highest for Lew-Lip, followed by PyD-Lip, Duo-Lip, and Amb-Lip.

Table 9.5: EA, protein adsorbed and hydrolytic activity of biocatalysts

Adsorbent	**Elemental Analysis (%)**			**Protein (%)**	**Hydrolytic activity [u g^{-1}]**[b] referred to biocatalyst *(referred to protein)*	**Esterification activity [umol min^{-1} g^{-1}]**[c] referred to biocatalyst (referred to protein)	**Ratio of esterification to hydrolytic activity**
	C	**H**	**N**				
-(Free enzyme)					9600[d]	0	
PyD-17	51.40	6.64					
PyD-Lip	52.37	6.78	0.86	5.37	1203 *(22400)*	249 *(4600)*	0.21
Duolite	61.32	7.23	8.38				
Duo-Lip	64.59	7.45	8.77	2.44	176 *(15700)*	67 *(6000)*	0.38
Amberlite	72.16	6.82					
Amb-Lip	72.26	5.55	0.18	1.12	222 *(9100)*	83 *(3400)*	0.37
Lewatit	68.16	7.75					
Lew-Lip	70.79	8.13	0.18	1.12	382 *(34100)*	83 *(7400)*	0.22

a: Protein present in the final dried biocatalyst (i.e. support + enzyme)

b: Hydrolytic activity units of lipase per g of the biocatalyst . 1 µmol of fatty acid consumed in the esterification reaction per minute per gram of biocatalyst [240]

c Esterification activity units of lipase per g of the biocatalyst, 1 u = 1 µmol of fatty acid consumed in the esterification reaction per minute per gram lipase

d Refers to pure enzyme while others refer to g of biocatalyst

The lipase binding capacity of PyD-17 with DS of 0.43, corresponding to 15% (w/w) of hydrophobic groups linked to the hydrophilic polysaccharide backbone, was 5.37% while with 1.12% it was lowest for both, Lewatit and Duolite (Table 9.5). In another study [251], 1.5% was reported for Lewatit. In that study, Lewatit was used without any pretreatment, while in the present work all supports were dried in vacuum before immobilization of lipase. Cabera *et al*. [234] reported a loading of 3% protein on Lewatit but for a different type of lipase and a different immobilization protocol (*Candida Antarctica*, CAL-B, 10 g support per 300 mL of lipase solution (1 mg lipase/mL) in 10 mM sodium phosphate for 4 hours) was used.

Like PgD, substitution pattern of PyD-17 showed a remarkable deviation from random distribution in the glucosyl units, which probably also means areas of high density of alkynyl residues and high portion of unsubstituted areas in the polymer chain which promises very good binding properties of PyD as already described in [251].

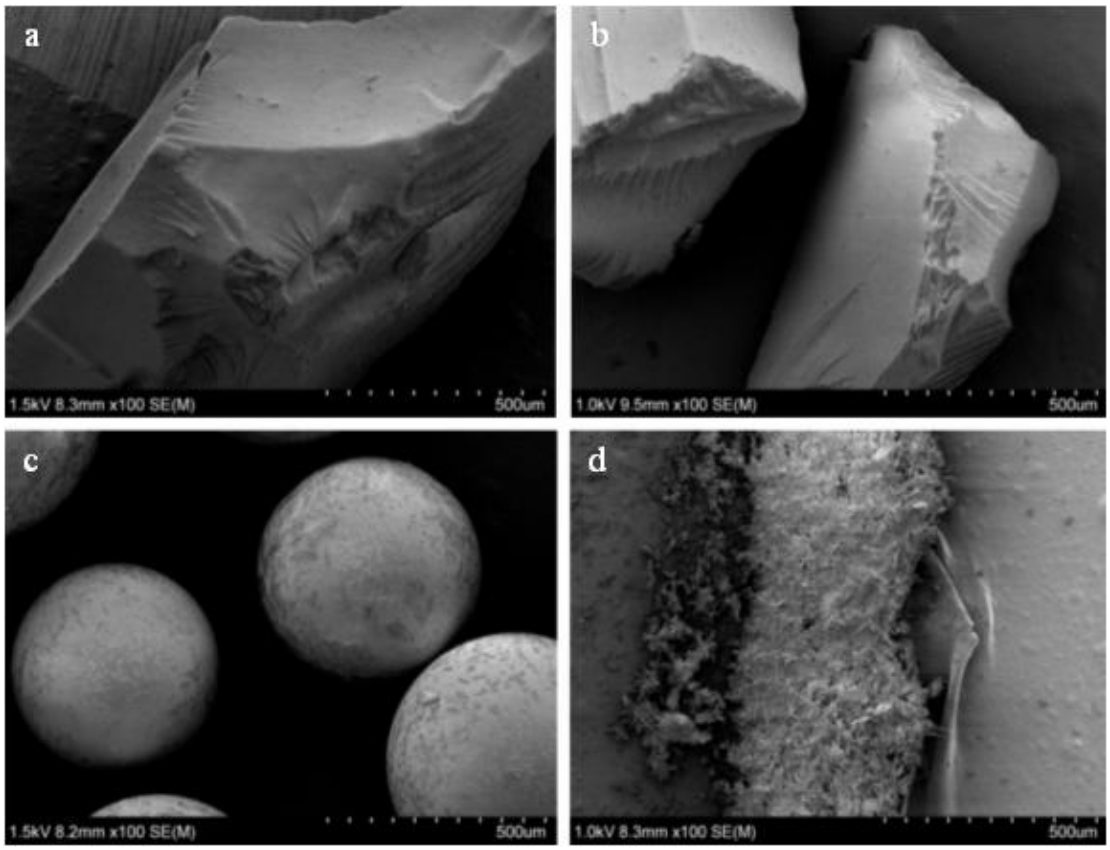

Fig. 9.5: SEM image of Amberlite XAD 761 (a) Duolite A568 (b) Lewatit VP OC 1600 (c) and pentynyl dextran, PyD-17(d) after immobilization of lipase of *Rhizopus arrhizus*

The surface area of PyD-17 was 3.3 ± 0.4 m^2/g while it was 130, 93 and 200 m^2/g for Lewatit, Duolite and Amberlite, respectively (according to technical data sheets). Although the surface area of PyD-17 is much lower than for the highly porous commercial adsorbents, it shows highest capacity for protein adsorption under the conditions used. The SEM images after immobilization show that except PyD, all supports have highly porous particles of specific size and shape which increases their interior surface area while in case of PyD, the average particle size is much smaller and thus the surface is mainly external (Fig. 9.5). In case of Lewatit, Amberlite and Duolite, due to porous structure, the large inner surface area was probably not or not fully accessible for the lipase, but most probably enzyme was immobilized only on the outer surface. In contrast, the much smaller surface area of PyD is probably well accessible by the enzyme molecules. Moreover, during esterification reaction, lipase adsorbed inside the pores would not be as active as on the surface which will be fully available for catalysis. Fibrous and sheet like structures as visible at higher magnification for PyD-17 (Fig. 9.6) are considered more suitable for lipase immobilization than spherical particles and other structures as has been reported by Fuentes *et al*. [252]. It is assumed that such structural differences are important for shifting the equilibrium between the enzyme's active ("open") and non-active ("closed") conformation in favor of the active form.

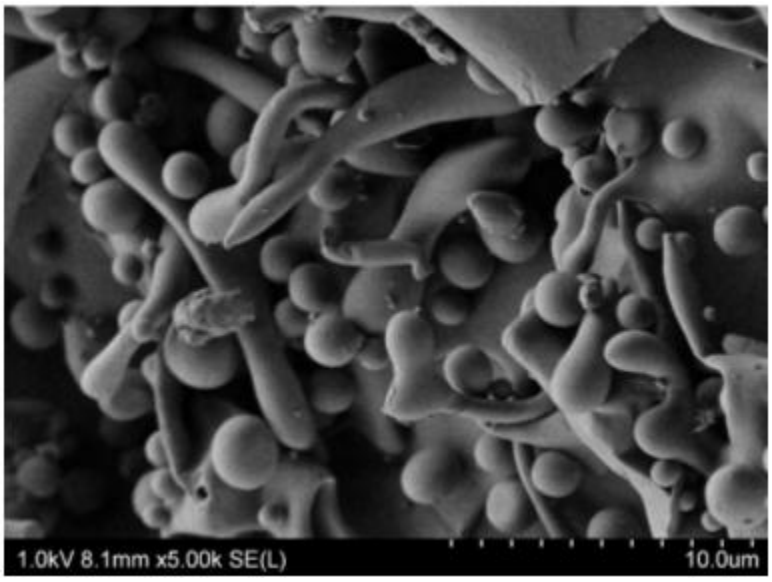

Fig. 9.6: SEM image of PyD-17 (without enzyme)

9.5.3 Evaluation of Lipase of *R. Arrhizus* Immobilized on PyD and other Adsorbents for Esterification of Geraniol and Octanoic acid

PyD-Lip, Lew-Lip, Amb-Lip and Duo-Lip was used to catalyze the esterification of geraniol (**42**) and octanoic acid (**43**) (Scheme 9.1). Reaction conditions optimized for lipase immobilized on PgD [251] were applied without any major change, using 500 mg of biocatalyst in each case.

9.5.4 Effect of Amount of Biocatalyst on Esterification Yield

In enzyme immobilization reactions, it is a general practice to refer to the amount of biocatalyst including the support, independent on its content of enzyme. The effect of the amount of biocatalyst on the final esterification yield was studied in model reaction. 500, 250, 125 and 75 mg of each type of biocatalyst was used in esterification reaction in 100 mL scale of 0.4 M geraniol and 0.4 M octanoic acid in *n*-hexane.

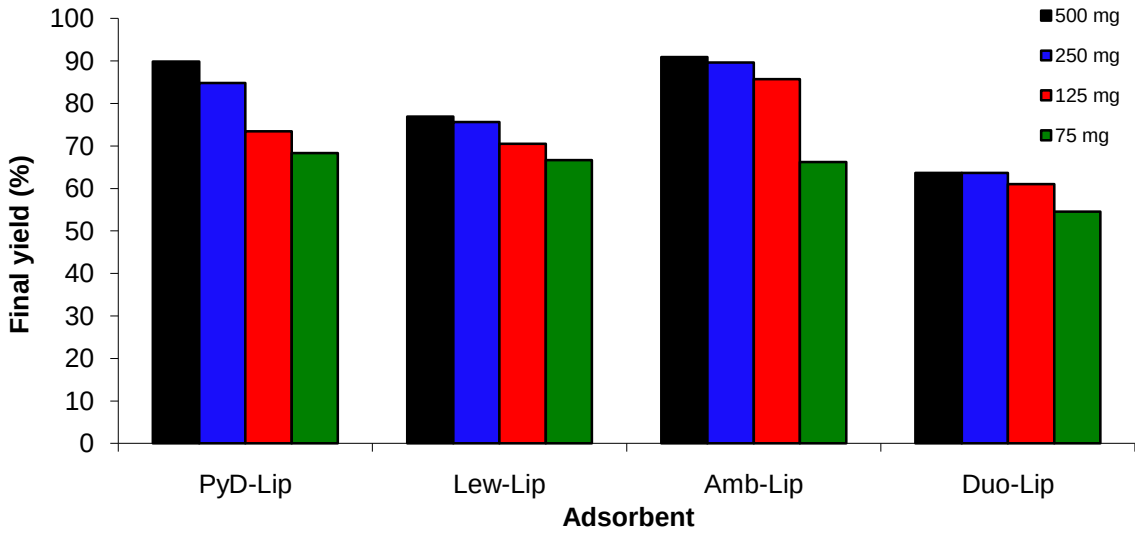

Fig. 9.7: Effect of amount of biocatalyst on final yield of geranyl octanoate from geraniol and octanoic acid. For the reaction times to achieve these yields see Table 9.6

Fig. 9.7 shows that the yields achieved in a reasonable time (for reaction times see Table 9.6) decreased when the amount of catalyst was reduced, as expected. For PyD-Lip, its final yield decreases continuously from 90 to 68% when reducing the amount of the biocatalyst from 500 to 75mg. The amount of biocatalyst did not affect the

esterification yield significantly until it is lowered below a certain limit, partly, since this was compensated by prolonged reaction time. Time to reach the apparent maximum yield, where no further conversion could be determined by the back-titration of residual acid, increased for all biocatalysts, e.g. from 160 h to 330 h for PyD-Lip when amount of biocatalyst was decreased from 500 mg to 75 mg. Maximum deceleration was observed for Lew-Lip where duration of reaction time increased from 72 to 330 h, while Duo-Lip was the least effected biocatalyst (from 235 to 330 h). Final esterification yield was also decreased, although not significantly (Table 9.6).

Table 9.6: Effect of amount of biocatalyst on final yield, and time required to achieve it in esterification reaction of geraniol and octanoic acid catalyzed by different biocatalysts

Biocatalyst	PyD-Lip		Lew-Lip		Amb-Lip		Duo-Lip	
amount (mg)	Time (h)	Yield (%)	Time (h)	Yield (%)	Time (h)	Yield (%)	Time (h)	Yield (%)
500	160	90	72	77	160	91	235	64
250	235	85	95	76	160	90	259	64
125	330	73	160	71	160	86	259	61
75	330	68	330	68	235	66	330	55

9.5.5 Storage Stability of Biocatalysts

After immobilization and drying, all biocatalysts were stored at -10 °C. Esterification activity was again determined after 8 weeks. All reaction conditions and amounts of biocatalysts were the same as used for freshly prepared biocatalysts. All biocatalysts show zero activity except PyD-Lip which did not show any loss of activity even after 14 weeks.

9.5.6 Repeated use of Biocatalysts

For lipase implementation at industrial scale, where many cycles of high yield are required, the stability of immobilized enzyme should permit its repeated reuse [247, 253]. For control, 500 mg of each biocatalyst was applied to an equimolar (0.4 M) mixture of geraniol and octanoic acid in 100 mL scale in repeated experiments. All biocatalysts maintained their esterification yield in the first two cycles (Fig. 9.8). For PyD-Lip, minimum time required to reach maximum yield of 90% increases from 160 to 284 h from the first to the forth cycle and then remained almost constant for the next cycles. In

case of Lew-Lip, it increased from 72 to 160 h, for Amb-Lip, from 160 to 185 h while for Duo-Lip it remained constant at 235 h in the first two cycles.

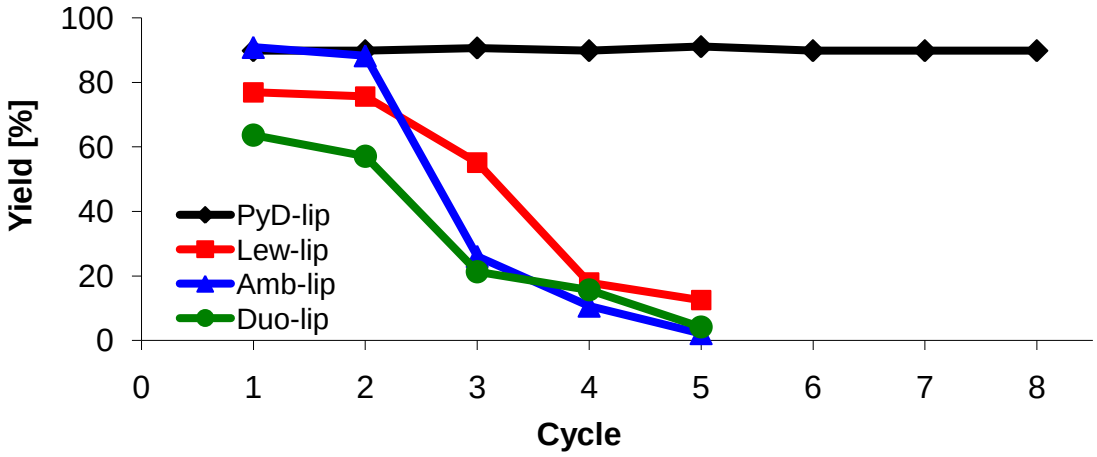

Fig. 9.8: Repeated use of lipase (*R. arrhizus*) immobilized on PyD-17 (PyD-Lip), Lewatit VP OC 1600 (Lew-Lip), Amberlite XAD 761 (Amb-Lip) and Duolite A568 (Duo-Lip). Biocatalysts were washed and freeze-dried after each cycle

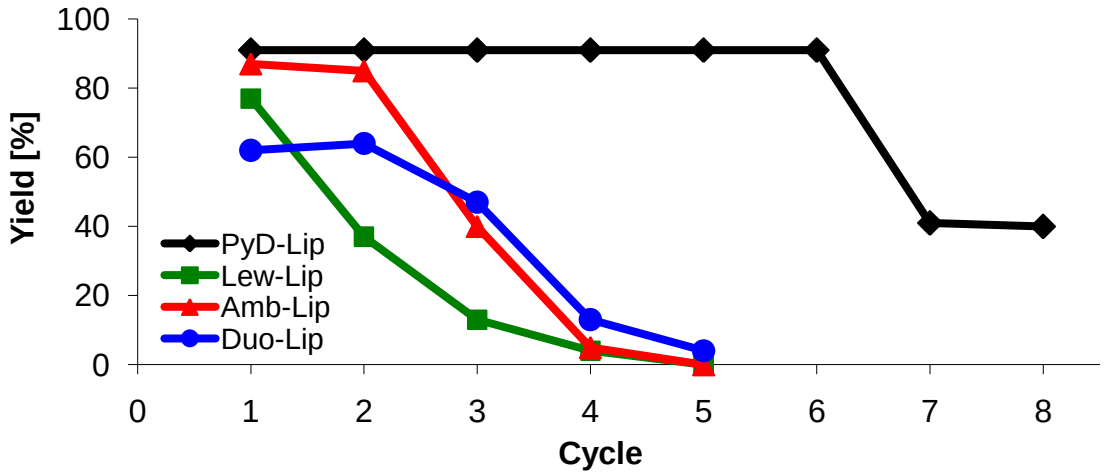

Fig. 9.9: Yields of esterification for repeated use of lipase (*R. arrhizus*) immobilized on PyD-17 (PyD-Lip), Lewatit VP OC 1600 (Lew-Lip), Amberlite XAD 761 (Amb-Lip) and Duolite A568 (Duo-Lip). Biocatalysts were washed with hexane and reused without freeze-drying

Final yield for all biocatalysts except PyD-Lip dropped rapidly after two cycles. In contrast, PyD-Lip still reached its maximum esterification yield even after eight cycles. For these experiments, all biocatalysts were filtered off, washed with *n*-hexane, dried at ambient atmosphere, and after addition of a small amount of water finally freeze-dried after each cycle. It was supposed that the addition of a small amount of water and

freeze-drying might be helpful to bring the enzyme back to its original conformation after each cycle.

However, considering only the final yields obtained without regarding the time required to achieve these, does not give a real image of the change of enzyme activities. While for the biocatalyst which had been freeze-dried before each new cycle, this time only slightly increases up to the 3rd cycle and then remained nearly constant, it was increasingly prolonged after each cycle, when the biocatalyst was only washed with hexane (Fig. 9.10).

Monitoring the conversion rate for each cycle of esterification using PyD-Lip indicated that there was nearly no difference for the first four cycles. However, in the following not only the slope of the initial conversion, which represents enzyme's activity, decreased, but at the same time an increasing incubation period was observed, until the reaction started (Fig. 9.13).

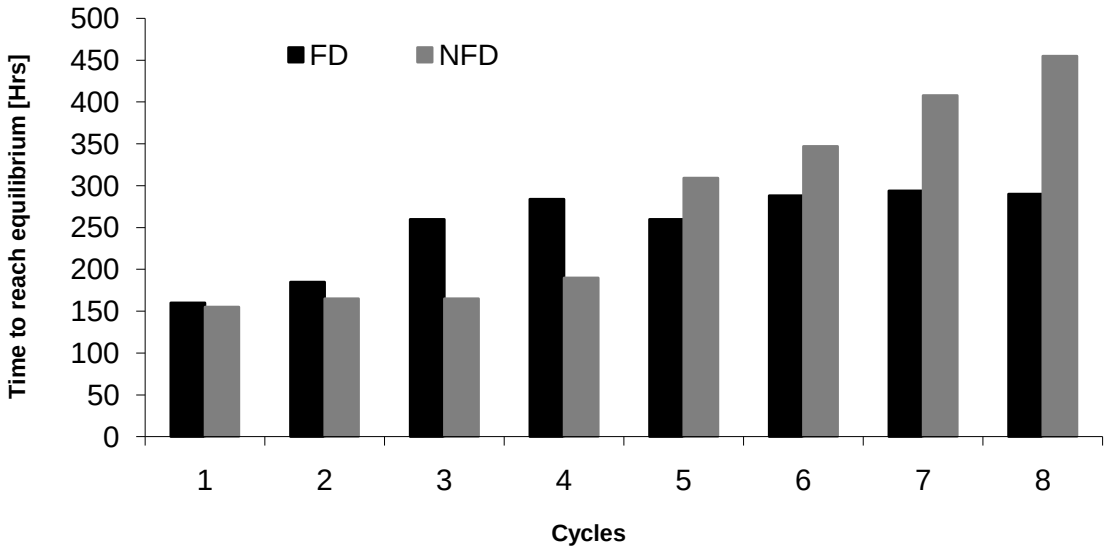

Fig. 9.10: Reaction time required to reach max. yield of esterification catalyzed by freeze-dried (FD) and non-freeze-dried (NFD) PyD-Lip in *n*-hexane. Biocatalyst was reused for eight cycles.

Esterification activities were calculated and shown to remain nearly constant for the first four cycles, and then to decrease rapidly (Fig. 9.12). Their change clearly correlates with the increased reaction time to achieve final yield. While the delay and slowing-down could be compensated for cycles 5 and 6 by prolonged reaction, the conversion rate is

already so slow in the subsequent cycles. Maximum yield cannot be achieved anymore in a reasonable time. Therefore, the exponential increase observed for the incubation period required until the enzyme recovers its reduced activity, probably better reflects the change of the biocatalyst.

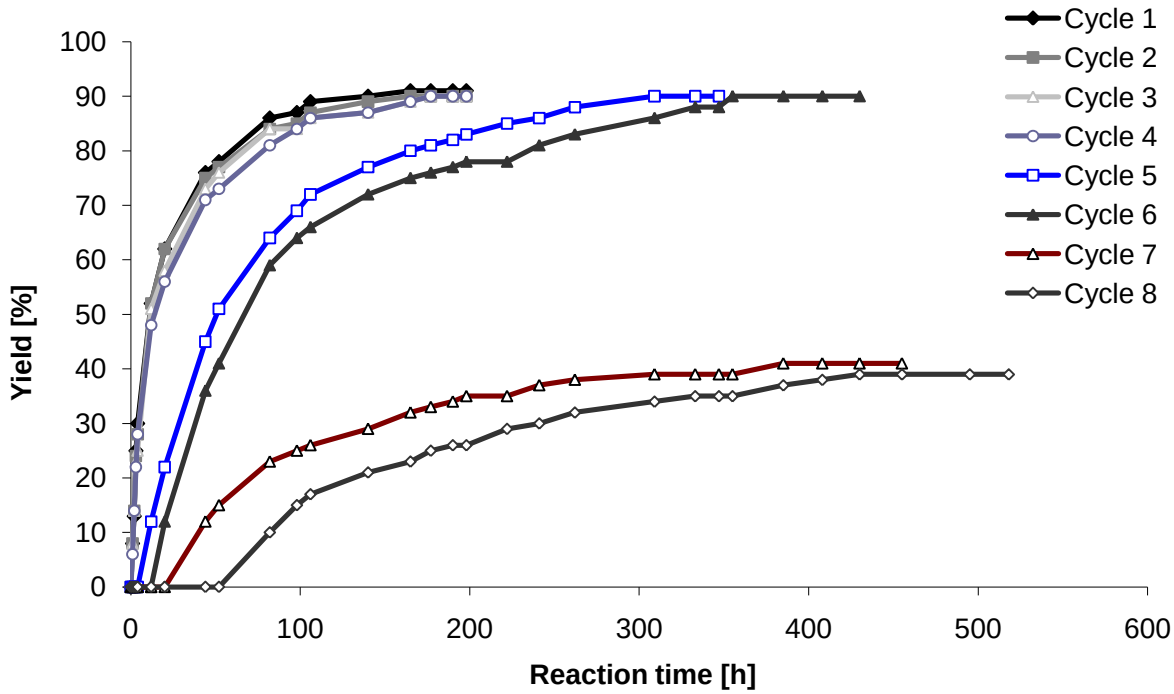

Fig. 9.11: Relation between final yield of esterification and time required. After 4 cycles, there was a delay in start of reaction. Biocatalyst was not freeze-dried after each cycle.

Although, the overall loss of activity was less pronounced in the first series, results from first four cycles without freeze-drying of the biocatalyst do not confirm the assumption that washing with water after washing with hexane and freeze-drying after each cycle, help to maintain activity by stabilizing the enzyme's conformation.

However, after four cycles the situation changed. Reason for the after 4 cycles prolonging incubation period for the non-freeze-dried biocatalyst (Figs. 9.11 and 9.13), and decrease in maximum yield after 6 cycles (Fig. 9.9) is possibly the inhibition of the enzyme by deposition of octanoic acid on the biocatalyst. This is already known from lipase immobilized on PgD-14 [251]. As the esterification yield did not decrease when the biocatalyst was washed with water and freeze-dried (Fig. 9.8), it is assumed that some octanoic acid on addition of substrates (geraniol, octanoic acid in *n*-hexane) was

deposited on the biocatalyst and partially inhibited the enzyme in each cycle, but was washed out with water after the reaction cycle. While solubility of octanoic acid in water is low, the accessibility is much better, since PyD-Lip is suspended in water, while it deposits in hexane and finally sticks at the wall of the reaction flask. Therefore, final yield was not affected even after 8 cycles in the first series (Fig. 9.8).

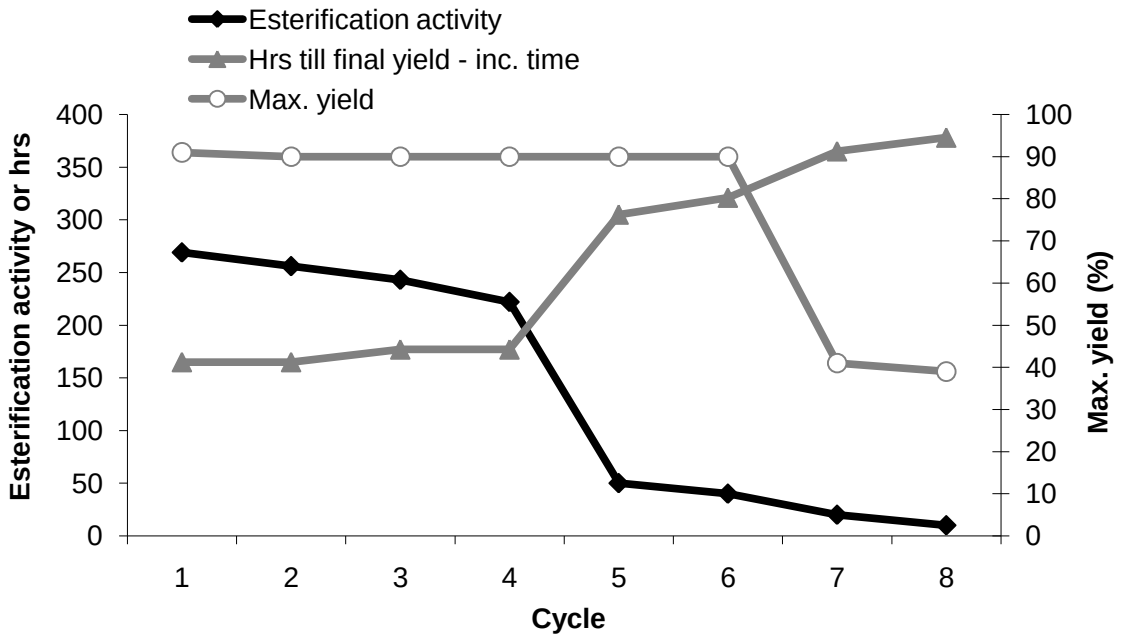

Fig. 9.12: Repeated use of lipase (*R. arrhizus*) immobilized on pentynyl dextran (PyD-Lip) without freeze-drying. Changes in esterification activity, time required to reach final yield corrected for incubation time required to start the reaction, and final maximum yield achieved in each cycle.

The study of reusability showed that all biocatalysts except PyD-Lip lose their esterification activity after 2-3 cycles, while, with PyD-Lip constant high esterification yield could be achieved, in spite of a slight loss of activities in the first cycles. The difference between PyD-Lip and the ion exchange support might be caused by their different structures. All adsorbents except PyD are spherical or irregular shaped particles which can be broken down during the reaction due to magnetic stirring, thus resulting into a vast activity loss of the enzyme. In contrast, PyD is a soft fluffy material having different kinds of morphologies (Figs. 9.5, 9.6) which not only helps to adsorb the enzyme very efficiently but is also not broken down under shear stress like other adsorbents. This assumption is based on the observation that after 2-3 cycles, a

significant portion of all biocatalysts except PyD-Lip was converted into fine powder. This drawback of granular particles used as immobilization supports was also indicated by some other researchers [254].

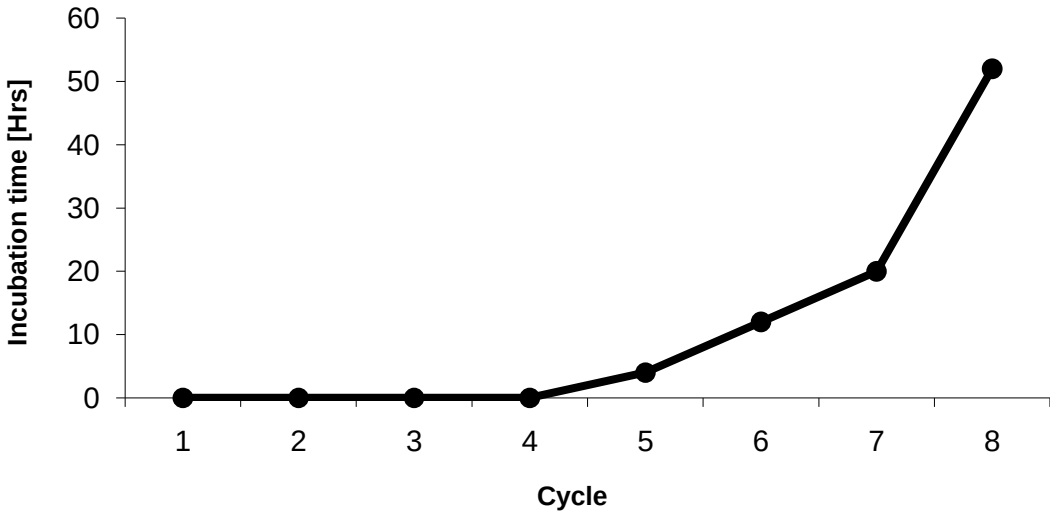

Fig. 9.13: Incubation time (h) until PyD-Lip has recovered its activity when starting a new cycle in repeated use. Biocatalyst was washed with hexane and reused without drying.

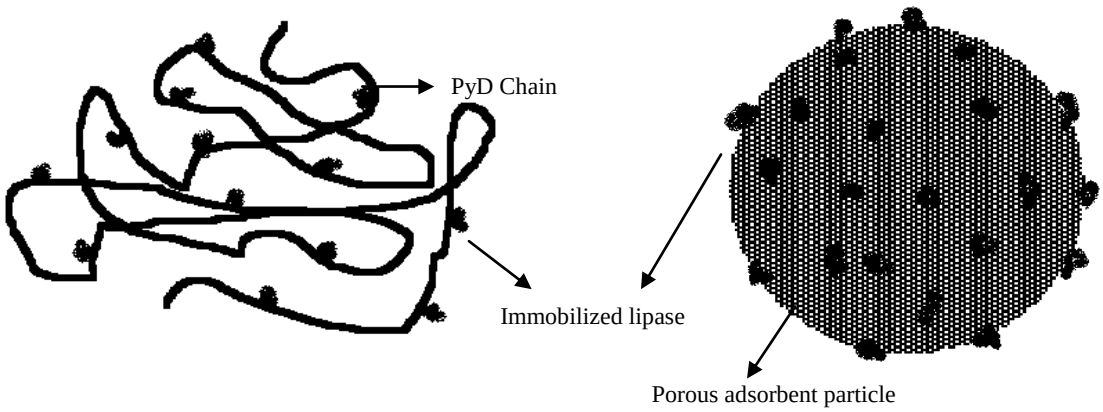

Fig. 9.14: Hypothetic model of different distribution of immobilized lipase on PyD and spherical ion exchange resin adsorbents

One could also assume that in case of PyD-Lip, enzyme is better protected against direct exposure to organic medium and shear stress due to cavities in the hyperbranched and

entangled PyD which is not the case in other adsorbents, where the enzyme is always exposed to organic medium due to adsorption on the external surface (Fig. 9.14).

Pentynyl dextran (PyD-17) has been proved being very successful candidate for lipase (*R.arrhizus*) immobilization and usage as biocatalyst for synthesis of geranyl octanoate. It was clearly superior compared to ion exchange resin-based adsorbents like Lewatit VP OC 1600, Amberlite XAD 761, and Duolite A568 with respect to biocatalyst activity, final esterification yield and storage stability, and repeated use.

10 SUMMARY

Due to its wide use in medical applications and biocompatibility, dextranis an interesting polysaccharide.By derivatization the spectrum of functionalities and applicabilities can be extended. In this thesis, *O*-alkynyl ethers of dextran were studied due to the special propertiesand reactivity of terminal alkynes, which make them ideal precursors for the introduction of various functional groups and signal molecules e.g. by "click-chemistry".

Propargyl dextrans (PgD) were prepared by etherification of dextran with propargyl bromide or propargyl chloride. Monomer analysis of PgD samples, recorded after storage for several months at room temperature indicated instability of propargyl residues. Along with instability in PgDs, a reasonable amount of side product was formed involving the dimsyl anion. All attempts to replace DMSO with other solvents like DMAc or THF failed.

Therefore, following the concept to prepare dextran alkynyl ethers as reactive intermediates with various spacer lengths, the alkynyl group was extended from three to five carbons. Pentynyl dextrans (PyD) were prepared using 5-chloro-1-pentyne and Li-dimsyl in DMSO. Products were characterized by elemental analysis, ATR-IR, and nuclear magnetic resonance (NMR) spectroscopy. Gas liquid chromatography (GLC) and electrospray ionization mass spectrometry (ESI-MS) were applied after depolymerisation. Repeated monomer analysis confirmed that PyD is a stable product. Formation of a side products from the alkynyl halide under basic conditions was much less pronounced for pentynylthan for propargyl halides. A yellow oil produced by oligomerisation of PyCl and alkynylation of DMSO waslargely removed by Soxhlet extraction with CH_2Cl_2 or treatment with cold THF GLC-analysis of methyl *O*-pentynyl-*O*-TMS-α,β-D-glucoside obtained from purified PyD after methanolysis and trimethylsilylation showed substitution following the order O-2 > O-4 ≥ O-3. Surprisingly for di-substitution patterns with vicinal pentynyl groups were enhanced compared to the 2,4-di-*O*-substituted glucose which was expected to be the most abundant due to the relative reactivities. The reason for "neighbor group effect" is not known but might be related to association properties of pentynyl halide. It was tried to fractionate PyD on the basis of DS by dissolving in H_2O, THF or a mixture of THF and

CH_2Cl_2 but was only partially successful, since fractions obtained showed only slight differences in distribution of substituents and could not undoubtedly retraced to the starting material. By dialysis from DMSO solution against water, spherical, rod- and sheet like structures were formed due to the amphipilic properties of the alkynyl dextran ethers,

PyD was employed in complexation studies with silver and iron salts. ´Dialysis against $AgNO_3$ solution resulted in a product containing 24% silver as determined by ICP-OES in accordance with a molar ratio of Ag/C≡C of 1.3:1. ATR-IR spectroscopy indicated Ag-acetylide salt formation. Transmission electron microscopy (TEM) after reduction with conc. formic acid displayed Ag nanoparticles of diameter 4-10 nm, along with *O*-formylation of dextran. In contrast to silver, iron did not show any complexation with PyD. However, dialysis of peracetylated pentynyl dextran (PyAcD) against iron salt solution yielded products containing ca. 10% iron. Product obtained with a Fe^{+2}/Fe^{+3}-mixture showed superparamagnetic properties during and after dialysis against water, which however, was lost after freeze-drying.

In the next step, the terminal alkynyl group of PyD was submitted to further functionalization. Different azides i.e. 2-azidoethylamine, 3-azido-1-propanol, 6-azido-*N*-Boc-hexylamine, 4-azidobutyric acid, 3-azido-1-propanethiol, *N*-biotinyl-2-aminoethylazide and α-tocopheryl azide were reacted in a copper-catalyzed 1,3-dipolar cycloaddition with PyD. By this "click-chemistry" 1,2,3-triazole between terminal alkyne of PyD and azides of respective compounds were formed. Characterization of the products was carried out by ATR-IR and NMR spectroscopy, and, after depolymerisation by methanolysis, by GLC and ESI-MS. Degree of conversion of alkyne groups to respective triazoles was calculated from ^{1}H-NMR spectra and from GLC after methanolysis and trimethylsilylation. In all reactions good to excellent conversion (ca. 60-100%) of pentynyl groups were achieved. In the ESI-mass spectra recorded after methanolysis of PyD-click products, $[M+H]^+$ and $[M+CH_3]^+$ ionsof fully and partially converted pentynyl-glucose were detected, the latter due to methylation of triazole under the methanolysis conditions, as was proved in an independent experiment.

Click product with a biotinyl derivative was shown to bind streptavidin, labeled with a fluorophor, by fluorimetry in solution, and also after spin coating of the biotinylated

dextran and incubation with the labeled streptavidin by fluorescence microscopy, ellipsometry and atomic force microscopy (AFM). The addition product of tocopheryl azide was tested with respect to its antioxidant activity in the TEAC test. During deprotection of the *O*-acetylated tocopherolthe dextran was depolymerized. Tocopheryl azide as well as the corresponding tocopheryl-triazolylpropyl ethers of methyl glucosides obtained by methanolysis showed high antioxidant activity, thus indicating that this is retained after coupling to the sugar backbone.

In further studies PgD and PyD were tested for their ability to immobilize lipase (from *Rhizopus arrhizus*) and were compared with some commercial adsorbents e.g. celite, fuller´s earth, silica gel, wood shavings, alumina, Lewatit VP OC 1600, Duolite A568 and Amberlite XAD 761. All biocatalysts (i.e. lipase on adsorbent) were used to catalyze esterification of octanoic acid with geraniol to geranyl octanoate which is one of the click beetle pheromones. Amount of immobilized lipase was estimated from nitrogen content. PgD (DS 0.69) with 12.1 and PyD (DS: 0.43) with 5.4% lipase show highest loading among all adsorbents, while on ion exchange resin-based supports only 1.1-2.4% enzyme were adsorbed. Due to stability and purity, PyD was chosen for more detailed investigations. Hydrolytic activity, determined by olive oil method, for lipase immobilized on PyD, Lewatit, Duolite and Amberlite was 1203, 382, 176 and 222 $u \cdot g^{-1}$,respectively. Average esterification activity in *n*-hexane, determined from first 60 minutes of esterification reaction for lipase immobilized on PyD was 249 $u \cdot g^{-1}$, while for the synthetic resins-based biocatalysts 67-83 $u \cdot g^{-1}$ were determined. In a comparative study on the reusability of lipase-biocatalysts for esterification, only PyD-Lip gave constantly 90% yield, even at prolonged reaction times and thus lower activity, while the activity of ion-exchange resin-based biocatalysts heavily decline after two cycles. However,A study about stability under storage showed that all biocatalysts become inactive after eight weeks storage at -10 °C, except PyD which was still fully active even after 14 weeks under the same conditions.

Thus, *O*-alkynyl dextrans turned out to be appropriate candidates for further functionalization and biconjugation, e.g. in combination with surface modification, and to have a high potential as support for the immobilization of enzymes, enabling esterification of lipases in organic solvents.

10 ZUSAMMENFASSUNG

Dextran ist aufgrund seiner Verwendung im medizinischen Bereich und seiner Biokompatibilität ein interessantes Polysaccharid. Durch Derivatisierung von Dextran können sein Eigenschaftsspektrum und seine Anwendungsmöglichkeiten erweitert werden. Die vorliegende Arbeit beschäftigt sich aufgrund der speziellen Eigenschaften und Reaktionen von terminalen Alkinen mit Alkinylethern von Dextran, die infolgedessen ideale Vorstufen für die Einführung verschiedener funktioneller Gruppen und Signalmoleküle, z.B. mittels „Click-Chemie“, darstellen. Propargyldextrane (PgD) wurden mittels Veretherung von Dextran mit Propargylbromid oder Propargylchlorid dargestellt.Die Monomeranalyse von PgD-Proben, die mehrere Monate bei Raumtemperatur gelagert worden waren, zeigtendie Instabilität der Propargylether an. Zusätzlich zu der Instabilität der PgDs bildete sich bei der Propargylierung unter Mitwirkung des Dimsyl-Anions eine nicht zu vernachlässigende Menge Nebenprodukt . Alle Versuche DMSO durch andere Lösemittel wie DMAc oder THF zu ersetzen blieben ohne Erfolg.

Daher wurde entsprechend dem Konzept von *O*-Alkinyldextranen als reaktiven Zwischenprodukten mit variablerSpacerlängedie Länge der Alkinylgruppe von drei auf fünf Kohlenstoffatome erweitert. Pentinyldextrane (PyD) wurden mit 5-Chlor-1-pentin und Li-Dimsyl in DMSO hergestellt. Die Produkte wurden mittels Elementaranalyse, ATR-IR- und Kernresonanzspektroskopie (NMR) analysiert. Nach Abbau zu Monomeren wurden Gaschromatographie und Elektrospray-Ionisation Massenspektrometrie (ESI-MS) eingesetzt. Wiederholte Monomeranalyse bestätigte, dass PyD ein stabiles Produkt ist. Die Bildung von Nebenprodukten aus dem Alkinylhalogenid während der Derivatisierung war sehr viel geringer als für die Propargylhalogenide beobachtet. Ein gelbes Öl, entstanden durch Oligomerisierung von PyCl und Alkinylierung von DMSO, wurde größtenteils mittels Soxhlet-Extraktion mit CH_2Cl_2 entfernt. Die GC-Analyse von Methyl-*O*-pentynyl-*O*-TMS-α,β-D-Glucosiden, dienach Methanolyse und Trimethylsilylierung von gereinigtem PyD erhalten wurden, zeigte die Reaktivitätsfolge O-2 > O-4 ≥ O-3. Der Anteil an DisubstitutionanvicinalenOH-Gruppen war höher als das 2,4-Di-*O*-pentinyl-Muster, was aufgrund der relativen Reaktivitäten den Erwartungen

widersprach. Diese Beobachtung kann durch einen bisher nicht beobachteten Nachbargruppeneffekt erklärt werden, welcher möglicherweise mit die Assoziation der sowohl H-Brückendonoren als auch –akzeptoren darstellenden Pentinylhalogenidezusammen hängt. Der Versuch PyD durch Extraktion mitWasser, THF oder einer Mischung aus THF und CH_2Cl_2nach DS zu fraktionieren,ergab Fraktionen, die leidernur geringfügige Unterschiede in der Verteilung der Substituenten aufwiesen und sich nichteindeutig aufAusgangsmaterial zur¨ckführen ließen. Die Dialyse aus Lösung in DMSO gegen Wasser ergab infolge des amphiphilen Charakters des heterogenen Pentinyldextrans sphärische, zylindrische und blattartige Strukturen

PyD wurde in Komplexierungsstudien mit Silber- und Eisensalzen verwendet. Die Dialyse gegen $AgNO_3$-Lösung ergab ein Produkt mit 24% Silberanteil (bestimmt mittels ICP-OES)entsprechend einem molaren Ag/C≡C Verhältnis von 1.3:1. Mittels ATR-IR-Spektroskopie konnte Ag-Acetylid-bildung nachgewiesen werden. Mit Hilfe der Transmissionselektronenmikroskopie (TEM) wurde nach Reduktion mit konz. Ameisensäure die Bildung von Ag-Nanopartikeln mit einem Durchmesser von 4 bis 10 nm nachgewiesen, während das IR die Rückbildung der terminalen Alkine und*O*-Formylierungdes Dextrans anzeigte. Im Gegensatz zu Silbersalzen zeigen Eisensalze keine Komplexierung mit PyD. Die Dialyse von peracetyliertem Pentinyldextran (PyAcD) gegen Eisensalzlösung ergab jedoch Produkte mit ca. 10 % Eisengehalt. Das mit einer Fe^{2+}/Fe^{3+}-Mischung erhaltene Produkt zeigte superparamagnetische Eigenschaften, die allerdings nach Gefriertrocknung nicht mehr auftraten.

Im nächsten Schritt, wurden die terminalen Alkinylgruppen des PyD weiter funktionalisiert. Verschiedene Azide -2-Azidoethylamin, 3-Azido-1-propanol, 6-Azido-*N*-Boc-hexylamin , 4-Azidobutansäure, 3-Azido-1-propanthiol, *N*-Biotinyl-2-aminoethylazide und α-Tocopherylazide wurden in eine 1,3-dipolaren Kupfer-katalysierten Cycloaddition mit PyD umgesetzt. Durch diese „Click-Reaktion“ wurden 1,2,3-Triazole zwischen den terminalen Alkinen des PyD und den Aziden in den entsprechenden Verbindungen gebildet. Das Produkt wurde mittels ATR-IR- und NMR-Spektroskopie analysiert und nach Depolymerisation durch Methanolyse wurdenGaschromatogramme und ESI-MS-Spektren aufgenommen. Der Umsatz von Alkinylgruppenen zu entsprechenden Triazolen wurde aus ^{1}H-NMR-Spektren unddem

gaschromatographisch bestimmten „Rest-DS“ abgeschätzt. In allen Reaktionen konnten gute bis ausgezeichnete Umsätze (ca. 60-100 %) der Pentinylgruppen erreicht werden. In den ESI-Massenspektren aufgenommen nach Methanolyse der PyD-„Click“-produkte, konnten $[M+H]^+$ und $[M+CH_3]^+$ Ionenvon vollständig und teilweise umgesetzten*O*-Pentinylglucosen detektiert werden, letztere aufgrund von Methylierung der Triazole unter Methanolysebedingungen, wie in einem unabhängigen Experiment bewiesen wurde.

Mit dem Biotinyl-dextranderivat konnte die spezifische Kopplung an Fluorophor-markiertes Streptavidingezeigt werden,. Der Nachweis konnte durch Fluorimetrie in Lösung und auch nach Spin-Coating des biotinylierten Dextrans und Inkubation mit dem markierten Streptavidin durch Fluoreszenz-Mikroskopie, Ellipsometrie und AFM geführt werden. Zusätzlich wurde die antioxidative Wirkung Tocopheryldextransmittels TEAC-Test untersucht. Tocopherylazid sowie die entsprechenden Methylglucosid-Derivate, diebei der Methanolyse zur Abspaltung der Acetyl-Schutzgruppe vom Tocopheryl enstanden, zeigten Tocopherol entsprechend antioxidative Aktivität, sodass diese auch nach Triazol-Kopplung an den Zucker erhalten bleibt.

In weiteren Studien wurden PgD und PyD auf ihre Fähigkeit, Lipase (von *Rhizopus Arrhizus*) zu immobilisieren getestet und mit einigen kommerziellen Adsorbentien verglichen, z.B. Celite, Fuller´s Erde, Kieselgel, Holzspäne, Tonerde, und die Ionenaustauscherharze Lewatit VP OC 1600, Duolite A568 und Amberlite XAD 761. Alle Biokatalysatoren (d.h. Lipase auf Adsorbens) wurden für die Veresterungvon Octansäure mit Geraniol zu Geranyloctanoate eingesetzt einBorkenkäfer-Pheromon. Der Gehalt immobilisierter Lipase wurde aus dem Stickstoffgehalt abgeschätzt. PgD (DS 0,69) mit 12.15 und PyD (DS 0.43) mit 5,4% Lipase zeigten die höchste Belegung unter alle Adsorbentien, während von den Ionenaustausch-Polyesterharzen nur 1,1-2,4% Enzym adsorbiert wurden. PyD wurde für ausführlichere Untersuchungen eingesetzt. Die mittels Olivenöl-Methode bestimmte Hydrolyse-Aktivität ergab für Lipase auf PyD 1203, immobilisiert auf Lewatit 382, auf Duolite 176 und auf Amberlite 222 $u \cdot g^{-1}$. Die durchschnittliche Veresterungsaktivität in *n*-Hexan, bestimmt für die ersten 60 Minuten der Reaktion von immobilisierter Lipase auf PyD,betrug 249 $u \cdot g^{-1}$, während für die auf den synthetischen Harzen basierenden Biokatalysatoren 67-83 $u \cdot g^{-1}$ bestimmt wurden.

Ineiner vergleichenden Studie überdie Wiederverwendbarkeit vonLipase-Biokatalysatoren für die Veresterung gab nurPyD-Lip auch bei längerenReaktionszeitenund damit geringererAktivität eine reproduzierbare Ausbeute von90%, währenddie Aktivität derIonenaustauscher-Harz-Basis Biokatalysatorennach zwei Zyklenstark zurückging.Jedoch zeigte eine UntersuchungderLagerstabilität, dass alleBiokatalysatoren mit Ausnahme von PyDnach acht WochenLagerung bei10 °C inaktivwurden., PyD war dagegen auch nach 14 Wochen unter denselben Bedingungen noch voll aktiv.

O-Alkynyldextrane erwiesen sich folglich als geeignete Kandidaten für die Einführung von verschiednen funktionellen Gruppen oder die Kopplung von bioaktiven Molekülen, z.B. auch in Verbindung mit Oberflächenfunktionalisierung. Darüberhinaus besitzen sie ein hohes Potenzial für die Immobilisierung von Lipase unter Erhalt der katalytischen Aktivität für Veresterungen in organischem Medium.

11 EXPERIMENTAL

11.1 General

All chemicals purchased from commercial sources were used without further purification if not mentioned.

11.2 Chemicals

Chemicals used are given in the following Table 11.1:

Table 11.1: Chemicals

Name	Purity	Producer	Remarks
2-Bromoethylaminehydrobromide	≥ 97%	Fluka	
t-Butyl alcohol	99.7%	Sigma-Aldrich	
3-Chloro-1-propanethiol	98%	Aldrich	
3-Chloro-1-propanol	98%	Aldrich	
4-Chlorobutyric acid	99%	Aldrich	
5-Chloro-1-pentyne	98%	Acros	
6-Azido-*N*-Boc-hexylamine		Fluorochem	
Acetic anhydride	≥ 99%	Fluka	
Acetone	99.98%	Fisher Scientific	
Amberlite XAD 761		Rohm and Haas	
Benzylazide	94%	Alfa Aesar	
D(+)-Biotin	98%	Acros	
BSTFA	≥ 99%	Fluka	
Calcium chloride		Merck	Water free
Copper sulphate -penta hydrate		Merck	Extra pure
Dextran (from *Leuconostoc sp*.)		Fluka	Mw ≈ 500 kD
Dichloromethane	99.99%	Fisher Scientific	
Diethyl ether		Fisher Scientific	
DMSO	99.99%	Sigma-Aldrich	
DMAc	99.9%	Fluka	
D-pinitol	95%	Aldrich	
Duolite A568		Rohm and Haas	
EDC	98%	Fluka	
Ethyl acetate	99%	Merck	
Ethyl alcohol	99.8%	Roth	
$FeCl_2.4H_2O$	≥ 99%	Riedel-de Häen	
$FeCl_3.6H_2O$	≥ 99%	Riedel-de Häen	

Formamide	99.5%	Sigma	
Geraniol	98%	Aldrich	
Gum acacia		Fluka	
Hydrochloric acid	37%	Riedel-de Häen	
Lewatit VP OC 1600		Lanxess	
Lipase	10.5 umg^{-1}	Fluka	From *Rhizopus arrhizus*
Magnesium sulphate	98%	Fluka	
Malic acid	98%	Fluka	
Methyl alcohol	99.99%	Fisher Scientific	
Methyl lithium		Acros	1.6 M in ether (± 5%)
N,*N*-dimethylformamide	99%	Fluka	
Na-L-ascorbate	≥ 99%	Fluka	
n-Hexane	95%	Fisher Scientific	
N-Hydroxysuccinimide	98%	Aldrich	
Nitric acid	69%	Fluka	
Octanoic acid	≥ 98%	Aldrich	
Olive oil			
Phenolphthalein	99%	Fluka	2% solution in ethanol
Phenylacetylene	≥ 97%	Fluka	
Phosphorus tribromide	98%	Fluka	
Potasium hydroxide			
Propargyl alcohol	99%	Fluka	
Propargyl chloride	98%	Aldrich	
Pyridine	≥ 99.8%	Fluka	
Silver nitrate	99.5%	Grüssing GmbH	
Sodium azide	99%	Fluka	
Sodium chloride			
Sodium hydride			
Sodium hydrogen carbonate	99%	Fluka	
Sodium Hydroxide	99%	Riedel-de Häen	
Sodium sulphate	96%	Merck	
Streptavidin		Fluka	Atto-550 labeling
TMCS	≥ 99%	Merck	
Toluene	99.99%	Fisher Scientific	
Triethylamine	≥ 99%	Sigma-Aldrich	
Trifluoroacetic acid	98%	Fluka	2 M aq. solution
Tris-(hydroxyethyl)aminomethane	99%	Fluka	

11.3 INSTRUMENTATION

11.3.1 Infrared Spectroscopy

Infrared spectra were recorded using a Bruker Tensor 27 attenuated total reflectance infrared (diamant-ATR-IR) spectrometer.

11.3.2 Gas Chromatography

Gas chromatographic analysis was carried out with a GLC-FID instrument Carlo Erba GLC 6000 Vega Series at 60 ºC for 1 minute, with 20 ºC/min. to 130 ºC, and with 4 ºC/min. to 290 ºC, kept constant for 30 minutes. Data were recorded with a Merck Hitachi D-2500 Chromato-Integrator. Alternatively, a Shimadzu GC 2010 with split / splitless injector, FID and coloumn (Phenomenex zebron ZB-5MS, 30 m, ID 0.25 mm, film thickness 0.25 µm and 1.5 m retention gap (methyl deact.)) was used. H_2 (40 cm/s, linear velocity mode) was used as carrier gas. Data were recorded with a Shimadzu GC solution Chromatography Data System Version 2.3. For quantitative evaluation, peaks were corrected according to ECR concept. Correction factors for PgD (glucose acetates, *O*-Pg/*O*-Ac): un-substituted: 1.000, mono-*O*-Pg:0.845, di-*O*-Pg: 0.731, tri-*O*-Pg: 0.645; and for PyD (methyl glucosides, *O*-Py/*O*-TMS): un-substituted: 1.000, mono-*O*-Py: 0.933, di-*O*-Py: 0.874, tri-*O*-Py: 0.823. Peaks were assigned by GCMS analysis.

11.3.3 GCMS Analysis

A Hewlett Packard 5890A gas chromatograph equipped with a 30 m analytical column (ZBI, Phenomenex, 30 m x 0.32 mm ID, t_f = 0.25 µm) was used.

Conditions: Injector 250 °C; temperature program was 100 °C (3min); 6 °C/min to 310 °C (3 min), split (ratio 1:20) or splitless mode, carrier gas He (1.6 ml min^{-1}) and the injection volume 1 µL. The capillary column was directly coupled to a triple quadrupole mass spectrometer Finnigan TSQ 700 (transfer line was set at 250 °C, ion source temperature was set at 150 °C and ionization voltage 70 eV).

11.3.4 Elemental Analysis

Elemental analysis was performed on Thermoquest flash EA 1112 (Institute of Pharmaceutical Chemistry, TU Braunschweig). Data were always the average of two measurements.

11.3.5 Scanning Electron Microscopy (SEM)

SEM images were recorded with a Hitachi Field-Emission Scanning Electron Microscope S-4800 at KTH Stockholm, Fibre and Polymer Technology, by Anna Risberg. Samples were prepared on colloidal graphite and subsequently dried in a desiccator for 2 days.

11.3.6 Transmission Electron Microscopy (TEM)

Transmission electron micrographs were obtained using a TEM Zeiss Leo 922 Omega microscope, operated at 200 kV,by Jennifer C. Horst and Christina Komoß, Institute for Pharmaceutical Technology, TU Braunschweig. Samples were prepared by placing a drop of dispersion on hydrophilized carbon film, which was supported by a copper grid (carbon only, copper grids 200 mesh). Excess dispersion was wiped off with filter paper and the sample was dried at room temperature for a few minutes. In case of freeze-dried samples, the material was redispersed in water or ethanol and treated analogously. Other techniques like freeze-fracture and negative staining did not lead to a satisfying result. All images were recorded with a Proscan CCD-camera system and processed by an ITEM image processing program.

11.3.7 Inductively Coupled Plasma Optical Emission spectroscopy (ICP-OES)

Quantitative measurement of Fe and Ag complexation was carried out on Radialen ICP-OES Vista MPX, Fe Varian, Darmstadt, Germany, by Christiane Schmidt, Institute of Ecological Chemistry. TU Braunschweig. Power: 1.20 kW, Plasma gas: 15 L/min, Auxiliary gas: Ar, 1.5 L/min, Atomizer pressure: 240 kPa, Pump speed: 20 rps. Atom

emission lines: Ag: 328.068, 338.289; ion emission lines: Fe: 238.204; Ag: 224.641, 241.318, 243.779; internal reference line: Ar: 470.067 nm.

11.3.8 Nuclear Magnetic Resonance (NMR) Spectroscopy

^{1}H- and ^{13}C-NMR spectra were recorded with a Bruker AMX 300 instrument (^{1}H: 300 MHz) or a Bruker AMX 400 (^{1}H: 400 MHz). Spectra were recorded in DMSO-d_6, pyridine-d_5 and $CDCl_3$. Chemical shifts were calibrated relative to the residual proton and carbon resonance of the solvent DMSO-d_6 (δ_H = 2.5), pyridine-d_5 (δ_H = 7.22, 7.58, 8.74) and $CDCl_3$ (δ_H = 7.25).

11.3.9 Electrospray Ionization Mass Spectrometry (ESI-MS)

ESI-MS spectra were recorded with an Esquire, Bruker Daltronic GmbH, Bremen and data was analyzed using software Bruker Data Analysis Esquire-LC, Bruker Dalronic GmbH, Bremen. Instrument parameters were set as:

Mode: Positive, Flow rate: 100-200 µL/h, Dry gas: 4 L/min, Dry Temperature: 325 °C, Capillary: -3500 V, End plate offset: -500 V, Nebulizer gas: N_2, 10 psi, Capillary exit: 120 V, Capillary exit offset: 90 V, Skim 1: 30 V, Skim 2: 10 V, Trap drive: 50.4.

Some of the ESI-MS spectra were recorded with HCT Ultra ETD-II, Bruker Daltronic GmbH, Bremen equipped with same software as for Esquire-LC. Instrument parameters were set as:

Mode: Positive, Flow rate: 100-200 µL/h, Dry gas: 5 L/min, Dry Temperature: 300 °C, Capillary: -3500 V, End plate offset: -500 V, Nebulizer gas: N_2, 5 psi, Capillary exit: 181.

11.3.10 Fluorimetry

Jasco Spectrofluorometer FP-6200 was used for fluorimetry. Biotinylated *O*-pentynyl dextran was treated with aqueous solution of labelled streptavidin and washed with water several times. After drying and dissolving in DMSO, fluorescence was recorded at 555 nm.

11.3.11 Ellipsometry

Ellipsometer DRE EL X-02C equipped with software EL X-1 2.0 was used. Parameters used were: λ = 632.80 nm, angle of incidence α = 70 °, RI_{Si}: 3.8816; RI_{SiO_2}: 1.4571, measured by Nico Lämmerhardt. RI applied for PyD and PyD-biotin: 1.56 (value reported for dextran films); RI applied for streptavidin-Atto550: 1.47 (value reported for unlabelled streptavidin).

11.4 Synthesis of Alkynyl Dextrans

11.4.1 Synthesis of Propargyl Bromide

Distillation apparatus was dried by heating under nitrogen. Water free propargyl alcohol (112 g, 2 mol) and water free pyridine (4 g) were added into three-necked round bottom flask placed in an ice bath. Phosphorus tribromide (126 g, 0.46 mol) and pyridine (1 mL) were added very slowly to the flask containing propargyl alcohol during stirring. The mixture was stirred at r.t. After 1 hour, color of the mixture turned from blackish brown to brown (or dark brown) which was the indication for completion of reaction. The temperature was increased up to the boiling point of propargyl bromide (84 ºC). Distilled propargyl bromide was collected in flasks containing K_2CO_3. Propargyl bromide was distilled again and stored in refrigerator (133.69 g, 1.12 mol, 56%).

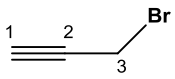

^{1}H-NMR (400 MHz, $CDCl_3$), δ = 2.51 (t, 1H, H-1, $J_{1,3}$= 2.6 Hz), 3.88 (d, 2H, H-3, $J_{1,3}$ = 2.6 Hz). ^{13}C-NMR (400 MHz, $CDCl_3$), δ = 13.31 (C-3), 74.82 (C-1), 78.70 (C-2).

11.4.2 Preparation of Li-Dimsyl

A round bottom flask with septum was dried by heating under nitrogen. 1.6 M Methyl lithium (5% solution in diethyl ether) was added to an equal volume of DMSO through a septum into the flask under nitrogen. A needle was inserted into the septum to release

methane and evaporate diethyl ether. The mixture was stirred under nitrogen for 90 minutes and freshly prepared Li-dimsyl was used immediately.

11.4.3 Synthesis of Propargyl Dextran (PgD)

In a typical procedure, 200 mg (1.23 mmol AGU, 3.70 mmol OH) dried dextran (M_w 500 000) was dissolved in 20 mL of DMSO (dry). Base (0.5-1.5 eq./OH of Li-dimsyl, pulverized NaOH or NaH) was added to the dextran solution. After 1 hour, propargyl bromide or propargyl chloride (2.0 eq./OH) was added slowly to the reaction mixture under ice cooling. After 24 hour stirring at room temperature, the product was purified by dialysis (MWCO 12-14000) against demineralized water (5×5L) for three days. IR (diamant-ATR): 3371-3501, depending on DS (s, OH), 3282 (s, C≡*C-H*), 2925, 2874 (m, CH, CH_2, aliph.), 2118 (w, C≡C, monosubst. acetylene), 1640 (m, OH), 1680, 1725 (from side product) 1445, 1345, 1285 (m, CH), 1153, 1076, 1008, 914 (s, CO), 632 cm^{-1} (acetylene). Detailed conditions, DS and yields etc. are given in [185].

11.4.4 Synthesis of Pentynyl Dextran (PyD)

O-pentynyl dextran (M_w 500 000) was prepared with Li-dimsyl and 5-chloro-1-pentyne according to the procedure described for PgD. Reaction time was increased from 24 to 48 hours. For subsequent reactions, PyD was prepared on gram scale.

Typical procedure: Dextran (M_w 500 000, 7.87 g, 48.6 mmol, 145.7 mmol OH) was dissolved in 310 mL DMSO. After formation of a clear solution, Li-dimsyl (145 mL, 1.5 eq./OH) was added. After 1 hour stirring at room temperature, 5-chloro-1-pentyne was added slowly under ice cooling and stirring was continued for 48 hours. The product was purified by dialysis against demineralized water. Water was changed 10 times in 5 days before freeze-drying (8.85 g, 46.44 mmol whitish solid). The product was further purified by Soxhlet extraction with CH_2Cl_2 for 24 hours.

EA (found): C 51.40%, H 6.64%; Calc. for PyD with DS 0.43: C 51.37%, H 6.65%. ØM (AGU) = 190.6, corresponding to a yield of 96%. IR (diamante-ATR-IR): 3385 (s, OH), 3280 (s, C≡C-*H*), 2924, 2880 (m, CH, CH_2, aliph.), 2117 (w, C≡C, monosubt. acetylene), 1640 (m, OH), 1445, 1345, 1285 (m, CH), 1150, 1086, 1022 (s, CO),

635 cm^{-1}(acetylene). ^{1}H-NMR (400 MHz, DMSO-d_6 + droplet of D_2O), δ = 1.67 (2H, H-2), 2.22 (2H, H-3'), 2.68 (H-5'), 3.0–3.9 (glucose ring H-2, H-3, H-4, H-5, H-6a'b and H-1'), 4.67 (H-1, 1,6-glc, unsubst. at *O*-2); 4.88 and 4.94 (H-1, 1,6-glc subst. at *O*-2, 1,3,6-glc, *t*-1,3-glc). ^{13}C-NMR (400 MHz, DMSO-d_6): 14.52 (C-3'), 28.61 (C-2'), 67.98 (C-6), 69.86 (C-1'), 70.15, 70.49, 71.17, 71.90, 73.37 (C-2–C-5), 79.91 (C-5'), 84.73 (C-4'), 96.0 (C-1, 2-*O*-subst.), 98.4 (C-1, unsubst. at *O*-2).

11.5 Monomer Analysis of Propargyl and Pentynyl Dextran by GLC

11.5.1 Monomer Analysis of Propargyl Dextran

Samples for the monomer analysis of PgD were prepared as follows:

Hydrolysis and acetylation:

1 mL Trifluoroacetic acid (TFA, 2M) was added to 2 mg of PgD in a 1 mL V-Vial followed by heating at 120 °C for 3 hours with continuous stirring. The reaction mixture was co-distilled with toluene under nitrogen to evaporate the acid. For acetylation, 200 µL acetic anhydride and 50 µL of pyridine was added and heated at 90 °C for 3 hours with stirring. Acetic anhydride was destroyed with sat. $NaHCO_3$ solution. The products were extracted with CH_2Cl_2 (4×15 mL), washed with sat. $NaHCO_3$ solution (2×15 mL), with cold 0.1 M HCl (1×20 mL), and with water (1×25 mL), filtered, and dried over $CaCl_2$. The dried organic phase was used for monomer analysis by GLC. The peak area was corrected according to the ECR concept[185].
Heating, stirring, and evaporating of solvents under nitrogen was carried out in a heating block from Barkey GmbH & Co. KG, Germany.

11.5.2 Monomer Analysis of Pentynyl Dextran (PyD)

Samples for the monomer analysis of PyD were prepared as follows:

Methanolysis and trimethylsilylation:

900 µL methanolic HCl (1.5 M) was added to 2 mg sample in 1 mL V-Vial followed by heating at 90 °C for 2 hours. After cooling to room temperature the reaction mixture was co-distilled with methanol under nitrogen to evaporate the acid. For trimethylsilylation, 50 µL CH_2Cl_2, 10 µL pyridine, 50 µL *N,O*-bis-(trimethylsilyl)-trifluoroacetamide (BSTFA), and 10 µL trimethylchlorosilane (TMCS) were added to the reaction mixture, and heated at 100 °C for 1 hour. The products were diluted with CH_2Cl_2 and analyzed by GLC.

For determination of the recovery of glucosyl units, D-pinitol (0.3 mg, 1.54 mmol) was added from a stock solution to the weighted PyD sample (about 5 mg). The peak area was corrected according to the ECR concept (factors: un: 1.000, mono: 0.933 (2,3 and 4); di: 0.874 (23, 24 and 34); tri: 0.823 for 234).

11.6 Peracetylation of Pentynyl Dextran

Peracetylated PyD (PyAcD) was prepared by dissolving PyD (DS 0.43, 200.9 mg, 1.05 mmol AGU, 2.7 mmol OH) in formamide ($HCONH_2$) (3.4 mL) and pyridine (4 mL) under stirring. After addition of acetic anhydride (2.85 mL, 30.2 mmol), the clear solution was stirred for 24 hours at 35 °C. The product was purified by dialysis against water and freeze-dried (253.8 mg; 100% d.Th. = 314.7 mg). Found: C 55.23%, H 5.90%, C/H 9.36; Calc.: C 53.46%, H 5.98%, C/H 8.94; ATR-IR: no OH absorption, strong C=O absorption at 1750 cm^{-1} and C-O absorption at 1220 cm^{-1}.

11.7 Alkynyl Dextran – Metal Complexation Studies

11.7.1 Dialysis of Pentynyl Dextran Against Silver Salt Solution

PyD (DS 0.43, 249 mg, 1.31 mmol AGU, 0.56 mmol C≡CH) was dissolved in DMSO (20 mL). After formation of a clear solution, it was dialyzed against aqueous $AgNO_3$ (2×100 mg) (MWCO 14000, 5L) and subsequently against deionized water (8×5L) to remove unbound salt, in the absence of light. A slight pink color developed during dialysis. The product was freeze-dried (290.6 mg, 100% d. Th.: 1:1-Ag-complex: 309 mg, 19.6% Ag). Ag content in the product was determined by elemental analysis and

ICP-OES. For ICP-OES, 3 mL of HNO_3 (65%) was added to the sample (61.5 mg) and heated at 85 °C for 4 hours. Solution was diluted to 10 mL with deionized water.
ICP-OES (Ag): 23.3%
EA: C 38.72%, H 5.18%, C/H 7.47, (calculated: 100 – CHO%: 24.5% Ag)
Molar ratio of Ag/C≡CH: 1.3

11.7.2 Dialysis of Peracetylated Pentynyl Dextran with Fe^{+3} Salt Solution

PyAcD (DS_{Py} 0.43, DS_{Ac} 2.57, 98.40 mg) was dissolved in DMAc (25 mL). Clear solution was formed within a few minutes but stirring was continued overnight. Solution was dialyzed against $FeCl_3.6H_2O$ (2×100 mg) in deionized water and subsequently without salt to remove unbound iron for 5 days (10×5L) before freeze-drying (81.1 mg).
For ICP-OES, 1.5 mL of HNO_3 (65%) and 0.5 mL of HCl (37%) was added to the sample (73.5 mg) and heated at 85 °C for 4 hours. Solution was diluted to 20 mL with deionized water.
ICP-OES (Fe): 9.4%
EA: C 46.78%, H 5.24%, C/H 8.93, (7.6% Fe)
In repeated experiment:
EA: C 46.91%, H 5.33%, C/H 8.80, (7.3% Fe)

11.7.3 Dialysis of Peracetylated Pentynyl Dextran with $Fe^{+2/+3}$ Salt Solution

PyAcD (DS_{Py} 0.43, DS_{Ac} 2.57, 76.60 mg) was dissolved in DMAc (15 mL). After formation of a clear solution, it was dialyzed against a mixture of $FeCl_2.4H_2O$ ((1) 70.1 mg, 0.353 mmol; (2) 70.6 mg, 0.355 mol), and $FeCl_3.6H_2O$ ((1) $FeCl_2.4H_2O$ 144.2 mg, 0.534 mmol, (2) 145.1 mg, 0.537 mmol) in a molar ratio of 1:1.5 in nanopure water treated wih UV raditions to avoid any microorganisms in water. All processes were carried out under nitrogen. Subsequently, to remove unbound salts, product was dialyzed against deionized water (7×5 L) for three days. During dialysis, it was observed that some part of material was precipitated while another part remained dissolved in the dialysis tube. After completion of dialysis process, soluble and precipitated fractions were separated and freeze-dried.

Weight of soluble part: 2.6 mg (3.75%)

Weight of insoluble part: 65.5 mg (96.25%)

Total weight: 68 mg

EA (soluble): C 17.14%, H 2.62%, C/H 6.54, corresponding to 39.8% Fe.

EA (precipitated): C 47.36%, H 6.42%, C/H 7.37, corresponding to 5.8% Fe.

11.7.4 Blank Experiment for Metal Complexation with Dextran

To check whether dextran itself can make any complexation with silver and iron, the following experiments were carried out.

11.7.4.1 Dialysis of Dextran Against Silver Salt Solution

Dextran (M_w 500 000, 288.6 mg) was dissolved in DMSO (25 mL). Solution was dialyzed two times against aqueous $AgNO_3$ (2×100 mg), and subsequently against deionized water (8×5 L) to remove unbound salt, and was then freeze-dried (270.6 mg, white solid).

EA: C 42.54%, H 6.49%, C/H 6.55, corresponding to 98.37% dextran.

11.7.4.2 Dialysis of Dextran Against Iron Salt Solution

Dextran (M_w 500 000, 288.6 mg) was dissolved in DMSO (25 mL). Solution was dialyzed two times against aqueous $FeCl_3.6H_2O$ (2×100 mg) and subsequently against deionized water (8×5 L) to remove unbound salt, and was then freeze-dried (273 mg, white solid).

EA: C 41.77%, H 6.63%, C/H 6.30, corresponding to 97.74% dextran.

11.8 Synthesis of Functionalized Azides

11.8.1 Synthesis of 2-Azidoethylamine (4)

2-Bromoethylamine hydrobromide (5.04 g, 24.60 mmol) was added to a solution of sodium azide (5.19 g, 79.83 mmol, 3.2 equiv.) in water (20 mL). The solution was heated to 75 ºC with continuous stirring for 21 hours before it was cooled to 0 ºC. Et_2O (20 mL) was added followed by solid KOH (8 g). The organic phase was separated and the aqueous layer was extracted with Et_2O (3×100 mL). The combined organic layers were dried over $MgSO_4$, filtered, and the solvent removed carefully by rotary evaporation (35 ºC, 750 mbar) to afford 2-azidoethylamine **4** (1.82 g, 21.13 mmol, 86%) as a colorless liquid.

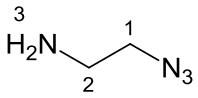

TLC: R_f = 0.39 (EtOAc/MeOH, 3:1)

^{1}H-NMR (400 MHz, $CDCl_3$): δ = 1.32 (s, 2H, H-3), 2.81-2.91 (t, 2H, H-1, *J* = 5.95), 3.26 (t, 2H, H-2, *J* = 5.93) ppm. ^{13}C-NMR (400 MHz, $CDCl_3$): δ = 41.34 (C-2), 54.65 (C-1) ppm.

11.8.2 Synthesis of 3-Azido-1-propanol (5)

Sodium azide (26.78 g; 412 mmol) was suspended in DMF (100 mL) with strong stirring followed by addition of 3-chloro-1-propanol (20.06 g, 213.36 mmol). Reaction mixture was heated at 100 °C for 48 hours before cooling to room termperature and extracted with diethyl ether (3×100 mL). The solution was washed with saturated NaCl solution (5×100 mL) and dried over Na_2SO_4. The solvent was evaporated to give 3-azido-1-propanol (**5**) as colorless liquid (19.18 g, 189.85 mmol, 89%).

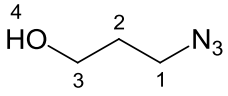

^{1}H-NMR (400 MHz, $CDCl_3$): δ = 1.83 (m, 2H, H-2), 3.47 (t, 2H, H-1, *J*= 6.84), 3.76 (t, 2H, H-3, *J* = 6.34) ppm. ^{13}C-NMR (400 MHz, $CDCl_3$): δ = 31.4 (C-2), 48.42 (C-1), 59.77 (C-3) ppm. NMR data were in accordance with [255].

11.8.3 Synthesis of 4-Azidobutyric Acid (6)

4-Chlorobutyric acid (5.0 g, 4.08 mL, 40.79 mmol) was added to water (10 mL) followed by the addition of NaN_3 (3.29 g, 50.65 mmol). Reaction mixture was refluxed for 24 hours before cooling to room temperature. 100 mL water was added to the reaction mixture. The product was extracted with diethylether (4×50 mL). Collected organic phases were washed with water (1×50 mL) and dried over $CaCl_2$. Diethylether was evaporated under reduced pressure to get 4-azido-butyricacid (**6**) as a yellow oil (4.27 g, 33.04 mmol, 81%).

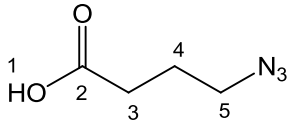

TLC R_f: 0.38 (MeOH/*n*-hexane 1:1)

^{1}H-NMR (300 MHz, $CDCl_3$): δ = 1.92 (m, 2H, H-4), 2.50 (m, 2H, H-5), 3.38 (m, 2H, H-3) ppm. ^{13}C-NMR (300 MHz, $CDCl_3$): δ = 24.13 (C-4), 30.93 (C-3), 50.63 (C-5), 178.09 (C-2) ppm.

11.8.4 Synthesis of 3-Azido-1-propanethiol (7)

3-Chloro-1-propanthiol (700 mg, 616.19 µL, 6.32 mmol) was added to a mixture of H_2O/C_2H_5OH (10 mL, 2:1) followed by the addition of NaN_3 (796.84 mg, 12.25 mmol). The reaction mixture was stirred for 24 hours at 110 °C before cooling down to room temperature, followed by addition of water (50 mL). The product was extracted with diethyl ether (4×50 mL), collected organic phases were washed with H_2O (1×50 mL) and dried over $CaCl_2$. Diethyl ether was evaporated and 3-azido-1-propanethiol (**7**) was obtained as yellow oil (554 mg, 4.72 mmol, 75%).

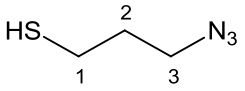

TLC R_f: 0.60 (MeOH/*n*-hexane 3:1)

^{1}H-NMR (300 MHz, $CDCl_3$): δ = 1.86 (m, 2H, H-2), 3.48 (m, 2H, H-3), 3.72 (m, 2H, H-1) ppm. ^{13}C-NMR (300 MHz, $CDCl_3$): δ = 28.25 (C-1), 35.26 (C-2), 49.69 (C-3) ppm.

11.8.5 Synthesis of *O*-Biotinyl-*N*- hydroxysuccinimide (8)

Biotin (204.4 mg, 0.836 mmol) was dissolved in DMF (15 mL) followed by the addition of 1-ethyl-3(3-dimethylaminopropyl)carbodiimide (EDC) (204.2 mg, 1.06 mmol) and *N*-hydroxysuccinimide (148 mg, 1.28 mmol). Stirring was continued for 48 hours at room temp. The solvent was evaporated in vacuum, and the residue was dissolved in CH_2Cl_2 (400 mL). The organic phase was washed with conc. $NaHCO_3$ solution (2×20 mL) and with conc. NaCl solution (1×20 mL), dried over $MgSO_4$ and filtered. CH_2Cl_2 was removed under vacuum to give pure biotin succinimide (**8**) (234 mg, 0.683 mmol, 82%).

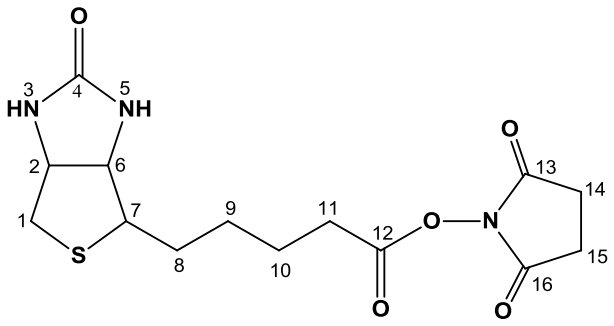

^{1}H-NMR (300 MHz, DMSO-d_6): δ = 1.50 (m, 3H, H-8$_{a/b}$, H-9), 1.71 (m, 3H, H-8$_{a/b}$, H-10), 2.72 (t, 4H, H-14, H-15, J = 7.34), 3.16 (m, 1H, H-7), 4.21 (m, 1H, H-6), 4.37 (m, 1H, H-2), 6.42 (s, 1H, H-3), 6.47 (s, 1H, H-5) ppm. ^{13}C-NMR (300 MHz, DMSO-d_6): δ = 24.3 (C-10), 25.4 (C-14, C-15), 27.6 (C-8), 27.8 (C-9), 30.0 (C-11), 55.2 (C-7), 59.2 (C-2), 61.0 (C-6), 162.7 (C-4), 168.9 (C-12), 170.3 (C-13, C-16) ppm. NMR data were in accordance with [256].

11.8.6 Synthesis of Biotin-*N*-(2-Azidoethyl)amide (9)

2-Azidoethylamine (60.35 mg, 0.70 mmol) was dissolved in DMF (8 mL) followed by the addition of triethylamine (65 µL, 0.0005 mmol) and biotin-succinimide **8** (152 mg, 0.44 mmol). The reaction mixture was stirred at room temperature for 48 hours. The solvent was evaporated under vacuum, and the residue was purified by flash column chromatography (acetone/MeOH, 10:1) to give pure biotin *N*-(2-azidoethyl)amide **9** (110.55 mg, 80 %).

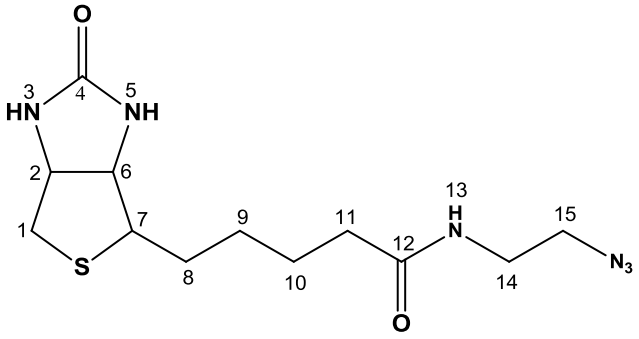

TLC: R_f = 0.29 (Acetone/MeOH, 10:1)

^{1}H-NMR (300 MHz, DMSO-d_6): δ = 1.20-1.38 (m, 2H, H-9), 1.40-1.55 (m, 3H, H-10, H-$8_{a/b}$), 1.55-1.69 (m, 1H, H-$8_{a/b}$), 2.08 (t, 2H, H-11, *J* = 7.32), 2.55 (d, 1H, H-1, *J* = 12.91), 2.80 (d, 1H, H-1, *J* = 12.42), 3.07-3.14 (m, 1H, H-7), 3.20-3.26 (m, 2H, H-14), 3.32 (d, 2H, H-15, *J* = 7.60), 4.10-4.17 (m, 1H, H-6), 4.28-4.35 (m, 1H, H-2), 6.35 (s, 1H, H-3), 6.42 (s, 1H, H-5), 8.04 (t, 1H, H-13) ppm. ^{13}C-NMR (300 MHz, DMSO-d_6): δ = 25.2 (C-10), 28.0 (C-8), 28.2 (C-9), 35.1 (C-11), 38.1 (C-14), 39.9 (C-1), 50.0 (C-15), 55.4 (C-7), 59.2 (C-2), 61.0 (C-6), 162.7 (C-4), 172.4 (C-12) ppm. NMR data were in accordance with [256].

11.8.7 6-Azido-*N*-hexyl-1-amine (10) and *O*-Acetyl-α-tocopherol Acetate Azide (11)

6-Azido-*N*-Boc-hexyl-1-amine (**10**) was commercially available while *O*-Acetyl-α-tocopherol acetate azide (**11**) was a gift from Prof. Thomas Rosenau, University of Natural Resources and Applied Life Sciences, Department of Chemistry, Vienna, Austria.

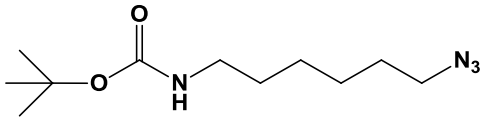

10

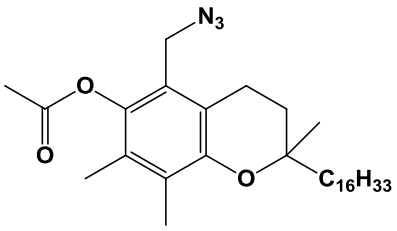

11

11.9 Click reaction of Pentynyl Dextran with Various Azides

In a typical procedure, PyD-17 (DS 0.43) was dissolved in DMSO/H_2O (4:1 v/v, 10-15 mL). After formation of a clear solution, any azide followed by freshly prepared 1M aq.solution of Na-L-ascorbate (20 mol% per alkynyl group), and $CuSO_4.5H_2O$ (5 mol% per alkynyl group) was added. The reaction mixture was stirred at room temperature for 96 hours. The product was purified by dialysis against deionized water and freeze-dried. Conversion of alkynyl groups into 1,2,3-triazole was calculated by EA, GLC and NMR (if soluble in an appropriate solvent).

Table 12.2: Click reaction of azides with PyD-17

PyD-17			Azide				Product	Conversion [%]		
mg	mmol	C≡CH mmol	compound	mg	mmol	eq./ C≡CH	mg	EA	GLC	NMR
200.8	1.05	0.45	(**4**)	94.2	1.10	2.4	254.5 (**12**)	95	98	
101.5	0.53	0.23	(**5**)	57.0	0.56	2.4	103.0 (**13**)	*140	98	100
112.6	0.59	0.25	(**6**)	64.7	0.50	2.0	177.4 (**14**)	83	85	78
113.9	0.60	0.26	(**7**)	65.7	0.56	2.2	185.5 (**15**)	*123	92	
1120.0	5.88	2.53	(**9**)	717.0	2.29	0.9	1420.1 (**16**)	76	63	72
180.0	0.94	0.40	(**10**)	95.0	0.39	1.0	268.2 (**17**)	86	77	95
142.0	0.75	0.32	(**11**)	333.9	0.65	2.0	246.6 (**18**)	*107	57	

* Apparent conversion

*Aminoethyl-triazole-PyD (**12**)*

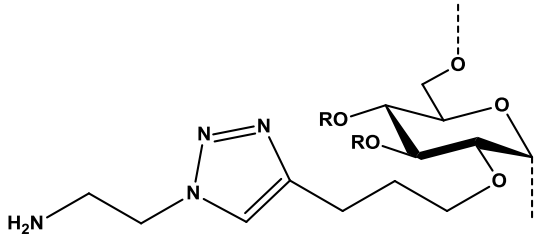

EA: C 44.07 %, H 6.50 %, N 10.11 %, C/H 6.78.

ATR-IR: $\tilde{\upsilon}$ [cm^{-1}] 3344, ν (O-H, s), 2925, 2883 ν (CH, CH_2, aliph., m), 1652 ν (C=C, v), 1519 ν (NH_2, m), 1436, 1352, 1280, δ (CH, m), 1148, 1102, 1014 ν (C-O).

*Propanol-triazole-PyD (**13**)*

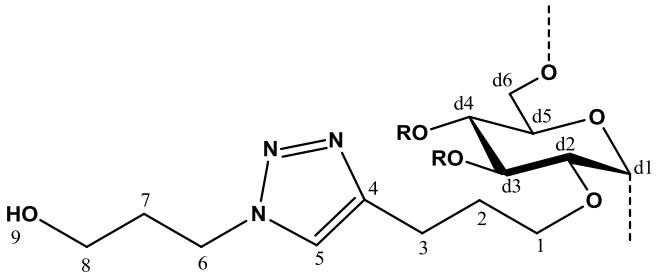

EA: C 43.95 %, H 6.60 %, N 10.05 %, C/H 6.66.

^{1}H-NMR (400 MHz, DMSO-d_6): δ = 1.80-2.67 (6H, H-2,-3, -7),3.0-4.0 (H-d2,3,4,5,6,6´,H-1), 4.35 (s, 2H, H-6), 4.69 (s, 1H, H-d1), 7.82 (s, 1H, H-5) ppm.

ATR-IR: $\tilde{\upsilon}$ [cm-1] 3349, ν (O-H, s), 2926, 2880 ν (CH, CH_2, aliph., m), 1647 ν (C=C, v), 1446, 1348, 1281, δ (CH, m), 1146, 1104, 1010 ν (C-O).

*Butyric acid-triazole-PyD (**14**)*

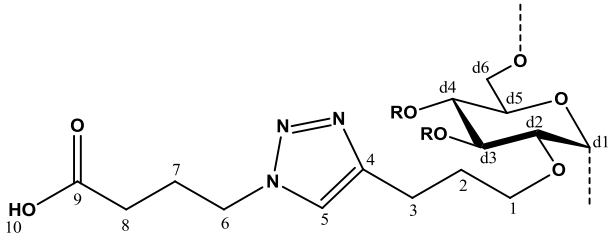

^{1}H-NMR (400 MHz, DMSO-d_6): δ = 1.79 (s, 2H, H-2), 2.21(6H, H-2, -3, -7),2.67 (s, H, CH, residualC≡CH), 3.0-4.0: glucose ring H and 2H, H-1, 4.67 (H, H-d1), 4.92: OH. 7.83 (s, 1H, H-5) ppm.

ATR-IR: $\tilde{\upsilon}$ [cm-1] 3375, ν (O-H, s), 2927, 2881 ν (CH, CH_2, aliph., m), 1712 ν (C=O, v), 1446, 1353, 1280, δ (CH, m), 1149, 1103, 1020 ν (C-O).

*Propanethiol-azide-PyD (**15**)*

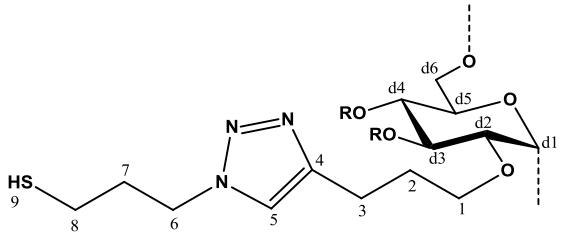

EA: C 42.85 %, H 6.05 %, N 8.83 %, S 9.08 %, C/H 7.08.

ATR-IR: $\tilde{\upsilon}$ [cm-1] 3371, ν (O-H, s), 2922, 2873 ν (CH, CH_2, aliph., m), 1645 ν (C=C, v), 1442, 1353, 1282, δ (CH, m), 1149, 1101, 1014 ν (C-O).

*Biotinethylamide-triazole-PyD (**16**)*

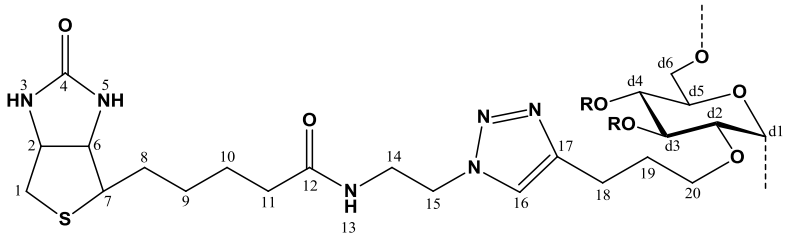

EA: C 48.78 %, H 6.62 %, N 9.32 %, S 3.03 %, C/H 7.37.

^{1}H-NMR (300 MHz, DMSO-d_6): δ = 1.25-2.24(12H, H-8, -9, -10, -11, -18, -19), (2H, H-18)2.60-4.00 (glucose ring H, H-20, H-1 and H-7), 4.15 (m, 1H, H-1), 4.35 (m, 1H, H-2), 4.50 (2H, H-15), 4.69 (H-d1), 6.39 (s, 1H, H-3), 6.44 (s, 1H, H-5), 7.80 (s, 1H, H-16), 7.96 (s, 1H, H-13) ppm.

ATR-IR: $\tilde{\upsilon}$ [cm^{-1}] 3347, ν (O-H, s), 2928, 2882 ν (CH, CH2, aliph., m), 1647 ν (C=C, v), 1552 ν (NH, w) 1448, 1348, 1277, δ (CH, m), 1148, 1104, 1015 ν (C-O).

*N-Boc-Hexylamine-triazole-PyD (**17**)*

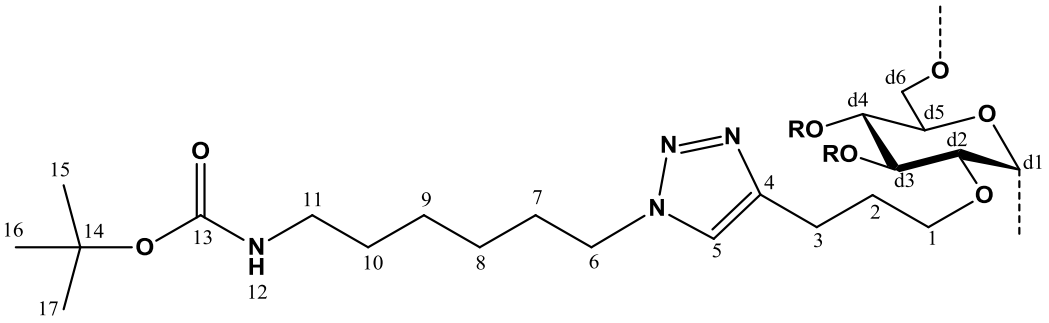

EA: C 51.47 %, H 7.69 %, N 7.41 %, C/H 6.69.

^{1}H-NMR (400 MHz, DMSO-d_6): δ = 1.23 (m, 4H, H-8, 9), 1.36 (s, 9H, H-15,16,17), 1.77-2.89 (10H, H-2, -3, -7, -10, -11), 3.0-4.0 (glucose ring H and H-1), 4.26 (2H, H-6), 4.69 and 4.85 (1H, H-d1), 6.72 (1H, H-12), 7.80 (s, 1H, H-5) ppm.

ATR-IR: $\tilde{\upsilon}$ [cm^{-1}] 3351, ν (O-H, s), 2932, 2884 ν (CH, CH_2, aliph., m), 1691 ν (RO*C*=*O*), 1650 ν (C=C, ν), 1524 ν (NH, m) 1455, 1365, 1237, δ (CH, m), 1156, 1104, 1015 ν (C-O).

*Tocopheryl-triazole-PyD (**18**)*

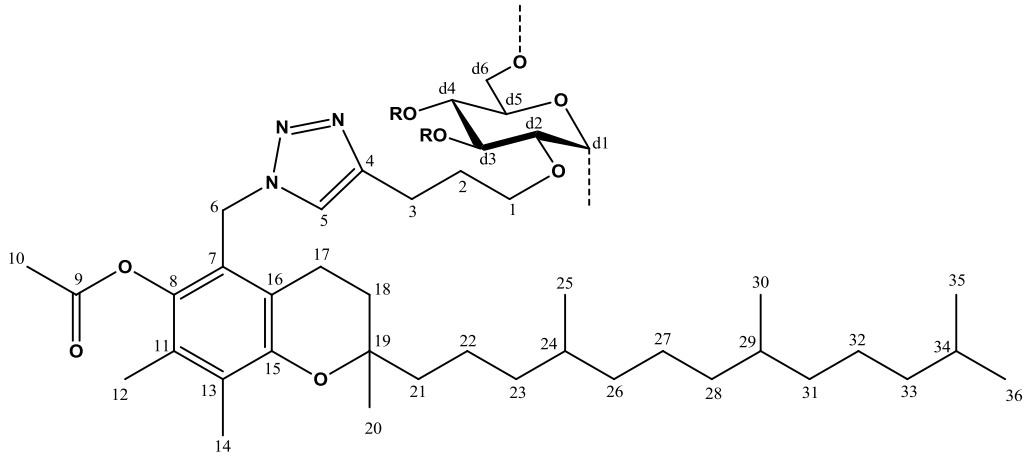

EA: C 61.29 %, H 8.38 %, N 4.54 %, C/N 13.5.

^{1}H-NMR (400 MHz, pyridine-d_5): δ = 0.89-1.90 (m, 33H, H-21 to H-36), 2.08-2.38 (8H, H-3, -12, -14), 3.0-4.6 (glucose ring H, H-1), 4.7-5.3 (glucose OH)., 7.75 (m, 1H,

H-5) ppm. ^{13}C-NMR (400 MHz, pyridine-d_5): δ = 12.38 (C-14), 13.24 (C-12), 19.85 (C-25, -30), 19.91 (C-22), 20.42 (C-10), 21.27 (C-17), 22.81 (C-35, -36), 23.86 (C-20), 25.10 (C-27 -32), 28.19 (C-34), 30.89 (C-18), 33.04 (C-14, -29), 37.66 (C-23, -26, -28, -31), 39.56 (C-21, -33), 46.49 (C-6), 75.87 (C-19), 118.74 (C-16), 128.37 (C-13), 126.90 (C-11), 141.99 (C-8), 169.72 (C-9) ppm. NMR data were in accordance with [257].
ATR-IR: $\tilde{\upsilon}$ [cm^{-1}] 3383, ν (O-H, s), 2950 ν (CH, arom., v), 2925, 2868 ν (CH, CH_2, aliph., m), 1641 ν (C=C, v), 1459, 1369, 1257, δ (CH, m), 1154, 1107, 1013 ν (C-O).

11.10 Synthesis of 1-Benzyl-4-phenyl-1,2,3-triazole (35)

Phenylacetylene (200.0 mg, 1.95 mmol) and benzylazide (260.7 mg, 1.95 mmol) were added to the solvent mixture of *t*-BuOH and H_2O (v/v, 1:1, 10 mL), followed by the addition of Na-L-ascorbate (160 mg, 0.81 mmol) and $CuSO_4.5H_2O$ (213.05 mg, 0.85 mmol). The reaction mixture was stirred at room temperature for 48 hours. Progress of the reaction was monitored by TLC. The product was purified by flash chromatography (EtOAc/*n*-hexane 1:3). The weight of the dried product was 318.0 mg (68%).

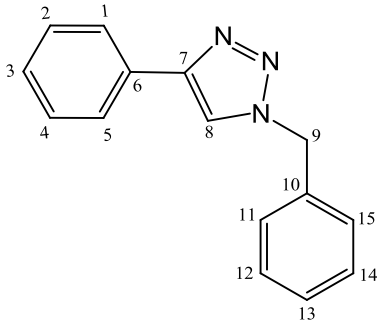

R_f: 0.27 (EtOAc/*n*-hexane 1:3)
^{1}H-NMR (300 MHz, $CDCl_3$): δ = 5.55(s, 2H, H-9), 7.25 (s, 1H, H-13), 7.29 (m, 2H, H-11, H-15), 7.36 (m, 2H, H-12, H-14), 7.35 (s, 1H, H-4), 7.41 (m, 2H, H-3, H-5), 7.65 (s, 1H, H-7), 7.78 (m, 2H, H-2, -6) ppm. ^{13}C-NMR (300 MHz, $CDCl_3$): δ = 54.17 (C-9), 119.47 (C-13), 125.67 (C-2, -6), 128.01 (C-11, -15), 128.11 (C-4), 128.72 (C-7), 128.76 (C-12, -14), 129.11 (C-3, -5), 130.54 (C-1), 134.68 (C-10), 148.18 (C-8) ppm.

11.11 Immobilization of Lipase

Lipase (*Rhizopus arrhizus*, 600 mg) was dissolved in water (30 mL) to form 2% solution. 7 mL of this solution was stirred with PyD-17 (DS 0.43), Lewatit VP OC 1600, Duolite A568 and Amberlite XAD 761 (700 mg of each) separately (1 mL per 100 mg of adsorbent) for 5 hours. The non-adsorbed enzyme was removed after centrifugation. The residue was washed with water and freeze-dried. The amount of enzyme protein adsorbed by the immobilization supports was determined on the basis of nitrogen content ($\text{protein (\%)} = \text{N \%} \times 6.25$). PyD (5.37%), Lewatit VP OC (1.12%), Duolite A568 (2.43%) and Amberlite XAD 761 (1.12%).

11.11.1 Determination of Surface Area of Pentynyl Dextran

Surface area of PyD-17 (DS 0.43) was determined by nitrogen adsorption with a Micrometric Flowsorb 2300 according to the BET-method at KTH Stockholm by Patricia Nordell. A mixture of 30% nitrogen in helium was used. Since the PyD adsorb moisture, sample was dried and directly measured. Average of two measurements: 3.3 ± 0.4 m^2/g.

11.11.2 Determination of Hydrolytic Activity of Immobilized Enzyme

The biocatalyst (10 mg) was added to the assay substrate containing 10 mL of 10% homogenized olive oil in 2 mL of a 10% gum acacia solution in 0.6% $CaCl_2$ and 5 mL 0.2 M tris maleate buffer of pH 7.0. A blank sample was also prepared containing all reagents in the same proportion but without biocatalyst. The enzyme substrate mixture was incubated at 30 °C in a shaking incubator at a speed of 100 rpm for 60 minutes. Ethanol-acetone mixture (v/v, 1:1, 20 mL) was added to stop the reaction. The liberated fatty acid was titrated with 0.1 M ethanolic KOH. A lipase unit was defined as the amount of enzyme, which releases 1 µmol fatty acids per minute at 30 °C. The hydrolytic activity was calculated using the following formula:

$\text{Hydrolytic activity} = V \times 166$ (u g^{-1} of biocatalyst)

V is the difference in volume of 0.1 M ethanolic KOH used for the biocatalyst and for the blank sample. Factor 166 in above equation was calculated as:

Suppose volume of 0.l M KOH used for neutralization of 1 mL fatty acid reaction mixture after 60 minutes = 1 mL

1000 mL of KOH can neutralize fatty acids mixture = 0.1moles

1 mL of KOH have neutralizes fatty acids mixture = $\frac{0.1}{1000}$ = 100 μ mol

So 100 μ mol. of fatty acids were released in first 60 min (first reading was recorded after 60 min)

Fatty acids released/min for 1 mL reaction mixture = $\frac{100}{60}$ = 1.66 μ mol min^{-1}

As amount of biocatalyst in fatty acids reaction mixture = 10 mg = 0.01 g

1g of biocatalyst can release fatty acids = $\frac{1.66}{0.01}$ = 166 μ mol $min^{-1}g^{-1}$

Thus hydrolytic activity = $V \times 166$ (u g^{-1} of biocatalyst)

Hydrolytic activity: PyD-Lip 1203, Lew-Lip 382, Duo-Lip 222 and Amb-Lip 176 ug^{-1} of biocatalyst.

11.11.3 Determination of Esterification Activity of Immobilized Enzyme and Synthesis of Geranyl Octanoate (37)

Geraniol (6.94 mL) and octanoic acid (6.34 mL) were dissolved in *n*-hexane (total volume 100 mL) to prepare 0.4 M solution for each, followed by addition of biocatalyst (500 mg). Samples were withdrawn after specific intervals and titrated with 0.05 M KOH (in EtOH) against phenolphthalein (0.1% in 60% ethanol) to follow the course of reaction.

TLC: R_f: 0.95 (EtOAc/*n*-hexane 1:1)

Esterification yield = $\frac{V_1 - V_2}{V_1} \times 100$

V_1 is the volume of 0.05 M KOH (in EtOH) used for 1 mL blank, and V_2 is the volume of 0.05 M KOH (ethanolic) used for 1 mL sample. Esterification activity was calculated after 60 minutes of the reaction.

12 APPENDIX

12.1 Determination of substituent distribution in PgD after hydrolysis and acetylation e.g. PgD-2

Peak No.	Position	Area	ECR	Factor	Corr.Area	Mol.[%]
1	un	11719	735	1.000	11719	6.97
2	un	8673	735	1.000	8673	5.16
3	2	44173	870	0.845	37326	22.19
4	2	35517	870	0.845	30012	17.84
5	3	0	870	0.845	0	0.00
6	3	0	870	0.845	0	0.00
7	4	0	870	0.845	0	0.00
8	4	0	870	0.845	0	0.00
9	23	16497	1005	0.731	12059	7.17
10	23	9962	1005	0.731	7282	4.33
11	24	32231	1005	0.731	23561	14.01
12	24	25917	1005	0.731	18945	11.26
13	34	0	1005	0.731	0	0.00
14	34	0	1005	0.731	0	0.00
15	234	18809	1140	0.645	12132	7.21
16	234	10095	1140	0.645	6511	3.87
Total					**168221**	**100.00**

Substitution in position	Mol %
un	12.12
2	40.03
3	0.00
4	0.00
23	11.49
24	25.27
34	0.00
234	11.08
Total	**100.00**

Mol fractions of un- (c_0), mono- (c_1), di- (c_2) and tri-substituted glucosyl units (c_3) was determined as:

$c_0 = s_0 = 12.12\%.$

$c_1 = s_2 + s_3 + s_4 = 40.03\%.$

$c_2 = s_{23} + s_{24} + s_{34} = 36.76\%.$

$c_3 = s_{234} = 11.08\%$

DS was calculated as:

$$\mathrm{DS} = \frac{c_1 + 2 \times c_2 + 3 \times c_3}{100} = 1.46$$

Partial DS (x_i) was calculated as:

$$x_2 = \frac{s_2 + s_{23} + s_{24} + s_{234}}{100} = 0.87$$

$$x_3 = \frac{s_3 + s_{23} + s_{34} + s_{234}}{100} = 0.22$$

$$x_4 = \frac{s_4 + s_{24} + s_{34} + s_{234}}{100} = 0.36$$

DS can also be calculated as:

$$\mathrm{DS} = x_2 + x_3 + x_4 = 1.46$$

12.2 Determination of substituent distribution in PyD after methanolysis and trimethylsilylation e.g. PyD-17

Peak No.	Bonding	Area	ECR	Factor	Corr.Area	Mol.[%]
1	un	2309478	1600	1.000	2309478	50.20
2	un	920011	1600	1.000	920011	20.00
3	2	387166	1715	0.933	361204	7.85
4	2	165395	1715	0.933	154304	3.35
5	3	69588	1715	0.933	64922	1.41
6	3	28747	1715	0.933	26819	0.58
7	4	166665	1715	0.933	155489	3.38
8	4	89262	1715	0.933	83277	1.81
9	23	63787	1830	0.874	55770	1.21
10	23	137916	1830	0.874	120582	2.62
11	24	25025	1830	0.874	21880	0.48
12	24	11574	1830	0.874	10120	0.22
13	34	92267	1830	0.874	80671	1.75
14	34	31759	1830	0.874	27767	0.60
15	234	50993	1945	0.823	41948	0.91
16	234	136910	1945	0.823	112625	2.45
Total					**4546867**	**100.00**

Substitution in position	Mol.%
un	70.20
2	11.21
3	1.99
4	5.19
23	3.83
24	0.70
34	2.36
234	3.36
Total	**100.00**

Mol fractions of un- (c_0), mono- (c_1), di- (c_2) and tri-substituted glucosyl units (c_3) was determined as:

$c_0 = s_0 = 70.20\%.$

$c_1 = s_2 + s_3 + s_4 = 18.39\%.$

$c_2 = s_{23} + s_{24} + s_{34} = 6.89\%.$

$c_3 = s_{234} = 3.36\%$

DS was calculated as:

$$\mathrm{DS} = \frac{c_1 + 2 \times c_2 + 3 \times c_3}{100} = 0.43$$

Partial DS (x_i) was calculated as:

$$x_2 = \frac{s_2 + s_{23} + s_{24} + s_{234}}{100} = 0.19$$

$$x_3 = \frac{s_3 + s_{23} + s_{34} + s_{234}}{100} = 0.12$$

$$x_4 = \frac{s_4 + s_{24} + s_{34} + s_{234}}{100} = 0.12$$

DS can also be calculated as:

$$\mathrm{DS} = x_2 + x_3 + x_4 = 0.43$$

12.3 Mass spectra of glucose derivatives obtained from propargyl dextran by hydrolysis and acetylation

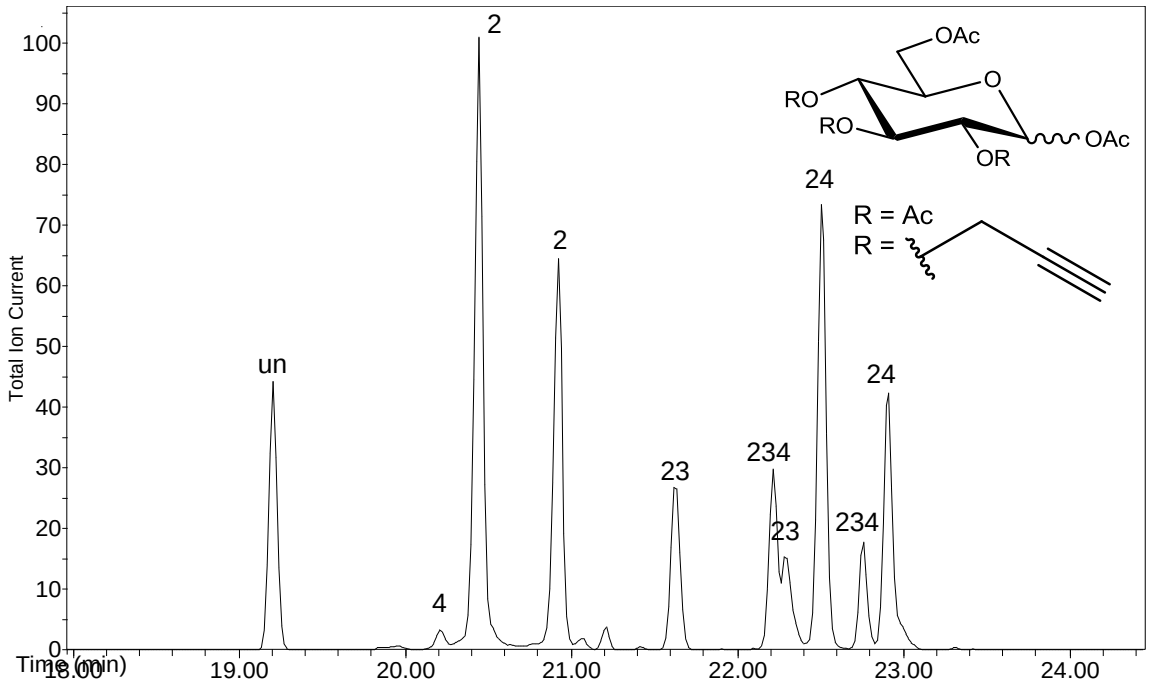

Gas chromatogram-mass spectrum of PgD-2 obtained by hydrolysis and acetylation. Temperature program: 100 °C (3 min); 6 °C/min to 310 °C (3 min), carrier gas He (1.6 mL min^{-1}), injection volume 1 μL.

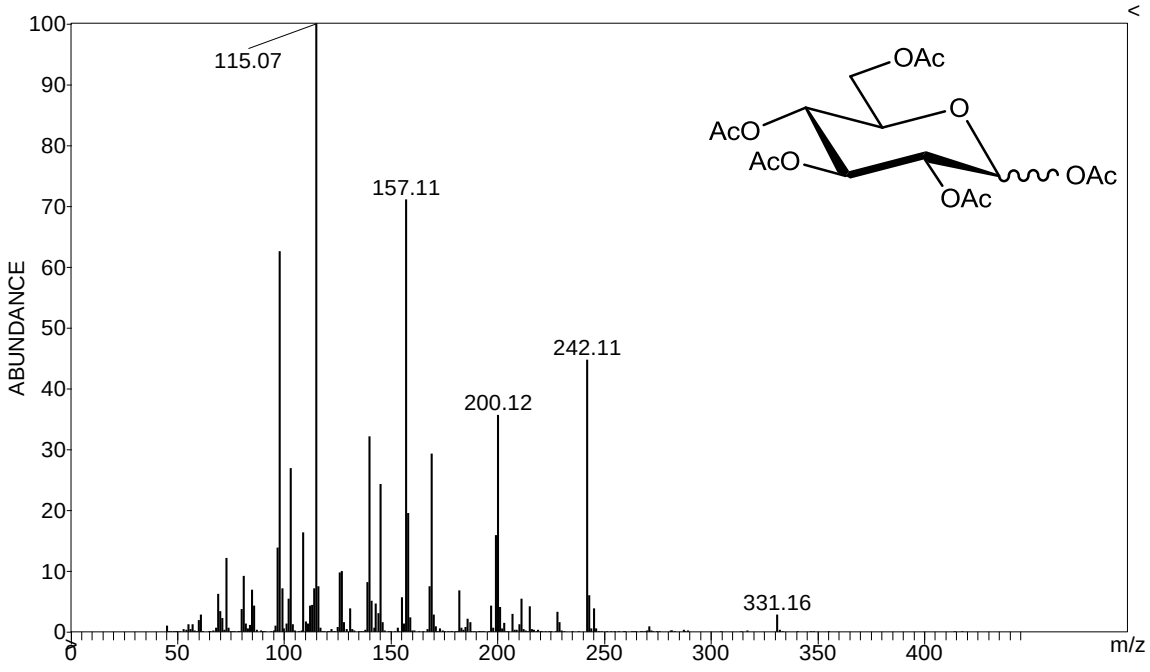

1,2,3,4,6-Penta-*O*-acetyl-α-D-glucopyranose (M = 390)

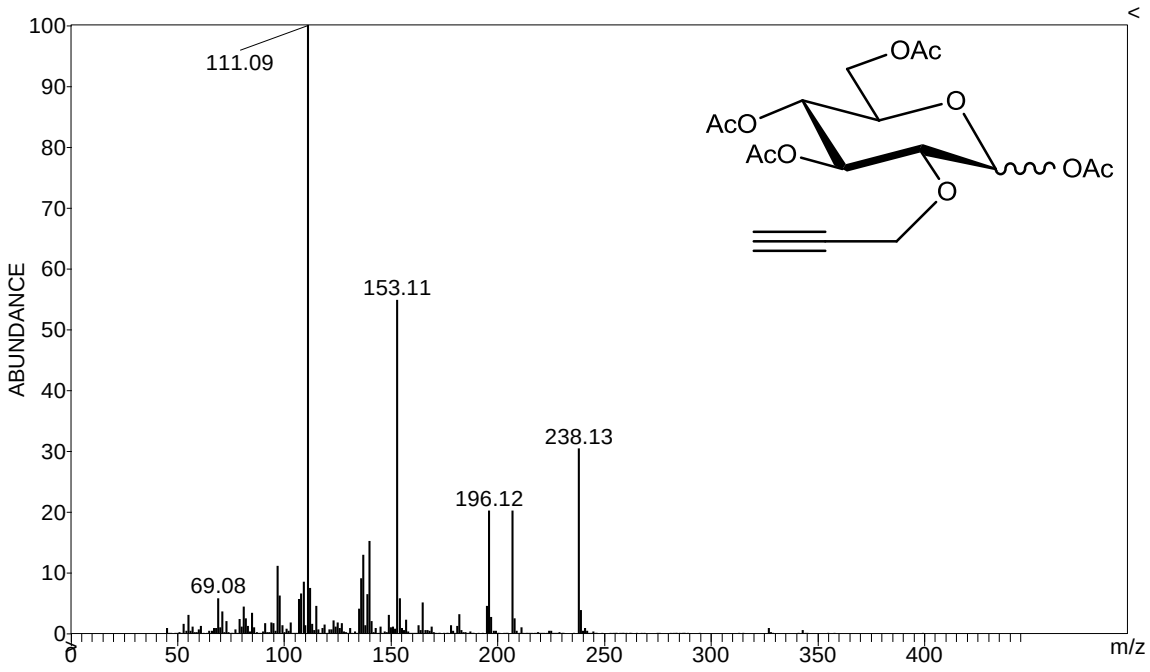

1,3,4,6-Tetra-*O*-acetyl-2-*O*-propargyl-α-D-glucopyranose (M = 386)

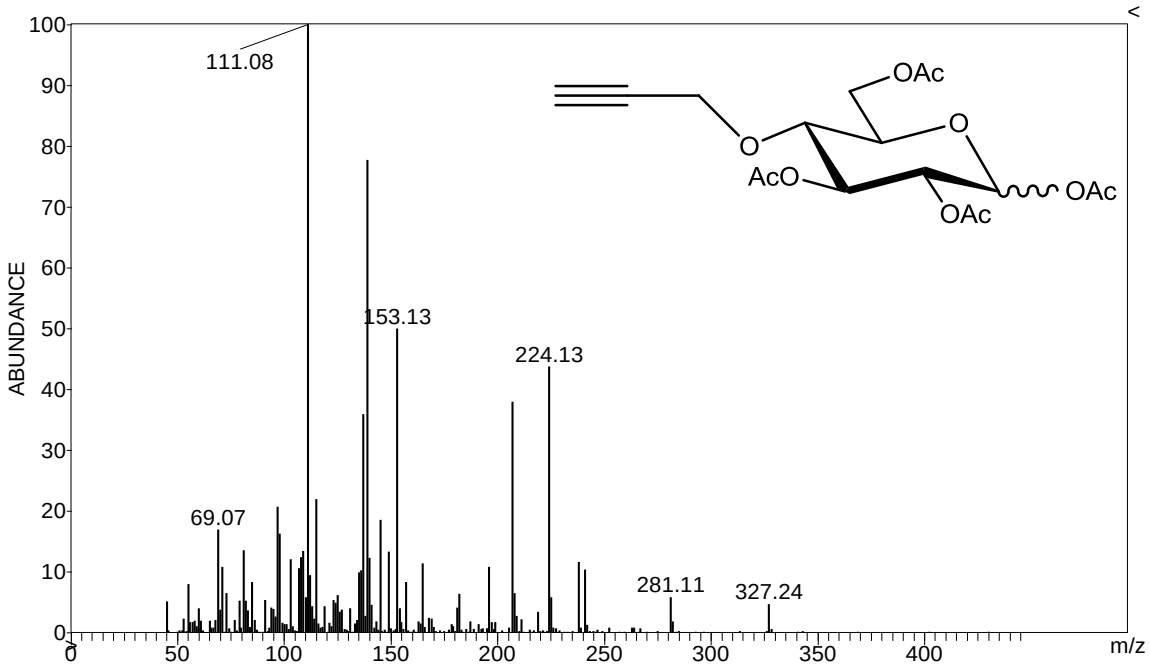

1,2,3,6-Tetra-*O*-acetyl-4-*O*-propargyl-α-D-glucopyranose (M = 386)

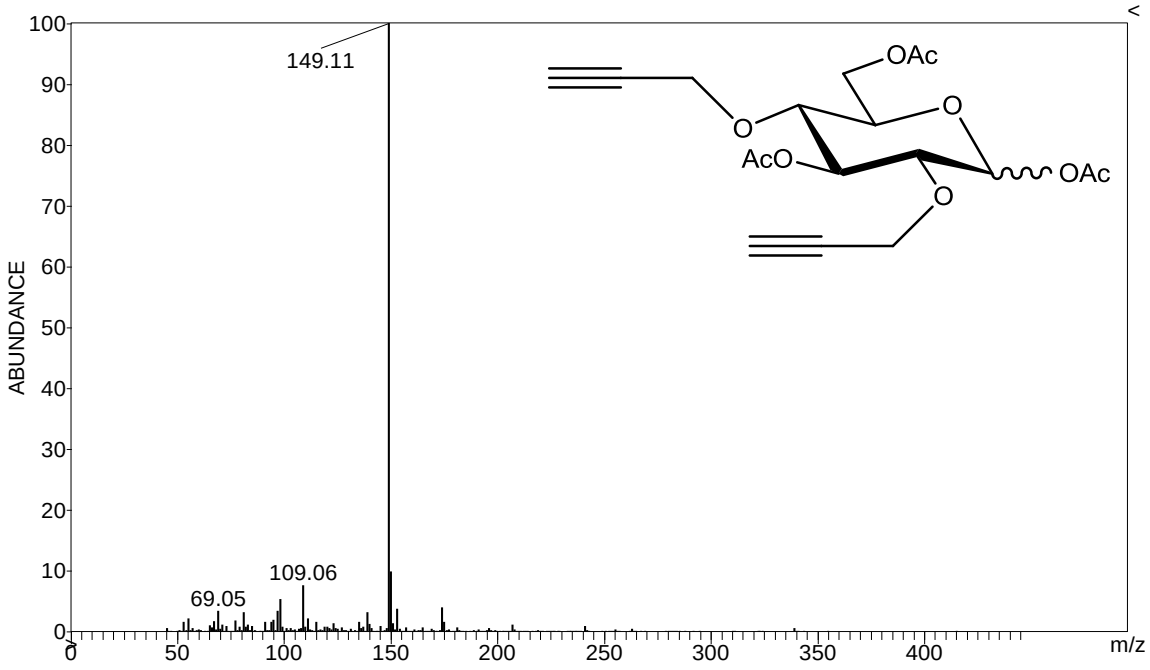

1,3,6-Tri-*O*-acetyl-2,4-di-*O*-propargyl-α-D-glucopyranose (M = 382)

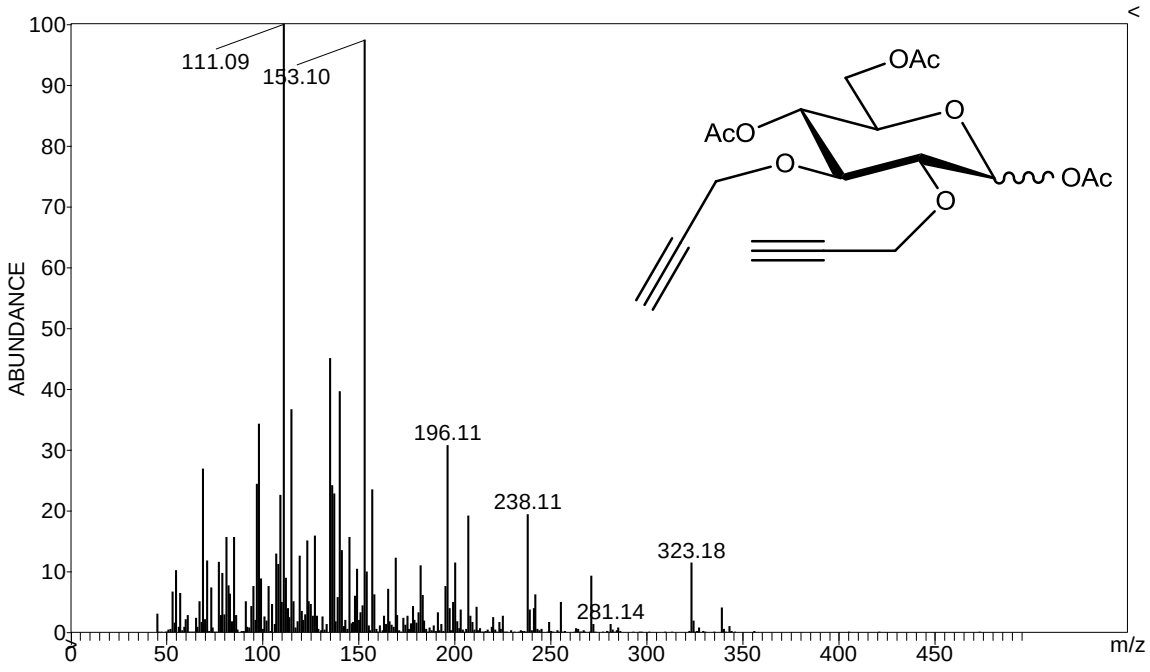

1,4,6-Tri-*O*-acetyl-2,3-di-*O*-propargyl-α-D-glucopyranose (M = 382)

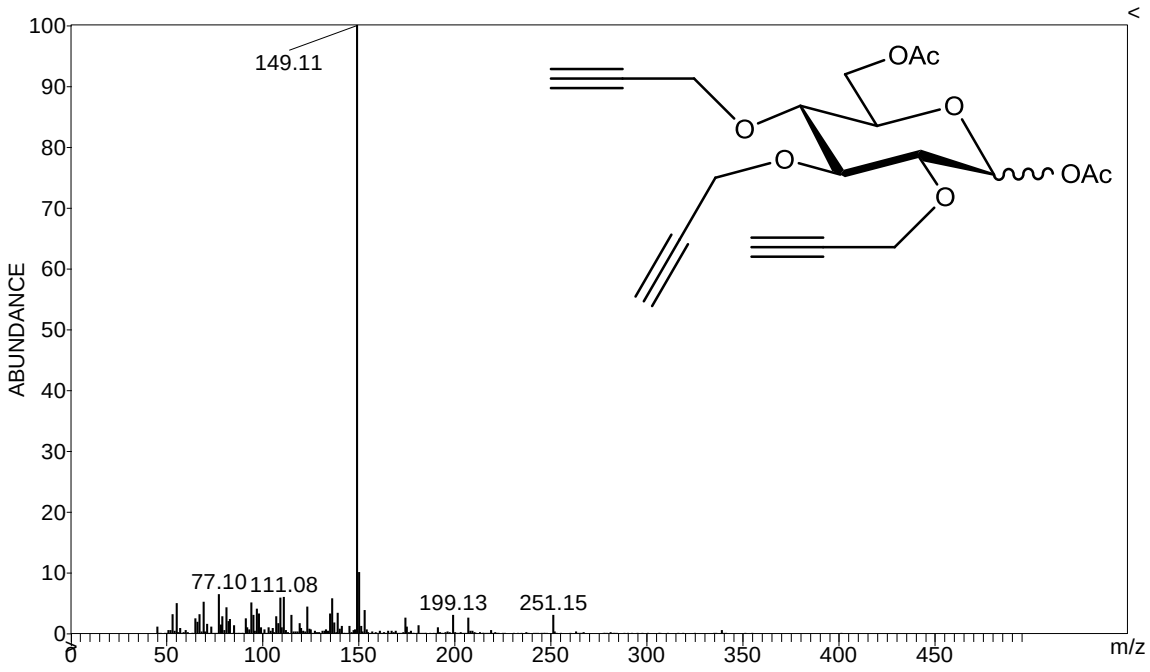

1,6-Di-*O*-acetyl-2,3,4-tri-*O*-propargyl-α-D-glucopyranose (M = 378)

12.4 Mass spectra of glucosides obtained from pentynyl dextran by methanolysis and trimethylsilylation

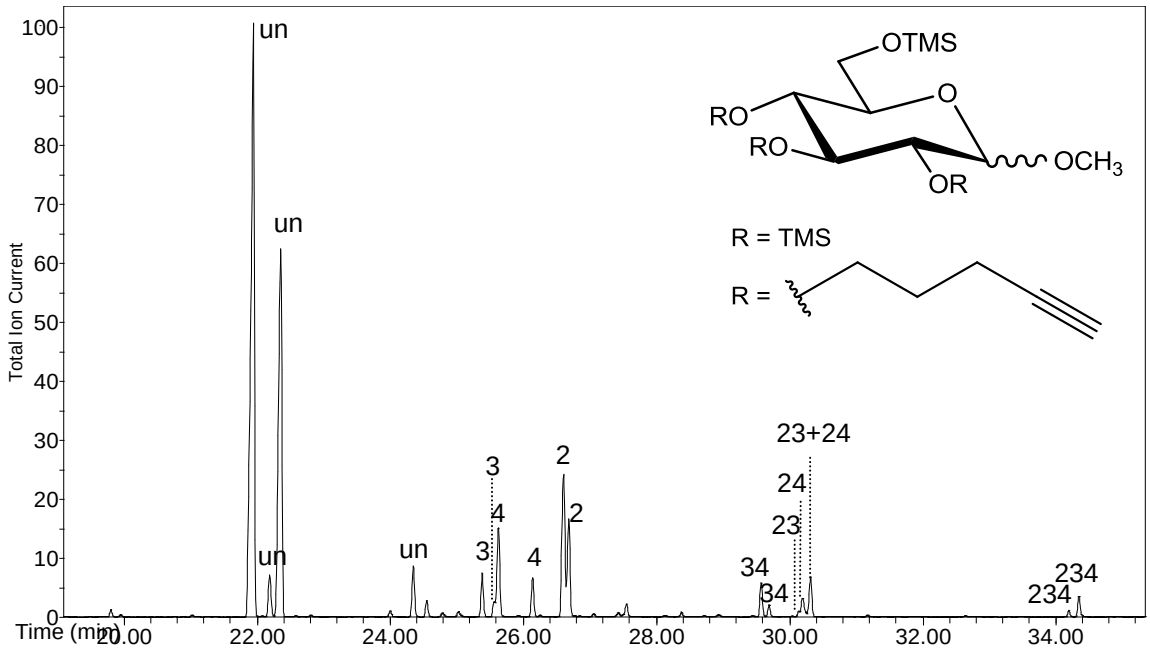

Gas chromatogram of PyD-16 (DS_{GC}: 0.43) after methanolysis and trimethylsilylation, column: zebron ZB 5 (5% phenylmethyl polysiloxan), carrier gas: He, temperature program: 60 °C (1 min) - 20 °C/min 130 °C - 4 °C/min 290 °C (10 min) - 20 °C/min 310 °C (10 min).

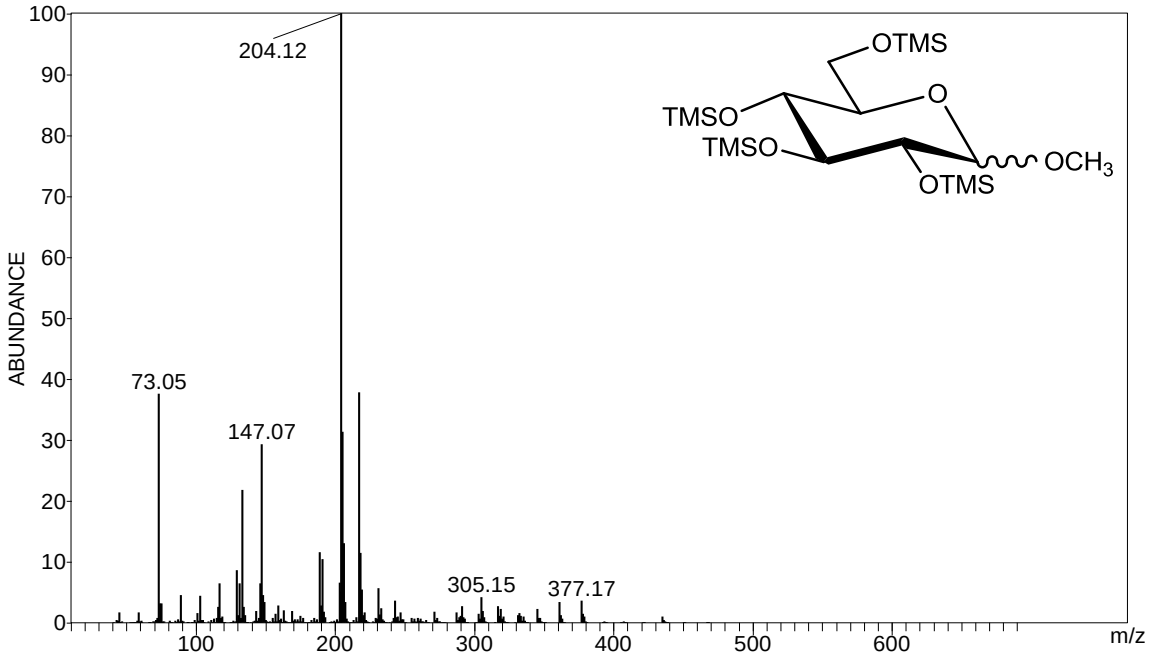

Methyl 2,3,4,6-tetra-*O*-trimethylsilyl-α,β-D-glucopyranoside (M = 482)

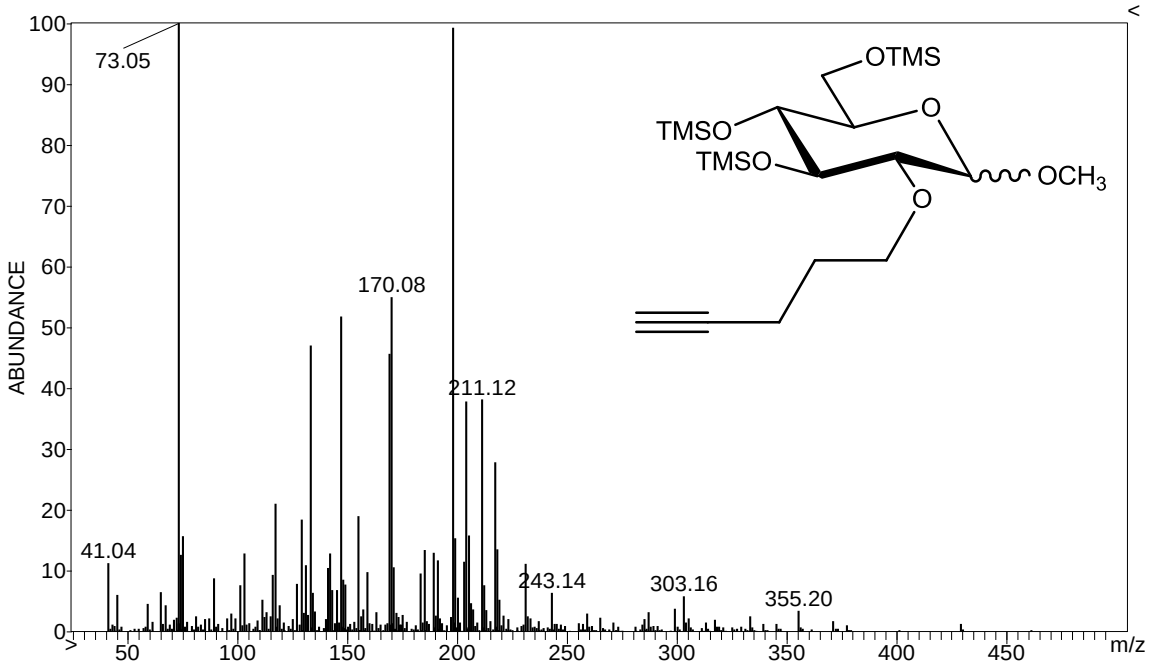

Methyl 3,4,6-tri-*O*-trimethylsilyl-2-*O*-pentynyl-α,β-D-glucopyranoside (M = 476)

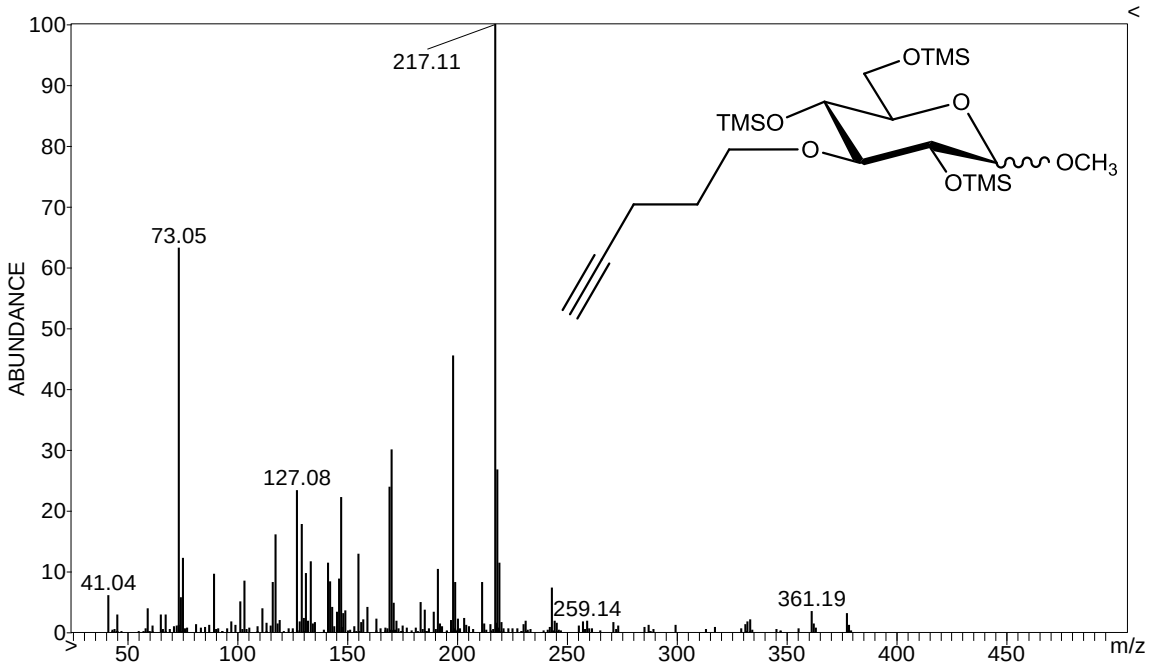

Methyl 2,4,6-tri-*O*-trimethylsilyl-3-*O*-pentynyl-α,β-D-glucopyranoside (M = 476)

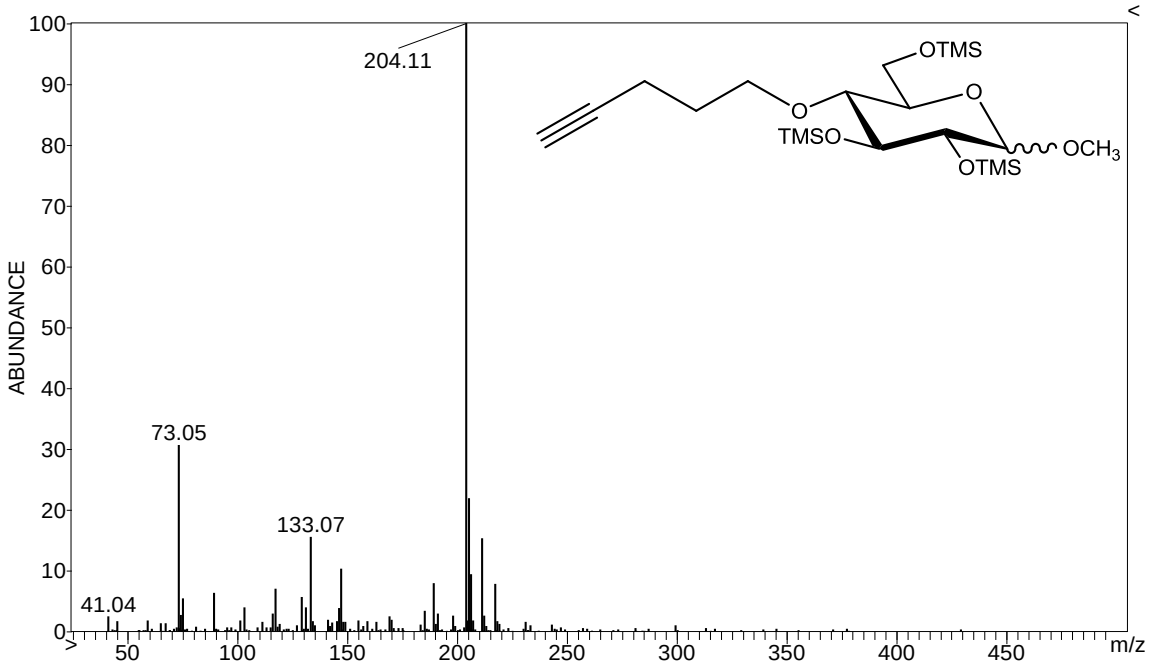

Methyl 2,3,6-tri-*O*-trimethylsilyl-4-*O*-pentynyl-α,β-D-glucopyranoside (M = 476)

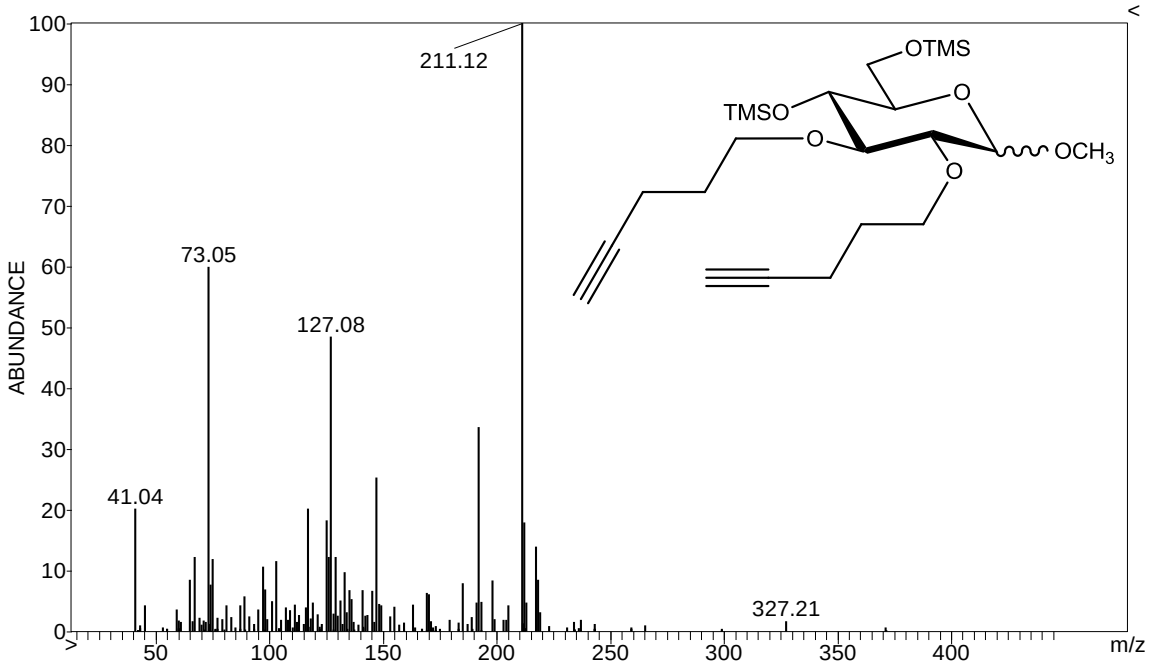

Methyl 4,6-di-*O*-trimethylsilyl-2,3-di-*O*-pentynyl-α,β-D-glucopyranoside (M = 470)

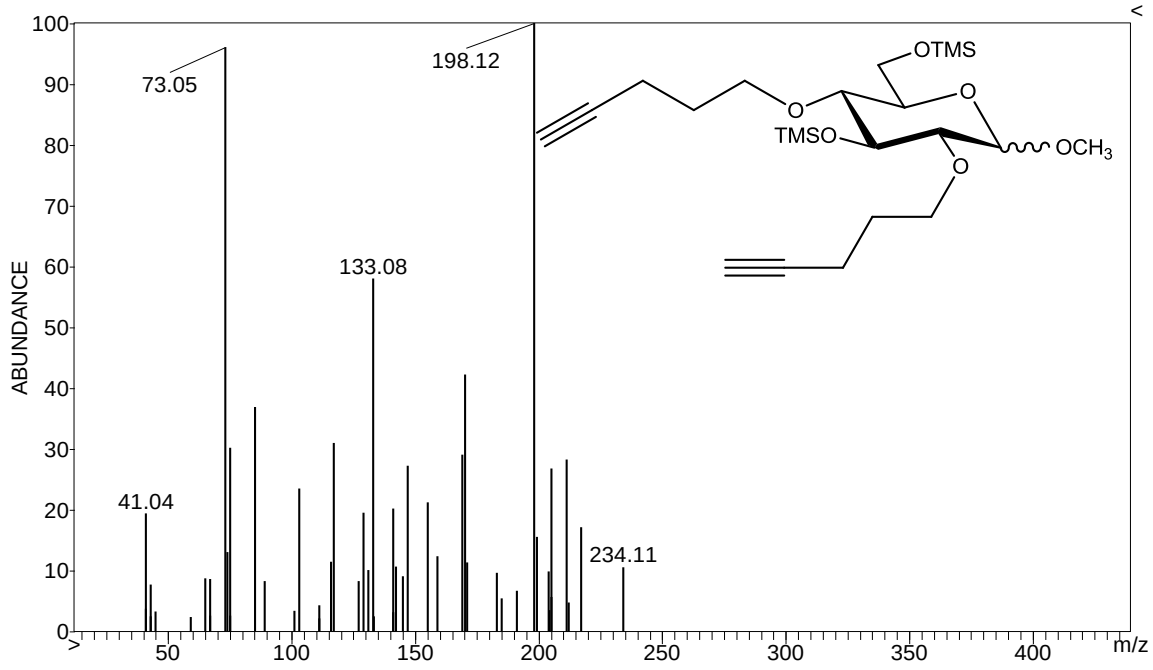

Methyl 4,6-di-*O*-trimethylsilyl-2,3-di-*O*-pentynyl-α,β-D-glucopyranoside (M = 470)

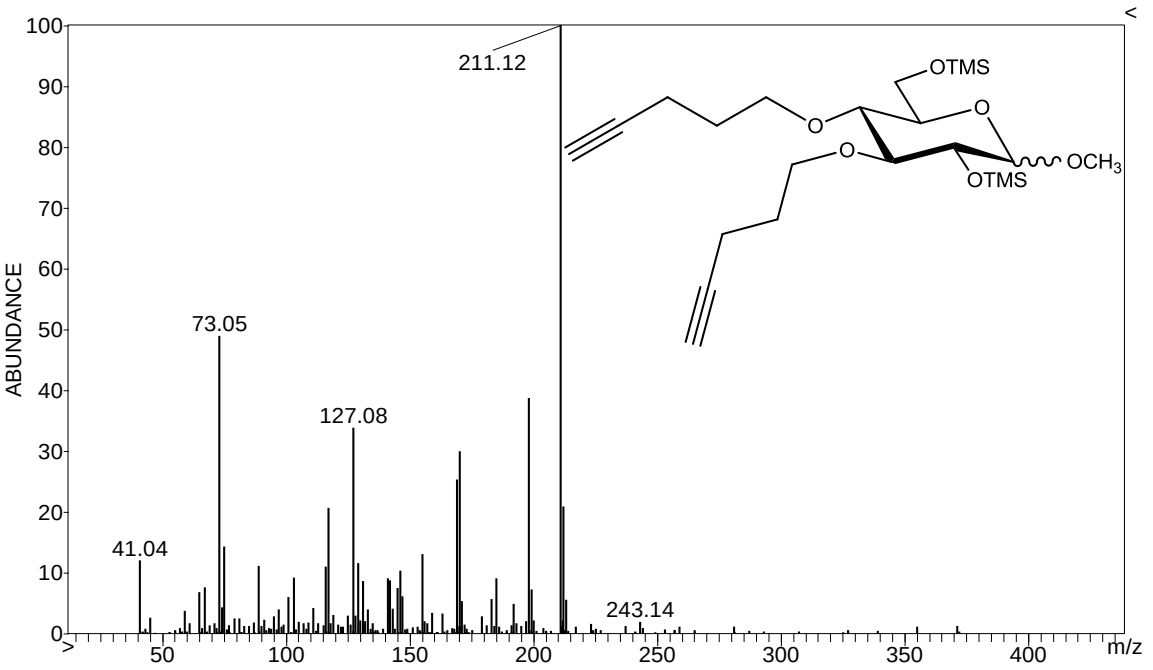

Methyl 2,6-di-*O*-trimethylsilyl-3,4-di-*O*-pentynyl-α,β-D-glucopyranoside (M = 470)

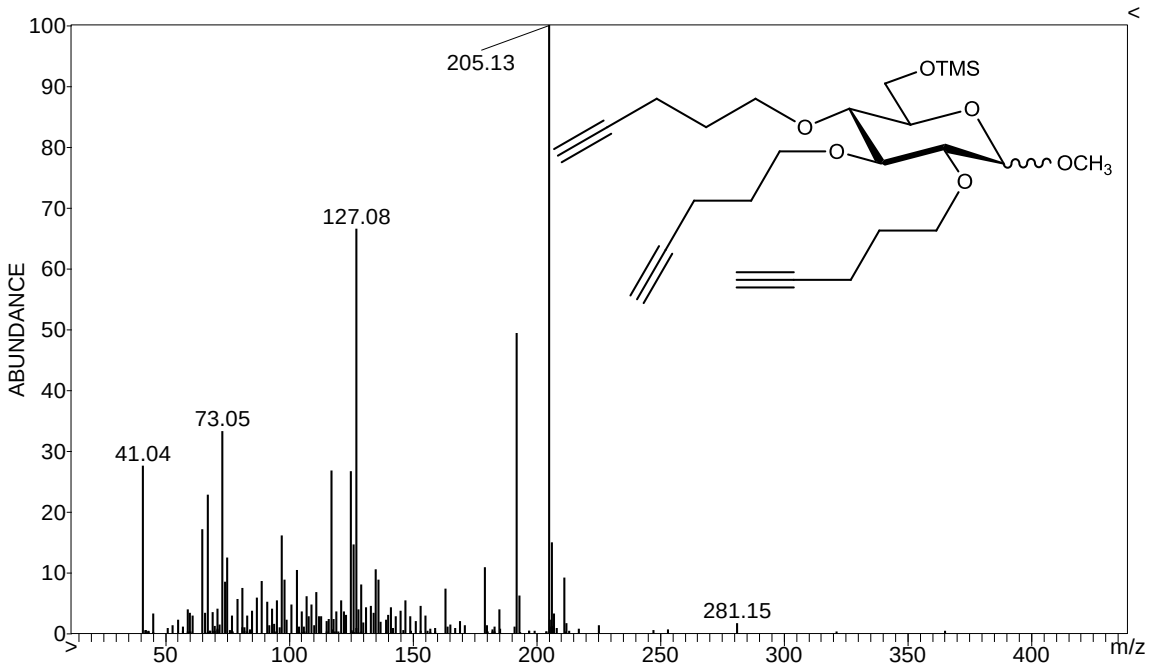

Methyl 6-*O*-trimethylsilyl-2,3,4-tri-*O*-pentynyl-α,β-D-glucopyranoside (M = 464)

13 REFERENCES

[1] Robyt JF, Essentials of carbohydrate chemistry. New York: Springer, **1998.**

[2] Gimelli SP, Carbohydrates: Fundamentals and applications. New York: Micelle Press, **2006**.

[3] Lutke-Eversloh T, Bergander K, Luftmann H, Steinbuchel A. Identification of a new class of biopolymer: Bacterial synthesis of a sulfur-containing polymer with thioester linkages. *Microbiology* **2006**; 147:11-19.

[4] Lehmann J, Carbohydrates: Structure and biology. Stuttgart: Thieme, **1998**.

[5] Biopolymers: Making materials natural way: US congress office of technology **1993**.

[6] Modern methods for theoretical physical chemistry of biopolymers. Elsevier Science & Technology Books, **2006**.

[7] Vishnyakov A, Laaksonen A, Widmalm G. Molecular dynamics simulations of α -D-Manp-(133)-ß-D-Glcp-OMe in methanol and in dimethyl sulfoxide solutions. *J Mol Graphics Modell* **2001**; 19:338-342.

[8] Montgomery R. Development of biobased products. *Bioresour Technol* **2004**; 91:1-29.

[9] Hofren J, Zou W, Cordova A. Heterogeneous 'organoclick' derivatization of polysaccharides. *Macromol Rapid Commum* **2006**; 27:1362-1366.

[10] Heinze T, Liebert T, Koschella A. Esterification of Polysaccharides. Heidelberg: Springer **2006**.

[11] Rinaudo M. Main properties and current applications of some polysaccharides as biomaterials. *Polym Int* **2008**; 57:397-430.

[12] Velde KVd, Kiekens P. Biopolymers: Overview of several properties and consequences on their applications. *Polym Test* **2002**; 21:433-442.

[13] Kjøniksen A-L, Beheshti N, Kotlar HK, Zhu K, Nyströma B. Modified polysaccharides for use in enhanced oil recovery applications. *Eur Polym J* **2008**; 44:959-967.

[14] Vaclavik VA, Christin EW, Essentials of Food Science 3rd ed. New York: Springer, **2008**.

[15] Vandamme EJ, DeBeats S, Steinbüchel A (editors). Biopolymers: Polysaccharides 1: Wiley-VCH, **2002**.

[16] Bösch A. *PhD thesis*, TU Braunschweig **2008**.

[17] De Belder AN. Dextran. Uppsala, Sweden: Amersham Biosciences **2003**.

[18] Ikai T, Okamoto Y. Structure control of polysaccharide derivatives for efficient separation of enantiomers by chromatography. *Chem Rev* **2009**; 109:6077-6101.

[19] Okamoto Y, Kawashima M, Hatada K. Useful chiral packing materials for high-performance liquid chromatographic resolution of enantiomers: Phenylcarbamates of polysaccharides coated on silica gel. *J Am Chem Soc* **1984**; 106:5357-5359.

[20] Okamoto Y, Noguchi J, Yashima E. Enantioseparation on 3,5-dichloro- and 3,5-dimethylphenylcarbamates of polysaccharides as chiral stationary phases for high-performance liquid chromatography. *React Func Polym* **1998**; 37:183-188.

[21] Seung-Hee S, Jonggeon J. Synthesis and characterization of the chiral stationary phase based on chitosan. *J Appl Polym Sci* **2007**; 106:2989-2996.

[22] Toga Y, Ichida A, Shibata T, Tachibana K, Namikoshi H. Chiral recognition ability of curdlan triacetate: Solvent and temperature effects. *Chirality* **2004**; 16:272-276.

[23] Kurauchi Y, Ono H, Wang B, Egashira N, Ohga K. Preparation of a β-cyclodextrin-modified *N*-carboxymethylchitosan and Its chromatographic behavior as a chiral HPLC stationary phase. *Anal Sci* **1997**; 13:47-52.

[24] Cass QB, Bassi AL, Matlin SA. Chiral discrimination by HPLC on aryl carbamate derivatives of chitin coated onto microporous aminopropyl silica. *Chirality* **1996**; 8:131-135.

[25] Ikai T, Okamoto Y. Structure control of polysaccharide derivatives for efficient separation of enantiomers by chromatography. *Chem Rev* **2009**; 109:6077-6101.

[26] Vollmer A, Voiges K, Bork C, Fiege K, Cuber K, Mischnick P. Comprehensive analysis of the substitution pattern in dextran ethers with respect to the reaction conditions. *Anal Bioanal Chem* **2009**; 395:1749-1768.

[27] Mischnick P, Momcilovic D. Chemical Structure Analysis of Starch and Cellulose Derivatives. *Adv Carbohyd Chem Biochem* **2010**; 64:117-210.

[28] Mischnick P, Heinrich J, Gohdes M, Wilke O, Rogmann N. Structure analysis of 1,4-glucan derivatives. *Macromol Chem Phys* **2000**; 201:1985-1995.

[29] Lee CK, Gray GR. Analysis of positions of substitution of *O*-acetyl groups in partially *O*-acetylated cellulose by the reductive-cleavage method. *Carbohydr Res* **1995**; 269:167-174.

[30] Mischnick P. Challenges in structure analysis of polysaccharide derivatives. *Cellulose* **2001**; 8:245-257.

[31] Mischnick P, Adden R. Fractionation of polysaccharide derivatives and subsequent analysis to differentiate heterogeneities on various hierarchical levels. *Macromol Symp* **2008**; 262:1-7.

[32] Biermann CJ, McGinnis GD (editors). Analysis of carbohydrates by GLC and MS. Boston: CRC, **1989**.

[33] Cheetham NWH, Sirimanne P. Methanolysis studies of carbohydrates, using H.P.L.C. *Carbohydr Res* **1983**; 112:1-10.

[34] Jentoft N. Analysis of sugars in glycoproteins by high-pressure liquid chromatography. *Anal Biochem* **1985**; 148:424-433.

[35] Sweeley CC, Bentley R, Makita M, Wells WW. Gas-liquid chromatography of trimethylsilyl derivatives of sugars and related substances. *J Am Chem Soc* **1963**; 85:2497-2507.

[36] Janauer GA, Englmaier P. Multi-step time program for the rapid gas-liquid chromatography of carbohydrates. *J Chromatogr A* **1978**; 153:539-542.

[37] Honda S, Yamauchi N, Kakehi K. Rapid gas chromatographic analysis of aldoses as their diethyl dithioacetal trimethylsilylates. *J Chromatogr A* **1979**; 169: 287-293.

[38] Honda S, Kakehi K, Okada K. Convenient method for the gas chromatographic analysis of hexosamines in the presence of neutral monosaccharides and uronic acids. *J Chromatogr A* **1979**; 176:367-373.

[39] Pelletier O, Cadieux S. Glass capillary or fused-silica gas chromatography-mass spectrometry of several monosaccharides and related sugars: Improved resolution. *J Chromatogr B* **1982**; 231:225-235.

[40] Albersheim P, Nevins DJ, English PD, Karr A. A method for the analysis of sugars in plant cell-wall polysaccharides by gas-liquid chromatography. *Carbohydr Res* **1967**; 5:340-345.

[41] Whiton RS, Lau P, Morgan SL, Gilbart J, Fox A. Modifications in the alditol acetate method for analysis of muramic acid and other neutral and amino sugars by capillary gas chromatography-mass spectrometry with selected ion monitoring. *J Chromatogr A* **1985**; 347:109-120.

[42] Sweet DP, Shapiro RH, Albersheim P. Quantitative analysis by various g.l.c. response-factor theories for partially methylated and partially ethylated alditol acetates. *Carbohydr Res* **1975**; 40:217-225.

[43] Addison RF, Ackman RG. Flame ionization detector molar responses for methyl esters of some polyfunctional metabolic acids. *J Gas Chromatogr* **1968**; 6: 135-138.

[44] Mischnick P, Kühn G. Model studies on methyl amyloses: Correlation between reaction conditions and primary structure. *Carbohydr Res* **1996**; 290:199-207.

[45] Manelius R, Buléon A, Nurmi K, Bertoft E. The substitution pattern in cationised and oxidised potato starch granules. *Carbohydr Res* **2000**; 329:621-633.

[46] Mischnick P, Hennig C. A new model for the substitution patterns in the polymer chain of polysaccharide derivatives. *Biomacromol* **2000**; 2:180-184.

[47] Kern H, Choi S, Wenz G, Heinrich J, Ehrhardt L, Mischnick P, Garidel P, Blume A. Synthesis, control of substitution pattern and phase transitions of 2,3-di-*O*-methylcellulose. *Carbohydr Res* **2000**; 326:67-79.

[48] Spurlin HM. Arrangement of substituents in cellulose derivatives. *J Am Chem Soc* **1939**; 61:2222-2227.

[49] Adden A. Substitution pattern in and over polymer chains -new approaches in carboxymethyl cellulose. *PhD thesis*, TU Braunschweig **2009**.

[50] Reuben J. Analysis of the 13C-n.m.r. spectra of hydrolyzed and methanolyzed *O*-methylcelluloses: Monomer compositions and models for their description. *Carbohydr Res* **1986**; 157:201-213.

[51] Reuben J, Casti TE. Distribution of substituents in *O*-(2-hydroxyethyl)cellulose: A 13C-N.M.R. approach. *Carbohydr Res* **1987**; 163:91-98.

[52] Heinze T, Liebert T, Heublein B, Hornig S. Functional polymers based on Dextran. *Adv Polym Sci* **2006**; 205:199-291.

[53] Abir F, Barkhordarian S, Sumpio BE. Efficiency of dextran solutions in vascular surgery. *Vasc Endovascular Surg* **2004**; 38:483-491.

[54] Catiker E, Güner A. Unperturbed molecular dimentions and the theta temperature of dextran in dimethylsulfoxide (DMSO) solutions. *Polym Bull* **1998**; 41:223-230.

[55] Jeanes A, Haynes WC, Wilham CA, Rankin CA, Melvin EH, Austin MJ, Cluskey JE, Fisher BE, Tsuchiya HM, Rest CE. Characterization and classification of dextrans form ninety-six strains of bacteria. *J Am Chem Soc* **1954**; 76:5041-5052.

[56] Collins PM (editor). Dictionary of carbohydrates, 2nd ed. New York: Chapman & Hall/CRC **2006**.

[57] Taylor C, Cheetham NWH, Walker GJ. Application of higher-performance liquid chromatography to a study of branching in dextrans. *Carbohydr Res* **1985**; 137: 1-12.

[58] vanTieghem P. *Ann Sci Nature Bot Biol Veg* **1878**; 7:180.
[59] Pasteur L. *Bull Soc Chim Paris* **1861**; 30.
[60] Beijerinck MWK. Akad Wetensch, *Amsterdam Proc sect Sc* **1910**; 12:635.
[61] Neill JM, Here EJ, Sugg JY, Jaffe E. Serological studies on sugar. *J Exp Med* **1939**; 70:427-442.
[62] Hehre EJ. Production from sucrose of a serologically reactive polysaccharide by a sterile bacterial extract. *Science* **1941**; 93:237-238.
[63] Wales M, Marshall PA, Weissberg SG. Intrinsic viscosity-molecular weight relationships for dextran. *J Polym Sci* **1953**; 10:229-240.
[64] Senti FR, Hellman NN, Ludwig NH, Babcock GE, Tobin R, Glass CA, Lamberts BL. Viscosity, sedimentation, and light-scattering properties of fractions of acid-hydrolyzed dextran. *J Polym Sci* **1955**; 17:527-546.
[65] Ebert KH, Brosche M. Origin of branches in native dextrans. *Biopolym* **1967**; 4:423-430.
[66] Robyt JF, Taniguchi H. The mechanism of dextransucrase action : Biosynthesis of branch linkages by acceptor reactions with dextran. *Arch Biochem Biophys* **1976**; 174:129-135.
[67] Rankin JC, Jeanes A. Evaluation of the periodate oxidation method for structural analysis of dextrans. *J Am Chem Soc* **1954**; 76:4435-4441.
[68] Dimler RJ, Wolff IA, Sloan JW, Rist CE. Interpretation of periodate oxidation data on degreded dextran. *J Am Chem Soc* **1955**; 77:6568-6573.
[69] Cleve JWV, Schaefer WC, Rist CE. The structure of NRRL B-512 dextran. Methylation studies. *J Am Chem Soc* **1956**; 78:4435-4438.
[70] Lindberg B, Svensson S. Structural studies on dextran from *Leuconostoc mesenteroides* NRRL B-512. *Acta Chem Scand* **1968**; 22:1907-1912.
[71] Capon B. Mechanism in carbohydrate chemistry. *Chem Rev* **1969**; 69:407-498.
[72] Bremner I, Cox JSG, Moss GF. Structural studies on iron-dextran: Characterization of an alkali-degreded dextran suitable for use in the production of parenteral iron-dextran complexes. *Carbohydr Res* **1969**; 11:77-84.
[73] Larm O, Lindberg B, Svensson S. Studies on the length of the side chains of the dextran eleborated by *Leuconostoc mesenteroides* NRRL B-512. *Carbohydr Res* **1971**; 20:39-48.
[74] Kuge T, Kobayashi K, Kitamura S, Tanahashi H. Degrees of long-chain branching in dextrans. *Carbohydr Res* **1987**; 160:205-214.
[75] Robyt JF, Kimble BK, Walseth TF. The mechanism of dextransucrase action: Direction of dextran biosynthesis. *Arch Biochem Biophys* **1974**; 165:634-640.
[76] van Dijk-Wolthuis WNE, Kettenes-van den Bosch JJ, van der Kerk-van Hoof A, Hennink WE. Reaction of dextran with glycidyl methacrylate: An unexpected transesterification. *Macromol* **1997**; 30:3411-3413.
[77] Cheetham NWH, Fiala-Beer E. Dextran structural details from high-field proton NMR spectroscopy. *Carbohydr Polym* **1991**; 14:149-158.
[78] Gottlieb HE, Kotlyar V, Nudelman A. NMR chemical shifts of common laboratory solvents as trace impurities. *J Org Chem* **1997**; 62:7512-7515.
[79] Suzuki N, Wada A. Study of dextran solutions by quasielastic light-scattering. *Carbohydr Res* **1982**; 109:249-258.

[80] Rolland-Sabaté A, Mendez-Montealvo MG, Colonna P, Planchot V. Online determination of structural properties and observation of deviations from power law behavior. *Biomacromol* **2008**; 9:1719-1730.

[81] Norrman B. Partial methylation of dextran. *Acta Chem Scand* **1968**; 22: 1381-1385.

[82] Croon I. Partial methylation of some glucose derivatives. *Acta Chem Scand* **1959**; 13:1235-1238.

[83] De-Belder AN, Lindberg B, Theander O. Partial methylation studies on methyl β-D-glucopyranoside and some derivatives. *Acta Chem Scand* **1962**; 16:2005-2009.

[84] Garegg PJ. Partial methylation of benzyl 4-*O*-methyl-β-D-xylopyranoside. *Acta Chem Scand* **1963**; 17:1343-1347.

[85] Zhang J, Pelton R, Wagberg L. Aqueous biphase formation by mixtures of dextran and hydrophobically modified dextran. *Colloid Polym Sci* **1998**; 276: 476-482.

[86] Kim S-H, Won C-Y, Chu C-C. Synthesis and characterization of dextran-maleic acid based hydrogels. *Biomed Mater Res* **1999**; 46:160-170.

[87] Norrman B. Partial methylation studies on pustulan, methyl α- and β-D-glucopyranoside and some derivatives. *Acta Chem Scand* **1968**; 22:1623-1627.

[88] Hall LD, Preston CM. A general survey of the proton spin-lattice relaxation-times of some oligo- and poly-saccharide derivatives. *Carbohydr Res* **1976**; 49:3-11.

[89] Gagnaire D, Vignon M. Carbon-13 NMR and proton NMR of dextran and its acetylated and benzylated derivatives. *Macromol Chem* **1977**; 178:2321-2333.

[90] Rees DA, Richardson NG, Wight NJ, Hirst SE. Characterisation of polysaccharide structures by glycoside stabilisation with toluene-p-sulphonates: model experiments with dextran. *Carbohydr Res* **1969**; 9:451-462.

[91] Harkness BR, Gray DG. Preparation and chiroptical properties of tritylated cellulose derivatives. *Macromol* **1990**; 23:1452-1457.

[92] Ydens I, Rutot D, Degee P, Six J-L, Dellacherie E, Dubois P. Controlled synthesis of poly(ε-caprolactone)-grafted dextran copolymers as potential environmentally friendly surfactants. *Macromol* **2000**; 33:6713-6721.

[93] Nouvel C, Dubois P, Dellacherie E, Six J-L. Silylation reaction of dextran: Effect of experimental conditions on silylation yield, regioselectivity, and chemical stability of silylated dextrans. *Biomacromol* **2003**; 4:1443-1450.

[94] Huynh R, Chaubet F, Jozefonvicz J. Carboxymethylation of dextran in aqueous alcohol as the first step of the preparation of derivatized dextrans. *Angew Makromol Chem* **1998**; 254:61-65.

[95] Maiga-Revel O, Chaubet F, Jozefonvicz J. New investigations on heparin-like derivatized dextrans: CMDBS, synergistic role of benzylamide and sulfate substituents in anticoagulant activity. *Carbohydr Polym* **1997**; 32:89-93.

[96] Bonnet J, Choe TB, Lee CH, Masse P, Verdier A. Selective elimination of Mercury using chemically modified biopolymers. In: L. Pawlowski GA, Lacy WJ (editors). Studies Environ Sci: Elsevier, **1986**: 421-435.

[97] Rogovin ZA, Vernik AD, Khomiakov KP, Laletina OP, Penenzhik MA. Study of the synthesis of dextran derivtives. *Macromol Sci A Chem* **1972**; 6:569 - 593.

[98] De Belder AN, Norrman B. The substitution patterns of *O*-(2-hydroxyethyl)starch and *O*-(2-hydroxyethyl)dextran. *Carbohydr Res* **1969**; 10:391-394.

[99] Kesler C, Hjermstad ET. Hydroxyethyl and hyroxypropyl starch. *Methods Carbohydr Chem* **1964**; 4:304-306.

[100] Rotureau E, Dellacherie E, Durand A. Concentration dependence of aqueous solution viscosities of amphiphilic polymers. *Macromol* **2005**; 38:4940-4941.

[101] Rotureau E, Chassenieux C, Dellacherie E, Durand A. Neutral polymeric surfactants derived from dextran: A study of their aqueous solution behavior. *Macromol Chem Phys* **2005**; 206:2038-2046.

[102] Durand A, Marie E, Rotureau E, Leonard M, Dellacherie E. Amphiphilic polysaccharides: Useful tools for the preparation of nanoparticles with controlled surface characteristics. *Langmuir* **2004**; 20:6956-6963.

[103] Imbert P, Sadtler VM, Dellacherie E. Phenoxy-substituted dextrans as emulsifying agent: Role of the substitution ratio on O/W emulsion stability and interfacial activity. *Colloids Surf A: Physicochem Eng Aspect* **2002**; 211: 157-164.

[104] Rogovin ZA, Vernik AD, Khomiakov KP, Laletina OP, Penenzhik MA. Study of the synthesis of dextran derivatives. *J Macromol Sci Chem* **1972**; 6:569 - 593.

[105] Mora M, Pato J. Synthesis and hydrolytic behaviour of dextran-bound anticancer agents. *Macromol Chem* **1990**; 191:1051-1056.

[106] Kubota N, Kikuchi Y. Preparation and properties of macromolecular complexes consisting of [2-(diethylamino)ethyl] dextran hydrochloride and potassium metaphosphate. *Appl Polym Sci* **1993**; 47:815-821.

[107] Hanselmann R, Burchard W. Characterization of DAEA-dextran by means of light scattering and combined size exclusion chromatography/low angle laser light scattering/viscometery. *Macromol Chem Phys* **1995**; 196:2259-2275.

[108] Grzeorz U, Maria C. Study of combinations of some dextran derivatives with salicylic acid. *Farmacja Polska* **1980**; 36:471-474.

[109] Bai G, Santos LMNBF, Nichifor M, Lopes A, Bastos M. Thermodynamics of the interaction between a hydrophobically modified polyelectrolyte and sodium dodecyl sulfate in aqueous solution. *J Phys ChemB* **2004**; 108:405-413.

[110] Bai G, Nichifor M, Lopes A, Bastos M. Thermodynamic characterization of the interaction behavior of a hydrophobically modified polyelectrolyte and oppositely charged surfactants in aqueous solution: Effect of surfactant alkyl chain length. *J Phys Chem B* **2004**; 109:518-525.

[111] Bai G, Nichifor M, Lopes A, Bastos M. Thermodynamics of self-assembling of hydrophobically modified cationic polysaccharides and their mixtures with oppositely charged surfactants in aqueous solution. *J Phys Chem B* **2005**; 109:21681-21689.

[112] Ghimici L, Nichifor M. Electrical conductivity of some cationic polysaccharides. I. Effects of polyelectrolyte concentration, charge density, substituent at the ionic group, and solvent polarity. *J polym Sci B Polym Phys* **2005**; 43:3584-3590.

[113] Francis MF, Lavoie L, Winnik FM, Leroux J-C. Solubilization of cyclosporin A in dextran-g-polyethyleneglycolalkyl ether polymeric micelles. *Eur J Pharm Biopharm* **2003**; 56:337-346.

[114] Virnik AD, Khomyakov KP, Skokova IF. Dextran and its derivatives. *Russ Chem Rev* **1975**; 44:588-602.

[115] Dijik-Wolthuis WNEV, Tsang SKY, Bosch JJK-vd, Hennink WE. A new class of polymerizable dextrans with hydrolyzable groups: Hydroxyethyl methacrylated dextran with and without oligolactate spacer. *Polymer* **1997**; 38:6235-6242.

[116] Dijk-Wolthuis WNEV, Steenbergen MJV, Underberg WJM, Hennink WE. Degredation kinetics of methycrylated dextrans in aqueous solution. *J PharmaceutSci* **1997**; 86:413-417.

[117] Denizli BK, Can HK, Rzaev ZMO, Guner A. Preparation conditions and swelling equilibria of dextran hydrogels prepared by some crosslinking agents. *Polymer* **2004**; 45:6431-6435.

[118] Hovgaard L, Brondsted H. Dextran hydrogels for colon-specific drug delivery. *J Controlled Release* **1995**; 36:159-166.

[119] Kim SH, Won CY, Chu CC. Synthesis and characterization of dextran-based hydrogels prepared by photocrosslinking. *Carbohydr Polym* **1999**; 40:183-190.

[120] Odavic R, Blom J, Beck EA, Bucher U. Cryoprotection of human bone marrow committed stem cells (CFU-c) by dextran, glycerol and dimethyl sulfoxide. *Experientia* **1980**; 36:1122-1124.

[121] Ashwood-Smith MJ, Warby C, Connor KW, Becker G. Low-temperature preservation of mammalian cells in tissue culture with polyvinylpyrolidone (PVP), dextrans, and hydroxyethyl strache (HES). *Cryobiol* **1972**; 9:441-449.

[122] Azzam T, Raskin A, Makovitzki A, Brem H, Vierling P, Lineal M, Domb AJ. Cationic polysaccharides for gene delivery. *Macromol* **2002**; 35:9947-9953.

[123] Mann JS, Hang JC, Keana JF. Molecular amplifiers: Synthesis and functionalization of a poly(aminopropyl)dextran bearing a uniquely reactive terminuus for univalent attachment to biomolecules. *Bioconjugate Chem* **1992**; 3:154-159.

[124] Rotureau E, Leonard M, Dellacherie E, Durand A. Amphiphilic derivatives of dextran: Adsorption at air/water and oil/water interfaces. *J Coli Interface Sci* **2004**; 279:68-77.

[125] Aumelas A, Serrero A, Durand A, Dellacherie E, Leonard M. Nanoparticles of hydrophobically modified dextrans as potential drug carrier systems. *Coll Surf B*: *Biointerfaces* **2007**; 59:74-80.

[126] Hornig S, Liebert T, Heinze T. Structure design of multifunctional furate and pyroglutamate esters of dextran by polymer-analogous reactions. *Macromol Biosci* **2007**; 7:297-306.

[127] Liebert T, Hornig S, Hesse S, Heinze T. Nanoparticles on the basis of highly functionalized dextrans. *J Am Chem Soc* **2005**; 127:10484-10485.

[128] Hornig S, Heinze T, Hesse S, Liebert T. Novel nano particles based on dextran esters with unsaturated moieties. *Macromol Rapid Commum* **2005**; 26:1908-1912.

[129] Hornig S, Heinze T. Nanoscale structures of dextran esters. *Carbohydr Polym* **2007**; 68:280-286.

[130] Stenekes RJH, Talsma H, Hennink WE. Formation of dextran hydrogels by crystallization. *Biomaterials* **2001**; 22:1891-1898.

[131] Haff LA, Easterday RL. Sephacryl gels: Physical properties and evaluation of performance in gel filteration. *J Liq Chromatogr* **1978**; 1:811-832.

[132] Ciucanu I, Kerek F. A simple and rapid method for the permethylation of carbohydrates. *Carbohydr Res* **1984**; 131:209-217.

[133] Purdie T, Irvine JC. C-The alkylation of sugars. *J Chem Soc* **1903**; 83:1021-1037.
[134] Whistler RL, Wolform ML. Methods in Carbohydrate Chemistry. New York: Academic Press, **1963**.
[135] Hodge EJ, Karjala SA, Hilbert GE. Methylation and ethylation of corn starch, amylose and amylopectin in liquid ammonia. *J Am Chem Soc* **1951**; 73: 3312-3316.
[136] Hakomori SI. Rapid permethylation of glycolipids and polysaccharides, catalyzed by methylsulfinyl in dimethylsulfoxide. *J Biochem (Tokyo)* **1964**; 55:205-208.
[137] Petrus L, Gray DG, BeMiller JN. Homogenious alkylation of cellulose in lithium chloride/dimethyl sulfoxide solvent with dimsyl sodium activation. A proposal for the mechenism of cellulose dissolution in lithium chloride/DMSO. *Carbohyd Res* **1995**; 268:319-323.
[138] Kvernheim AL. Methylation analysis of polysaccharides with butyllithium in dimethylsulfoxide. *Acta Chem Scand Ser B* **1987**; B41:150-152.
[139] Isogai A, Ishizu A, Nakano J. A new facile methylation method for cell-wall polysaccharides. *Carbohydr Res* **1985**; 138:99-108.
[140] Ciucanu I. Per-*O*-methylation reaction for structural analysis of carbohydrates by mass spectrometry. *Anal Chim Acta* **2006**; 576:147-155.
[141] Falconer EL, Adams GA. The aldobiouronic acids of hemicellulose B of oat hulls. *Cand J Chem* **1956**; 34:338-344.
[142] Ciucanu I, Kerek F. A simple and rapid method for the permethylation of carbohydrates. *Carbohyd Res* **1984**; 131:209-217.
[143] Ciucanu I, kerek F. Proceedings of the international conference on chemistry and biotechnology of natural products. Budapest, Hungary. **1983**.
[144] Lemal DM, Pacht PD, Woodward RB. The synthesis of L-(-)-mycarose and L-(-)-cladinose. *Tetrahedron* **1962**; 18:1275-1293.
[145] Bromberg L. Salt-mediated miscibility of proteins and polymers. *J Phy Chem* **1994**; 98:10628-10633.
[146] Isogai A, Ishizu A, Nakano J. Preparation of tri-*O*-substituted cellulose ethers by the use of a nanoaqueous cellulose solvent.*J Appl Polym Sci* **1984**; 29: 3873-3882.
[147] Brimacombe JS, Jones BD, Stacey M, Willard JJ. Alkylation of carbohydrates by using sodium hydride. *Carbohydr Res* **1966**; 2:167-169.
[148] Blakeney AB, Stone BA. Methylation of carbohydrates with lithium methylsulfinyl carbanion. *Carbohydr Res* **1985**; 140:319-324.
[149] Parente JP, Cardon P, Leroy Y, Montreuil J, Fournet B, Ricart G. A convenient method for methylation of glycoprotein glycans in small amounts by using lithium methylsulfinyl carbanion. *Carbohydr Res* **1985**; 141:41-47.
[150] Tankam PF, Mischnick P, Hopf H, Jones PG. Modification of methyl *O*-propargyl-D-glucosides: Model studies for the synthesis of alkynyl based functional polysaccharides. *Carbohydr Res* **2007;** 342:2031-2048.
[151] Tankam PF, Müller R, Mischnick P, Hopf H. Alkynyl polysaccharides: Synthesis of propargyl potato starch followed by subsequent derivatization. *Carbohydr Res* **2007**; 342:2049-2060.

[152] Belghiti T, Joly J-P, Didierjean C, Dahaoui S, Chapleura Y. Synthesis of strained glycophanes from D-glucal by oxidative homocoupling of propargyl ethers. *Tetrahedron Lett* **2002**; 43:1441-1443.

[153] Aversa MC, Barattucci A, Bilardo MC, Bonaccorsi P, Giannetto P, Rollin P, Tatibouet A.Sulfenic acids in the carbohydrate field. An example of straightforward access to novel multivalent thiosaccharides. *J org Chem* **2005**; 70:7389-7396.

[154] Bernett B, Vasella A. Acetylenosaccharides in Acetylene Chemistry. Chemistry, Biology and Material Science, Diederich F, Stang PJ, Tykwinski RR (editors). Weinhein: Wiley-VCH, **2005**.

[155] Alzeer J, Cai C, Vasella A.Oligosaccharide analogues of polysaccharides: Part 1: Concept and synthesis of monosaccharide-derived monomers. *Helv Chim Acta* **1995**; 78:242-264.

[156] Murty KVSN, Xie T, Bernet B, Vasella A. Oligosaccharide analogues of polysaccharides: Part 26: Mimics of cellulose I and cellulose II: Di- and monoalkynyl C-cellosides of 1,8-disubstituted anthraquinones. *Helv Chim Acta* **2006**; 89:675-730.

[157] Hoffmann B, Bernet B, Vasella A. Oligosaccharide analogues of polysaccharides Part 24: Synthesis of cyclodextrin analogues containing substituted buta-1,3-diyne or a 1,2,3-triazole unit and analysis of intramolecular hydrogen bonds. *Helv Chim Acta* **2002**; 85:265-287.

[158] Masaidova GS, Yakunina AS, Gal´braik LS, rogovin ZA. Structure and properties of cellulose and its derivatives. CXCVI. Synthesis of cellulose ethers containing C-C triple bonds. *Vysokomolekulyarnye Soedineniya* **1966**; 8:865-869.

[159] Bhatt IG, Lyer V, Sundaram V. Synthesis of propargyl cellulose. *Ind J Text Res* **1981**; 6:43-44.

[160] Avny Y, Rahman R, Zilkha A. Some complexation reactions of cellulosic ethers. *J Macromol Sci Chem* **1972**; 6:1427-1434.

[161] Rashidova SS, Valie AK. Aminomethylation of cellulose propargyl ether. *Uzbekskii Khimicheskii Zhurnal* **1977**; 5:44-47.

[162] Gal'braikh LS, Masaidova GS, Rogovin ZA. Synthesis of new cellulose derivatives with acetylenic links, and their chemical transformations. *Cellulose Chem Technol* **1969**; 3:455-467.

[163] Tomoe CW, Meldal M. Peptidotriazoles: Copper (1) - catalyzed 1,3-dipolar cycloadditions on solid phase. In Peptides: The wave of the future: Proceedings of the 2nd international and the 17th American peptide symposium: Label M, HoughtenRA (Editors).San Diago: Americam peptide society and Kluwer Academic Publishers, **2001**.

[164] Tornoe CW, Christensen C, Meldal M. Peptidotriazoles on solid phase: [1,2,3]-Triazoles by regiospecific Copper(I)-catalyzed 1,3-dipolar cycloadditions of terminal alkynes to azides. *J org Chem* **2002**; 67:3057-3064.

[165] Vsevolod VR, Luke GG, Valery VF, Sharpless KB. A stepwise Huisgen cycloaddition process: Copper(1)-catalyzed regioselective "ligation" of azides and terminal alkynes. *Angew Chem Int Ed* **2002**; 41:2596-2599.

[166] Huisgen R. Cycloaddition - defination, classification, and characterization. *Angew Chem Int Ed* **1968**; 7:321-406.

[167] Huisgen R, Szeimies G, Mobius L. 1,3-Dipolare Cycloadditionen, XXXII. Kinetik der additionen organischer azide an CC-Mehrfachbindugren. *Chem Ber* **1967**; 100:2494-2507.

[168] Zhang L, Chen X, Xue P, Sun HHY, Williams ID, Sharpless KB, Fokin VV, Jia G. Ruthenium-catalyzed cycloaddition of alkynes and organic azides. *J Am Chem Soc***2005**; 127:15998-15999.

[169] Christopher B-K, Andrew JI. Has *click chemistry* lead to a paradigm shift in polymer material design? *Macromol Chem Phys* **2009**; 210:987-992.

[170] Lodge TP. A Virtual Issue of Macromolecules: "Click chemistry in macromolecular science". *Macromol* **2009**; 42:3827-3829.

[171] Sumerlin BS, Vogt AP. Macromolecular engineering through click chemistry and other efficient transformations. *Macromol* **2010**; 43:1-13.

[172] van Dijk M, Rijkers DTS, Liskamp RMJ, van Nostrum CF, Hennink WE. Synthesis and applications of biomedical and pharmaceutical polymers via click chemistry methodologies. *Bioconjugate Chem* **2009**; 20:2001-2016.

[173] Jin T, Kamijo S, Yamamoto Y. Copper-catalyzed synthesis of *N*-unsubstituted 1,2,3-triazoles from nonactivated terminal alkynes. *Eur J Org Chem* **2004**; 2004:3789-3791.

[174] Pahimanolis N, Vesterinen A-H, Rich J, Seppala J. Modification of dextran using click-chemistry approach in aqueous media. *Carbohydr Polym* **2010**; 82:78-82.

[175] Yeoh KK, Butters TD, Wilkinson BL, Fairbanks AJ. Probing replacement of pyrophosphate via click chemistry; synthesis of UDP-sugar analogues as potential glycosyl transferase inhibitors. *Carbohyd Res* **2009**; 344:586-591.

[176] Srinivasachari S, Liu Y, Zhang G, Prevette L, Reineke TM. Trehalose click polymers inhibit nanoparticle aggregation and promote pDNA delivery in serum. *J Am Chem Soc* **2006**; 128:8176-8184.

[177] Srinivasachari S, Liu Y, Prevette LE, Reineke TM. Effects of trehalose click polymer length on pDNA complex stability and delivery efficacy. *Biomaterials* **2007**; 28:2885-2898.

[178] Horne WS, Yadav MK, Stout CD, Ghadiri MR. Heterocyclic peptide backbone modifications in an α-helical coiled coil. *J Am Chem Soc* **2004**; 126: 15366-15367.

[179] Angelo NG, Arora PS. Nonpeptidic foldamers from amino acids: Synthesis and characterization of 1,3-substituted triazole oligomers. *J Am Chem Soc* **2005**; 127:17134-17135.

[180] Opsteen JA, van Hest JCM. Modular synthesis of block copolymers via cycloaddition of terminal azide and alkyne functionalized polymers. *Chem Commun* **2005**; 1:57-59.

[181] John AFJ, Niels THT, Fatna Ait El M, Arwin JB, Esse GW, Dirk TSR, Rob MJL, Roland JP.High-yielding microwave-assisted synthesis of triazole-linked glycodendrimers by copper-catalyzed [3+2] cycloaddition. *Eur J Org Chem* **2005**; 2005:3182-3185.

[182] Xia Y. Nanomaterials at work in biomedical research. *Nat Mater* **2008**; 7: 758-760.

[183] Such GK, Quinn JF, Quinn A, Tjipto E, Caruso F. Assembly of ultrathin polymer multilayer films by click chemistry. *J Am Chem Soc* **2006**; 128:9318-9319.

[184] Such GK, Tjipto E, Postma A, Johnston APR, Caruso F. Ultrathin, responsive polymer click capsules. *Nano Lett* **2007**; 7:1706-1710.
[185] Tahir MN. Alkynyl ethers of dextrans as intermediates for new functional biopolymers. *Master Thesis,* Technissche Universität Braunschweig, Germany **2007**.
[186] Sharma YR. Elementary organic spectroscopy. New Delhi: S. Chand & Company Ltd., **2000**.
[187] Siskos MG, Kyriakakou G, Zarkadis AK. The polymerization of propargyl halides (CI, Br) using $M(CO)_5PPh3/RxAICl_{3-x}$ (M=Mo,W) as catalysts.*Polym Bull* **1994**; 33:295-300.
[188] Klusener PAA, Hommes H, Hanekamp JC, Kerk ACHTMVd, Brandsma L. Butyllithium-induced dimerization of pent-3-en-1-yne and related additions. *J Organomet Chem* **1991**; 409:67-81.
[189] Kunzler J, Perces V. The polymerization of 3-chloro-1-propyne and 3-bromo-1-propyne with $MoCl_3$ and WCl_6 based initiators and the structure of the resulting polymers. *J Polym Sci, Part A: Polym Chem* **1990**; 28:1043-1057.
[190] Kabanov VA, Aliev KV, Richmond J. The polymerization of propargyl chloride activated by interaction with poly(4-vinylpyridine). *J Maromol Sci Part A* **1975**; 9:273-283.
[191] Gal Y-S, Lee W-C, Choi S-K. A water-soluble pyridine-containing polyacetylene: Poly(2-ethynylpyridine bromide) having propargyl side chains. *Bull Korean Chem Soc* **1997**; 18:265-266.
[192] Balcar H, Kalisz T, Sedlácek J, Blechta V, Matejka P. Polymerization of nitrophenyl propargyl ethers with transition metal catalysts and characterization of polymers. *Polymer* **1998**; 39:4443-4447.
[193] Tahir MN, Bork C, Risberg A, Horst JC, KomoßC, Vollmer A, Mischnick P. Alkynyl ethers of glucans: Substituent distribution in propagyl-, pentynyl- and hexynyldextrans and -amyloses and support for silver nanoparticle formation. *MacromolChem Phys* **2010**; 211:1648-1662.
[194] Barlow SJ, Bondarenko GV, Gorbaty YE, Yamaguchi T, Poliakoff M. An IR study of hydrogen bonding in liquid and supercritical alcohols. *J PhyChemA* **2002**; 106:10452-10460.
[195] Sokolova M, Barlow SJ, Bondarenko GV, Gorbaty YE, Poliakoff M. Comparison between IR absorption and Raman scattering spectra of liquid and supercritical 1-Butanol. *JPhyChemA* **2006**; 110:3882-3885.
[196] Horner S. *PhD thesis*, University of Hamburg. **1999**.
[197] Montando G, Lattimer RP, editors, Mass spectrometry of polymers. London: CRC Press, **2002**.
[198] Cech NB, Enke CG. Practical implications of some recent studies in electrospray ionization fundamentals. *Mass Spectrom Rev* **2001**; 20:362-387.
[199] Adden R, Mischnick P. A novel method for the analysis of the substitution pattern of *O*-methyl-[alpha]- and [beta]-1,4-glucans by means of electrospray ionisation-mass spectrometry/collision induced dissociation. *Int J Mass Spectrom* **2005**; 242:63-73.
[200] Tüting W, Adden R, Mischnick P. Fragmentation pattern of regioselectively *O*-methylated maltooligosaccharides in electrospray ionisation-mass

spectrometry/collision induced dissociation. *Int J Mass Spectrom* **2004**; 232: 107-115.

[201] Kochetkov NK, Chizhov OS. Mass spectrometry of methylated methyl glycosides : Principles and analytical application. *Tetrahedron* **1965**; 21:2029-2047.

[202] Chen M-L, Xu X-F, Cao Z-X, Wang Q-M. Ligand- and anion-controlled formation of silver alkynyl oligomers from soluble precursors. *Inorg Chem* **2008**; 47:1877-1879.

[203] Abu-Salah OM, Ja'far MH, Al-Ohaly AR, Al-Farhan KA, Al-Enzi HS, Dolomanov OV, Howard JAK. Synthesis and structural characterization of a halide-free rhombohedral Silver-alkynyl cage complex $[Ag_{14}(C_2tBu)_{12}][BF_4]_2$. *Eur J Inorg Chem* **2006**; 2006:2353-2356.

[204] Zhang L, Eisenberg A. Multiple morphologies of "crew-cut" aggregates of polystyrene-b-poly(acrylic acid) block copolymers. *Science* **1995**; 268: 1728-1731.

[205] Begtrup M, Hansen K, Pedersen C. Studies on methylated 1,2,3-triazoles. *Acta Chem Scand* **1967**; 21:1234-1238.

[206] Geest BGD, Camp WV, Prez FED, Smedt SCD, Demeester J, Hennink WE. Biodegradable microcapsules designed via 'click' chemistry. *Chem Commun* **2008**:190-192.

[207] Butler JE, Ni L, Nessler R, Joshi KS, Suter M, Rosenberg B, Chang J, Brown WR, Cantarero LA. The physical and functional behavior of capture antibodies adsorbed on polystyrene. *J Immunol Meth* **1992**; 150:77-90.

[208] Green NM. Avidin. *Adv Protein Chem* **1975**; 29:85-133.

[209] http://en.wikipedia.org/wiki/Streptavidin, 26.07. **2010**.

[210] Weber P, Ohlendorf D, Wendoloski J, Salemme F. Structural origins of high-affinity biotin binding to streptavidin. *Science* **1989**; 243:85-88.

[211] Hendrickson WA, Pähler A, Smith JL, Satow Y, Merritt EA, Phizackerley RP. Crystal structure of core streptavidin determined from multiwavelength anomalous diffraction of synchrotron radiation. *PNAS* **1989**; 86:2190-2194.

[212] Mathe G, Albersdörfer A, Neumaier KR, Sackmann E. Disjoining pressure and swelling dynamics of thin adsorbed polymer films under controlled hydration conditions. *Langmuir* **1999**; 15:8726-8735.

[213] Scouten WH, Konecny P. Reversible immobilization of antibodies on magnetic beads. *Anal Biochem* **1992**; 205:313-318.

[214] Blanco RM, Terreros P, Munoz N, Serra E. Ethanol improves immobilization on a hydrophobic support. *J Mol Catal B: Enzym* **2007**; 47:13-20.

[215] Bhushan I, Parsad R, Qazi GN, Ingavle G, Rajan CR, Ponrathram S, Gupta VK. Lipase enzyme immobilization on synthetic macroporous copolymers for kinetic resolution of chiral drugs intermediates. *Process Biochem* **2008**; 43:321-330.

[216] Kobayashi J, Mori Y, Kobayashi S. Novel immobilization method of enzymes using a hydrophilic polymer support. *Chem Commun* **2006**:4227-4229.

[217] Brigida AIS, Pinheiro ADT, Ferreira ALO, Pinto GAS, Goncalves LRB. Immobilization of *Candida antartica* lipase B by covalent attachment to green coconut fiber. *Appl Biochem Biotechnol* **2007**; 136-140:67-80.

[218] Fernandez-Lorente G, Cabrera Z, Godoy C, Fernandez-Lafuente R, Palomo JM, Guisan JM. Interfacially activated lipases against hydrophobic supports: Effect of the support on the biocatalytic propeties. *Process Biochem* **2008**; 43:1061-1067.

[219] Awang R, Ghazuli MR, Basri M. Immobilization of lipase from *Candida rugosa* on palm-based polyurethane foam as a support material. *Am J Biochem Biotechnol* **2007**; 3:163-166.

[220] Chang SW, Shaw JF, Yang KH, Chang SF, Shieh CJ. Studies of optimum conditions for covalent immobilization of *Candida rugosa* lipase on poly(γ-glutamic acid) by RSM. *Bioresour Technol* **2008**; 99:2800-2805.

[221] Vaidya A, Gera G, Ramakrishna S. Evaluation and optimization of immobilized lipase for esterification of fatty acid and monohydric alcohol. *W J Microbial Biotechnol* **2008**; 24:2987-2995.

[222] Alloue WAM, Destain J, Medjoub TE, Ghalfi H, Kabran P, Thonart P. Comparison of *Yarrowia lipolytica* lipase immobolization yield of entrapment, adsorption and covalent bond techniques. *Appl Biochem Biotechnol* **2008**; 150:51-63.

[223] Rao N, Shanmugam V. Lipase-mediated synthesis of dodecyl oleate and oleyl oleate in aqueous foams. *J Am Oil Chem Soc* **2000**; 77:605-608.

[224] Jonzo MD, Hiol A, Druet D, Comeau LC. Application of immobilized lipase from *Candida rugosa* to synthesis of Cholesterol oleate. *J Chem Technol Biotechnol* **1997**; 69:463-469.

[225] Yang G, Wu J, Xu G, Yang L. Enhancement of the activity and enantioselectivity of lipase in organic systems by immobilization onto low-cost support. *J Mol Catal B: Enzym* **2009**; 57:96-103.

[226] Gomes FM, Silva GS, Pinatti DG, Conte RA, Castro HFD. Wood cellulignin as an alternative matrix for enzyme immobilization. *Appl Biochem Biotechnol* **2005**; 121-124:255-268.

[227] Jiang Y, Guo C, Xia H, Mahmood I, Liu C, Liu H. Magnetic nanoparticles supported ionic liquids for lipase immobilization: Enzyme activity in catalyzing esterification. *J Mol Catal B: Enzym* **2009**; 58:103-109.

[228] Ozman EY, Sezgin M, Yilmaz M. Synthesis and characterization of cyclodextran-based polymers as a support for immobilization of *Candida rugosa* lipase.*J Mol Catal B: Enzym* **2009**; 57:109-114.

[229] Lee DH, Park CH, Yeo JM, Kim SW. Lipase immobilization on silica gel using cross-linking method. *J Ind Eng Chem* **2006**; 12:777-782.

[230] Christensen MW, Anderson L, Husum TL, Kirk O. Industrial lipase immobilization. *Eur J Lipid Sci Technol* **2003**; 105:318-321.

[231] Kotha A, Raman RC, Ponrathnam S, Kumar KK, Shewale JG. Beaded reactive polymers, 2. Immobilization of pencillin G acylase on glycidyl methacrylate-divinyl benzene copolymers of different pore size and its distribution. *React Funct Polym* **1996**; 28:235-242.

[232] Liu X, Guan Y, Shen R, Liu H. Immobilization of lipase onto micron-size magnetic beads. *J Chromatogr B* **2005**; 822:91-97.

[233] Gabel D, Vretblad P, Axen R, Porath J. Insolubilized trypsin with activity in 8 M urea. *Biochem Biophys Acta* **1970**; 198:559-561.

[234] Cabrera Z, Fernandez-Lorente G, Fernandez-Lafuente R, Palomo JM, Guisan JM. Novozym 435 displays very different selectivity compared to lipase from *candida antartica* B adsorbed on other hydrophiobic supports. *J Mol Catal B: Enzym* **2009**; 57:171-176.

[235] Kosaka PM, Kawano Y, Seoud OAE, Petri DFS. Catalytic activity of lipase immobilized onto ultrathin films of cellulose esters. *Langmuir* **2007**; 23: 12167-12173.

[236] Fernandez-Lorente G, Palomo JM, Cabrera Z, Fernandez-Lafuente R, Guisan JM. Improved catalytic properties of immobilized lipases by the presence of very low concentration of detergents in the reaction medium. *Biotechnol Bioeng* **2007**; 97:242-250.

[237] Mariotti F, Tome D, Mirand PP. Converting nitrogen into protein-beyond 6.25 and Jones factor. *Crit Rev Food Sci Nutr* **2008**; 48:177-184.

[238] Naka K, Yamashita R, Nakamura T, Ohki A, Maeda S, Aoi K, Takasu A, Okada M.Chitin-graft-poly(2-methyl-2-oxazoline) enhanced solubility and activity of catalase in organic solvent. *Int J Biol Macromol* **1998**; 23:259-262.

[239] Samad MYA, Salleh AB, Razak CNA, Ampon K, Younus WMZW, Basri M. A lipase from newly isolated thermophilic *Rhizopus rhizopodiformis*. *W J Microbiol Technol* **1990**; 6:390-394.

[240] Toth M, Furlan L, Szarukan I, Ujvary I. Geranyl hexanoate attracting male click beetles *Agriotes rufipalpis* brulle and *Agriotes sordidus* illiger (Col., Elateridae). *J Appl Ent* **2002**; 126:312-314.

[241] Toth M, Furlan L, Yatsynin VG, Ujvary I, Szarukan I, Imrei Z, Subchev M, Tolasch T, Francke W. Identification of sex pheromones composition of click beetle *Agriotes brevis* candeze. *J Chem Ecol* **2002**; 28:1641-1652.

[242] Toth M, Furlan L, Yatsynin VG, Ujvary I, Szarukan I, Imrei Z, Tolasch T, Francke W, Jossi W. Identification of pheromones and optimization of bait composition for click beetle pests (Coleoptera: Elateridae) in central and western europe. *Pest Manag Sci* **2003**; 59:417-425.

[243] Toth M, Furlan L, Xavier A, Vuts J, Toshova T, Subschev M, Szarukan I, Yatsynin VG. New sex attractant composition for the click beetle *Agriotes proximus*: Similarity to the pheromone of *Agriotes lineatus*. *J Chem Ecol* **2008**; 34:107-111.

[244] Adnan A, Qadeer MA, Iqbal MZ. Production of fragrance esters fusal oil by mycelial lipase of *Rhizopus arrhizus*. *Pak J Sci IndRes* **1994**; 3:449-452.

[245] Miller C, Austin H, Porsorske L. Characterization of an immobilized lipase for the commercial synthesis of esters. *J Am Oil Chem Soc* **1988**; 65:927-931.

[246] Pereira EB, Zanin GM, Castro HF. Immobilization and catalytic properties of lipase on chitosan for hydrolysis and esterification reactions. Braz *J Chem Eng* **2003**; 20:343-355.

[247] Mateo C, Palomo JM, Fernandez-Lorente G, Guisan JM, Fernandez-Lafuente R. Improvement of enzyme activity, stability and selectivity via immobilization techniques. *Enzyme Microb Technol* **2007**; 40:1451-1463.

[248] Fernandez-Lafuente R, Armisen P, Sabuquillo P, Fernandez-Lorente G, Guisan JM. Immobilization of lipases by selective adsorption on hydrophobic supports. *Chem Phys Lipids* **1998**; 93:185-197.

[249] Brady L, Brozozowsky AM, Derewenda ZS, Dodson E, Dodson G. A serine protease triad forms the catalytic center of a triacylglycerol lipase. *Nature* **1990**; 343:767-770.

[250] Naoe K, Ohsa T, Kawagoe M, Imai M. Esterification by Rhizopus delemar lipase in organic solvent using sugar ester reverse micelles. *Biochem Eng J* **2001**; 9: 67-72.

[251] Tahir MN, Adnan A, Mischnick P. Lipase immobilization on *O*-propargyl and *O*-pentynyl dextrans and its application for the synthesis of click beetle pheromones. *Process Biochem* **2009**; 44:1276-1283.

[252] Fuentes IED, Viseras CA, Ubiali D, Terreni M, Alcantara AR. Different phyllosilicates as asupports for lipase immobilization. *J Mol Catal B: Enzym* **2001**; 11:657-663.

[253] Chatterjee S, Barbora L, Cameotra SS, Mahanta P, Goswami P. Silk-fiber immobilized lipase-catalyzed hydrolysis of emusified sunflower oil. *Appl Biochem Biotechnol* **2009**; 157:593-600.

[254] Deng L, Tan T, Wang F, Xu X. Enzymatic production of fatty acid alkyl esters with a lipase preparation from *Candida sp*. 99-125. *Eur J Lipid Sci Technol* **2003**; 105:727-734.

[255] Liu X-M, Thakur A, Wang D. Efficient synthesis of linear multifunctional poly(ethylene glycol) by Copper(I)-catalyzed Huisgen 1,3-dipolar cycloaddition. *Biomacromol* **2007**; 8:2653-2658.

[256] Mayer T, Maier ME. Design and synthesis of a tag-free chemical probe for photoaffinity labeling. *Eur J Org Chem* **2007**; 2007:4711-4720.

[257] Adelwöhrer C, Rosenau T, Kloser E, Mereiter K, Netscher T. Synthesis of 5a-α-tocopheryl azide and its reaction to 1-(5a-α-tocopheryl)-1,2,3-triazols by [2+3]-cycloaddition. *Eur J Org Chem* **2006**; 2006:2081-2086.